



Unione europea
Fondo sociale europeo



Ministero dell'Università
e della Ricerca



Università degli Studi
di Palermo

arXiv:cond-mat/0703130v1 [cond-mat.mtrl-sci] 5 Mar 2007

**Role of hydrogen on the generation
and decay of point defects
in amorphous silica exposed
to UV laser radiation**

Ph. D. Thesis

Fabrizio Messina

Supervisore: *Prof. Marco Cannas*

Il Coordinatore: *Prof. Natale Robba*

Tesi cofinanziata dal Fondo Sociale Europeo

PROGRAMMA OPERATIVO NAZIONALE 2000/2006

“Ricerca Scientifica, Sviluppo Tecnologico, Alta Formazione”
Misura III.4, “Formazione Superiore e Universitaria”

Palermo (Italy)
January 2007

Acknowledgements

The time spent in writing a doctoral Thesis provides a rather unique opportunity to look back and gain a new perspective on several years of work. In doing so, I feel the need to thank the many people that have contributed in different ways to the realization of this work.

I wish to express my sincerest gratitude to Prof. Marco Cannas, for generously sharing with me his scientific experience, which has permitted me to continuously improve my skills while allowing the progressive development of my autonomy. But even more, I thank him for his persistent support, and for being gifted with a firm enthusiasm and a solid optimism which really help to transform even the hard work in an enjoyable experience. It is also a real pleasure for me to thank Prof. R. Boscaino. Aside from his outstanding ability to suggest, direct and organize future research work, I am grateful to him for having closely followed my activity, thus allowing me to benefit from his very large experience and knowledge. I thank Dr. S. Agnello, who has always been exceedingly generous in sharing his time in plenty of stimulating scientific discussions, and whose experimental support has been always at hand. Moreover, I genuinely acknowledge the many important suggestions that during these years have repeatedly come from Prof. F. M. Gelardi and Prof. M. Leone, whether during formal or informal discussions. With all these people I am really indebted for having given an invaluable contribution to this work and, even more, to my formation as a young researcher.

I wish to spend also a few words on the colleagues who have shared with me the PhD experience. The peculiar mix of friendship and professional collaboration which I have been establishing with them, particularly with the members of my research group, is a very important part of the human experience I have gone through during the last years. It has been a real pleasure to work among these people.

In these years I have been given several occasions to get advantage from valuable discussions with scientists from all around the world. Apart from improving my formation as a physicist, these meetings have provided important steps forward in the understanding of the experimental results which I was working on. Among these people, I express a particular gratitude to Prof. V. A. Radzig., Prof. A. Shluger, Prof. A. Thrukhin, and especially to Dr. L. Skuja, who offered me very detailed and useful comments, suggestions and corrections on the Thesis. I thank also Prof F. Persico, for providing me with a wider standpoint on my research, as well as for carefully proofreading my English. Finally, I would like to express my appreciation for the work of Prof. N. Robba, the coordinator of the PhD activities in my department, and I gratefully acknowledge the technical assistance received by Mr. G. Lapis, Mr. G. Napoli, and Mr. G. Tricomi.

I wish this to be an occasion to thank my family. Among the many reasons that I could choose to motivate my gratitude, I would like to mention their everlasting support and their commitment in setting up throughout the years the necessary boundary conditions which have permitted me to arrive here. Also my friends in my private life truly deserve my most sincere gratefulness for being close to me during these years and for helping me in times of trouble.

Last but not least, I thank Elisa. You have been at my side and believed in me during these years, and your enduring love is a privilege that I really hope to deserve. This Thesis is dedicated to you because I regard every achievement in my life as a success of the two of us.

To Elisa

Contents

Contents	vii
Introduction	1
I Background	3
1 Effects of laser irradiation on amorphous silica	5
1.1 Structure and basic point defects in silica	5
1.2 Exposure of a -SiO ₂ to laser radiation	11
1.2.1 Overview	11
1.2.2 Generation of E' center	12
1.2.3 Ge-related defects	24
2 Diffusion and reaction of mobile species in a-SiO₂	33
2.1 Post-irradiation kinetics and annealing of radiation-induced defects	33
2.2 Diffusion in silica	36
2.3 Theoretical treatment of the reaction kinetics	41
2.4 Hydrogen in silica and its interaction with point defects	47
2.4.1 Forms of hydrogen in a -SiO ₂	47
2.4.2 Reaction of NBOHC center with H ₂	49
2.4.3 Reaction of E' center with H ₂	54
3 Experimental techniques: a theoretical background	57

3.1	Optical properties of a point defect	57
3.2	Magnetic resonance of a point defect	61
II	Experiments and Results	67
4	Materials and experimental setups	69
4.1	Silica samples	69
4.2	Irradiations and <i>in situ</i> optical measurements	71
4.2.1	The Nd:YAG laser system	71
4.2.2	The optical fiber spectrophotometer	73
4.2.3	The cryostat	75
4.3	Photoluminescence measurements	75
4.3.1	The instrument	75
4.3.2	Correction procedures	76
4.3.3	Time-resolved photoluminescence measurements	78
4.4	Electron spin resonance measurements	78
4.4.1	The instrument	78
4.4.2	Absolute concentration measurements	80
4.5	Raman measurements	81
5	Effects induced on silica by 4.7eV laser radiation	83
5.1	Introduction	83
5.2	Optical properties of the as-grown samples	84
5.3	<i>In situ</i> observation of the generation and decay of E' center	86
5.4	Response of Ge-related defects to irradiation	93
5.5	Discussion	97
5.6	Conclusions	101
6	Generation of E' center	103
6.1	Introduction	103

6.2	E' center in natural wet α -SiO ₂	104
6.2.1	Experiment	104
6.2.2	Results	104
6.2.3	Discussion I: Precursor of E' center	107
6.2.4	Discussion II: Generation mechanism	112
6.2.5	Discussion III: Generation kinetics	115
6.2.6	Previous literature on the Si-H generation model	120
6.3	E' center in other types of α -SiO ₂	122
6.3.1	Dry natural silica	122
6.3.2	Synthetic silica	126
6.4	Conclusions	127
7	Post-irradiation conversion processes at room temperature	129
7.1	Introduction	129
7.2	Conversion processes of GLPC center	131
7.2.1	Results	131
7.2.2	Discussion I: Correlation between GLPC and H(II) centers	135
7.2.3	Discussion II: Correlation under repeated irradiations and photo-induced decay of H(II) center	140
7.3	Modeling the reaction kinetics	143
7.4	Conclusions	148
8	Temperature dependence of the generation and decay of E' center	149
8.1	Introduction	149
8.2	Experiments and Results	150
8.3	Discussion I: Character of the reaction between E' center and H ₂	157
8.3.1	Rate constant of the reaction	157
8.3.2	Comparison with theoretical models and previous literature	160
8.4	Discussion II: Temperature dependence of the generation process	162

8.5	Conclusions	165
9	Conclusions	167
	List of related papers	171
	References	173

Introduction

Amorphous silicon dioxide, or silica ($a\text{-SiO}_2$), is a material of major scientific and technological interest, which has been for several decades a very active subject of investigation frequently crossing the border between physics and materials science. Research has been motivated by the circumstance that silica may be regarded as a simple archetypal system helpful to understand the general properties of amorphous insulators, as well as by the several applications of the material, which at the moment remains one of the most important in optical and microelectronic technologies. Notwithstanding many years of research and the wide availability of the basic experimental techniques necessary for the investigation, many of the properties of silica still remain poorly understood and lively debated, so that the subject continues to attract an intense research activity aiming to completely unravel the complex puzzle of its physical properties.¹⁻³

Many investigations dealing with $a\text{-SiO}_2$ focus their attention on the properties of point defects, usually generated by exposure of the material to laser or ionizing radiation. On the one hand, the presence of defects may significantly affect the properties of silica that are exploited by applications. On the other hand, some basic physical properties of the defects embedded in an amorphous solid are not thoroughly understood at the moment, and it took considerable ingenuity to elucidate the microscopic structure of even the most common defects in $a\text{-SiO}_2$.¹⁻³ The generation of defects upon irradiation features quite a complex phenomenology. In particular, the type of centers produced by radiation and their concentration strongly depend on several factors, such as the presence of even small concentration of impurities, or the characteristics of the radiation being used. A common means of inducing point defects in silica is exposure of the material to laser radiation. Not surprisingly, apart from being a useful tool to generate defects to be studied, the interaction of laser light with the material has become in the years a research field in itself, also in this case motivated by strong technological demands due to the wide use of lasers in applications. A specific defect may usually be generated by several mechanisms depending on the experimental conditions, but the current understanding of several of these processes is still qualitative, and many important questions are unanswered at the moment. For these reasons, the interest in performing further investigations on these topics is still alive.¹⁻³

This Thesis reports an experimental research work on the effects of laser irradiation on amorphous silica. The investigation is mainly focused on the kinetics of generation and decay of point defects induced by laser radiation. As we are going to show, these processes are strongly conditioned by the presence of hydrogen, which is able to diffuse spontaneously in silica even at room tempera-

ture. In the specialized literature on $a\text{-SiO}_2$, most of the current knowledge on defect-related issues is based on stationary studies, namely investigations that look at the defects mainly after the end of any possible time-dependent effect altering their concentration. In contrast, we argue that kinetic investigations often provide additional information worthy to be collected and discussed. This idea underlies all this work. Our experimental approach is based on the combined use of several spectroscopic techniques, as mandatory to perform comprehensive studies in this field. In particular, some of the most valuable information come from the use of *in situ* optical absorption to investigate the transient kinetics of point defects generated by laser radiation.

The Thesis is organized in a Part I, comprising chapters 1-3, and a Part II, comprising chapters 4-9. The purpose of Part I is to provide a background on the specialized literature dealing with the effects of laser irradiation on $a\text{-SiO}_2$. The approach is by no means comprehensive, as the attention is mainly focused on a selection of relevant and interconnected topics that our work aims to clarify. The last chapter of Part I includes a brief theoretical background on the experimental methodologies used in our investigation. Part II reports the experiments and their main results. After the description of the experimental setups and of the instruments (chapter 4), the chapters from 5 to 8 present the results of our investigation; the order is dictated by the sake of clarity rather than by relevance reasons. Finally, in chapter 9 we draw the main conclusions and briefly sketch some proposals for further work. Most of the results presented in this work have been published as papers on scientific Journals. Bibliographic references to these papers and to a few others on closely related topics are available in a "List of related papers" included at the end of Part II.

Part I

Background

Chapter 1

Effects of laser irradiation on amorphous silica

In this chapter we open the background part of the Thesis with a discussion of some general properties of amorphous silica and its defects, after which we propose a review of the current knowledge on some of the most important effects induced by laser irradiation in $a\text{-SiO}_2$.

1.1 Structure and basic point defects in silica

The most widely accepted description of the microscopic structure of amorphous silica is known as the Continuous Random Network (CRN) model, and is mainly based upon the evidences coming from X-ray and neutron scattering studies of the solid.^{1,2,4-6} Within the CRN model, the basic structural unit of silica is a SiO_4 tetrahedron with each silicon atom forming four bonds with oxygen first neighbors (Figure 1.1), while the solid consists in an infinite repetition of basic units connected by sharing an oxygen atom. For what concerns the basic unit (with an O-Si-O angle of 109.5°), the structure of silica closely resembles that of the crystalline solid with the same chemical composition, i.e. quartz, at least in its most common crystalline form, α -quartz. The main structural difference is that the angles defining the relative spatial orientation of each pair of connected tetrahedra are statistically distributed in silica, differently from quartz where they assume fixed values. Due to the stochastic nature of the spatial configuration, the structure of silica is amorphous in that it lacks translational invariance, and thus long-range order. Although the term is sometimes used to indicate both the crystalline and the amorphous form of silicon dioxide, in this work only the latter will be referred to as *silica*.

From the standpoint of solid state physics, silica is a wide bandgap insulator. Due to its large bandgap ($\sim 9\text{ eV}$) the material, when pure, is optically transparent from infrared (IR) up to ultraviolet (UV). In addition, it is characterized by excellent insulating properties, a high radiation resistance and good mechanical and thermal stability. For these reasons, silica is one of the key materials at the basis of the current telecommunication and computing technologies. Indeed, it is

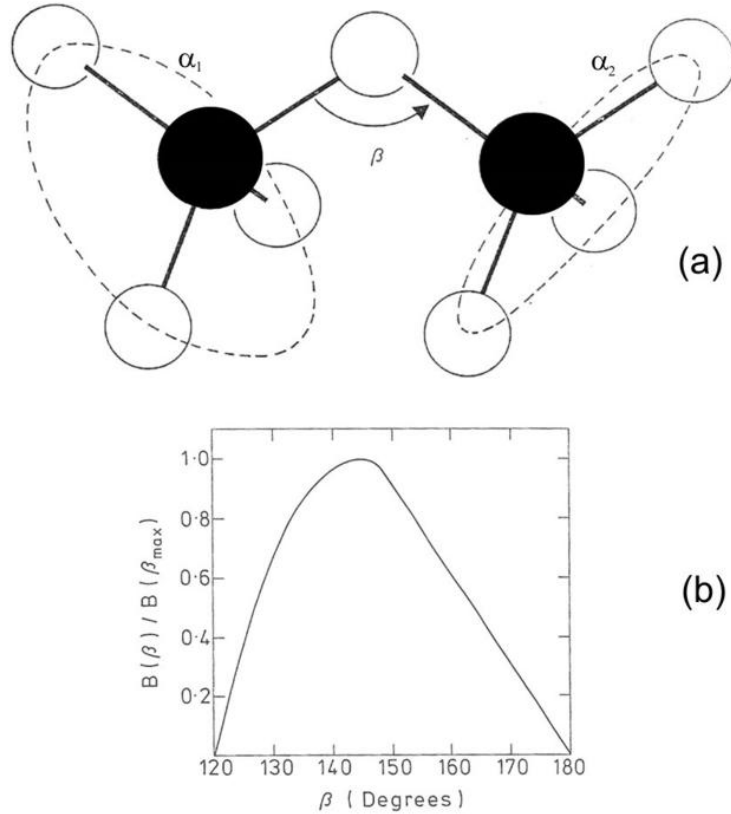


Figure 1.1: Panel (a): structure of a -SiO₂, with Si atoms in black and O atoms in white. The three angles α_1 , α_2 and β define the spatial configuration of two connected tetrahedra. Panel (b): statistical distribution of β , as derived from X-ray scattering measures. Figure adapted from Mozzi *et al.*⁵ and Bell *et al.*⁶ Other more recent investigations of the distribution of β based on different experimental techniques have suggested a significantly narrower distribution than panel (b).¹

the material of choice for many optical applications, ranging from photolithography to optical fibers, particularly when usability in the far UV is required, while in electronics it is found as a thin insulating layer covering silicon, in metal-oxide-semiconductor (MOS) transistors and other components.^{1-3,7,8} Finally, silica is being used to manufacture novel experimental devices, such as photonic crystal fibers and nanowires.^{9,10} Although in recent years other insulators, such as ZrO₂ and HfO₂, have been proposed to substitute silica in selected applications, particularly in microelectronics,¹¹ at the moment a -SiO₂ still remains one of the most important technological materials, so that investigation is in progress with the purpose of further improving our ability to control its macroscopic properties.

One of the basic issues in research on silica is the study of point defects and of their generation and conversion processes. A point defect in the intrinsically disordered structure of silica can be defined as any deviation from the 'perfect' structure, as described by definition by the CRN model, provided that it is localized in a region whose dimensions are comparable to the interatomic distance.¹ The experimental investigation of point defects is founded on the use of several spectroscopic techniques. Each of them may be sensitive only to some types of defects, depending on their properties, and is characterized by its own advantages and drawbacks. The most common are Electron

Spin Resonance (ESR), Optical Absorption (OA) in the visible, in the UV, or in the infrared, Raman and photoluminescence (PL) spectroscopies. The minimum defect concentration detectable by typical^a ESR, OA, PL measurements usually ranges from $\sim 10^{13}\text{cm}^{-3}$ to $\sim 10^{16}\text{cm}^{-3}$ depending on the specific defect, although the sensitivity can be much higher in particular experimental conditions^b. Often, the combined use of different techniques allows to infer information not available by examining separately the results of the single observations.¹ Among these different techniques, the ESR, albeit applicable only to paramagnetic centers, possesses an unsurpassed ability to yield direct structural information on the defects, thereby allowing the development of their microscopic models. Indeed, also the structural models for diamagnetic defects are often founded on the observed conversion into a paramagnetic defect whose structure is known by ESR.

From a historical point of view, it was initially thought that the knowledge accumulated on crystalline point defects could be straightforwardly extended to defects embedded in an amorphous structure. Nonetheless, the study of simple model systems such as amorphous silica and silicon, showed that the defects found in a disordered solid feature new and different characteristics peculiar of the amorphous state, with a quite unforeseen complexity that still prevents a thorough understanding comparable to that available for the crystalline case.^{1,12} In particular, some types of defects that exist in silica are not found in quartz, meaning that the amorphous structure provides new degrees of freedom to incorporate or stabilize the defects. An example of an amorphous-specific defect class is that of *isolated dangling bonds*, namely under-coordinated atoms surrounded by a defect-free network in which all other atoms are regularly coordinated.¹² Besides, the properties of 'amorphous defects' are conditioned by the characteristic inhomogeneous site-to-site distribution of structural parameters, such as bond length and angles, with relevant consequences on their spectroscopic features. At the moment, the current understanding of these issues is mostly qualitative.^{8,12}

The study of point defects is also connected to the issue of investigating the effects of irradiation. As anticipated, exposure of the material to several forms of radiation, from lasers to γ , X, or β , results in the generation of defects; actually, this often occurs by transformation, or *conversion*, of other defects preexisting in the *as-grown* material before irradiation, and known as *precursors*. Generally the defects found in the as-grown material are prevalently diamagnetic, whereas paramagnetic centers are detected in measurable concentrations only in irradiated specimens. In several cases, the growth of point defects alters the macroscopic properties of the material with subsequent degradation of the technological performance, an important example being the loss of optical transparency due to the absorption bands associated to most centers. Still, in other cases the generation or conversion of point defects can be exploited to induce *ad hoc* new and useful properties.^{1-3,7,8,13} In this context, most investigation efforts in recent times focus on the effects of *laser* irradiation.⁸ Indeed, exposure of silica to laser light is common in many applications, such as photolithography, a technique used to produce micro-electronics circuits by irradiation of a sensitive material with laser light through a mask.³ Here, the progressive reduction of the typical circuit dimensions has led to an increase

^aHere and in the following, the detection limits refer to standard commercial instruments, and to sample sizes of the order of 1 mm.

^bIn particular, PL measurements with high power laser sources and very low-noise detectors, may allow in some cases to detect even a single luminescent center.¹

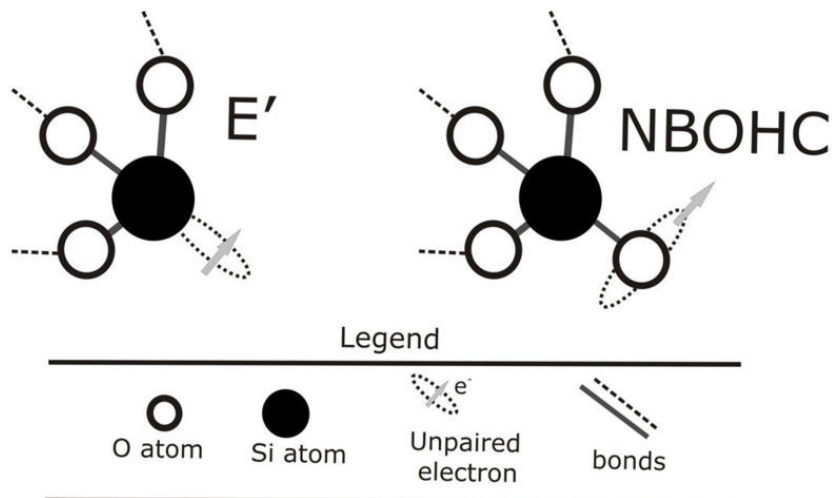


Figure 1.2: Schematic representation of the structure of the E' and NBOHC centers in $a\text{-SiO}_2$

of the photon energy hc/λ used in the process, resulting in an increasing tendency of laser photons to damage the optical components used in the lithographic system; hence, the need to understand and control the basic laser-induced damage processes in $a\text{-SiO}_2$. On the other hand, lasers have been found to be particularly effective in inducing *controlled* variations of the properties of silica, in particular when the material is conveniently doped with suitable impurities.^{1,3,13} As many of these processes are related to point defects, it is easily understandable why the investigation of laser-induced generation and conversion of defects in $a\text{-SiO}_2$ is currently a very active field.

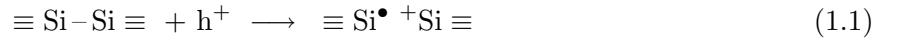
Two among the simplest defects that may be expected *a priori* to exist in the structure of amorphous silica are the *silicon dangling bond* ($\equiv\text{Si}\bullet$) and the *oxygen dangling bond*, ($\equiv\text{Si}-\text{O}\bullet$), where each symbol "—" indicates a bond with an oxygen atom, and the symbol "•" represents an unpaired electron. Both centers are expected to be paramagnetic due to the presence of an unpaired electron in their structure. Indeed, research has demonstrated that these two structures (represented in Figure 1.2) are actually very common in $a\text{-SiO}_2$ after irradiation. In the specialized literature, they are referred to as the E' center,^{1,7,8,14,15} and the Non Bridging Oxygen Hole Center (**NBOHC**),^{1,7,8,16–18} respectively.

The NBOHC center is detectable in silica by its characteristic ESR signal, as well as by its optical activity, consisting in three absorption bands, at 2.0 eV, 4.8 eV and 6.4–6.8 eV, which excite a photoluminescence emission peaked at 1.9 eV.^{1,16–20} The structure of the defect, featuring an unpaired p electron on an O atom bonded to a 3-fold coordinated Si ($\equiv\text{Si}-\text{O}\bullet$), was consistently inferred by ESR investigations, radio-chemical arguments, and by the detailed study of its photoluminescence activity.^{1,16–18}

The E' center is an almost ubiquitous defect in irradiated silica: it is found virtually in every specimen exposed to radiation. It is accompanied by a characteristic absorption band peaked at 5.8 eV, which is going to play a central role in our experimental investigation.^{1,3,8,21,22} In discussing

the properties of the E' center, it is necessary to go beyond the scheme in Figure 1.2. Indeed, to be precise the expression " E' -center" is used in literature to refer to a *variety* of paramagnetic defects in amorphous silica or crystalline quartz that share a common property: their unpaired electron spin is localized on a sp^3 orbital of a 3-fold coordinated Si atom ($\equiv\text{Si}\bullet$).^{1,7,8} However, several possible varieties of the E' center have been proposed to exist in silica glass,^{7,23} their structure still representing a quite debated problem in the current literature: all of them *comprise* the $\equiv\text{Si}\bullet$ basic moiety, whose structure was unambiguously clarified by the careful analysis of the spectroscopic properties of the ESR signal,^{1,7,14,24–27} but they differ for the environment of the primary structure, and are distinguishable, at least in principle, either by their spectroscopic properties or on the basis of their generation mechanism.

Historically, the first variety of E' to be identified was the $\equiv\text{Si}\bullet + \text{Si}\equiv$ structure in crystalline quartz, which is generated by hole trapping on a pre-existing oxygen vacancy ($\equiv\text{Si}-\text{Si}\equiv$):



The Si–Si bond in the vacancy initially involves two electrons. After hole trapping, the remaining electron localizes asymmetrically on only one of the two Si atoms, thus giving the structure at the right side of (1.1).^{1,7,8,24,25} This type of E' is widely believed to exist also in amorphous silica, generated either by laser or ionizing radiation.^{1,2,8,12,23,28,29} In this work, it will be referred to as *vacancy- E'* .^c However, differently from the case of quartz, in principle the $\equiv\text{Si}\bullet$ defect can exist in silica also as an **isolated dangling bond**.⁸ It is unclear at the moment which of the two is prevalent in the amorphous material. A further type of E' which will be referred to in the following, is the so-called E'_β center,^{7,23} whose currently accepted model is $\equiv\text{Si}-\text{H}\equiv\text{Si}\bullet$; this defect is supposed to arise from trapping of a H atom on an oxygen vacancy^d, followed by a structural relaxation at the end of which the unpaired electron points away from the former vacancy.^{1,7,12} Such a local rearrangement must be supposed in order to account for the unobserved hyperfine interaction (see chapter 3) between the electron and the proton. For completeness, we recall that at least two more types of E' have been proposed by the several studies on point defects in silicon dioxide:^{1,7,12,23} the E'_δ and the E'_α . Recent investigations have provided strong evidence that the structure of the former consists in an unpaired electron delocalized over four sp^3 orbitals of nearly equivalent Si atoms^e,^{29–31} while the E'_α has been proposed to be a variant of the *vacancy- E'* in which the unpaired electron points away from the vacancy and interacts with an extra oxygen in the a -SiO₂ network.³²

Apart from the detailed structure of the several sub-types of E' , it is still discussed at the moment if all of them contribute to the "usual" 5.8 eV absorption band.¹² This problem is complicated by the circumstance that the electronic transition responsible for this absorption has not been clarified yet. In particular, theoretical calculations have ascribed the optical transition to a "charge transfer" of

^cThe traditional classification of the sub-types of the E' center in a -SiO₂ is mainly based on the differences among their ESR signals, rather than on their structural properties.^{1,7,23} In literature, the *vacancy- E'* is often referred to as the E'_γ center;^{1,7,12,23} we prefer here to use an alternative denomination in order to better emphasize the structural difference with respect to the isolated dangling bond.

^dnamely the reaction: $\equiv\text{Si}-\text{Si}\equiv + \text{H} \Longrightarrow \equiv\text{Si}-\text{H}\equiv\text{Si}\bullet$

^eAccepting this structural model, the inclusion of the E'_δ within the category of E' centers relies on a broader interpretation of the above definition of E' .

the unpaired electron from the dangling bond to the positively charged $^+Si\equiv$ group which is expected according to (1.1);^{33,34} on this basis, the 5.8 eV band should be a property of the *vacancy- E'* defect, but certainly not of the isolated dangling bond. However, other theoretical works have questioned this finding,^{12,35} and it has been also predicted a weaker transition falling in the same energy region but entirely comprised within the silicon dangling bond.^{33,34} For these reasons, the character of the 5.8 eV absorption band of E' has not been conclusively established.^{8,12}

As common in literature, in this work the term " E' center", as well as the expression "silicon dangling bond", will be used in the general sense of a defect comprising the $\equiv Si^\bullet$ fragment *and* absorbing at 5.8 eV, as these are the two most basic features of this defect in $a-SiO_2$. More specifically, the expression "isolated" dangling bond will be used for the E' center that consists *only* in the $\equiv Si^\bullet$ structure.

Aside from being the two most "basic" defects in $a-SiO_2$, E' and NBOHC are very important also from the technological point of view. In fact, the generation of these two centers is the main cause of degradation of the UV transparency of silica upon irradiation, due to their wide absorption bands peaked at 5.8 eV and 4.8 eV (Figure 1.3).^{1,3,8} Several works have investigated the generation processes of the two defects under laser irradiation, showing a complex landscape in which many formation channels are possible, depending on the specific laser wavelength and intensity being used, as well as on the manufacturing procedure of the material. However, the understanding of the generation mechanisms often remains at a qualitative level, thus calling for more investigations to clarify the several open issues.^{1-3,8,12,36}

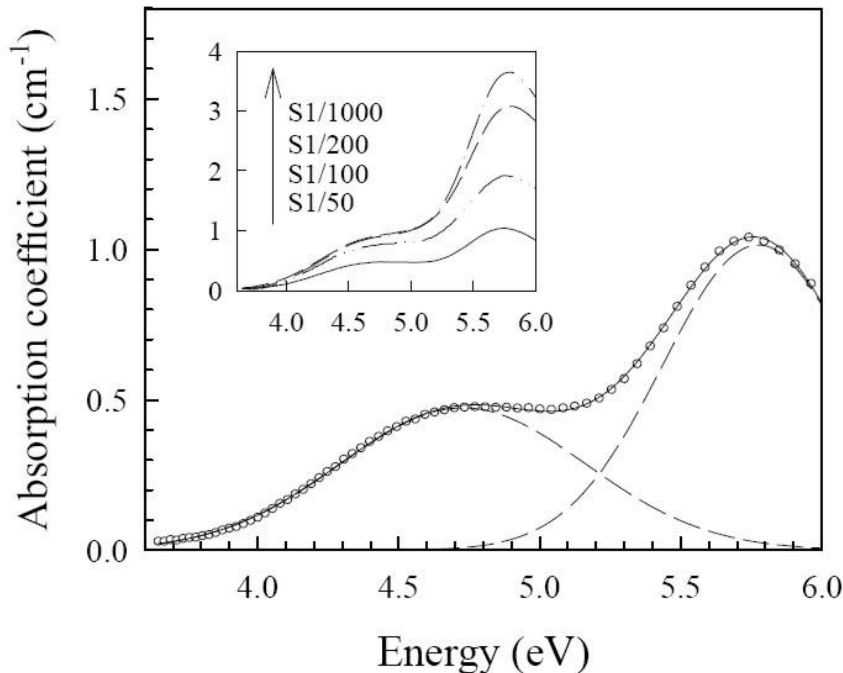


Figure 1.3: Optical absorption induced in a synthetic silica sample by γ irradiation, showing the 5.8 eV and 4.8 eV bands related to E' and NBOHC centers respectively. Figure taken from Cannas *et al.*³⁶

Many other defects, such as oxygen-deficient centers, peroxy radicals, interstitial oxygen, and so on have been identified, some of them still being actively studied, and the picture becomes even more complicated if we include another important class of defects in silica: impurity-related centers. In this context we recall that point defects are usually classified in extrinsic or intrinsic depending on the presence or absence of an impurity in their structure, respectively (in the specific case of $a\text{-SiO}_2$, the term "impurity" indicates any chemical element which is neither Si nor O). E' and NBOHC are examples of intrinsic defects; extrinsic defects due to the presence of impurities are always present in variable concentrations in the material. On the other hand, selected impurities can be deliberately added by doping to induce many useful properties.^{1-3,7,8,12} Germanium and Hydrogen have assumed a particularly important role in the last two decades. In fact, Ge-doped silica has been shown to feature interesting optical properties, such as photosensitivity and nonlinearity, not observed in pure $a\text{-SiO}_2$ and partially related to point defects.^{1,3,13} Hydrogen is by far the most common impurity in $a\text{-SiO}_2$, whose presence is basically unavoidable also in high purity samples. Hydrogen is able to diffuse in silica, even at low temperatures, and conditions the response of the material to irradiation by reacting with point defects. Furthermore, diffusion and reaction of mobile species like hydrogen in $a\text{-SiO}_2$ are quite interesting also from a fundamental point of view, as their features are a fingerprint of the amorphous nature of the solid.³⁷⁻⁴²

The experiments presented in this Thesis are relevant to the understanding of the generation mechanisms and the properties of laser-induced E' centers in silica. In addition, some of our findings concern conversion processes of Ge-related defects. Hence, to provide a background for the presentation of the results, in the following sections of this chapter we are going to review in more detail the current understanding of laser-induced effects in $a\text{-SiO}_2$, particularly with regard to the generation of E' and the conversion of Ge-related defects.

1.2 Exposure of $a\text{-SiO}_2$ to laser radiation

1.2.1 Overview

The complex interaction processes between laser radiation and matter are a very timely research subject. In general, laser light interacts with solids by coupling with electron or nuclear degrees of freedom, resulting in articulated photothermal and photochemical effects of which the generation of point defects is just one of the end products. The availability of progressively increasing laser intensities in a wide range of wavelengths has provided research and industry with an invaluable set of tools for material processing. In fact, lasers are currently used for deposition, etching, ablation, and controlled amorphization, they are capable to generate hot plasmas, to induce controllable modifications in the optical properties, and so on.^{8,43} In this sense two categories of lasers have been found to be particularly effective, thus being the subject of strong technological and scientific interest: pulsed high-power UV lasers and femtosecond pulsed lasers. The former emit pulses with a few ns duration, and typical energy density from tens to hundreds mJcm^{-2} per pulse, this corresponding

to peak intensities^f around 10^{10} Wcm^{-2} . The most commonly used are excimer lasers (using KrF, ArF, XeCl, F₂ as the active medium) or frequency multiplied Nd:YAG lasers. Femtosecond lasers (the most common being the Ti:Sapphire) emit in the infrared (IR) spectral range and have a much higher peak intensity due to the very short pulse duration. Also, they can be converted to shorter wavelengths by using frequency-multiplying nonlinear devices.⁴³

In regard to silica, the effects of laser radiation began to be intensively studied during the eighties, following the first observation in 1984 of the E' center induced by laser radiation.⁴⁴ Nowadays, laser irradiation has been demonstrated to induce a variety of macroscopic effects in pure or doped silica. The most common and relevant for applications is transparency loss, but more complex modifications of the material have been demonstrated, such as variations of the refractive index,^{45–48} laser-induced birefringence,⁴⁹ or optical nonlinearity,⁵⁰ ablation,^{47, 51} densification,^{47, 52–54} crystallization,² and more. From the microscopic standpoint, many of these effects are at least partially ascribable to generation and conversion of point defects, although laser irradiation may also cause extended (non-local) structural rearrangements of the $a\text{-SiO}_2$ matrix. Finally, some of these processes are strongly enhanced when the material is enriched in some impurities like Germanium, as we are going to see in more detail in the following.^{1–3, 13}

After two decades of research on laser-induced processes in $a\text{-SiO}_2$ it is now known that every defect induced by ionizing radiation can be observed, under suitable conditions, in laser-irradiated silica.⁸ From a purely structural point of view, laser-induced defects are virtually identical to those growing upon much more energetic γ or β exposure; on the other hand, processes caused by laser irradiation are characterized by some peculiarities, such as *selectivity*, i.e. laser light at a given wavelength often acts only on a specific precursor, thereby exciting only a particular defect generation process among the many which can be induced simultaneously by ionizing radiation.⁸ In this sense, laser irradiation may be a very useful tool if the aim is to study selectively the properties and the generation mechanisms of a specific point defect.

1.2.2 Generation of E' center

Stathis and Kastner were the first to report the generation of point defects in $a\text{-SiO}_2$ upon exposure to laser light:⁴⁴ irradiation of a high purity silica sample with KrF and ArF pulsed excimer lasers (photon energies 5.0 eV and 6.4 eV respectively) or with a F₂ pulsed laser (7.9 eV) was observed to generate the E' center, detected by electron spin resonance (ESR) spectroscopy. The effect was found to be strongly dependent on laser photon energy.⁴⁴

High purity silica samples like those used by Stathis and Kastner are basically transparent to excimer laser photons (whose energies are lower than the silica bandgap ~ 9 eV) due to the absence of midgap electronic levels that may be introduced by the presence of impurities or pre-existing intrinsic defects^g. Hence, at that time, it was somewhat unexpectedly found that photons with

^fThe intensities, however, can be highly increased above these values by focusing the laser beam.

^gThis is not completely true for the F₂ laser, which features a 7.9 eV photon energy close to the bandgap. Indeed, as a consequence of its amorphous nature, $a\text{-SiO}_2$ features localized electronic states just below the conduction band

energies lower than the bandgap, which excite the material in an optical transparency region, are able to produce defects efficiently. Indeed, prior to this work, point defect generation in α -SiO₂ had been observed only under high energy radiation, such as γ , β , electrons or neutrons. Therefore, many authors tried to investigate in more detail the defects generation mechanism, suggesting in particular that it could involve multi-photon processes. Convincing experimental proofs followed a few years after, when several independent experiments evidenced that the concentration of induced E' centers depends quadratically on incident KrF or ArF laser power (Figure 1.4), strongly suggesting two photon absorption to be involved in E' generation.⁵⁵⁻⁵⁷

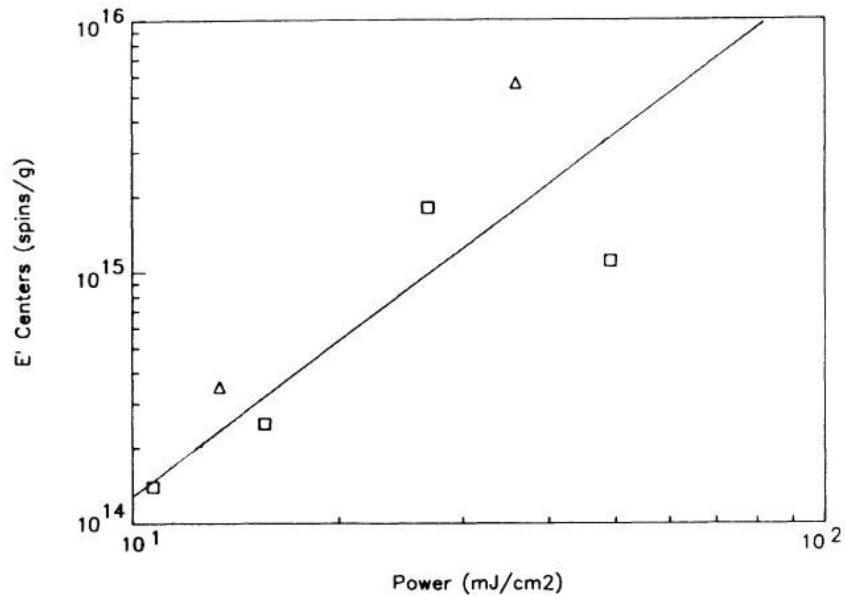


Figure 1.4: Concentration ρ of E' centers induced in a synthetic silica sample by 6.4eV ArF pulsed laser radiation, as a function of energy density per pulse I . The line with slope $\alpha=1.9\pm 0.7$ is a least-square fit of the experimental data with the function $\rho=kI^\alpha$. The value of α , close to 2, evidences the involvement of a two photon process. Squares and triangles represent two different irradiations. Figure taken from Tsai *et al.*⁵⁵

Nevertheless, the specific mechanism at the basis of laser-induced damage remained quite debated. Broadly speaking, the immediate consequence of a two photon absorption by the α -SiO₂ matrix is the generation of free electron-hole pairs or excitons,⁵⁸⁻⁶⁰ depending on the excitation energy. If free charges are made available, they can move and get trapped at a suitable precursor site, when available, forming paramagnetic defects. Alternatively, they can recombine in an exciton. The successive dynamics of the excitons is strongly conditioned by the electron-phonon coupling. In fact in silica, similarly to other solids, elementary excitations such as excitons can spontaneously get trapped at a regular lattice site and become immobile at low temperature.^{2,58,61-63} This occurs because the electron-hole pair is able to create a localized distortion in the lattice, which decreases the total energy, resulting in the formation of a potential well in which the quasi-particle is then trapped. In both silica and quartz this process is spontaneous, and is accompanied by a transition of

and above the valence band,¹ which are responsible for an interband absorption "tail" extending to energies smaller than the bandgap

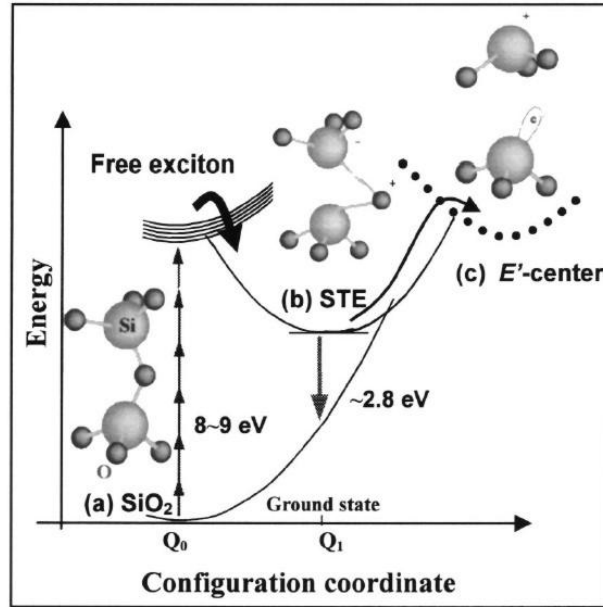


Figure 1.5: Configuration coordinate diagram representing the generation and self trapping processes of an exciton in (crystalline) SiO_2 , triggered by absorption of $\sim 9\text{ eV}$ radiation. After self trapping, the exciton can either decay radiatively (2.8 eV emission) or non radiatively; in the second case, a stable E' center is supposedly generated. Figure taken from Fukata *et al.*⁷⁶

the exciton to a triplet electronic state. The result of the trapping is referred to as the *self-trapped-exciton (STE)*. The STE has been for years the subject of intensive experimental and theoretical work, aimed to elucidate accurately its transient structure, dynamics and formation mechanism. Once formed, the STE decays radiatively (with a measurable luminescence band peaked between $2.0\text{ eV} - 2.3\text{ eV}$ and a $\sim 1\text{ ms}$ radiative lifetime) or non-radiatively. The luminescence decay time of the exciton results from a combination of the parallel radiative and non-radiative channels; as a result, it decreases with temperature due to the progressive thermal activation of the non-radiative decay mechanisms.^{2,58,61-71}

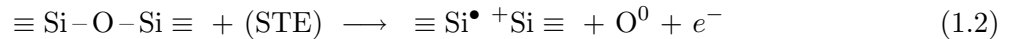
The relevance of the STE in the present context arises from the fact that it can serve as a transient product of irradiation whose energy may be eventually spent in the formation of a point defect. The non-radiative decay of a STE on an (initially) defect-free lattice has been recognized in silica, as well as in other solids, as one of the fundamental mechanisms for defect formation, which allows to break the original Si–O–Si matrix locally, so as to form a permanent defect.^{1,2,55,58,61-63,65,68-76} Due to the very nature of the process, in which the electron-phonon coupling is involved, this defect generation mechanism is characterized by an efficiency that is highly temperature-dependent. The main experimental evidences supporting this process, which permits E' generation in $a\text{-SiO}_2$ under laser irradiation, are reviewed in the next subsection A. After that, in the following two subsections B and C we discuss other two classes of generation mechanisms of E' that have been proposed in literature; both of them, differently from the decay of STE on the defect-free silica matrix, require the presence of pre-existing precursor defects.

A. Excitonic mechanism and generation from a regular lattice site

It was reported that XeCl laser radiation at 4.0 eV, lower than KrF and ArF lasers energy and less than one *half* of the silica bandgap, is unable to generate E' at comparable power levels.⁵⁶ This is consistent with the idea that electron-hole pairs formation is the first step of the E' generation process, since with 4.0 eV radiation *three* photons are required to bridge the silica bandgap, resulting in a much lower efficiency. A further step was made by Tsai *et al.*,^{55,74} which analyzed the effect of highly focused ArF laser radiation on synthetic silica: they were able to demonstrate experimentally that actually no *free* electrons in conduction band are generated by absorption of two 6.4 eV photons, in spite of the very high laser intensity ($>100 \text{ J cm}^2$ per pulse) used in their experiment. Hence, it was argued that most of the energy deposited by laser radiation results in the formation of excitons. Moreover, they measured a very high E' concentration up to 10^{18} cm^{-3} , higher than any possible precursor, and reached without any tendency to saturation with increasing irradiation dose. The experimental evidences led the authors to propose the following model: laser-induced generation of E' occurs by non-radiative decay of STE on the defect-free silica matrix, leading to the formation of a persistent defect.

The involvement of STE in defect generation was also confirmed by other two experimental findings. First, studying the concentration of laser-induced E' as a function of temperature, it was found that the generation of defects is quenched below $\sim 150 \text{ K}$ under radiation at 5.0 eV (Figure 1.6),^{77,78} or grows with temperature up to 400 K under radiation at 6.4 eV.⁷⁹ This behavior resulted to be anticorrelated with the luminescence decay time of the exciton (as measured in quartz), as expected from the idea that the generation of E' is the end-product of the non-radiative decay of STE. Second, another work focused on the comparison between laser- and γ -induced concentrations of E' .⁸⁰ It is known that the primary effect of γ exposure is creation of electron-hole pairs by the Compton effect, which are expected to spontaneously combine in STEs; hence, it was found that the growth curves of E' under γ and laser are identical, if the irradiation dose is expressed in both cases as the number of generated electron-hole pairs. This finding strongly suggests the existence of a common generation process for E' , independent of the radiation source, and occurring via the excitonic mechanism.

Up to this point, we have described the E' generation process as due to the decay of a STE at a regular lattice site, without mentioning the specific reaction by which the decay creates the defect. In a first stage, this was supposed to be:^{73,74}



where O^0 is an interstitial oxygen atom, e^- is an electron, and the first term at the right side is the E' center. Reaction (1.2) can be read saying that the self trapping and the successive non-radiative decay of the exciton causes the displacement of an oxygen ion to an interstitial position; of course, one must assume that the transient structure is eventually stabilized by migration of the oxygen, preventing recombination with the E' . One of the most convincing proofs of this generation scheme was the demonstration^h of the presence in the lattice of interstitial oxygen O_2 of radiolytic origin (presumably formed by diffusion and dimerization of O atoms), after high power ArF irradiation of

^hThe presence of radiolytic O_2 was indirectly inferred by the observed decay of E' correlated to the formation of

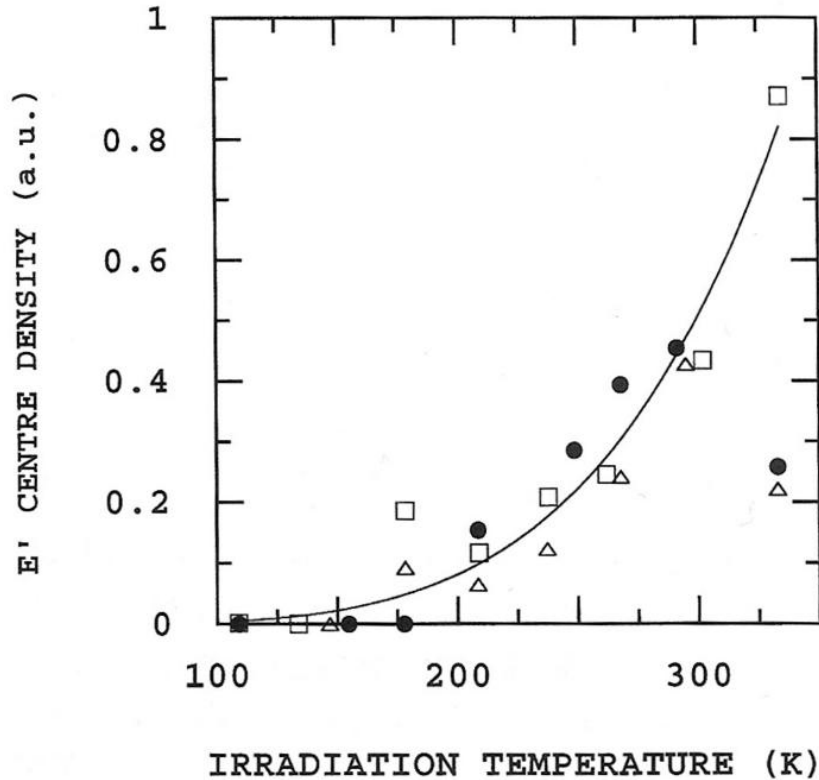
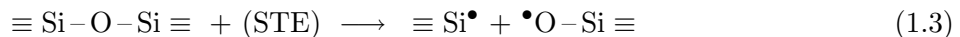


Figure 1.6: Defect density as a function of irradiation temperature in bulk a - SiO_2 samples exposed to 5.0 eV irradiation with 300 mJcm^{-2} energy density per pulse. Circles and triangles are the concentrations of induced E' , while the squares represent the concentrations of peroxy radicals produced by a post-irradiation thermal treatment at 600 K for one hour. Figure taken from Devine *et al.*²

samples where O_2 was initially absent.^{74,78} Process (1.2) is in some sense the analogous under laser radiation of the so-called *knock on* process induced by γ rays, namely the displacement of an oxygen atom due to the impact on a lattice site of a sufficiently energetic Compton electron.^{2,55}

Another group of experiments suggested a slightly different picture of defect generation upon non-radiative decay of STE. In fact, several works reported a correlated growth of E' and NBOHC centers either under γ or laser radiation,^{28,73,75,79,81,82} both defects being usually monitored with ESR spectroscopy. This finding can be explained as a consequence of another possible rupture mechanism of the Si–O–Si bond:



where the two terms at the right side are the E' and the NBOHC respectively. To accept reaction (1.3), it is necessary to explain the absence of broadening in the measured ESR signal of the E' and NBOHC centers, which would be expected due to dipole-dipole interaction. To this aim, it was supposed that the two defects after generation undergo a separation process so as to be far enough

peroxy radicals PRs ($\equiv \text{Si}-\text{O}-\text{O}^\bullet$), after a high temperature treatment, supposedly as a consequence of the reaction of O_2 with E' .^{74,78}

(tens of angstroms) that this effect is negligible. Only the defects that separate enough can survive recombination and become permanent centers.^{75,82,83}

More recently, time-resolved pump-and-probe experiments on the femtosecond scale have been carried out to study the self trapping process of the exciton in α -SiO₂, demonstrating that it is actually well represented by reaction (1.3), rather than (1.2). In other words, the exciton self trapping leads to the generation of a transient E' -NBOHC pair, occurring in roughly 250 fs.⁶² Similar results have been obtained by theoretical calculations.^{63,65} These studies, however, cannot investigate the long-term stabilization of the defect pair leading to the formation of a pair of *permanent* centers; for this reason, reaction (1.2) still cannot be excluded, because after reaction (1.3), oxygen may be eventually formed by decomposition of NBOHC, leading to the same net effect as reaction (1.2).

Finally, in some works it has been proposed that the occurrence of process (1.2) or (1.3) upon STE decay could be *site-selective*. In particular, process (1.3) may occur preferably on *strained bonds*, namely sites in the inhomogenous structure of α -SiO₂ where the Si-O-Si bonds are weaker and can be more easily cleaved.⁸³⁻⁸⁵ Strained bonds can be detected by vacuum ultraviolet (6 eV–9 eV) OA or Raman measurements;⁸⁴ they are expected to be particularly abundant in optical fibers,⁸⁶ as a consequence of the manufacturing process itself, or in silica densified with suitable techniques. Consistently, correlated E' and NBOHC generation has been reported in optical fibers,⁸⁷ and its efficiency in bulk silica was observed to grow after densification.⁷³ More recently, process (1.3) has been proposed to occur under F₂ laser radiation (7.9 eV),⁸⁵ by selective breaking of the strained bonds; with such a high photon energy, the process can occur even by single photon absorption, since the first electronic transition of the strained bond falls at energies slightly lower than the silica bandgap.

B. Generation from Oxygen Deficient Centers

Up to this point, we have described the experimental evidences regarding generation of E' from an initially unperturbed silica matrix. Other works have pointed out that processes starting from preexisting precursor defects are often important and can prevail on the simpler Si-O-Si bond breaking.^{56,57,72,88-90} In particular,⁷² some studies have shown quite a complex phenomenology not easily reducible to the picture proposed so far: by comparing samples prepared with a variety of manufacturing techniques it was pointed out a very strong dependence of the induced defect species and of their concentrations on the type of silica, as shown for example in Figure 1.7.

Such a variability strongly suggests that defect generation from precursors, rather than transformation of the pure silica matrix, is much more important than initially supposed. Nowadays it is generally believed that generation from the defect-free matrix is the prevailing generation mechanism of point defects and yields high defect concentrations ($>10^{16}$ cm⁻³) only under very high power focused excimer laser or femtosecond laser radiation, as it occurs in a minority of experiments.^{55,62,74,76,91} After recognizing the important role of precursors, the comparison of samples prepared with different techniques has become nowadays a standard approach to investigate the generation processes of point defects.

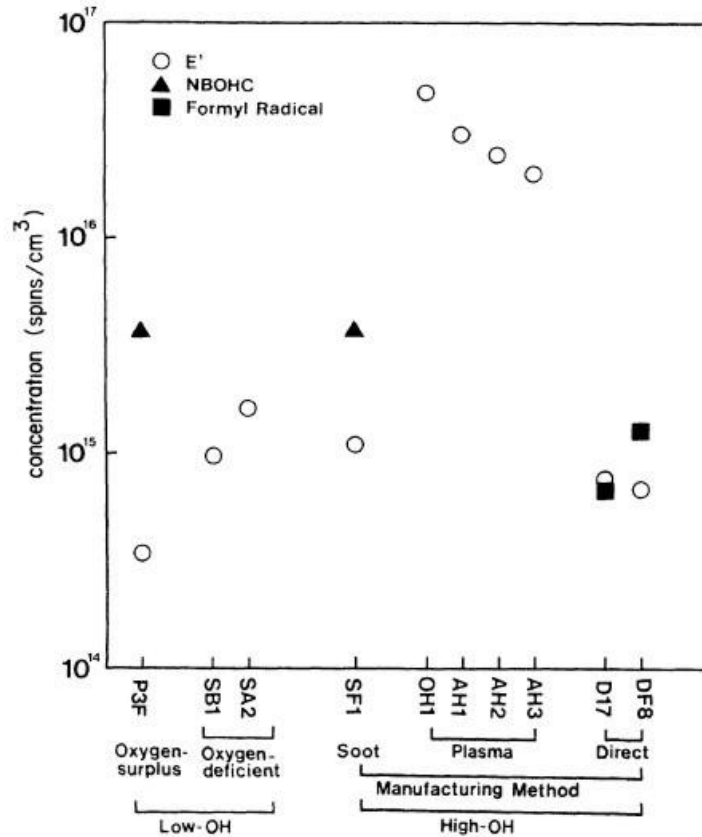


Figure 1.7: Concentrations of several centers induced by 6.4 eV ArF laser radiation in silica samples prepared with different manufacturing techniques. Figure taken from Nishikawa *et al.*⁷²

In general, the transformation of a precursor into another point defect under laser radiation may occur by several processes: **(i)** direct one-, two-, or many- photon absorption at the defect site (depending on the level scheme of the defect and on the laser photon energy), which may result in a permanent transformation of the structure, usually as a consequence of ionization or of the breaking of a chemical bond. **(ii)** Trapping at the precursor site of free electrons or holes made available by ionization of another precursor or by two photon absorption by the α -SiO₂ matrix. **(iii)** Non-radiative decay at the precursor site of STEs created in a first stage by two photon absorption by the α -SiO₂ matrix.^{1,56,72,88,89} **(iv)** Processes mediated by the diffusion to the precursor site of mobile ions, atoms or molecules made available by irradiation. This class of mechanisms will be discussed in more detail in the next chapter.

Some of the first experimental investigations dealing with generation of E' from precursors focused on oxygen-deficient silica samples,^{56,57,88-90} where a specific class of generation mechanisms for E' was pointed out, namely conversion of pre-existing oxygen-deficient-centers (ODCs). The ODCs in silica are found in two varieties: the **ODC(I)**, absorbing at 7.6 eV, and the **ODC(II)**, which absorbs at 5.0 eV and emits photoluminescence at 2.7 eV and 4.4 eV.^{8,12,92,93} Both are usually found in significant concentrations in oxygen-deficient silica due to the substoichiometry of the specimens and have been supposed to be precursors for generation of E' under laser radiation.

The detailed understanding of the generation processes of E' from ODCs is a problem linked with that of elucidating the exact structure of the two varieties of the oxygen vacancy. In detail, the commonly accepted structural model for the ODC(I), based upon several experimental evidences, is an oxygen vacancy, with a $\equiv\text{Si}-\text{Si}\equiv$ structure.^{12,88,94} Under ArF or F₂ laser radiation, it was observed a reduction (*bleaching*) of the ODC(I) 7.6 eV band concurrent to the growth of E' .⁵⁷ This finding suggests that the ODC(I) can be a precursor for E' by the following reaction:



where the ionization of the vacancy (under laser radiation at energies lower than 7.6 eV) may occur by direct two photon ionization or by hole trappingⁱ. As already mentioned, for reaction (1.4) to occur we must assume that after ionization the remaining electron spontaneously localizes on only one of the two adjacent Si atoms; in regard to oxygen vacancies in quartz, this scheme has been supported by theoretical calculations.²⁴ It is worth noting that the laser-induced reduction of ODC(I) concentration is usually much larger than the concentration of generated paramagnetic defects,^{8,12,57} this meaning that other unknown channels besides reaction (1.4) contribute to the bleaching of the 7.6 eV absorption band. The generation of E' by hole trapping on the oxygen vacancy is generally regarded as one of the main mechanisms triggered by γ -irradiation of amorphous silica.^{1,2,28,29,32}

In contrast, the understanding of the role of ODC(II) is less straightforward. Indeed, also in this case it has been observed a reduction of ODC(II) absorption and luminescence signals accompanied by a growth of E' , usually in concentration of a few 10^{15} cm^{-3} .^{88,89} From this result, and from the analysis of the power dependence, it was inferred that ODC(II) can serve as a precursor for generation of the E' by a two photon process. Moreover, in samples that contain a high native concentration of ODC(II) centers, a high concentration of induced E' is usually observed upon irradiation.¹² Starting from these observations, in literature it was proposed for the ODC(II) a model of *unrelaxed* oxygen vacancy, i.e. a vacancy similar to the ODC(I) but with a different value of the Si-Si bond length corresponding to another potential energy minimum.^{88,95}

On the other hand, another structural scheme has been proposed for the same defect based on completely different observations: the *twofold coordinated Si* model, in which ODC(II) corresponds to the structure $=\text{Si}^{\bullet\bullet}$, a silicon bonded with two oxygen atoms and hosting an electron lone pair.^{92,93} This model has its own quite convincing proofs, among which the observed conversion by hydrogen trapping to **H(I)** center ($=\text{Si}-\text{H}^{\bullet}$), whose structure has been established unambiguously by ESR spectroscopy and calculations.^{92,93,96-100} Starting from the twofold coordinated Si model, it is not immediately understandable how ODC(II) may be transformed in E' after ionization; even so, theoretical calculations have suggested this to be possible via a spontaneous local structural rearrangement^{j,101}. In conclusion, the issue of the ODCs structural models, as well as the possible generation of E' from these precursors are two connected problems not completely clarified and both still open at the moment.

ⁱin the latter case, it coincides with reaction (1.1)

^jTo further complicate the whole picture, several experimental evidences and theoretical calculations have also suggested that excitation of the ODC(I) in the 7.6 eV absorption band can result in its conversion to a transient ODC(II) center (in the excited singlet electronic state). Such unstable defect manifests itself by emitting a luminescence emission signal very similar to that associated to the standard ODC(II)^{12,101-105}

C. The Si–H precursor and instability of E'

Apart from the oxygen deficient centers, it was argued that another class of possible precursors exists for the E' center: they are extrinsic defects in the form Si–X, where X is an impurity. One of the most important in literature and in relation to the results of this Thesis is the Si–H group.

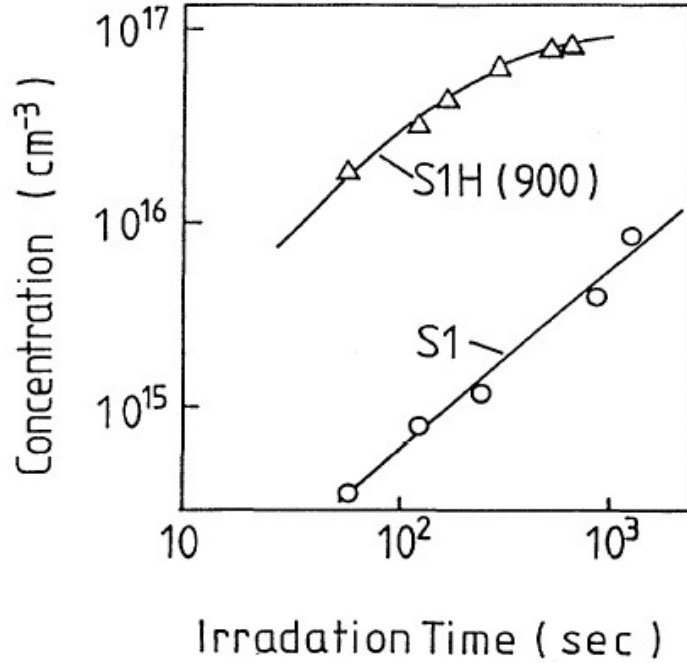


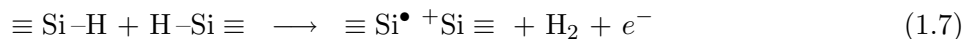
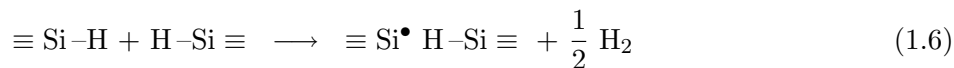
Figure 1.8: Concentrations of E' (measured by ESR) as a function of ArF laser irradiation time, in a oxygen-deficient glass before (S1) and after (S1H(900)) thermal treatment in hydrogen. Figure taken from Imai *et al.*⁸⁹

One of the strongest evidences that Si–H can be a precursor for E' came from an experiment in which an oxygen-deficient sample was treated at high temperatures ($T > 600\text{ C}^\circ$) in a H_2 atmosphere. Upon thermal treatment, it was observed a reduction of the 7.6 eV absorption band due to the ODC(I) vacancies, accompanied by an increase of the concentration of Si–H groups, as evidenced by the growth of their typical Raman spectroscopic signal at 2250 cm^{-1} .⁸⁹ This observation suggests that the vacancies can be converted to Si–H groups by the following reaction:



Due to reaction (1.5), Si–H becomes the dominant defect species in the H_2 -treated substoichiometric material. Then, it was observed that glasses prepared by (1.5) are characterized by a much higher efficiency for E' generation (under 6.4 eV laser irradiation) than before H_2 treatment (Figure 1.8).⁸⁹ This experimental evidence in itself strongly suggests that Si–H groups can be efficient precursors for the E' . Two^k possible photo-induced reactions were put forward:⁸⁹

^kIt is worth noting that the two reactions (1.6) and (1.7) give rise in principle to two different varieties of E' . In



supposedly occurring by a two-photon process, on the basis of theoretical calculations that had predicted the lowest σ - σ^* electronic transition of the Si-H group to be at about 8 eV.¹⁰⁶

The issue of E' generation from Si-H is closely connected to the problem of *stability* vs *instability* of the paramagnetic center. In fact, as apparent from the above reactions, the rupture of Si-H precursors gives rise both to E' centers and hydrogen (atoms or molecules). Now, it is known that H₂ in silica is able to diffuse, even at room temperature, and spontaneously reacts with some paramagnetic point defects.^{38,39} Hence, if E' centers are generated from Si-H, we should expect that after the end of irradiation molecular hydrogen diffuses and recombines back with the defect restoring the Si-H bond by the *inverse* of reactions (1.6) and (1.7). Imai *et al.* confirmed this prediction by observing a partial post-irradiation decay of the induced E' taking place in a few hours at room temperature (Figure 1.9), as apparent from ESR measurements performed at several delays from the end of exposure. On the one hand, the observation of the anticipated decay further supports the proposal of Si-H groups as possible precursors of the E' center under laser radiation; on the other hand, however, we note that if one assumed E' to be generated *only* by the above reactions, the concentration of hydrogen produced together with E' should be sufficient to *completely* cancel the paramagnetic defects in the post-irradiation stage. Hence, the *partial* decay in Figure 1.9 indicates that, in the experimental conditions explored by Imai *et al.*, either a portion of hydrogen was involved in a reaction with another unknown defect, or that a second generation channel of E' was active besides Si-H breaking. Instability of point defects in α -SiO₂ due to reaction with mobile species is a much more general issue that extends beyond this particular case. Since the study of the reaction between E' and H₂ is a central topic for this work, these problems will be discussed in more detail in the next chapter.

The possibility that Si-H can be a precursor of E' (both under laser and ionizing radiation), at least in materials where its concentration is increased artificially by a thermal treatment in H₂, has been suggested in several other works.^{28,72,75,90,107} It is worth noting that, while in the H₂-treated samples used by Imai *et al.* Si-H should be present mainly in the form predicted by eq. (6.17), i.e. a hydrogen-decorated vacancy, in principle it is conceivable that Si-H may also exist simply as an isolated defect, depending from the manufacturing procedure of the material. Besides, Si-H can be found in couple with Si-OH if the two are formed together by reaction of H₂ with Si-O-Si during the high temperature manufacturing process of the silica specimen being used.^{40,108} Since these varieties of Si-H are not straightforwardly distinguishable by their IR or Raman spectroscopic features, it is not easy to know at the moment what is the prevalent arrangement of the Si-H groups in a given silica sample.

particular, the former may be very similar to the so-called E'_β center, introduced in section 1.1, while the latter is the usual *vacancy*- E' center.

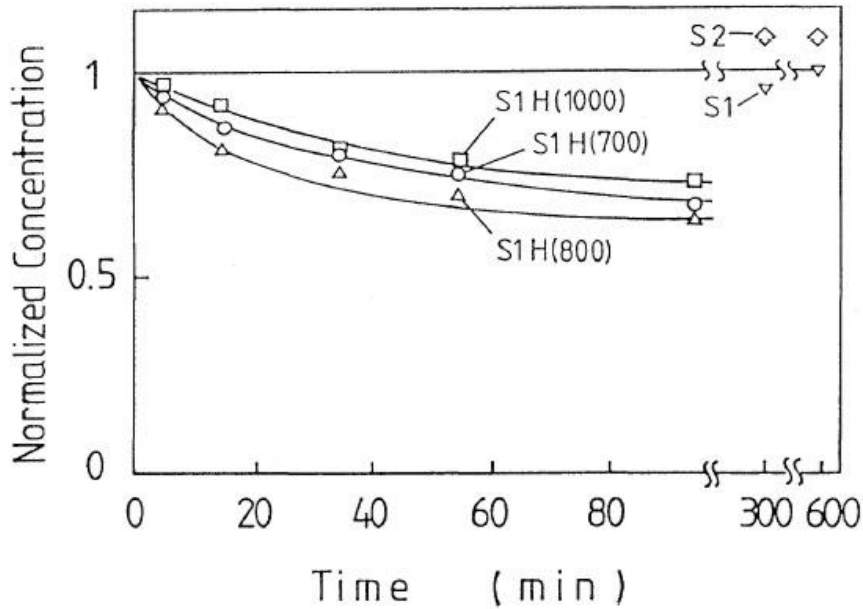


Figure 1.9: Decay of E' concentration after the end of laser irradiation in the sample containing ODC [S1] and a sample containing Si-H [S1H(900)], obtained by the high temperature treatment of [S1] in a H_2 atmosphere. Figure taken from Imai *et al.*⁸⁹

Neglecting for the moment this rather subtle point, we return now to the properties of the E' center created from Si-H, whose basic feature is that it is *unstable* and decays, due to recombination in the post-irradiation stage with free hydrogen coming from the same generation process. In this respect, the E' coming from Si-H is different from the E' generated by the previously described mechanisms, which is not reported to be unstable at room temperature.

Since the E' created by Si-H rupture is transient due to the very nature of its generation process, ordinary (*ex situ*) measurements, usually performed starting from a few minutes after the end of irradiation, are inappropriate to thoroughly investigate its properties and dynamics. In contrast, some papers proposed a more deep investigation of the *transient* E' induced by laser irradiation, by employing *in situ* optical absorption techniques.¹⁰⁹⁻¹¹⁵ *In situ* OA techniques are measurements of the induced OA spectrum or absorption coefficient at some fixed wavelength (for instance 215 nm, corresponding to the peak of the 5.8 eV absorption band of E' center) performed while the specimen is being exposed to laser light. Measures usually continue also after the end of laser irradiation, to investigate the post-irradiation kinetics of the defect. As opposed to *ex situ* measurements, the *in situ* techniques allow to investigate also the growth kinetics of the defects and to access the first stages of the decay, so that this approach is mandatory to obtain a satisfactory understanding of the generation of the transient E' coming from Si-H.¹ The diffusion of *in situ* techniques is relatively recent in literature: in particular, PL *in situ* measurements have been applied to study the laser-induced generation and decay of NBOHC by monitoring its emission at 1.9 eV,^{42,116,117} and OA *in*

¹Or in any other experimental situation in which the generated defects are unstable and decay in the post-irradiation stage.

in situ has been recently employed to study the kinetics of defect generation under ionizing radiation.¹¹⁸

One of the first *in situ* studies was performed by Leclerc *et al.*,^{109,110} first in bulk $a\text{-SiO}_2$ and later on optical fibers.¹¹¹ The authors examined the kinetics of E' under KrF 5.0 eV laser radiation in samples of high purity silica with high Si–OH content by *in situ* optical absorption. They found that the defects are almost completely transient and rapidly disappear after the end of irradiation (Figure 1.10). Such a relaxation was not observed in samples with a low Si–OH content.

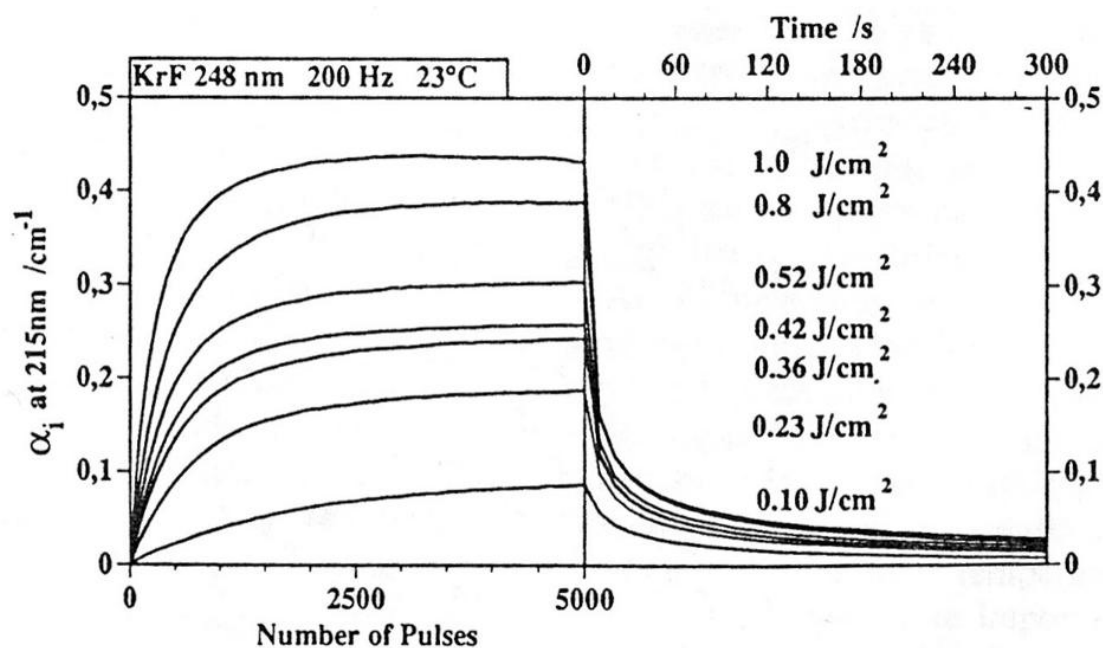


Figure 1.10: Induced absorption coefficient at 5.8eV in high OH fused silica during and after irradiation with KrF laser with several different energy densities per pulse. Figure taken from Leclerc *et al.*¹¹⁰

On the basis of the results, the authors put forward a model in which the E' center, which may be initially created from any precursor, is converted by the relaxation process to some unknown state $\overline{E'}$, spectroscopically invisible. Then, the $\overline{E'}$ can be reconverted very efficiently to E' by a successive irradiation. Based on the observed temperature dependence, they proposed that the relaxation is due to reaction with H_2 , and that the $\overline{E'}$ can actually be identified with the Si–H. From the study of the dependence of process on laser power, they concluded that generation of E' occurs by a single-photon process. It is worth noting that this finding is apparently at variance with the above reported theoretical predictions on the Si–H electronic transition; this issue is even more controversial because no experimental data are available at the moment on the UV absorption spectrum of Si–H. Finally, Leclerc *et al.* suggested on a qualitative basis that the saturation of E' concentration reached during laser exposure is due to an equilibrium between generation and decay.

Other studies by Shimbo *et al.*, dealing with transient E' generated by KrF and ArF laser radiation,^{112,115} examined in more detail the dependence on the Si–OH content, finding that the maximum induced absorption coefficient is inversely correlated to the native concentration of Si–OH. In contrast to Leclerc *et al.*, the power dependence of the transient E' generation rate was found to

be sublinear.

Finally, Smith *et al.* distinguished a fast and a slow decay of E' , respectively due to recombination with atomic and molecular hydrogen.¹¹⁴ Furthermore, their data showed that the decay of E' is observed only in samples that already contain dissolved hydrogen in *free* form (H_2) prior to irradiation. This conclusion contrasts with the original results by Imai *et al.* where the decay was observed even if hydrogen was initially stored entirely as Si–H or Si–OH bonds. Therefore, it is not clear whether in this case the E' centers were actually generated from Si–H. Finally, the results by Smith *et al.* suggested a linear single-photon E' generation process.

In summary, although the application of *in situ* measurement techniques to the laser-induced E' center has permitted several step forwards in the understanding of its transient dynamics, many issues are still debated due to the report of contradictory results. In particular, given that Si–H has been regarded as one of the main generation mechanism of transient E' centers, an important unclarified point is whether Si–H rupture occurs by a one- or a two-photon process. In addition, some questions have never been investigated, such as the detailed mathematical modeling of the growth kinetics^m.

1.2.3 Ge-related defects

From the technological point of view, Ge-doped a -SiO₂ has a very important application in the fabrication of optical fibers, where it is commonly used as the *core* material, surrounded by a pure silica *cladding*. In fact, Ge-doping increases the refractive index of silica thus permitting the guidance of light in this geometry by total refraction.³ The scientific interest for Ge-doped silica increased abruptly after the experimental demonstration by Hill *et al.* of the strong *photosensitivity* of this material.¹¹⁹ In this context, the term photosensitivity indicates the phenomenon by which exposure to laser irradiation induces a modification of the refractive index n .

In the original experimental scheme by Hill *et al.* (Figure 1.11), two interfering coherent high-intensity laser beams of the same wavelength λ_0 propagate within the fiber in opposite directions, creating a standing wave pattern. The exposure of the core material to laser radiation induces a variation in the refractive index, which is modulated according to the intensity pattern. The modulation of the refractive index may be regarded as a grating-like structure, so that the fiber then behaves like a filter; as a result, it reflects selectively at the entrance light signals with wavelength near λ_0 .¹¹⁹ Such a device is referred to as a *fiber bragg grating* (FBG) and results to be a very versatile tool, both in telecommunications, where it is used in multiplexing devices, and as a temperature or stress sensor.^{1–3, 120}

^mFor completeness we also recall that Si–Cl groups, sometimes abundant in synthetic silica depending on the manufacturing procedure, have been argued to be possible precursors of the defect by a radiation-induced breaking process similar to what occurs in the case of Si–H. In contrast, breaking of Si–F, another relatively common impurity in a -SiO₂, is generally considered much less likely under laser radiation due to the greater strength of the silicon-fluorine bond.^{28, 57, 72, 75, 107} Both Si–Cl and Si–F impurities in a -SiO₂ can be detected by Raman spectroscopy, sensitive to their stretching vibrational modes.

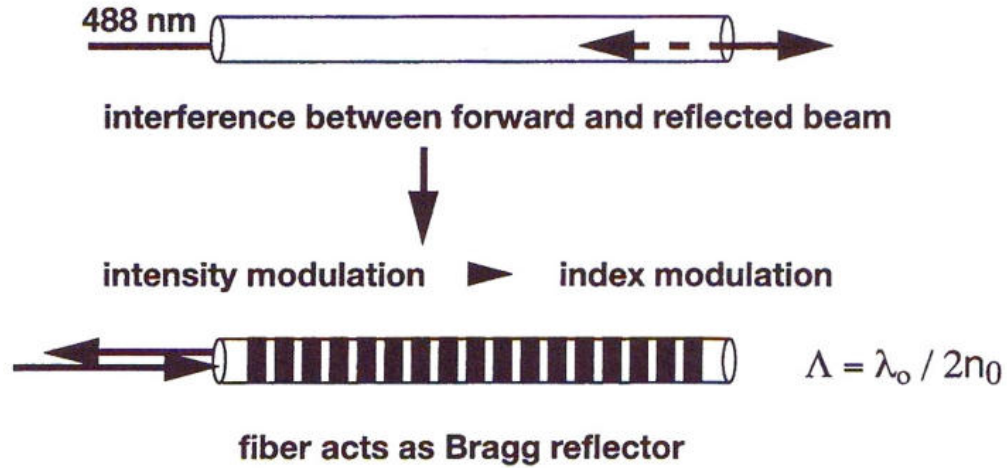


Figure 1.11: Inscription of a Fiber Bragg Grating in a Ge-doped core optical fiber. Figure adapted from Devine *et al.*²

More recent studies have demonstrated photosensitivity also in glasses with different chemical compositions, including pure silica under femtosecond laser radiation, but Ge-doped $a\text{-SiO}_2$ remains one of the most apt to technological purposes.^{45,46,121} It is thought that photosensitivity may be exploited to build low-cost advanced optical devices, as for example optical waveguides inscribed in the bulk of glass by focused laser irradiation,⁴⁵ or the recently demonstrated three-dimensional optical memories, namely devices where the "bit" is recorded as a localized modification of n , with achieved storage densities of $10^{12} - 10^{13}$ bits cm^{-3} .^{46,122}

Another very interesting optical property that can be induced in Ge-doped $a\text{-SiO}_2$ by particular procedures is optical nonlinearity. It was first observed by Osterberg and Margulis that prolonged exposure of an optical fiber to 1064 nm light from a Nd:YAG laser results in the generation of second harmonic light at 532 nm, with progressively increasing efficiency.^{123,124} This finding came as a great surprise, because it is widely known that glass, being a centrosymmetric material, has a zero second-order nonlinear coefficient.^{125,126} Obviously the induced nonlinearity must be due to the breaking of the native symmetry property of the material. In the following years, special techniques have been proposed, which are able to confer to Ge-doped silica an artificial nonlinearity comparable to that of crystalline materials commonly used in applications, e.g. LiNbO_3 . One of most effective is UV poling, consisting in laser UV irradiation under a strong electric field.^{13,127-129} From the technological point of view, the usability of glass as a nonlinear active medium would bear many advantages, such as the low cost and the straightforward integrability with other optical components.^{3,13,130}

Hence, the demonstration of these properties of Ge-doped $a\text{-SiO}_2$ led to a strong interest in understanding the microscopic mechanisms at the basis of photosensitivity and induced optical nonlinearity, with the aim to control and enhance these properties of the material. It was soon realized that photosensitivity is partly due to laser-induced conversion processes of Ge-related point defects, resulting in variations of the OA spectrum, which cause the modification of n through the Kramers-Kronig relationships. Beyond point defect conversions also other mechanisms, such as laser-induced

densification, are supposed to contribute to photosensitivity.^{1,3,59,131–133} Similarly, also optical non-linearity is linked to Ge-related point defects. In particular, it has been proposed that one of the action mechanisms of UV poling is ionization of Ge-related precursors followed by trapping of the produced electrons in a non-homogeneous spatial distribution, due to the presence of the electric poling field. This charge redistribution implies the breaking of the symmetry of the material so as to allow for second order nonlinearity.^{13,129}

A. Defect models

On these grounds, many studies have tried to shed light on the problem of Ge-related defects in silica. Germanium may be arranged within a -SiO₂ in many different configurations, each of which constitutes a specific point defect. Since Ge and Si are isoelectronic elements, it is qualitatively expected that many Ge-related point defects are structurally identical to Si-related centers apart from the substitution of Si with Ge. Actually, some exceptions are known to this simple scheme. Research aims to clarify two main issues: to associate the observed spectroscopic signals to specific structural models, and to elucidate the photochemical processes induced by irradiation, which usually convert diamagnetic precursors into paramagnetic defects. The two problems are clearly connected, because important clues to identify the structure of diamagnetic defects often come from the observation of their conversion processes.^{1,3,134} As outlined hereafter, the picture that has emerged from these studies is quite complicated and still leaves many open questions.

Ge-containing silica samples usually present a native absorption band peaked at ~ 5.1 eV (often referred to as B_{2 β} band¹³⁵) prior to any irradiation. This signal has been connected with Germanium oxygen deficient centers (GeODCs) and it has been suggested to play a key role in the point defect conversion processes at the basis of photosensitivity and nonlinear effects. In fact, in experiments with excimer laser or UV lamp radiation, an intensity reduction (*bleaching*) of the native ~ 5.1 eV OA band has been repeatedly observed, associated to the growth of several paramagnetic signals and of new absorption signals (see an example in Figure 1.12). This observation clearly suggests that the defect(s) responsible for the B_{2 β} band are converted by UV radiation to other centers.^{134,136–141}

The most common Ge-related paramagnetic defects that are detected by ESR in irradiated Ge-doped a -SiO₂ are the **Ge–E'** center, the Germanium Electron Centers (GECs) **Ge(1)** and **Ge(2)** and the **H(II)** center. The microscopic structures of three of them, Ge–E', Ge(1) and H(II), have been unambiguously identified by ESR studies, further supported by theoretical calculations, and are now widely accepted. The Ge–E', which is observed also in pure GeO₂, is structurally identical to the E' apart from substitution of Si with Ge ($\equiv \text{Ge}^\bullet$).^{142–146} An absorption band at 6.2 eV–6.4 eV has been attributed to this center,^{134,147–149} which is considered the most important in causing the refractive index variation in FBGs.^{150,151} The Ge(1) consists in an electron trapped at the site of a substitutional 4-fold coordinated Ge precursor (GeO₄^{•-}).^{134,145,152–154} A wide absorption band peaked at 4.4 eV–4.6 eV has been correlated with this defect.^{134,147,153} Finally, the H(II) center consists in a Ge atom bonded to two oxygens and one hydrogen, and hosting an unpaired electron ($=\text{Ge}^\bullet-\text{H}$).^{93,96,98,155} No detailed information is available on the absorption properties of the H(II)

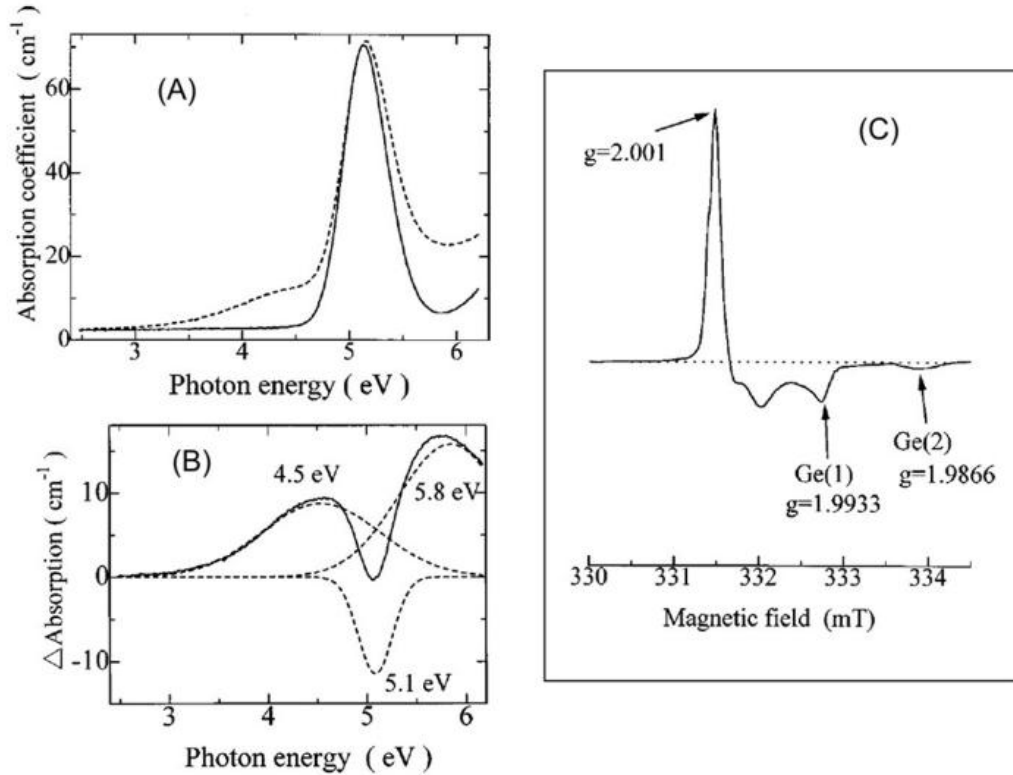


Figure 1.12: Panel (A): native OA spectrum of a Ge-doped silica sample (full line) and spectrum after irradiation (dashed line). Panel (B): difference OA, showing the bleaching of the 5.1 eV band and the growth of two components at 4.5 eV and 5.8 eV. Panel (C): ESR signal of the irradiated sample, resulting from the superposition of components due to three Ge-related defects. Figure adapted from Fujimaki *et al.*¹³⁹

centers, although they have been proposed to feature an emission at 1.83 eV, excited by energy transfer from a nearby GeODC center.¹⁵⁶

In regard to the Ge(2), this is the paramagnetic Ge-related center whose structural model is most controversial at the moment. Indeed, it was initially considered as a variant of the Ge(1), i.e. an electron trapped at the site of a GeO₄ unit, but differing from Ge(1) for the number of Ge nearest neighbors ions; besides, it was put in relationship with an absorption at 5.8 eV.^{138, 152–154, 157} However, subsequent studies suggested that Ge(2) can be annihilated by capturing an electron released by a donor ion,^{134, 147} or that it can be created by ionization of preexisting twofold coordinated Ge centers.^{139, 158} On this basis, the alternative model of a ionized twofold coordinated Ge (=Ge[•]) was proposed. Also the attribution of the OA has been criticized, as some authors have proposed the 5.8 eV (in addition to the above mentioned 4.4 eV) band to be related to Ge(1) rather than to Ge(2),^{139, 149} and recent theoretical and experimental investigations, some of which based upon Optically Detected Magnetic Resonance (ODMR) spectroscopy, have suggested that the absorption at 5.8 eV may be due to a Ge-related diamagnetic center, thus being unrelated to the Ge(2).^{159–162}

Also the structural model of the diamagnetic oxygen-deficient precursor responsible of the

~ 5.1 eV band very common in as-grown Ge-doped silica has been debated, similarly to what we have seen for the Si-related ODCs, ODC(I) and ODC(II), introduced in subsection 1.2.2-B. In detail, two defects have been proposed to contribute to the Ge-related ~ 5.1 eV band: the Germanium Lone Pair Center (**GLPC**) and the Neutral Oxygen Vacancy (**NOV**).

GLPC: Exciting in the 5.1 eV band two luminescence bands, peaked at 3.1–3.2 eV and 4.2–4.3 eV, are detected (Figure 1.13).^{93,164–166} The linear correlation between the three optical bands found in a large number of samples, strongly suggests to ascribe them to a single defect. The overall optical activity was attributed to a twofold coordinated Ge structure ($=\text{Ge}^{\bullet\bullet}$), also known as GLPC or GeODC(II),^{93,164–166} which has the same chemical structure of the intrinsic ODC(II), apart from substitution of the silicon atom with the isoelectronic Ge. The GLPC model is based on two main

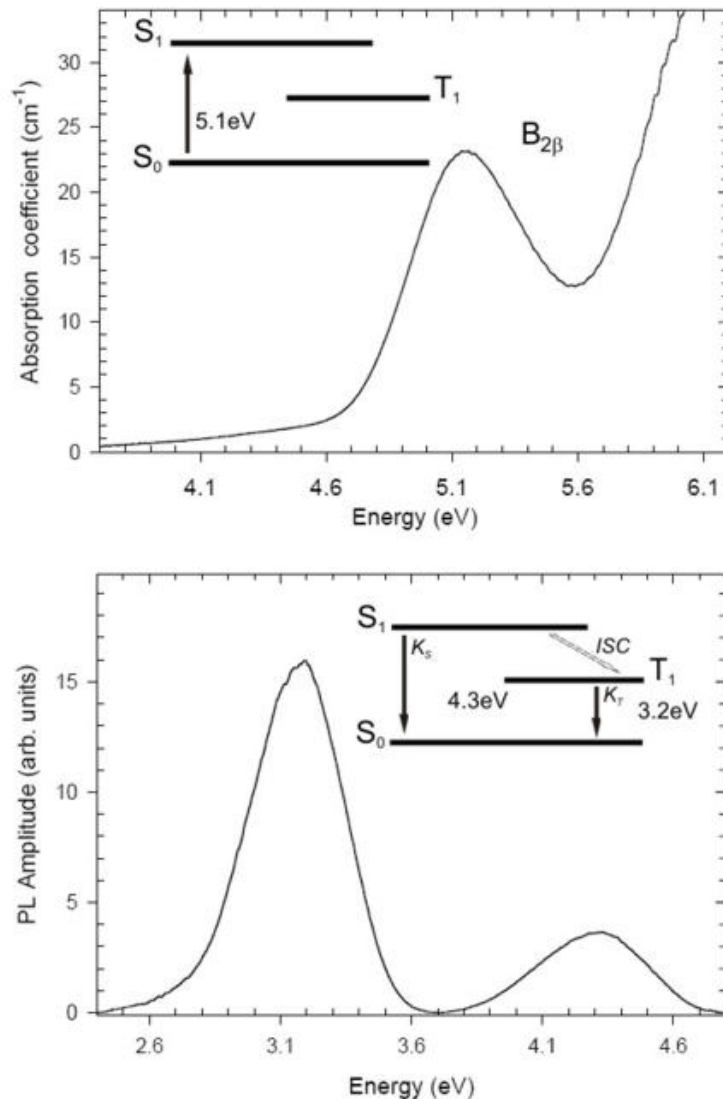


Figure 1.13: Panel (A): $B_{2\beta}$ OA band as measured in a Ge-doped silica sample. Panel (B): emission bands at 3.2 eV (triplet) and 4.3 eV (singlet) detected under excitation at 5.0 eV. In both panels: graphical representation of the electronic levels and transitions responsible for the optical activity. Figure adapted from Cannizzo.¹⁶³

evidences: (i) the symmetry properties of the center, deduced by PL polarization data, suggest the defect to be in a twofold coordinated configuration,^{93,166} and (ii) the observed conversion (eq. 1.8) by hydrogenⁿ trapping into H(II):^{12,98,167}



which strongly suggests the GLPC model thanks to the unambiguous knowledge of the structure of the H(II) center obtained by ESR. This is an example of how the structural information available on a paramagnetic defect (H(II)) can be an indirect, though powerful, means of inferring the structure of its diamagnetic precursor (GLPC). Finally, the twofold coordinated model has been also confirmed by computational works.^{155,168}

From the detailed experimental and theoretical study of the optical properties of the GLPC, it has been also clarified the scheme of its electronic levels and transitions (see Figure 1.13),^{3,93,155,163,164} which we briefly describe here as the spectroscopic signals of the GLPC will be reported among the results. The optical absorption band at 5.1 eV is associated to the promotion of the defect from the ground singlet state S₀ to an excited singlet state S₁. From the spectroscopic point of view, the OA is reported to peak at 5.13–5.16 eV with a 0.45–0.48 eV FWHM.^{3,93,136,163,164} From S₁ the center can either go back to S₀ by the radiative decay channel k_S , giving rise to the 4.2–4.3 eV (singlet) band, or undergo a non radiative transition (known as intersystem crossing, or ISC) to the excited triplet state T₁. From T₁, the defect decays radiatively to the ground state (channel k_T), emitting in the 3.1–3.2 eV (triplet) band^o. In this context, it is worth noting that the intrinsic Si-related ODC(II) defect features a very similar level scheme, mainly differing for the values of the transition energies and of the decay rates.^{3,93,155,163,164}

Although the optical activity pattern of the GLPC has been confirmed by several experimental investigations, it is not universally accepted at the moment. In fact, some authors have recently pointed out a lack of correlation between the 5.1 eV absorption and the two luminescence bands,¹⁶⁹ or between the two luminescence bands,¹⁷⁰ under irradiation, thereby concluding that the three signals cannot be attributed to a single center.

NOV: On the other hand, it has been proposed that another variety of oxygen-deficient Ge-related defect besides GLPC contributes to the absorption at ~ 5.1 eV, but *not* to the two luminescence signals: the Neutral Ge-related Oxygen Vacancy (NOV) ($=Ge-Ge=$ or $=Ge-Si=$).¹³⁶ The main evidence of this model comes from the observation under exposure to UV *lamp* of the bleaching of an OA band peaked at 5.06 eV with 0.38 eV FWHM (compare with the above reported parameters of GLPC absorption), not accompanied by any reduction of the singlet and triplet luminescence bands, but correlated to the growth of an ESR signal due to the Ge- E' center. This observation suggests that the defect responsible for this 5.06 eV component can be ionized to give the Ge- E' center. Based on

ⁿA diffusing hydrogen *atom* is often indicated in the specialized literature by H⁰, so as to emphasize its charge neutrality and distinguish it from the H⁺ (proton) and H⁻ ions. Since this distinction is not necessary here, throughout this Thesis we are going to use simply the symbol "H".

^oThe level scheme of the center includes another excited singlet state S₂ (not included in Figure 1.13), which can be excited at ~ 7.4 eV, and from which a similar decay pattern is observed.^{163,164}

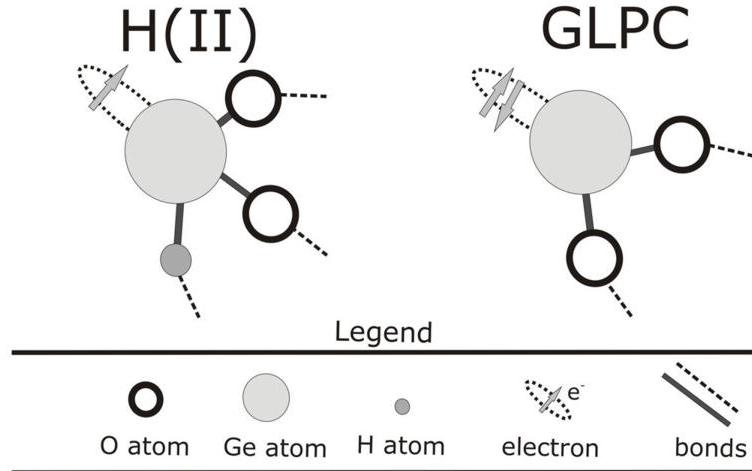


Figure 1.14: Schematic representation of the structure of the GLPC and H(II) centers in $a\text{-SiO}_2$. We stress that in the H(II) center, a (not represented) significant portion of the wave function of the unpaired electron is localized on the hydrogen atom, thus giving rise to an hyperfine interaction between the electron and proton spins.

the structure of the $\text{Ge}-E'$, the simplest hypothesis is that such defect consists in a Ge-related oxygen vacancy, the ionization of which generates the $\text{Ge}-E'$ just as the ionization of an ordinary vacancy can generate E' (process 1.4). Ionization of the Ge-related vacancy is believed to occur by a single-photon process, because an UV lamp is incapable of efficiently inducing multi-photon processes due to its low intensity.¹³⁶ The NOV model has been recently confirmed by theoretical calculations;¹⁴⁶ nonetheless, adding more complexity to the problem, other simulations have suggested that, aside from the NOV, also the GLPC can be converted to $\text{Ge}-E'$ by a photochemical laser-induced reaction.¹⁶⁰

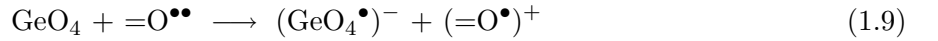
Although the issue of the GeODC remains open at the moment, based upon the available experimental evidences it is likely that both GLPC and NOV exists and contribute to the native ~ 5.1 eV absorption of native Ge-doped $a\text{-SiO}_2$, while only the GLPC is responsible for the luminescence activity. Finally, apart from twofold (GLPC) and threefold (NOV) coordinated configurations, it is generally accepted that Ge can be incorporated in $a\text{-SiO}_2$ also as substitutional four-fold coordinated Ge or as Ge nanoclusters.^{136,171,172} Given the Ge-doping level, the prevalent arrangement of Ge in the as-grown sample is expected to determine the effects of irradiation, and in particular the paramagnetic defects appearing as a consequence of laser exposure. Nevertheless, the pattern by which the population of Ge impurities in the as-grown material distributes itself among the several possible configurations, seems to strongly depend on the details of the manufacturing procedure, in a way which is not fully clarified.^{136,171,172} As we are going to see in the following, among the several possible Ge-related defects in $a\text{-SiO}_2$, GLPC and H(II) play a particularly important role in this work: in fact, GLPC happens to be the prevalent arrangement of Ge in our samples prior to any treatment, while the generation of H(II) after irradiation by reaction (1.8) will indicate the presence of diffusing hydrogen in the material. The structure of these two defects is represented in Figure 1.14.

B. Conversion processes

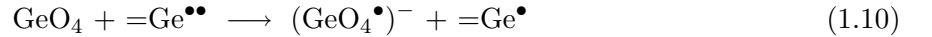
These controversies about the structural models of some Ge-related defects correspond to a parallel debate about the defect conversions triggered by UV lamp or by excimer laser radiation.

We have already discussed the ionization of the NOV towards a Ge- E' center occurring by absorption of (single) $\sim 5\text{eV}$ photons from an UV lamp.¹³⁶ In successive studies the action mechanism of laser radiation was investigated,^{138, 139, 157, 173–175} resulting in the proposal of two main models of laser-induced processes in Ge-doped silica.

A first group of works,^{138, 157, 173} suggested that the primary process triggered by laser radiation on Ge-related defects is the following: two-photon band to band excitation results in pair generation of Self-Trapped *Holes*, (STH),^P whose structure is $(=\text{O}^\bullet)^+$, and GECs (i.e. Ge(1) and Ge(2) centers), here modeled as electrons captured by a GeO₄ unit $(\text{GeO}_4^\bullet)^-$:



The efficiency of the band to band excitation process was reported to be much higher than in pure silica, partly because Germanium doping decreases the bandgap. Reaction (1.9) was proposed on the basis of the correlated growth of the ESR signals of STH and GECs. However, this model leaves aside the GLPC center, being unable to explain the reduction of its PL signal which is also observed upon laser irradiation. Hence, in other studies,^{139, 174, 175} a different model able to explain the role of the GLPC was suggested, based on the picture in which the Ge(2) center corresponds to an ionized GLPC. Within this alternative scheme, Ge(1) $(\text{GeO}_4^\bullet)^-$ and Ge(2) $(=\text{Ge}^\bullet)$ are generated together by two-photon ionization of pre-existing twofold coordinated Ge and subsequent electron trapping at GeO₄ sites (eq. 1.10):



It is worth noting, however, that reactions (1.10) and (1.9) are not incompatible in principle, provided that we identify the $(\text{GeO}_4^\bullet)^-$ at the right side of (1.9) with the Ge(1) center and the $=\text{Ge}^\bullet$ at the right side of (1.10) with the Ge(2) center.

Finally, it has been pointed out that the presence of *hydrogen* can strongly influence Ge-related processes.^{1, 134, 150, 151, 175–179} In particular, loading of Ge-doped core optical fibers with H₂ is known to increase photosensitivity of the material, so that it has become a standard technique used to produce fibers suitable to manufacture FBGs.^{1, 134, 176} From the microscopic point of view, it was found that the presence of H₂ strongly enhances the generation of Ge- E' ,^{150, 151, 175, 177, 178} which could explain the increasing photosensitivity, assuming that the variations of the refractive index are due to the growth of the Ge- E' absorption band. According to a model proposed by Awazu *et al.*,¹⁵⁰ the enhancement of Ge- E' creation in the presence of H₂ may be due to the formation of Ge-H bonds, which then act as efficient precursors for the paramagnetic center. Nonetheless, the question is still open since it is unclear how Ge-H can be efficiently formed upon H₂ treatment at *room temperature*,^{176, 180} and it appears strange that the Ge- E' center features interaction properties

^PThe STH in α -SiO₂ is a hole that gets spontaneously trapped at the site of a bridging oxygen $(=\text{O}^{\bullet\bullet})$. It is visible by ESR spectroscopy^{1, 138}

with hydrogen so different from the usual Si-related E' , which is known to be *passivated*, and not enhanced, by the mobile species (as discussed in detail in the next chapter). Aside from the generation of Ge- E' , the presence of hydrogen is reported to influence also other Ge-related processes: in particular, it has been reported that in H₂-loaded fibers or bulk samples, no Ge(2) centers are observed after laser exposure, whereas H(II) is detected in much higher concentration than in the unloaded materials.^{175,177} This observation suggests that Ge(2) can be passivated by reaction with hydrogen, forming a hypothetical defect (=Ge-H)⁺ that can be easily converted into H(II) by electron trapping.¹⁷⁵ At the moment, further studies are needed to thoroughly elucidate the interaction between hydrogen and laser-induced conversion processes of Ge-related defects.

Chapter 2

Diffusion and reaction of mobile species in $a\text{-SiO}_2$

The results presented in this Thesis deal with the generation and decay kinetics of point defects induced in silica by UV laser irradiation. As anticipated, we are going to show that these effects are strongly conditioned by diffusion and reaction of mobile hydrogen in the material. Hence, in this chapter we provide a general background on diffusion- and hydrogen-related effects in amorphous silica, in order to better contextualize our work with respect to the available literature on related subjects.

2.1 Post-irradiation kinetics and annealing of radiation-induced defects

In some experiments it is found that the point defects induced by irradiation at a temperature T_i are unstable after the end of exposure, and their concentration continues to vary with time even after removal of the sample from (or switching off) the irradiation source. These processes are referred to as *post-irradiation kinetics*: their most usual consequence is a spontaneous decay of the generated defects after that the irradiation is interrupted. Depending on the experimental conditions, the decay can be partial or complete and its typical time scale may vary from seconds to years, after which the defects reach stationary concentrations.^{1, 2, 7, 39, 89, 110, 114, 181–186} More in general, the concentration of a specific defect can *grow*, rather than decay, in the post-irradiation stage, and the observed effects can involve also centers that pre-existed in the material before irradiation. We have already seen some examples of post-irradiation kinetics in Figure 1.9 and Figure 1.10. Similar effects have also been observed and studied in irradiated optical fibers, where they result in a partial recovery after the end of exposure of the transparency lost due to the formation of point defects. (Figure 2.1).^{182, 183, 186}

After that the defects generated by irradiation at the temperature T_i have reached their sta-

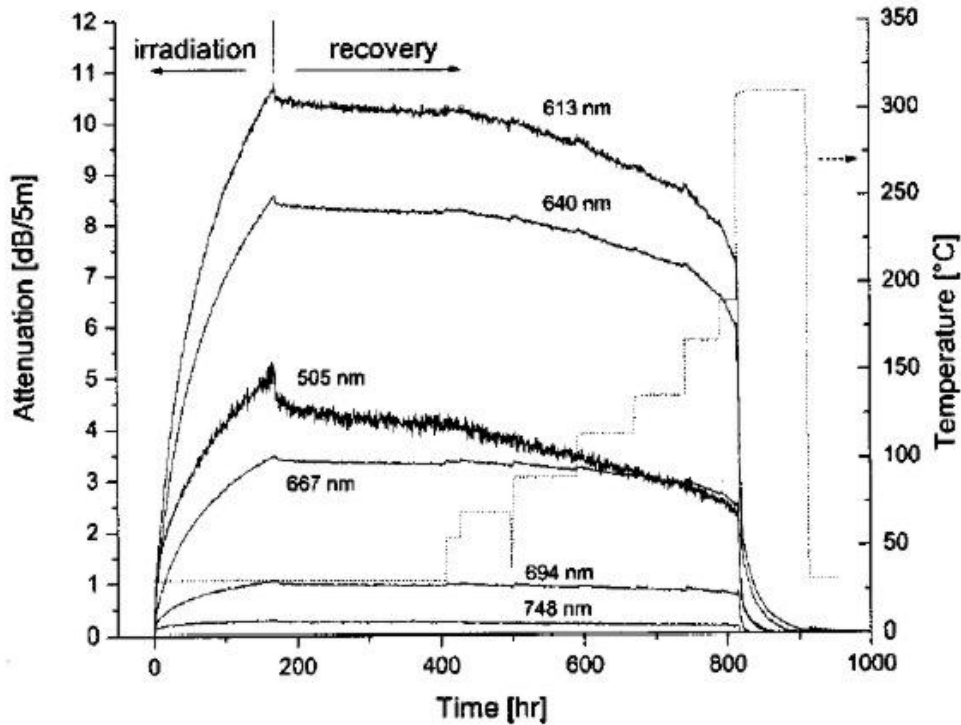


Figure 2.1: Growth and recovery of the attenuation at several wavelengths, as observed during and after γ irradiation at room temperature of an optical fiber. After a few days, the specimen is thermal treated up to ~ 600 K (following the sequence represented by the dotted line) to completely anneal the residual induced absorption. Figure taken from Borgermans *et al.*¹⁸⁶

tionary concentrations, it is commonly observed that they become again unstable if the specimen is heated at temperatures higher than a given threshold $T_d > T_i$. Hence, upon such a *thermal treatment* one observes some of the radiation-induced defects to disappear by conversion in other centers, the conversion processes strongly depending on the temperature range, on the sample and on the irradiation conditions.^a Nevertheless, a general rule of thumb is that the *paramagnetic* centers appeared as a consequence of irradiation disappear, or are *annealed*, when a sufficiently high temperature is reached, as shown for example in Figure 2.2. A thermal treatment can be a useful method to "cancel" the effects of irradiation.^{1,2,7,181} While a complete erasure of the induced defects is always possible, a thermal treatment sometimes allows a selective cancelation of radiation damage by a proper choice of a (not too high) temperature T_d . From another point of view, thermal treatments are a common means to investigate the stability of the induced point defects as a function of temperature so as to indirectly infer information on their properties.^b

^aAlso by a thermal treatment, in general the defects can either grow or decrease in concentration, and the observed effects can involve also centers that pre-existed in the material before irradiation.

^bThermal treatments can be distinguished in two categories. Given a base temperature T_b (typically coinciding with T_i), and a time interval Δt , an *isochronous* treatment consists in a sequence of cycles in each of which the sample is kept at some $T_d > T_b$ for a Δt , and then brought back to T_b to perform measurements. After that, the procedure is repeated at a higher T but using the same Δt , so that the process can be followed as a function of temperature. The other possibility is an *isothermal* treatment, in which both T_d and Δt are the same for all the cycles, so as to study

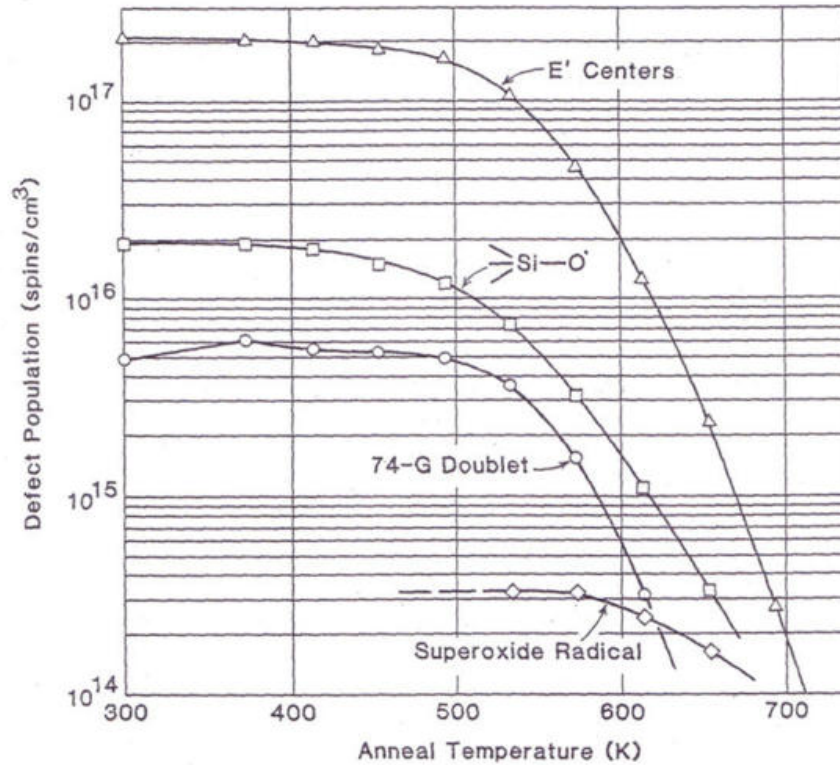


Figure 2.2: Concentration variations of E' , NBOHC ($\equiv\text{Si}-\text{O}^\bullet$), H(I) centers (referred to as 74 G doublet) and peroxy radicals ($\equiv\text{Si}-\text{O}-\text{O}^\bullet$, referred to as Superoxide Radical) observed during an isochronous thermal treatment performed up to 700 K. In this case, the defects had been induced in the sample by γ irradiation at room temperature, and their decay after heating the specimen is due to reactions with diffusing water of radiolytic origin. Figure taken from Griscom.¹⁸⁷

Although the occurrence of post-irradiation kinetics and annealing effects has been known for a long time, its influence on the concentration of defects induced by irradiation has been in some sense underestimated in literature. Indeed, most works on point defect generation in $a\text{-SiO}_2$ have investigated only the stationary concentrations of induced centers, measured after the conclusion of the post-irradiation kinetics, or have simply not discussed the possible influence of the post-irradiation effects. In contrast, it is worth pointing out that only the observation of the complete growth and decay kinetics of the defects can give detailed information on their dynamics and properties. In particular, the stationary concentrations generally represent only the net result of generation and annealing at the temperature T_i .

Several physical processes may in principle contribute to the annealing of defects. Historically, the basic mechanism was first believed to be the recombination of electron-hole pairs produced by irradiation. Nonetheless, successive studies led to recognize that the prevalent process is often the diffusion and reaction in $a\text{-SiO}_2$ of small chemical species like hydrogen, oxygen, or water, which are able to react with point defects thus resulting in their conversion in other centers. Nowadays, the idea that several molecules are able to diffuse in $a\text{-SiO}_2$ in a wide temperature range and react

the process as a function of time.

with defects is widely accepted and supported by a large set of experimental data.^{1,2,7,38,181,187} Consistently with this interpretation, it is usually found that the annealing temperature of a given point defect strongly depends on the history of the specific sample being used, which is thought to determine the nature and the concentration of the diffusing agents that cause the disappearance of the center. Often, the reaction with a diffusing chemical species converts an optically active defect to another center that is "invisible" for what concerns optical absorption in a range of technological interest: in this case, the reaction is usually referred to as the *passivation* of the defect.

Since diffusion in a solid is a thermally activated process (see next section), each mobile species is characterized by a typical minimum temperature that must be reached to activate its migration through the silica matrix. Hence, the temperature determines the possible chemical species that, if present in sufficient concentration, can influence the effects of irradiation by reacting with point defects. In general, the diffusing species may be either already present in the $a\text{-SiO}_2$ matrix before irradiation, depending on the manufacturing procedure of the material, or they can be made available in the sample as a consequence of the irradiation itself, typically by a radiolysis process. Another important general rule is that paramagnetic defects, due to the presence of an unpaired electron, are much more reactive than diamagnetic defects, so that they are more easily passivated by reaction with hydrogen, oxygen or water.^{1,2,7,38,181,187}

Diffusion-related effects in $a\text{-SiO}_2$ are a very lively research topic; indeed, also in recent times many experimental and computational works continue to investigate the diffusion mechanisms of several mobile species in silica and their interactions with the matrix and with point defects.^{42,188–193} In this context, *hydrogen* assumes a particular importance because it is the most reactive among the chemical species that efficiently diffuse in silica already at room temperature or below.^{38,40,42,185} Furthermore, hydrogen is the most common impurity in silica, virtually present in every variety of the material. In the next section we give a general background of diffusion processes in silica and diffusion-limited reactions, after which we proceed to describe the main experimental results concerning the reactivity of point defects in $a\text{-SiO}_2$ with hydrogen.

2.2 Diffusion in silica

By definition, diffusion is the motion of a chemical species driven by a gradient of chemical potential, which in the simplest case arises from a concentration gradient.^{108,194} It is often a good approximation to suppose the flux density \vec{J} of the chemical species to be linearly proportional to the spatial gradient of its concentration ρ :

$$\vec{J} = -D\nabla\rho \quad (2.1)$$

Eq. (2.1) is called the first Fick law, and defines a proportionality constant D called the *diffusion constant*. Diffusion can be regarded as the continuum limit of the well-known problem of random walk in a lattice. The mathematical problem of diffusion can be treated by adding to the Fick law the continuity equation and setting appropriate boundary conditions. Without entering in the detail of the solutions, it is useful for the present purposes to introduce another quantity of interest: the

mean diffusion length L_d , which represents the mean distance covered by a diffusing molecule in a given time interval t . In a three-dimensional geometry, L_d is given by $L_d = \sqrt{6Dt}$.^{108,194,195}

Diffusion in solids is a complex problem discussed in many experimental and theoretical works. Both the detailed understanding of the microscopic mechanisms at the basis of diffusion and the measure of the diffusion coefficients are still open problems in some systems, among which the amorphous solids. In general, the principal and simplest microscopic diffusion mechanisms in a solid are two: *vacancy* diffusion and *interstitial* diffusion. In vacancy diffusion, the elementary process at the basis of the macroscopic transport of matter is the jump of an atom to a neighboring vacancy of the lattice^c. This mechanism is very important for substitutional impurities in metals and alloys and is active also in ionic solids.^{108,196} In the alternative scheme, *interstitial* diffusion, small molecules of a given chemical species are dissolved in the solid by being incorporated in interstitial positions, and diffuse by jumping to one of the nearest-neighbor solubility sites.^{108,196} This mechanism is dominant in many covalent solids, such as α -SiO₂, which have relatively open structures, so as to allow for an easy dissolution of sufficiently small molecules in interstitial positions, and where the energy to break bonds is large, so that vacancy formation is unfavorable.^{108,196}

In the study of diffusion, apart from the interest connected to the present work, silica glass is particularly important as it is the only solid for which extensive measurements for many atoms and molecules in a wide temperature range have been performed.^{108,196} From the microscopic point of view, the motion of a molecule from an interstitial site to the neighboring one in the solid requires to overcome a potential barrier due to the necessary rearrangement of the closest atoms; hence, diffusion is an *activated* process, and the macroscopic diffusion coefficient usually depends on temperature according to an *Arrhenius equation*:

$$D = D_0 \exp\left(-\frac{E_a}{k_B T}\right) \quad (2.2)$$

where D_0 is called the pre-exponential factor, k_B is the Boltzmann constant, T is the absolute temperature and E_a is the activation energy for the process. From an experimental point of view, the parameters E_a and D_0 can be determined by a simple linear fit after reporting the diffusion coefficient measured at several temperatures in a so-called *Arrhenius plot* ($\log D$ vs $1/T$). Indeed, in such a graph eq. (2.2) corresponds to a straight line (see for example Figure 2.3).

Physically, the value of E_a (typically a fraction of 1 eV) may be interpreted as an estimate of the potential barrier that separates neighboring interstitial sites. It has been pointed out that for a given solid, E_a is closely connected to the dimensions^d of the diffusing species, being lowest for atoms

^cVacancies are always present even in a "perfect" lattice, as inferred by simple thermodynamic considerations⁵⁹

^dIn the simplest treatment of the problem of interstitial diffusion in a solid, the mobile atom or molecule is regarded for simplicity as a not deformable object characterized by a size d . d is assumed to be unaffected by the insertion of the molecule in the solid; therefore, it is usually estimated from the kinetic theory of gases starting from measurements of the viscosity of the mobile specie in gaseous form outside the solid.¹⁰⁸ It was found that the functional dependence between E_a and d in α -SiO₂ is remarkably well reproduced by the equation: $E_a = \alpha(d - d_0)^2$, where α and $d_0 = 0.38 \text{ \AA}$ are constants. This finding can be interpreted by the following very simple argument: one imagines that the mobile species dissolves within the solid in interstices connected by doorways of average radius d_0 : then, E_a is proportional to the elastic energy required to dilate such doorways from d_0 to d , so as to allow the jump of the diffuser from one interstice to a neighboring one.¹⁰⁸

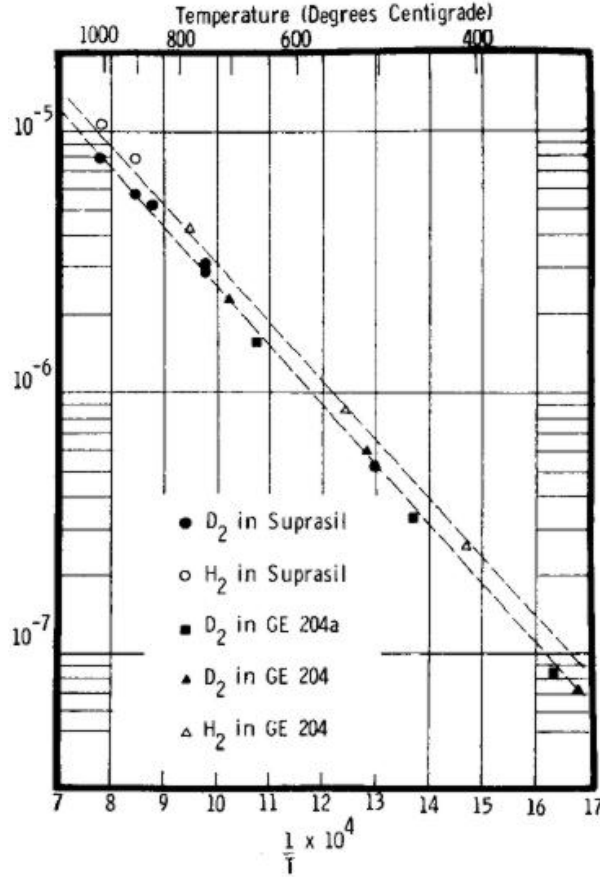


Figure 2.3: Arrhenius plot of the diffusion coefficient of molecular hydrogen and deuterium measured in several types of silica samples. The straight lines correspond to Arrhenius temperature dependences, eq. (2.2). Figure adapted from Lee.¹⁹⁷

or small molecules like H_2 . For what concerns silica, its microscopic structure is relatively porous, meaning that the fraction of space occupied by the Si and O ions and by their electronic clouds is lower than in many other solids. For this reason, the measured values of E_a are usually lower than in other insulators.¹⁰⁸ The pre-exponential factor D_0 can be connected to the entropy of activation for diffusion and the vibrational frequency of the molecule inside each interstitial position.^{108,196} Its typical order of magnitude in α -SiO₂ is $10^{-4} \text{ cm}^2\text{s}^{-1}$. Up to this point, we have described diffusion in α -SiO₂ as the thermally activated motion of a chemical species described by the simple eqs. (2.1) and (2.2). Actually, there are at least two additional complications that must be taken into account for a thorough description of this process.

Reaction with the matrix: When the temperature is increased above a certain limit, which may depend on the experimental conditions, the solid cannot be more regarded as a passive lattice within which the migration of the mobile species takes place. For example, at $T < 700 \text{ K}$ H_2 diffuses with essentially no chemical interaction with the silica matrix, but at increasing temperatures the picture gets more complicated because of the occurrence of chemical reactions of H_2 with the glass, the most

basic being the reaction of H_2 with Si-O-Si groups.^e At even higher temperatures, one must take into account also the spontaneous decomposition of preexisting Si-OH groups, which makes available additional hydrogen.^{37, 38, 108, 197–200} When measuring the diffusion coefficient D , these processes influence the estimated values, so that one has to introduce an *effective* diffusion coefficient D_e . The actual D can still be estimated from D_e by more or less complex treatments, as thoroughly discussed in specialized texts.¹⁰⁸ Such diffusion-reaction kinetics are particularly important for water, which significantly reacts with the lattice in most of the temperature range in which it is mobile.^{3, 108} Due to these effects, the values of D for H_2O in $\alpha\text{-SiO}_2$ reported in literature appear to be very variable according to the experimental conditions.^{108, 201} For what concerns the present work, the main mobile species we are interested with is H_2 . From this point of view, we stress that the temperature of our experiments ($<500\text{ K}$) was in any case low enough to neglect the influence of any reaction with the matrix on the diffusion process.

Non-Arrhenius behavior: The diffusion constant is usually measured by experiments founded on the controlled permeation of a gas through a membrane at several temperatures^f. When the measurements are carried out on a sufficiently extensive temperature range, often it is evidenced that the experimental data present small deviations from a precise Arrhenius behavior, eq. (2.2). In particular, it is often observed that the slope in an Arrhenius plot tends to increase with temperature. In silica, this has been experimentally evidenced in a clear way at least for helium and neon.^{38, 108, 204–206} More in general, slightly different values of the diffusion parameters of a given species are often obtained by fitting with eq. (2.2) data collected in different temperature ranges. For example, for He it was reported by Swets *et al.* that $D_0=3.0\times 10^{-4}\text{ cm}^2\text{ s}^{-1}$ and $E_a=0.24\text{ eV}$ for $300\text{ K}<T<600\text{ K}$ while $D_0=7.4\times 10^{-4}\text{ cm}^2\text{ s}^{-1}$ and $E_a=0.29\text{ eV}$ for $600\text{ K}<T<1300\text{ K}$.²⁰⁴ The observed deviations from a purely Arrhenius behavior are usually interpreted by theoretical arguments suggesting that D_0 should be proportional either to T or to \sqrt{T} ,^{37, 108} namely the pre-exponential "constant" actually depends on temperature.

Nevertheless, in regard to silica, Shelby and Keeton proposed another interpretation, which appears to be closer to our qualitative understanding of the properties of amorphous solids. In fact, to explain the increase with temperature of the pre-exponential factor for diffusion of He in $\alpha\text{-SiO}_2$, they hypothesized that in the amorphous matrix the activation energy must be regarded as a randomized parameter, which statistically fluctuates from site to site following a Gaussian distribution centered on some value ϵ and with a width (standard deviation) σ . Qualitatively, it can be argued that the local diffusivity in the glass is necessarily nonuniform because the moving species traverse interstitial voids of various shapes and sizes.^{38, 42, 185, 189, 206} Hence, following Shelby and Keeton, the value of D measured by the classical experiment based on permeation through a membrane must be actually

^eNamely the reaction $\text{Si-O-Si} + \text{H}_2 \implies \text{Si-OH} + \text{H-Si}$, that produces Si-OH and Si-H (immobile) impurities in the network.

^fA notable exception to this approach is atomic hydrogen H, whose value of D was estimated by experiments dealing with its reactions with point defects^{39, 202, 203}

interpreted as the *mean* D value on the distribution of E_a , which is:^{205,206}

$$\begin{aligned} \langle D \rangle &= \int D_0 \exp\left(-\frac{E_a}{k_B T}\right) \times \frac{1}{\sigma\sqrt{2\pi}} \exp\left[-\frac{(E_a - \langle E_a \rangle)^2}{2\sigma^2}\right] dE_a \\ &= D_0 \exp\left[\frac{\sigma^2}{2k_B^2 T^2}\right] \exp\left(-\frac{\langle E_a \rangle}{k_B T}\right) \end{aligned} \quad (2.3)$$

eq. (2.3) deviates from the Arrhenius behavior in that it contains the additional T -dependent term $\exp[\sigma^2/(2k_B^2 T^2)]$, leading to an *increase* of the effective diffusion coefficient from the value $D_0 \exp(-\langle E_a \rangle/k_B T)$ corresponding to the mean activation energy $\langle E_a \rangle$. The authors found that eq. (2.3) is able to reproduce a large set of experimental data on He diffusion in $a\text{-SiO}_2$ at $300\text{ K} < T < 1300\text{ K}$, with $\langle E_a \rangle = 0.33\text{ eV}$ and $\sigma = 0.057\text{ eV}$. In particular, with these parameters it is possible to reproduce quite well both temperature intervals investigated by Swets *et al.* (see above). Similarly to the case of He, slightly temperature-dependent values of the activation energy for molecular hydrogen or deuterium^g diffusion in the interval $0.38\text{ eV} - 0.45\text{ eV}$ have been measured by several studies performed in different temperature ranges.^{37,197,198,207} Actually, when one considers not too wide temperature intervals (typically up to $\sim 300\text{ K} - 500\text{ K}$ wide), the expression (2.2) remains a very good approximation for many purposes and is commonly used in reporting the diffusing parameters and in the analysis of diffusion processes.¹⁰⁸ Even so, for the above discussed reasons D_0 and E_a are characterized by some "intrinsic" indeterminacy. In regard to E_a , which influences the diffusion coefficient much more strongly than D_0 , these effects typically lead to fluctuations within $\sim 10\%$ of the reported values. Hence, when using literature diffusion parameters, one should always keep in mind the specific temperature interval in which the values have been measured. On the other hand, eq. (2.3) implies an important step forward in the understanding of the diffusion process in an amorphous matrix. Indeed, as it will be discussed in the following, the introduction of distributed activation energies becomes mandatory to describe the reaction kinetics of point defects with diffusing molecules.

Once clarified the framework in which the description of diffusion by eq. (2.2) is valid, we report in Table (2.1) some representative values of the diffusion parameters of common chemical species in silica, as estimated by the work of several authors. From the reported parameters, we note that the species featuring the lowest activation energies for diffusion are He, Ne, atomic and molecular hydrogen. The mean diffusion length of these species at $T = 300\text{ K}$ on a time scale of a few hours is $10^3 - 10^6$ times a typical interatomic distance: $\sim 5 \times 10^{-8}\text{ cm}$. Since the noble gases are basically inert from the chemical point of view, hydrogen can now be anticipated to be the diffusing species most able to influence the properties of the material in experiments performed at room temperature or below.

^gThe dimension and the electronic structure of the H_2 and D_2 molecules are essentially the same. As expected, the two activation energies for diffusion are found to be almost identical. In contrast, the pre-exponential factor D_0 scales as $\text{m}^{-1/2}$.^{37,38,108,196,198}

	$D_0[\text{cm}^2 \text{s}^{-1}]$	$E_a[\text{eV}]$	Reference	Range(K)	$D(300\text{K})[\text{cm}^2 \text{s}^{-1}]$	$L(\text{h})[\text{cm}]$
H	1.0×10^{-4}	0.18	39	77-130	9.5×10^{-8}	4.5×10^{-2}
H ₂	5.7×10^{-4}	0.45	197	570-1270	1.5×10^{-11}	5.6×10^{-4}
O ₂	2.9×10^{-4}	1.17	208	1220-1350	5.9×10^{-24}	$< 10^{-8}$
H ₂ O	1.7×10^{-4}	0.76	209	400-1500	3.4×10^{-17}	8.6×10^{-7}
He	3.0×10^{-4}	0.24	204	300-600	2.8×10^{-8}	2.5×10^{-2}
Ne	5.1×10^{-4}	0.41	207	300-770	6.7×10^{-12}	3.8×10^{-4}

Table 2.1: Diffusion parameters of some common chemical species in amorphous silica. The column "Range" reports the temperature intervals in which the diffusion parameters in the first two columns were measured. $D(300\text{K})$ is the diffusion constant extrapolated at room temperature. $L(\text{h})$ is the mean diffusion length in a time interval of one hour, calculated from $D(300\text{K})$.

2.3 Theoretical treatment of the reaction kinetics

In this section, we introduce some theoretical approaches that permit to describe chemical reaction kinetics in $a\text{-SiO}_2$. Consider the following generic bimolecular reaction, in which two species A and B combine to form C:



Due to reaction (2.4) the concentrations $[\text{A}]$, $[\text{B}]$ and $[\text{C}]$ depend on time. In many cases, the time variations can be described by a simple second order rate equation in which the time derivative of the concentrations (called the *reaction rate*) is proportional to the product of the concentrations of the two reagents.

$$\frac{d[\text{A}]}{dt} = \frac{d[\text{B}]}{dt} = -\frac{d[\text{C}]}{dt} = -k[\text{A}][\text{B}] \quad (2.5)$$

The constant k is known as the *rate constant* of process (2.4), and can be estimated experimentally by measuring the concentrations of the reagents as a function of time.

Several theoretical treatments have been proposed to derive an explicit expression for the rate constant, as a function of microscopic parameters related to A and B, to be compared with experimental data.^{194,210} Before discussing some of them, let us start with a qualitative discussion of the physical factors determining the rate of reaction (2.4). For the reaction to occur, the species A and B must first encounter each other during their random diffusive motion, thereby forming an (A–B) pair separated by a distance short enough (a few Å) to allow for the chemical interaction. Then, the fate of the encounter can be one of the following two: A and B can either react forming C, or diffuse away thus breaking the pair. In this sense, the overall rate of the reaction depends on two factors: the diffusion constant, which determines the rate at which the pairs form and break, and the reaction rate, namely the probability per unit time that a pair reacts resulting in the formation of C. Therefore, we can define two typical time scales: the reaction time τ_R , which is the typical time required for a pair to react, provided that it is not separated by diffusion, and the diffusion time τ_D , which is the lifetime of a pair before A and B diffuse away, provided that they do not react. Let us suppose now for simplicity that A and B interact only below a certain distance r_0 . Then, the order of magnitude of τ_D is the time required to diffuse out of a sphere with radius r_0 : $\tau_D \sim r_0^2/D$.

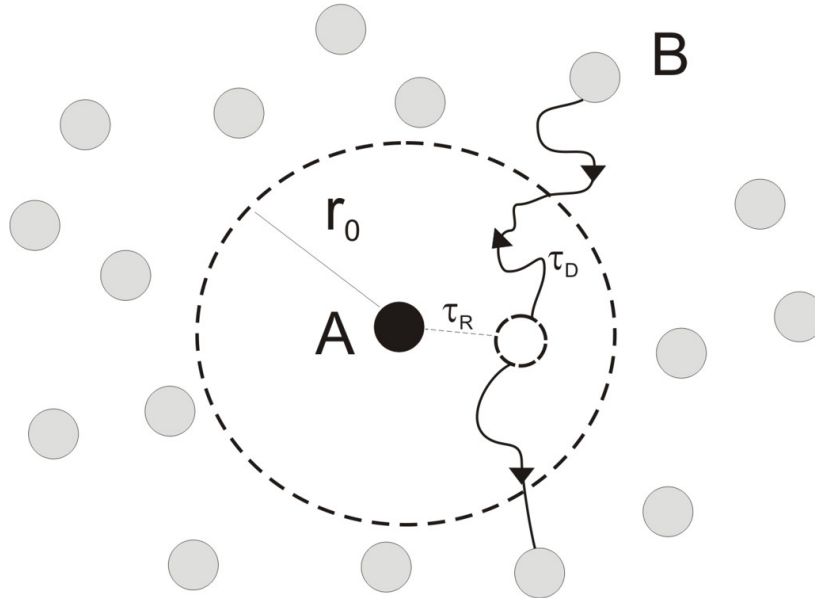


Figure 2.4: Pictorial representation of a reaction between two species A (supposed immobile for simplicity) and B (diffuser) within a solid. The continuous line with arrows represents the random diffusion trajectory of B. The typical time scale required for B to move across the interaction sphere of radius r_0 is τ_D , while τ_R is the typical time required for reaction.

Now, the reactions can be classified according to the relation between the two time scales. Indeed, if $\tau_D \gg \tau_R$, almost each encounter is successful in forming C: in fact, the diffusion is so slow that the reagents, after an encounter, remain close for much more time than typically required for the reaction. Hence, the reaction is mainly controlled by the rate at which (A–B) pairs form by diffusion, so as to say that the process is *diffusion-limited*. In the opposite case, if $\tau_D \ll \tau_R$, the reagents need to meet many times before they actually react. In this case, the process is said to be *reaction-limited* and is mainly controlled by the local interaction between A and B rather than by the migration of the species. Finally, it is worth noting that intermediate situations are obviously possible. For reactions occurring in solution or in solids, the diffusive motion is so slow that it often represent the actual bottleneck for the process; therefore, most reactions in solids involving mobile species are diffusion-limited processes.^{194,210}

To describe a diffusion-limited reaction, it is expected that the details of the short-range interaction between the reagents are unimportant. For this reason, one can try to describe the process on the basis of a somewhat crude approximation first proposed by Smoluchowski:²¹¹ the two species instantaneously react when their distance falls below a given distance r_0 , called the *capture radius*. From the mathematical point of view, this represents a boundary condition for the diffusive motion, which allows to model the occurrence of the reaction. On these grounds, we are going now to derive an explicit expression for the reaction constant of a diffusion-limited reaction. We start with introducing a simple heuristic model called *the trapping problem*, discussed in many standard textbooks.^{194,195} Suppose that in reaction (2.4) A represents a static point defect, whereas B is a mobile diffusing species. For the sake of simplicity, we imagine a particle A as a perfect spherical

trap of radius r_0 centered at the origin of the axis and surrounded by an infinite sea of diffusing particles B with spatial density $\rho(r)$, which move following the Fick law, here written in spherical coordinates:

$$J_r = -D \frac{\partial \rho(r)}{\partial r} \quad (2.6)$$

now, the total flux \mathbb{J} of the species B through a sphere of radius r centered at the origin must be independent of r in stationary conditions, since the only sink for the diffusive motion of B is represented by the spherical trap A:

$$\mathbb{J} = 4\pi r^2 J_r = -4\pi D r^2 \frac{\partial \rho(r)}{\partial r} = \text{constant} \quad (2.7)$$

\mathbb{J} is a negative quantity representing the variation per unit time of the total number N_B of B particles due to trapping.

$$\mathbb{J} = \frac{dN_B}{dt} \quad (2.8)$$

The aforementioned hypothesis, i.e. particles B are instantaneously trapped by A as soon as they arrive at r_0 , can be incorporated in the model as the condition $\rho(r_0) = 0$ (Smoluchowski boundary condition). Using this relation, we can now solve eq. (2.7) for $\rho(r)$:

$$\rho(r) = -\frac{\mathbb{J}}{4\pi D} \left(\frac{1}{r_0} - \frac{1}{r} \right) \quad (2.9)$$

the last expression shows that in proximity of the trap the concentration of B is depleted with respect to the value ρ_∞ at distances $r \gg r_0$. Besides, the unperturbed value ρ_∞ must be identified with the macroscopic measured concentration of the chemical species B. If we take the limit for $r \rightarrow \infty$ in the expression for $\rho(r)$, we find \mathbb{J} :

$$\mathbb{J} = -4\pi r_0 D \rho_\infty = -4\pi r_0 D [\text{B}] \quad (2.10)$$

This expression has been derived assuming a single trapping center A. Therefore, \mathbb{J} has to be multiplied for the number N_A of A particles. Finally, since the macroscopic reaction rate is the derivative of the concentration, rather than of the number of B particles, \mathbb{J} must also be scaled for the volume V of the sample. On this basis, starting from (2.8) and (2.10) we get:

$$\frac{d[\text{B}]}{dt} = V^{-1} \frac{dN_B}{dt} = \mathbb{J} \frac{N_A}{V} = -4\pi r_0 D [\text{A}] [\text{B}] \quad (2.11)$$

and comparing with eq. (2.5), we finally obtain the well known expression for the diffusion-limited reaction rate:^{194, 195}

$$k_d = 4\pi r_0 D \quad (2.12)$$

it is worth noting that the capture radius r_0 is expected to be of the order of the interatomic distance (a few Å) if the above arguments make sense at all. As an example, for the case of a process at room temperature in α -SiO₂ limited by H₂ diffusion, substituting in eq. (2.12) the value of $D(300\text{ K})$ from Table (2.1), we estimate the reaction constant to be of the order of: $4\pi r_0 D(300\text{ K}) \sim 10^{-17} \text{ cm}^3 \text{ s}^{-1}$.

It is clear that this very simple approach bears many limitations. In particular, it does not take into account the removal of the traps upon reaction, the occurrence of an initial arbitrary non-stationary spatial distribution of the reagents and the possibility that both A and B diffuse. In

literature, diffusion-limited reaction kinetics have been described by other techniques that permit to take into account these effects. Among the available approaches, we are going to focus on that proposed by Waite, which is a theoretical treatment formulated in terms of the pair probability densities of the reacting particles.²¹⁰ Hypothesizing uniform and uncorrelated initial distributions of A and B, and based upon the Smoluchowski boundary condition, Waite found that the rate "constant" k of reaction (2.4) actually depends on time, and is given by the following expression.

$$k_d = 4\pi r_0 D \left(1 + \frac{r_0}{\sqrt{\pi D t}} \right) \quad (2.13)$$

Physically, the time-dependent term $\sqrt{\pi D t}$ accounts for a transient regime during which the initial uniform distribution of A and B, which also includes a fraction of particles that are initially closer than the capture radius, spontaneously evolves towards a situation in which the concentration of B particles is depleted around A. After a time much longer than r_0^2/D , the time-dependent term in (2.13) becomes negligible, the spatial distribution of reagents resembles eq. (2.9), and the rate constant coincides *de facto* with the expression (2.12). Finally, eq. (2.13) is valid also if both species are mobile, with the substitution $D = D_A + D_B$.

The treatment by Waite can be extended also to situations in which the reaction is not purely diffusion-limited. To this aim, it may be used another boundary condition, originally proposed by Collins.²¹² The author suggested to define a interval of pair separations, from $r_0 - \Delta r$ to r_0 , within which the reaction is no longer controlled by diffusion, but follows a first order rate equation. In other words

$$\frac{d[C]}{dt} = w[(A-B)] \quad (2.14)$$

where $[(A-B)]$ is the concentration of (A-B) pairs whose distance falls within the above defined interval, and w is a constant [s⁻¹]. On this basis, it can be derived a generalized expression for the reaction constant:²¹⁰ similarly to eq. (2.13), k is found to be time-dependent but, once the initial transient is completed, the following approximate time-independent expression holds:^{210,213}

$$k_r = 4\pi r_0 D \frac{w}{w + D(r_0 \Delta r)^{-1}} \quad (2.15)$$

which generalizes eq. (2.12). This expression allows to make quantitative the distinction among diffusion- and reaction- limited processes, depending on the relation existing between diffusion and reaction time scales.^{210,213} Indeed from (2.15), when $w \gg D(r_0 \Delta r)^{-1}$, $k_r \sim k_d$ (compare with eq. (2.12)), and the reaction is a purely diffusion-limited process; in particular, the diffusion-limited reaction rate depends on D but not on w . In contrast, if $w \ll D(r_0 \Delta r)^{-1}$, one gets $k_r \sim 4\pi r_0^2 \Delta r w$. In these conditions, the reaction constant depends on w and not on D and the process is reaction-limited. If $r_0 \sim \Delta r$, the quantity $D(r_0 \Delta r)^{-1}$ can be interpreted as the inverse of the time necessary for the diffusing species to move a distance r_0 . Hence, the condition $w \gg D(r_0 \Delta r)^{-1}$ can be simply stated as follows: a reaction is diffusion-limited if the time necessary for the mobile species to diffuse away from the capture radius is much longer than the mean time (w^{-1}) necessary for reaction. This confirms our previous conclusions based on qualitative arguments.

Solving the rate equations

We are going now to briefly sketch the structure of the solutions of the chemical rate equations. The simplest situation is that of a single diffusion-limited bimolecular reaction, described by the second order rate equation (2.5). The parameter k will be supposed to be independent of time, which is basically true apart from an initial transient of duration r_0^2/D . In this case, it is easy to find the following analytical solutions of eq. 2.5. If the initial concentration $[A](0)$ is higher than $[B](0)$:

$$[A](t) = \frac{\delta}{1 - \lambda \exp(-k\delta t)} \quad (2.16)$$

$$[B](t) = \frac{\delta}{\lambda^{-1} \exp(k\delta t) - 1} \quad (2.17)$$

where $\delta = [A](0) - [B](0)$ and $\lambda = [B](0)/[A](0)$. For the particular initial condition $[A](0) = [B](0) = c$, the solution assumes a different form:

$$[A](t) = [B](t) = \frac{c}{1 + kct} \quad (2.18)$$

This initial condition, which may appear quite unlikely, can actually be realized if A and B are introduced in the sample as a consequence of a common mechanism. Both in eq. (2.16) and eq. (2.18), the typical time scale over which the reaction occurs is given by the product of the reaction constant k times a concentration, either δ or c .

A more complex situation is that in which n reactions proceed together. In this case, a rate equation can be written for each chemical species, containing a sum of terms each describing the variation rate of the concentration of that species due to a given reaction. In this way, one obtains a system of nonlinear differential equations whose solutions can be compared with experimental data. Some approximations can be often made which help to simplify the system, typically based upon the orders of magnitude of the reaction coefficients. To illustrate this approach, we analyze a case that will be of much interest in the following, namely the passivation of a defect X by molecular hydrogen in silica at room temperature. To fix ideas, we can further specify X to be a *paramagnetic* defect: indeed, as molecular hydrogen is a very stable molecule, usually it reacts efficiently only with paramagnetic (rather than diamagnetic) centers, very reactive due to the presence of an unpaired spin.^{38,214} The treatment we are about to follow has been used in literature to describe the reaction of NBOHC centers with H_2 ,^{38,185} while in the following of this work it will be applied to the passivation of E' . The generic reaction with X and H_2 can be written



and results in the conversion of the paramagnetic X into the diamagnetic $X-H$ as well as in the production of a free hydrogen atom H . Then, H diffuses and can encounter another X , passivating it:



but another possibility is that H made available by (2.19) meets another H and dimerizes forming H_2 .



In order to find out the time dependence of the concentrations of [X], [H₂] and [H], we write down the system of rate equations derived from the three above reactions:

$$\frac{d[X]}{dt} = -k_1[X][H_2] - k_2[X][H] \quad (2.22)$$

$$\frac{d[H_2]}{dt} = -k_1[X][H_2] + k_3[H]^2 \quad (2.23)$$

$$\frac{d[H]}{dt} = k_1[X][H_2] - k_2[X][H] - 2k_3[H]^2 \quad (2.24)$$

where k_1 , k_2 , k_3 are the rate constants of reactions (2.19), (2.20), (2.21), respectively. The three equations are self-explanatory generalizations of eq. (2.5). Now, we start with proposing a qualitative view of the solutions of this system. Let us suppose that the initial concentrations of X and H₂ are comparable, being of order c . Due to the reactions, the concentration of these two species are progressively reduced until one of the two is exhausted. In contrast, H plays quite a different role. Indeed, this species is an *intermediate* product, meaning that it is produced by reaction (2.19) and consumed by (2.20) and (2.21). In addition, we observe that k_1 is a reaction constant limited by the diffusion of *molecular* hydrogen, whereas k_2 and k_3 are limited by the much faster *atomic* hydrogen diffusion. Based on the values of Table (2.1) and on the expression (2.12) for the diffusion-limited reaction constant (where the order of magnitude of the capture radius is a few Å), it is evident that the following condition holds: $k_1 \ll k_2, k_3$. In other words, the typical time scale for H₂ diffusion and reaction is much longer than for H. From these considerations, one can draw the following qualitative picture: H that is "slowly" produced by reaction (2.19) (controlled by k_1) is very rapidly consumed by reactions (2.20) and (2.21) (k_2, k_3); hence, H is expected to behave as a *transient* species, whose concentration always remains much lower than H₂ and X: $[H] \ll [H_2], [X]$. Even if an initial anomalously high concentration of H is present, it is going to be rapidly consumed by reactions (2.20) and (2.21), at most in a time of $\sim k_2 c$, during which the much slower reaction (2.19) is actually frozen. Apart from this possible fast transient, H just follows adiabatically the "slow" decrease of the other two species, whose typical time scale is $\sim k_1 c$, but keeping a much lower concentration. On this basis, one can make the following approximation, called *stationary state approximation*:^{39,194}

$$\frac{d[H]}{dt} \sim 0 \implies k_1[X][H_2] - k_2[X][H] - 2k_3[H]^2 \sim 0 \quad (2.25)$$

The stationary state approximation is widely applicable to reactions involving a highly reactive intermediate product.¹⁹⁴ Now, since the concentration [X] is much higher than [H], and k_2 and k_3 are comparable, the following relation holds: $k_3[H]^2 \ll k_2[X][H]$. Therefore, we can neglect the quadratic term in [H] with respect to the linear one, and from eq. (2.25) we finally find:

$$[H] \sim \frac{k_1}{k_2}[H_2] \quad (2.26)$$

Using eq. (2.26), the stationary state approximation allows to eliminate the concentration [H] that can be simply expressed as a function of [H₂]. It is worth noting that, since $k_1 \ll k_2$, eq. (2.26) confirms *a posteriori* that $[H] \ll [H_2]$, so that the approximation gives self-consistent results. At $T=300$ K, from Table (2.1) we estimate $[H]/[H_2] \sim k_1/k_2 \sim 10^{-4}$: due to the very high diffusivity and reactivity of H, the stable form of hydrogen at room temperature is molecular rather than atomic.

Finally, we can substitute eq. (2.26) in eqs. (2.22) and (2.23) and neglect again the quadratic term in the latter, to get:

$$\frac{d[X]}{dt} = 2\frac{d[H_2]}{dt} = -2k_1[X][H_2] \quad (2.27)$$

the factor 2 has a very simple interpretation: each H_2 molecule actually reacts with *two* X centers, because the hydrogen atom produced by reaction (2.19) readily recombines with another X (2.20). The expression (2.27) represents now a system of two equations in the form (2.5), and can be solved exactly to give $[X](t)$. Using the expression (2.12) for k_1 , indicating with D_{H_2} the diffusion constant of H_2 and with $[X](0)$ and $[H_2](0)$ the initial concentrations, and substituting in (2.16), we eventually obtain:

$$[X](t) = \frac{([X](0) - 2[H_2](0))[X](0)}{[X](0) - 2[H_2](0) \exp[-4\pi r_0 D_{H_2}([X](0) - 2[H_2](0))t]} \quad (2.28)$$

from this expression, we see that $[X](t)$ tends asymptotically to $[X]_\infty = [X](0) - 2[H_2](0)$ (provided that $[X](0) > 2[H_2](0)$). The time constant of the exponential appearing at the denominator, can be regarded as the typical timescale τ in which the process occurs:

$$\begin{aligned} \tau &\sim [4\pi r_0 D_{H_2} \{[X](0) - 2[H_2](0)\}]^{-1} \\ &= [4\pi r_0 D_{H_2} [X]_\infty]^{-1} \\ &\sim 10^{17} \text{cm}^{-3} \text{s} \cdot [X]_\infty^{-1} \quad (\text{for } H_2 \text{ at } T=300 \text{ K}) \end{aligned} \quad (2.29)$$

using the values of Table 2.1 for the diffusion parameters of H_2 . As a final remark, we stress that even if in this particular case we were able to find an analytical, albeit approximate, expression for the time dependence of the concentrations of the reacting species, in general the rate equation system can be solved only numerically.

2.4 Hydrogen in silica and its interaction with point defects

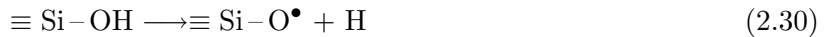
2.4.1 Forms of hydrogen in α - SiO_2

The presence of hydrogen is so common in silica that it can be barely considered as an impurity. It can be found in *free* form, as H atoms or H_2 molecules dissolved in the matrix, or in *bonded form*. Only in the first case it is mobile and potentially able to diffuse in the matrix (provided that the temperature is not too low). The most common bonded configurations are Si–OH and Si–H groups. In the following, we provide some more additional information about these species and their detection techniques, and then we discuss in detail the interaction of hydrogen with the two major point defects in α - SiO_2 , NBOHC and E' .

Si–OH: Si–OH groups are the most known and common form of bonded hydrogen in α - SiO_2 . They can be incorporated in silica in concentrations exceeding 10^{20}cm^{-3} , and they can be detected both by IR absorption and Raman spectroscopy by the signal around 3700cm^{-1} associated to their stretching mode.^{8,40,41} Typical sensitivity of IR and Raman (see footnote a of the previous chapter) allows to measure a minimum concentration of Si–OH of $\sim 10^{17} \text{cm}^{-3}$. The IR absorption band

associated to Si–OH is detrimental to the telecommunications technologies, since its first overtone at $\sim 1.4 \mu\text{m}$ falls in the wavelength range commonly used for transmitting signals in optical fibers.^{1–3, 108} Silica samples are commonly classified as "wet" or "dry" according to the high (100–1000 parts per million in weight) or low (1–100 ppm) concentration of Si–OH groups, which mainly depends on the water content of the atmosphere in which the sample is synthesized.^{215, 216}

An important property of this hydrogen-related center is that it serves as a precursor for the NBOHC. Indeed, many experimental evidences have demonstrated that irradiation can break the oxygen-hydrogen bond in Si–OH generating NBOHC and atomic hydrogen.^{1, 8, 38, 42, 85}



This process is observed under γ or X-ray radiation, and can be induced with high efficiency by F₂ laser radiation, which photolyzes the bond by exciting the bonding-nonbonding electronic transition of Si–OH at $E > 7.4 \text{ eV}$.^{8, 42, 85}

Si–H: Si–H groups can form in reactions of hydrogen with the silica network or with preexisting oxygen vacancies. They can be detected by IR absorption or Raman measurements on their vibration mode at about 2250 cm^{-1} , with a typical sensitivity of $\sim 10^{17} - 10^{18} \text{ cm}^{-3}$.^{40, 41} The 2250 cm^{-1} signal overlaps with a strong absorption due to an intrinsic vibration mode of the Si–O–Si silica network. As a consequence, the reliable observation of the Si–H signal by IR absorption is usually possible only in difference spectra. Very few experiments have investigated how the presence of hydrogen incorporated in Si–H form depends on the manufacturing procedure of α -SiO₂. As already discussed, it has been argued for a long time that photo- (or radio-) induced breaking of the silicon-hydrogen bond in Si–H generates E' and H:



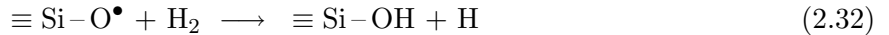
for this reason, Si–H is generally regarded as an important precursor for the paramagnetic defect;^{8, 28, 57, 72, 75, 89, 90, 107, 114} nevertheless, the understanding of process (2.31) at the moment is basically qualitative.

Other bonded forms: Aside from Si–H and Si–OH, hydrogen can be bonded in several other configurations, two examples of which are the H(I) and the H(II) centers introduced in the previous chapter. However, these structures usually appear only in irradiated samples and store only a minor portion of the total hydrogen population.

H: Atomic hydrogen is very reactive, and spontaneously combines with many point defects or dimerizes to form H₂, thus being highly unstable except at low temperatures. For this reason, at $T > 150 \text{ K}$ it exists only as a transient species, generated by radiolysis or photolysis of Si–H or Si–OH bonds or as a subproduct of the reaction of H₂ with defects. H can be detected by ESR spectroscopy at $T < 150 \text{ K}$ by its typical signal, which consists in a doublet split by 50mT due to the hyperfine interaction of the electron and the proton spins.^{38, 217, 218}

H₂ : The concentration of available solubility sites for molecular hydrogen in silica glass at room temperature has been estimated to be $\sim 10^{21} \text{ cm}^{-3}$, corresponding to a 4.6% molar concentration.³⁷ H₂ in vacuum does not absorb in the infrared due to its symmetry resulting in a zero dipole moment.¹²⁶ In contrast, when incorporated in silica, the structure of the molecule is slightly distorted, so as to activate a weak IR absorption band at 4130–4140 cm^{-1} associated to its fundamental stretching mode.^{40,41,108} The vibration of the species can be also detected with higher sensitivity by Raman spectroscopy, with a typical minimum detectable concentration of $10^{17} - 10^{18} \text{ cm}^{-3}$.^{40,41,219,220} Several studies have shown that usually H₂ is already present in variable concentration in as-grown commercial silica materials.^{42,221} As anticipated, due to its high bond energy ($\sim 4.5 \text{ eV}$) H₂ is a very stable molecule, which usually reacts only with paramagnetic centers^{h,38,214}

We have already mentioned several times that the presence of H₂ has important consequences on the response of silica to radiation, partly as a consequence of its high diffusivity. Indeed, often its concentration is increased by *loading* techniques for several technological purposes. One example is H₂-loading of Ge-doped *a*-SiO₂, a procedure which, as we have seen, tends to enhance point defect conversion processes leading to photosensitivity. On the contrary, in *pure* silica the presence of H₂ has in some sense the opposite effect: it tends to passivate radiation-induced defects. In particular, many experimental evidences have suggested that the two main paramagnetic defects in *a*-SiO₂, the *E'* ($\equiv \text{Si}^\bullet$) and the NBOHC ($\equiv \text{Si}-\text{O}^\bullet$), can react with H₂ by the following reactions:



as discussed in the previous section, atomic hydrogen produced at the right side of these reactions may dimerize in H₂, or passivate another defect:



In the presence of H₂, these reactions lead to a partial or complete passivation of *E'* and NBOHC produced by irradiation. Hence, as the two defects absorb in the UV, hydrogen allows for a recovery of the native transparency of the material compromised by the presence of these centers. In this sense, loading with a high concentration of H₂ is a standard technique used to make silica materials more resistant to transparency loss upon exposure to radiation, as common for example in multimode optical fibers to be used to transmit deep UV (200 nm–300 nm) light. In the following, we discuss what is known about the reaction properties of these two defects with H₂.

2.4.2 Reaction of NBOHC center with H₂

One of the first systematic investigations of the interaction between diffusing hydrogen and point defects in *a*-SiO₂ was carried out and reported by Griscom in a 1984 paper.³⁸ In that experiment, a

^hIt may occur, however, that H₂ reacts efficiently with a diamagnetic center in an excited electronic state, examples being the breaking of H₂ molecules by ODC(II) centers,²¹⁴ or (possibly) by GLPC centers in the S₁ state (see Figure 1.13).¹⁷⁹

synthetic silica specimen was first exposed to X-ray radiation at $T=77$ K. Then, thermal treatments were performed at $77\text{K} < T < 300\text{K}$, accompanied by ESR measurements, to investigate the annealing properties of the generated defects. Data obtained during an isochronous treatment are collected in Figure 2.5.

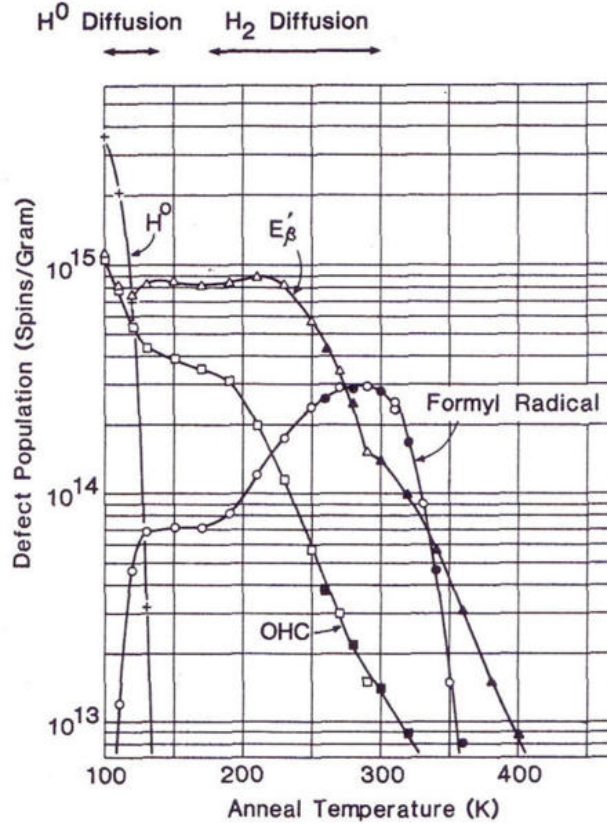


Figure 2.5: Concentration of several paramagnetic defects during an isochronous thermal treatment after X-ray irradiation at $T=77$ K. Figure adapted from Griscom.³⁹

The main experimental evidences are: (i) just after X-ray irradiation NBOHC and H are detected in the sample in comparable concentrations. (ii) Between 100 K and 150 K, H and NBOHC decrease in concentration; in particular, the H signal completely disappears. Also, it is observed the growth of two more signals, called the E'_β and Formyl Radical (FR). The former is a variety of E' center already introduced in section 1.1, while the latter was identified as a HCO structure. (iii) The concentrations of all the species remain relatively constant until $\sim 200\text{K}$ is reached. (iv) Above 200 K, a new stage of the process begins: in particular it is observed a further anneal of NBOHC and an increase of the FR. These results can be interpreted as follows: X-ray irradiation at 77 K generates NBOHC and H by breaking the oxygen-hydrogen bond on pre-existing Si-OH precursors. This result is particularly clear thanks to the direct observation by ESR of both NBOHC and H, roughly in the same concentration. Then, between ~ 130 K and 150 K, *atomic* hydrogen diffusion is activated, so that H partly recombines with NBOHC (Reaction (2.34)) and partly dimerizes in H_2 . Above 200 K, *molecular* hydrogen diffusion is activated, and the remaining portion of NBOHC are annealed by reaction with H_2 (Reaction (2.32)). In this context, the observed growth of the

hydrogen-related Formyl Radical (HCO) plays an important role: in fact, the FR is formed by reaction of (a portion of) atomic hydrogen with pre-existing precursors in the CO form; hence, the growth of FR represents an independent and clear indication of the presence of diffusing hydrogen in the matrix, which corroborates the attribution of the decay of NBOHC to reactions with H and H₂. By demonstrating that NBOHC can be passivated by reactions (2.32) and (2.34), the experiment by Griscom was the first to clearly evidence the role of diffusing hydrogen species in annealing the defects generated at cryogenic temperatures. Furthermore, it permitted to individuate the typical temperature ranges for atomic ($T > 130$ K) and molecular ($T > 200$ K) hydrogen diffusion in α -SiO₂.

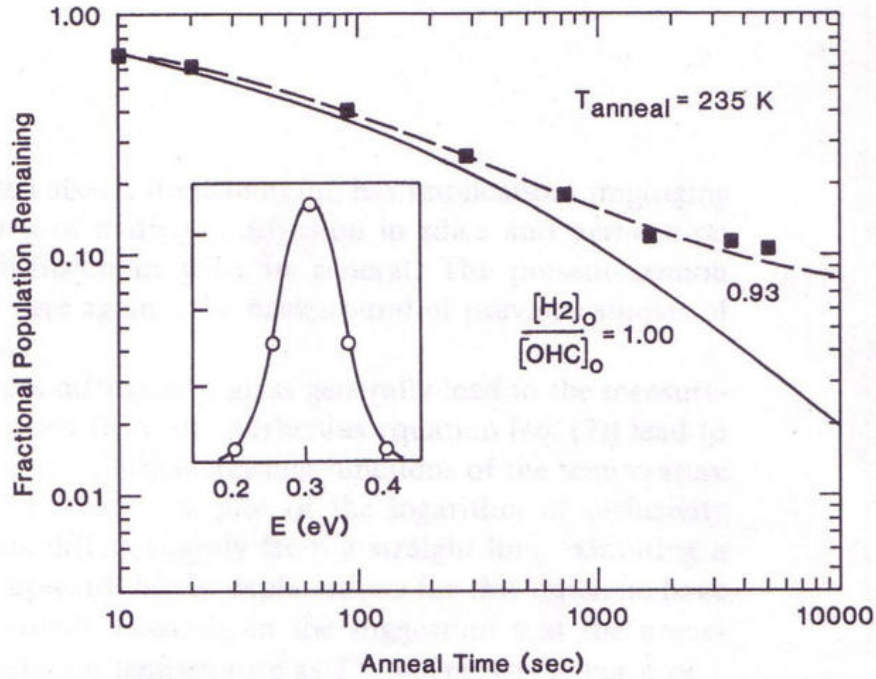


Figure 2.6: Time dependence of the concentration of NBOHC induced by irradiation at $T=77$ K, as measured during an isothermal thermal treatment at $T=235$ K. The decay of NBOHC is due to reaction with H₂. The fitting curves are obtained by a linear combination of expressions (2.28), weighted by a Gaussian distribution (inset) of hydrogen diffusion activation energy. The ratio between the initial concentrations of hydrogen and NBOHC is used as a fitting parameter, with a best fit value of 0.93. Figure adapted from Griscom.³⁹

Within this interpretation, the author made a step forward and tried to fit the measured annealing kinetics on the basis of the Waite model for diffusion-limited reactions, in the temperature range ($T > 200$ K) in which the annealing is due to reaction with molecular hydrogen H₂. However, it was found that satisfactory fits cannot be obtained by the expression (2.28) for H₂ diffusion-limited kinetics. In contrast, a good fit could be obtained only by a *linear combination* of these expressions, obtained by different values of D_{H_2} weighted by a Gaussian distribution of the activation energy for H₂ diffusion. This is shown for an isothermal decay curve at $T=235$ K in Figure 2.6. This finding must be interpreted as another manifestation of the existence of a statistical distribution of diffusion activation energies, consequent to the amorphous structure of silica; we have already introduced this idea when discussing the non-Arrhenius behavior of the diffusion constant D . In this sense, it is worth noting that point defects like NBOHC may be considered an indirect tool to study the properties of

diffusion in glass.

Nonetheless, there is now a very important point to be stressed. We have seen that the non-Arrhenius dependence of D measured by macroscopic diffusion experiments can be described by introducing a Gaussian distribution in E_a and identifying the measured value of D with the *mean* diffusion constant calculated on the distribution.^{205,206} On the contrary, when fitting the data in Figure 2.6, the use of a linear combination of expressions (2.28) is *not equivalent* to using a *single* expression calculated by simply substituting in (2.28) the *mean* diffusion constant. Qualitatively, this suggests that the diffusing species, in the typical experimental times, do not move enough to experience the full range of activation energies, so as to be characterizable by an "average diffusivity".³⁸ In contrast, one can imagine a set of H_2 molecules diffusing along many independent and not crossing paths until encountering and passivating a NBOHC, each path being characterized by a different value for activation energy. As a consequence of this interpretation, it was also suggested that the parameters of the distribution of activation energy necessary to fit the reaction kinetics may be slightly dependent on the explored concentration range, which determines the mean free path of the diffusers.³⁸ This overall approach undoubtedly gives a powerful insight on the diffusion in disordered solids and is quite reasonable from a qualitative point of view; nevertheless, at the moment it remains heuristic and lacks a solid theoretical basis founded on a detailed microscopic modeling of the diffusion phenomenon. Further experimental and theoretical studies are needed to provide a thorough understanding of the problem.

Finally, we point out an important point that was left unsolved by Griscom: the mean value ~ 0.3 eV of the activation energy (inset of Figure 2.6), which was found by fitting the reaction kinetics, is significantly lower than the (mean) activation energy for diffusion of H_2 in $a\text{-SiO}_2$ known from classical diffusion studies, 0.38–0.45 eV (Table 2.1). This poses a relevant problem in the interpretation of the results, being apparently inconsistent with the attribution of the decay of NBOHC to a diffusion-limited reaction with H_2 .

Today the reaction between NBOHC and H_2 , the role of hydrogen as an important passivating agent in $a\text{-SiO}_2$, and the existence of a site-to-site distribution of diffusion activation energies are well established results. To overcome the limitations inherent in the pioneering work by Griscom, the reaction properties of NBOHC with hydrogen have been recently investigated again using a different experimental approach, based on monitoring the NBOHC center by observing its luminescence emission at 1.9 eV. In detail, a pump and probe PL technique has been applied to observe *in situ* the recombination of hydrogen and NBOHC centers, generated together by breaking of Si–OH bonds (process 2.30) induced by F_2 laser photons.^{42,85,116,185} Similarly to the experiment by Griscom, by performing measurements in different temperature ranges this experiment has permitted to investigate both the reactions of NBOHC with H and H_2 , the latter species being formed by spontaneous dimerization of H atoms.

This investigation has permitted several steps forward in the understanding of the problem. First, the study was performed starting from very low (10 K) temperatures, and it was found that atomic H becomes mobile and starts to passivate NBOHC at temperatures much lower than initially thought, i.e. ~ 30 K (Figure 2.7). Second, it was confirmed that the kinetics of the reactions (2.32)

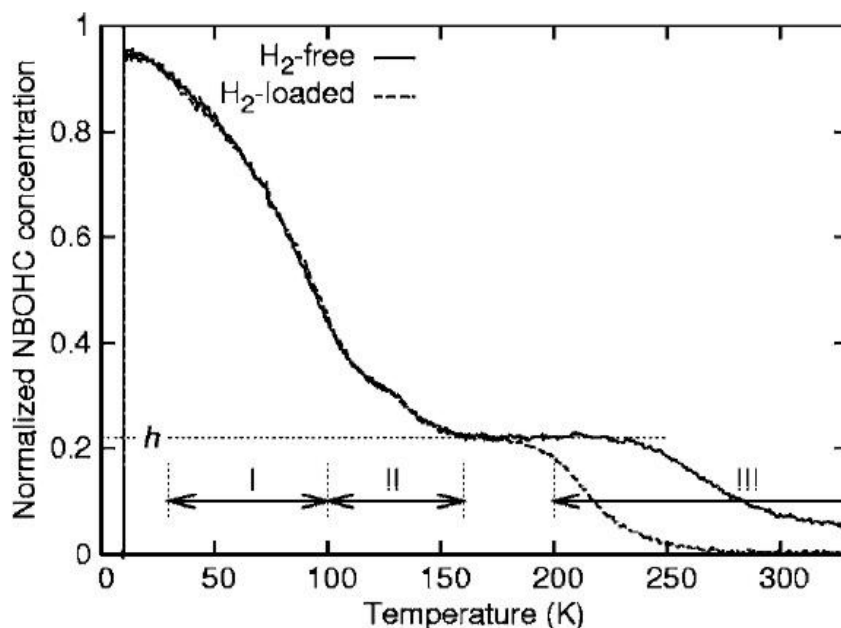


Figure 2.7: Decay curves of NBOHC generated at 10 K by a F_2 laser pulse, as observed in a thermal annealing experiment in which the sample was subjected to a progressive temperature increase from 10 K with a constant rate of 3 Kmin^{-1} . Results obtained in a H_2 -loaded material are compared with those in a sample initially free of H_2 . Figure adapted from Kajihara *et al.*¹⁸⁵

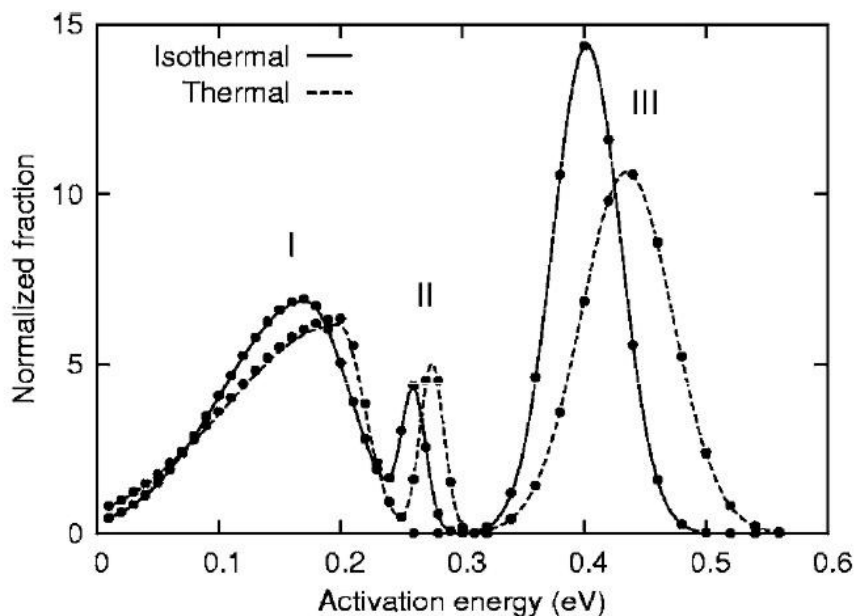


Figure 2.8: Statistical distribution of activation energy for diffusion of hydrogenous species, as obtained from the analysis of the kinetics of isothermal and thermal (see Figure 2.7) decay curves. Figure adapted from Kajihara *et al.*¹⁸⁵

and (2.34) are not describable by ordinary diffusion-limited reactions theory, but they can be accounted for by including a distribution of diffusion activation energies. Within this approach, from the accurate analysis of the measured thermal and isochronous decay kinetics, it was possible to accurately calculate the distribution of the activation energy E_a for diffusion of hydrogenous species in $a\text{-SiO}_2$, reported in Figure 2.8. Apart from some difference between the results found from isothermal data with respect to isochronous data, we see that the distribution of E_a of *atomic* H diffusion is strongly asymmetrical (peak I), whereas that of H_2 (III) is well represented by a Gaussian. An additional peak (peak II) is found that may be due to H trapped within shallow traps in the silica matrix. The three peaks correspond to temperature regions (Figure 2.7) in which the diffusion of H and H_2 are thermally activated. Moreover, the mean activation energy for H_2 diffusion is now found to be ~ 0.42 eV, and the pre-exponential factor is $\sim 8.5 \times 10^{-5} \text{ cm}^2\text{s}^{-1}$, both in a good agreement with the values in Table 2.1. This demonstrates very clearly that the reaction between NBOHC and H_2 is diffusion-limited, solving the problem of the too small mean value of $E_a \sim 0.3$ eV found by Griscom.ⁱ

As a last remark we mention that, apart from the distribution of activation energy, another model has been proposed in literature to explain the "anomalous" decay kinetics in glasses, which as we have seen cannot be fitted by standard chemical rate equations. The model is based upon the idea of diffusion in fractal spaces. It is known that fractals are geometrical structures characterized by a set of properties in which they differ from "Euclidean" spaces, such as self-similarity and fractional dimension. Fractals can derive either from deterministic or from stochastic construction rules, and a particular class of random fractals, the so-called percolation cluster, is thought to well describe, at least from a qualitative point of view, the structure of vitreous materials.^{184,195} Now, it is known from simulations and theoretical considerations that when diffusion takes place in a fractal space, such as the percolation cluster, the simple Fick law is not more valid. In particular, the relation $L_d \propto (Dt)^{1/2}$ is substituted by $L_d \propto (D't)^\gamma$, where $\gamma < 1/2$; it can be shown that this is formally equivalent to the introduction of a time-dependent diffusion coefficient. This situation is usually referred to as *anomalous diffusion*. As a consequence, the kinetics of diffusion-limited reactions is anomalous as well, and can be described by rate equations similar to the ordinary but having time-dependent rate "constants".^{184,195,222} Therefore, in some works the decay curves of point defects in silica have been fitted with success by so-obtained fractal kinetic curves; the parameters were found to be near to the values expected from the mathematical theory of fractals.^{184,195,222} This approach is alternative to (but not incompatible with) the introduction of a distribution of activation energies for diffusion. Also in this case, further investigation is needed to found on a more rigorous basis the fractal representation of the microscopic structure of silica.

2.4.3 Reaction of E' center with H_2

With respect to the NBOHC, much less is known about the other basic hydrogen-defect reaction in $a\text{-SiO}_2$, namely passivation of E' by hydrogen (Reactions (2.33) and (2.35)). We had previously

ⁱThe discrepancy with the results by Griscom was explained by hypothesizing the presence in the first investigation of a certain amount of hydrogen already dissolved in form of H_2 in the as-grown samples (as opposed to hydrogen of radiolytic origin), and not taken into account.¹⁸⁵

mentioned this process when discussing the generation of E' from Si–H precursors (Reaction 1.6). In this case, hydrogen atoms are generated as a co-product of E' . Therefore, H dimerizes in H_2 that recombines with E' in the post-irradiation stage (Reaction 2.33) causing the partial disappearance of E' centers in a time scale of a few hours at room temperature (Figure 1.9).^{89,114,223,224} More in general, hydrogen can also be not of radiolytic origin and react with E' centers generated from other precursors. For example, passivation of E' has been observed to occur in silica films irradiated with γ , UV or X-rays or in activated surfaces, after exposition of the sample to gaseous H_2 in a vessel.^{107,214,225–228} Apart from being relevant for the general understanding of diffusion and reaction dynamics in glass, reaction (2.33) has a notable practical importance as it allows to reduce the 5.8 eV absorption band of E' detrimental for the UV transparency of the glass. Even so, the main features of this process have been quite debated in literature and at the moment a full understanding is lacking.

First, although many experimental observations demonstrate that reaction (2.33) proceeds spontaneously at room temperature, some theoretical calculations contrast with these results, suggesting instead that the dissociation of a H_2 molecule on E' is an endothermic process, so that E' should not be an efficient cracking center for H_2 , differently from NBOHC.^{1,229,230,234} Besides, theoretical works and experimental results obtained in MOS systems have suggested that the process can occur efficiently in the *opposite* direction, i.e. spontaneous reaction of H with preexisting Si–H bonds de-passivates the dangling bond and generates a H_2 molecule.^{230,231}

Second, in experiments on E' centers generated by laser irradiation at room temperature, it was observed that the defects partially decay in the post-irradiation stage, likely by reaction with H_2 . However, when trying to fit with eq. (2.28) the time dependence of $[E']$, it was found an unrealistically small capture radius of the order of $\sim 10^{-2}$ Å.^{89,224} This is tantamount to saying that the kinetics is much slower than expected for a H_2 -diffusion-limited reaction. A possible interpretation of this finding is that the passivation of E' by H_2 is reaction-limited rather than purely diffusion-limited, namely its rate is significantly conditioned by the short-distance interaction between the two species;^{213,224,226} however, this is contrary to what occurs for NBOHC or for many other reactions in solids, and has been questioned by several other theoretical and experimental works.^{194,210,223,232,233}

From the experimental point of view, the character (diffusion- or reaction- limited) of the reaction between E' and H_2 could be clarified by an accurate kinetic study able to estimate the reaction rate as a function of temperature. Unfortunately, until now such measurements have been carried out only for surface E' centers,²¹⁴ or for E' centers in thin silica films,²²⁶ systems where the reaction can be directly investigated by exposure of the surfaces to gaseous H_2 in a vessel. These two works report disagreeing results: the measured rates of reaction (2.33) at $T=300$ K differ by two orders of magnitude, while the two activation energies are 0.4 eV and 0.3 eV respectively^{214,226} (data for E' in a thin silica film are reported in Figure 2.9). In regard to theoretical studies, the process was shown to require an activation energy ranging from 0.2 eV to 0.7 eV depending on the calculation methods.^{229,230,232,234} For E' centers in *bulk* silica, the task of studying experimentally the reaction becomes more difficult, since here the concentration of available H_2 is not an external controllable parameter depending on the pressure in the vessel, and diffusion of H_2 in the bulk a -SiO₂ matrix becomes a necessary step to bring the reagents in contact. Furthermore, it is needed to measure *in situ*

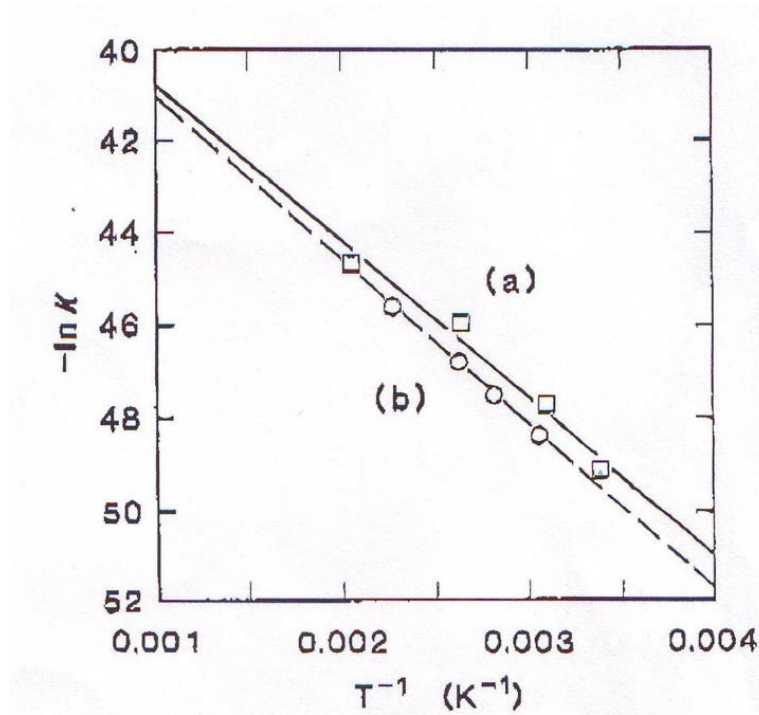


Figure 2.9: Arrhenius plot of the reaction constant between E' centers and H_2 in irradiated $a\text{-SiO}_2$ films of different thicknesses (450 nm (a) and 100 nm (b)) on a Si substrate. The activation energy for reaction (2.33) derived from these data is 0.3 eV. Figure taken from Li *et al.*²²⁶

the kinetics of the transient defects generated by irradiation in temperature-controlled experiments. For these reasons, the thermal activation properties of the reaction between E' and H_2 , as well as the limiting factor of its kinetics, have still to be thoroughly investigated. Finally, no experimental data exist about the influence on this process of the statistical distribution of the activation energy that characterizes the diffusion of H_2 in $a\text{-SiO}_2$. A contribution to the understanding of these problems represents one of the most relevant results of this PhD Thesis.

Chapter 3

Experimental techniques: a theoretical background

The purpose of this chapter is to provide a basic theoretical background for the interpretation of the parameters deduced from the investigation of point defects in α -SiO₂ by optical and magnetic resonance spectroscopic techniques.

3.1 Optical properties of a point defect

Optical absorption spectroscopy investigates the properties of a point defect embedded in a solid by the observation of the absorption band(s) associated with the transitions of the center from the electronic ground state to the excited state(s)^a. Consider the simple two-level scheme of a point defect represented in Figure 3.1. To describe the optical properties of this center, one must take into account the coupling between the electronic and the vibrational degrees of freedom. Within the Born-Oppenheimer and the Condon approximations, this can be done by describing the state of the system as the (tensorial) product of an electronic wave function and a nuclear wave function; on this basis, the general state of the system is characterized by a pair of quantum numbers (N, i) , describing the state of the electronic and vibrational subsystems respectively.^{1,3}

Suppose now that the system is initially in its electronic *and* vibrational ground state $(0, 0)$, as expected in particular at $T=0$. After optical excitation it can be promoted to each of the vibrational sublevels $(1, i)$ within the excited electronic state, the transition at lowest energy being that from $(0, 0)$ to $(1, 0)$, called the *zero phonon line* (ZPL). The set of $(0, 0) \rightarrow (1, i)$ combined electronic-vibrational transitions (*vibronic* transitions) is characterized by a specific distribution of transition rates, which can be predicted theoretically and depends on the extent to which the equilibrium position of the nuclei in the excited electronic state differs from the ground state. This problem is treated in many standard texts^{1,3} and is not discussed in detail here. However, we recall that: **(i)**

^aWe refer here only to electronic transitions, whose typical energies (generally of the order of a few eV) fall in the range probed by UV or visible optical absorption spectroscopy.

very often the $(0, 0) \rightarrow (1, i)$ vibronic transitions cannot be resolved in the optical absorption spectrum, which therefore appears as a single bell-shaped broad band^b, given by the envelope of many narrow subbands each due to a given transition.^{1,3} We have already seen typical examples of such broad absorption bands in Figure 1.3 for the case of E' and NBOHC centers. (ii) The energy E_{OA}^{pk} at which falls the maximum of the absorption band corresponds to the most probable vibronic transition, which is generally higher than the "pure" ZPL (see Figure 3.1).

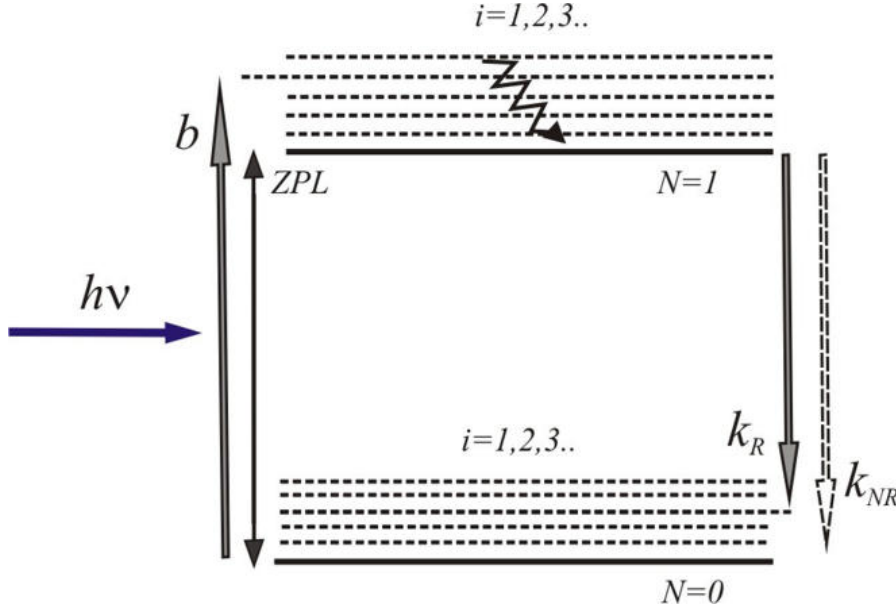


Figure 3.1: Idealized electronic-vibrational level scheme of a two levels point defect. The horizontal arrow represents an incoming photon. The continuous arrow oriented upward represents one of the possible absorption transitions (from the $(0, 0)$ to the $(1, 4)$ state). The continuous arrow oriented downward represents spontaneous emission from $(1, 0)$ to $(0, 3)$. The dotted arrow represents the non-radiative decay process. The double arrow indicates the ZPL transition. The arrow within the $(1, j)$ levels represents the internal relaxation process.

If a light beam propagates along the x direction within a sample containing absorbing point defects, its intensity is progressively reduced according to an exponential equation:^{1,3}

$$I(\lambda, x) = I_0(\lambda) \exp(-\alpha(\lambda)x) \quad (3.1)$$

where $I(\lambda, x)$ is the intensity of the monochromatic component of wavelength λ in the position x . The last equation defines implicitly the *absorption coefficient* $\alpha(\lambda)$, which characterizes the OA profile of the point defect. The quantity that is directly measured by an absorption spectrophotometer is the *optical density* $OD(\lambda)$ of the sample. It is defined by:

$$OD(\lambda) = \log_{10} \frac{I_0(\lambda)}{I(\lambda, d)} \quad (3.2)$$

and is obtained by measuring for each λ the light intensity before ($I_0(\lambda)$) and after ($I(\lambda, d)$) the sample. OD is related to α by the following relationship

$$\alpha = \ln(10) \frac{OD}{d} \sim 2.303 \frac{OD}{d} \quad (3.3)$$

^bAside from electron-phonon coupling, which leads to so-called homogeneous broadening, in amorphous silica the absorption bands of point defects are further broadened by inhomogeneity effects.

where d is the thickness of the sample. Finally, we note that the absorption coefficient can be equivalently expressed as $\alpha(E)$, namely as a function of the photon energy $E = 2\pi\hbar c/\lambda$, \hbar and c being the Planck constant and the speed of light respectively.

Consider a silica sample containing a single species of absorbing point defects in concentration ρ . As anticipated, the absorption profile $\alpha(E)$ due to the presence of the centers is typically bell-shaped with a width between 0.1 eV and 1 eV. The value of α at a given spectral position is proportional to ρ through the absorption cross section $\sigma(E)$:^{1,3}

$$\alpha(E) = \sigma(E)\rho \quad (3.4)$$

in turn, $\sigma(E)$ is connected to the Einstein coefficient b for absorption and stimulated emission^{c:1,3,126}

$$b = \frac{c}{2n\pi\hbar} \int \frac{\sigma(E)dE}{E} \quad (3.5)$$

where n is the refractive index of the medium in which the defect is embedded. In the case of a very narrow absorption band, the energy dependence of the denominator can be neglected, thus giving the following approximate expression:

$$b \sim \frac{c}{2n\pi\hbar^2\omega} \int \sigma(E)dE \quad (3.6)$$

which is equivalent to regarding the absorption process as a simple transition between narrow, "atomic"-like levels separated by an energy $\hbar\omega$.

The absorption properties of a point defect can be characterized either by using the "local" (function of E) property $\sigma(E)$ or by a dimensionless integrated parameter known as the *oscillator strength*. The two are alternative but equivalent ways to express the strength of the absorption signal arising from a given concentration of the defect. In detail, the oscillator strength f of an electric dipole transition of frequency ω is given by:^{1,3,126}

$$f = \frac{2m\omega}{3\hbar e^2} |\langle \psi_1 | D | \psi_2 \rangle|^2 \quad (3.7)$$

where m and e are electron's mass and charge, respectively, D is the electric dipole moment operator and ψ_1 and ψ_2 indicate the quantum initial and final states of the transition. f can be connected to the *integral* of the measured OA band. In fact, it can be shown that:¹

$$\int \alpha(E)dE = \frac{\rho}{n} \left(\frac{E_e}{E_0} \right)^2 \frac{2\pi^2 e^2 \hbar}{mc} f \quad (3.8)$$

where the E_e/E_0 term is called the *effective field correction*, and takes into account the difference existing between the macroscopic electric field E_0 and the *local* microscopic field E_e acting at the position of the defect.^{1,59} Several treatments of the problem of the effective field are available in standard texts, resulting in different mathematical expressions of the correction. One of the most

^cFrom now on we suppose for simplicity that both the initial and the final electronic state are non-degenerate. Generalizing the equations to take into account electronic degeneracy is straightforward.

commonly used is called the Lorentz-Lorenz correction: within this approach, and in the case of a Gaussian absorption band, eq. (3.8) can be approximated as follows:¹

$$\rho f \sim 8.72 \times 10^{16} \frac{n}{(n^2 + 2)^2} \alpha_{max} \Delta \times [cm^{-2} eV^{-1}] \quad (3.9)$$

where α_{max} is the maximum amplitude of the band and Δ is the width (full width at half maximum) of the band.

The experimental estimate of the oscillator strength (or of the cross section) of a point defect can be made using (3.8) (or (3.4)) on the basis of the measured absorption band, only if the concentration is already known from an independent approach. For paramagnetic centers this is usually accomplished by ESR measurements, which permit to estimate the absolute concentration of the defects by comparison with a reference sample. For example, for the 5.8 eV absorption band of the E' center it was determined that the *peak* absorption cross section is $\sigma(5.8 \text{ eV}) = 6.4 \times 10^{-17} \text{ cm}^2$.^{3,224} In the case of photoluminescent centers, the oscillator strength can be estimated from the knowledge of the luminescence radiative decay lifetime (as explained below). If a center is neither paramagnetic nor luminescent, the task becomes much more complicated and must be solved indirectly, for example on the basis of the observed conversion in another defect of known concentration.

Another optical property of great importance in the study of point defects is photoluminescence (PL), i.e. the process by which a system excited by light with wavelength λ_0 emits light at $\lambda_e > \lambda_0$ while decaying back to its ground state. Under excitation with constant intensity, we indicate the spectral density of the emitted light as

$$\frac{dI_e}{d\lambda_e}(\lambda_0, \lambda_e) \quad (3.10)$$

which is considered as a function of λ_e , while λ_0 may be regarded as a parameter. A measurement of the emitted spectral profile $dI_e/d\lambda_e$ (as a function of λ_e) under excitation at a given λ_0 is called *emission* spectrum of the center. Not all the point defects that feature a measurable absorption band decay by emitting luminescence, but when this occurs, their study by PL spectroscopy has some important advantages with respect to OA. In particular, PL is more *selective*, as it often allows to *isolate* a center whose absorption band overlaps to those arising from other defects, based on the different emission properties.

To picture the physical processes determining the PL emission band, let us consider again the two-level system of Figure 3.1. Excitation to one of the $(1, j)$ states is followed by a rapid *internal relaxation*, which drives the system all the way down to the $(1, 0)$ state (if at $T=0 \text{ K}$), within a time scale comparable to that of nuclear vibrations: 10^{-12} – 10^{-11} s .²³⁵ Then, in general the center relaxes back to the ground state either by *radiative* emission (photoluminescence) or by a temperature-dependent *non-radiative* process in which the energy is dissipated by emission of phonons. The two processes can be characterized by a radiative decay rate k_R and a non-radiative decay rate k_{NR} . The radiative decay is the origin of the emission band, consisting in the combination of several $(1, 0) \rightarrow (0, j)$ vibronic transitions. The most probable of such transitions determines the peak spectral position E_{PL}^{pk} of emission. From Figure 3.1 it is apparent that E_{PL}^{pk} must be *lower* than the ZPL; Hence, it is also lower than the spectral position of the absorption peak $E_{OA}^{pk} > \text{ZPL}$. This results in a shift ($E_{OA}^{pk} - E_{PL}^{pk}$) between the peak positions of absorption and emission spectra, called

Stokes shift.^{1,3} It can be demonstrated that the absorption and emission spectra are approximately symmetric (*mirror symmetry*) with respect to the ZPL position.^{1,3}

When a defect emits by photoluminescence under excitation of constant intensity within its absorption band (stationary photoluminescence), the efficiency of the luminescence process can be characterized by a parameter η known as *luminescence quantum yield*, defined as the ratio between emitted photons and absorbed photons. η is determined by the competition between radiative and non-radiative decay processes. For the case of Figure 3.1, it can be easily demonstrated that $\eta = k_R/(k_{NR} + k_R)$. Differently from stationary PL measurements, in a *time-resolved* PL measurement, it is studied the time decay of the emitted light after an exciting light *pulse*. By this technique, it is possible to directly estimate the decay time $\tau_e = (k_{NR} + k_R)^{-1}$ from the excited state. At sufficiently low temperatures, the non-radiative decay channels are usually quenched, i.e. $k_{NR} \ll k_R$, so that the measurement directly yields the *radiative* decay time $\tau = 1/k_R$. The importance of the knowledge of τ relies in the possibility of calculating the oscillator strength f of the center. To see this, we observe that $1/\tau = k_R$ equals the *a* Einstein coefficient for spontaneous emission, which is connected to the *b* coefficient by the relation $a = 2\hbar\omega^3 n^3 b \pi^{-1} c^{-3}$. Hence, combining with (3.6) and (3.4), the following relationship between $1/\tau$ and the absorption profile $\alpha(E)$ is derived:

$$\frac{\rho}{\tau} = \frac{n^2 \omega^2}{\pi^2 c^2 \hbar} \int \alpha(E) dE \quad (3.11)$$

Based on the knowledge of τ , if the absorption profile of the defects $\alpha(E)$ has been measured, this equation can be used to find the concentration ρ , which in turn can be inserted in eq. (3.8) to estimate f . Nonetheless, eq. (3.11) has been deduced within the scheme of an "atomic" two level system, in which there is no electron-phonon coupling and absorption and emission occur at the same energy. For point defects in solids, this treatment must be carried out singularly for *each* vibronic transition. Then, the radiative transition rates must be integrated over the whole spectrum. On this basis, one can generalize eq. (3.11) to an equation (Förster equation) applicable to the case of point defects in *a-SiO₂*:¹

$$\frac{\rho}{\tau} = \frac{n^2}{\pi^2 c^2 \hbar^3} \int (2E_0 - E)^3 \frac{\alpha(E) dE}{E} \quad (3.12)$$

where E_0 is the position of the ZPL, which can be estimated experimentally on the basis of the mirror symmetry between emission and absorption spectra.

3.2 Magnetic resonance of a point defect

Electron Spin Resonance (ESR) is the resonant absorption of electromagnetic radiation by an electronic spin system coupled to a static magnetic field, which takes place when the frequency of the radiation matches one of the characteristic transition frequencies of the system. For typical laboratory magnetic fields of the order of 10^3 G, the resonance frequency ω_0 falls in the microwave range (10^9 – 10^{10} Hz). A typical ESR spectrometer explores the resonance condition by exposing the sample to a fixed microwave frequency ω_0 and varying the static magnetic field, and not *vice versa*, since an accurate control of a varying frequency would be technically more difficult. Moreover, to

increase sensitivity, a modulation magnetic field of frequency $\omega_m \ll \omega_0$ and small amplitude A_m is superimposed to the static field; hence, it is used the so-called "lock-in" detection technique, which is selective with respect to the frequency ω_m and sensitive to the phase of the detected signal. As a consequence, it can be shown that the spectrometer is sensitive to the *first derivative of the energy absorption curve*.

The ESR technique is applicable to a variety of systems, including paramagnetic point defects, which possess a nonzero spin in their lowest electronic state due to the presence of an unpaired electron. We have already seen important examples of such defects in α -SiO₂, in particular the E' and the NBOHC. The ESR technique possesses an unsurpassed ability to provide detailed structural information about the centers: in some sense, it can be argued that most of the current knowledge about the structure of *all* defects in α -SiO₂ is based, directly or indirectly, on the models of paramagnetic defects elucidated by means of ESR investigation.¹

From the theoretical standpoint, the interaction of an electronic spin with its surroundings can be described by the introduction of the *spin hamiltonian* \mathcal{H}_0 .^{1,217,218} The basic term of the spin hamiltonian is the Zeeman contribution, which accounts for the interaction of the magnetic moment associated to the spin \vec{S} with the magnetic field. For a field of intensity B_z directed along the z axis of the laboratory frame:

$$\mathcal{H}_0 = -\vec{\mu} \cdot \vec{B} = g\beta\vec{S} \cdot \vec{B} = g\beta S_z B_z \quad (3.13)$$

where $\beta = |e|\hbar/(2mc)$ is the Bohr magneton and g is the spectroscopic splitting factor (the gyromagnetic ratio). This Hamiltonian gives rise to two electronic levels, from which it is found the following resonance condition:

$$B_z = \frac{\hbar\omega_0}{g\beta} \quad (3.14)$$

hence, the quantity g can be measured from eq. (3.14), based upon the observation of the field position at which the resonance occurs.

A thorough description of the magnetic resonance phenomenon in a solid requires not only to find the positions of the resonance line(s), but also to deal with the interaction *dynamics* of the spin with the magnetic field. To this end, it is mandatory to take into account the effects of the spin-lattice coupling, allowing for the dissipation of energy, and of the spin-spin interaction, which lead to a homogeneous broadening of the resonance line.^{1,217,218} Without entering into the details, we recall that this problem was treated by Bloch, who proposed a set of equations able to describe the interaction of the macroscopic magnetization \vec{M} of a solid containing paramagnetic centers with a time-dependent magnetic field. In particular, the spin-lattice and spin-spin interactions were dealt with by the introduction of two phenomenological relaxation times T_1 and T_2 , respectively. In the presence of the static field B_z and of a perpendicular microwave field B_x oscillating at the frequency ω_0 , if we define a complex magnetic susceptibility χ :

$$M_x = \chi B_x e^{j\omega_0 t} \quad (3.15)$$

then the energy absorption of the system is connected to the imaginary part χ'' of the susceptibility. χ'' can be equivalently considered as a function of ω_0 or B_z ; as expected from (3.14), it can be

demonstrated that $\chi''(B_z)$ shows a resonance for $B_z = \hbar\omega_0/(g\beta)$ described by the following equation:^{1,217,218}

$$\chi''(B_z) = \frac{1}{2}\gamma M_z^0 T_2 \frac{1}{1 + T_2^2(\gamma B_z - \omega_0)^2 + \frac{1}{4}\gamma^2 B_x^2 T_1 T_2} \quad (3.16)$$

where M_z^0 is the z magnetization at thermal equilibrium, proportional to the number of spins N , and $\gamma = g\beta/\hbar$. As apparent from eq. (3.16), the shape and the intensity of the resonance generally depend on the incident microwave power through the term in B_x^2 appearing on the denominator. However, a particular condition (called *non-saturation condition*) is realized when $\gamma^2 B_x^2 T_1 T_2 \ll 1$, which physically means that the incident microwave power is low enough to allow for the relaxation channels to efficiently dissipate the absorbed energy. When the non-saturation condition is verified, the term in B_x^2 can be neglected from eq. (3.16), and the resonance line acquires a Lorentzian shape independent of incident power and with a $(T_2\gamma)^{-1}$ width.

As described in more detail in the next chapter, the measured *ESR spectrum* $S(B_z)$ is proportional to the derivative of the absorption curve multiplied by the amplitude B_x of the microwave field and the modulation amplitude A_m defined at the beginning of this section:

$$S(B_z) \propto \frac{d\chi''}{dB_z} B_x A_m \quad (3.17)$$

Hence, substituting χ'' from (3.16), the *doubly-integrated* signal gives the following quantity Γ .

$$\Gamma = \int_{-\infty}^{+\infty} dy \int_{-\infty}^y dB_z \frac{d\chi''}{dB_z} B_x A_m = \frac{\pi M_z^0 A_m}{2} \frac{B_x}{\sqrt{(1 + \frac{1}{4}\gamma^2 B_x^2 T_1 T_2)}} \quad (3.18)$$

If we define $\Gamma' = \Gamma/(B_x A_m)$, far from saturation ($\gamma^2 B_x^2 T_1 T_2 \ll 1$), the last equation can be approximated as $\Gamma' \sim \pi M_z^0/2$. Therefore, the doubly-integrated signal normalized for the microwave (B_x) and the modulation (A_m) amplitudes, Γ' , is proportional to the number of spins N through M_z^0 , so as to represent a *relative* measurement of N . Γ' can be converted to an *absolute* concentration measurement by comparison with a reference sample in which the concentration of a given defect is known by an independent technique. This interpretation of Γ' is lost when the transition is saturated, because in this case (see (3.18)) the proportionality factor depends on T_1 and T_2 , making impossible a comparison between different centers or samples.

For a free electron, $g = g_e = 2.0023$; in the case of a point defect in a solid, the situation becomes more complicated because of the admixture of *angular* momentum into the spin ground state of the center. In particular, this leads to the *anisotropy* of the Zeeman interaction, which is accounted for by promoting g to a *tensorial* quantity \underline{g} , whose principal values g_1, g_2, g_3 generally differ from g_e . Hence, the hamiltonian assumes the following form:^{1,217,218}

$$\mathcal{H}_0 = \beta \vec{B} \cdot \underline{g} \cdot \vec{S} \quad (3.19)$$

and the resonance condition becomes:

$$B_z = \frac{\hbar\omega_0}{\beta \sqrt{g_1^2 \cos^2 \theta_1 + g_2^2 \cos^2 \theta_2 + g_3^2 \cos^2 \theta_3}} \quad (3.20)$$

where θ_i are the angles between the direction of the magnetic field (i.e. the z axis of the laboratory frame), fixed by the geometry of the spectrometer, and the principal axes of the g tensor, dictated by the local symmetry properties of the defect.

If we execute a measurement on a *powdered* crystal sample, in which the defects are randomly oriented in all directions, the observed resonance line results to be the envelope of many narrow Lorentzian lines at the positions given by (3.20) for all the possible values of the random θ_i . This gives rise to the so-called *powder lineshape*. From the mathematical point of view, the isotropic distribution of the defect orientations can be represented by statistical distributions of the three angles θ_i proportional to $\sin(\theta_i)$; then, one has to use eq. (3.20) to find the corresponding distribution of $g = \sqrt{g_1^2 \cos^2 \theta_1 + g_2^2 \cos^2 \theta_2 + g_3^2 \cos^2 \theta_3}$, which must finally be convoluted with the single-packet lineshape given by eq. (3.16) to obtain the overall resonance curve.¹ A typical result is sketched in Figure 3.2: it is worth noting that from the observation of the powder lineshape it is still possible to extract the three principal values g_i , which correspond to specific field positions detectable by inspection of the curve. Finally, when one considers defects in an *amorphous* matrix, another effect

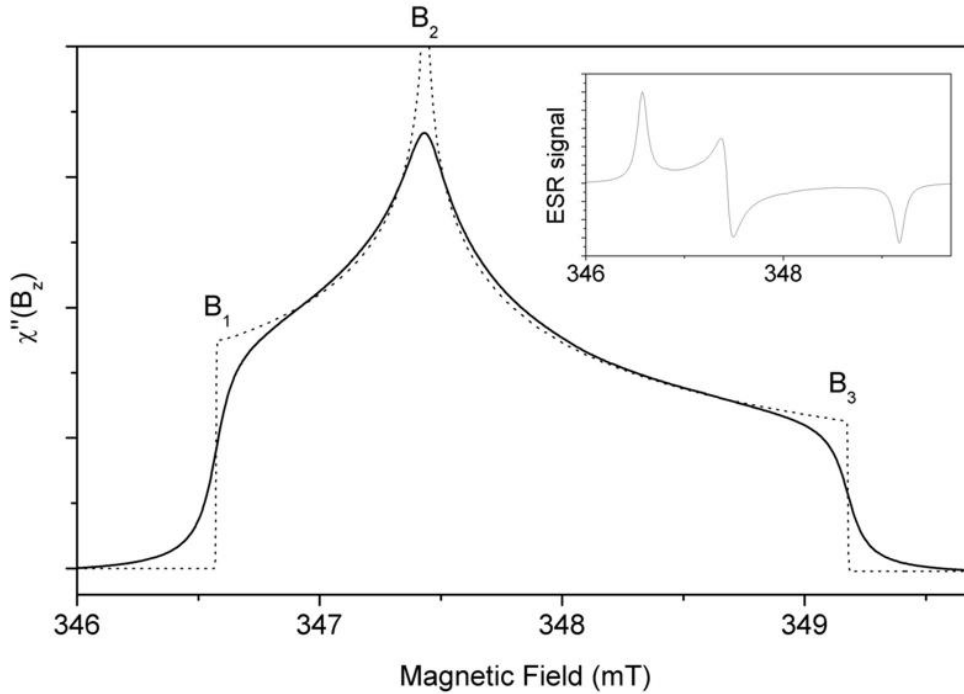


Figure 3.2: Simulated ESR absorption curve ($\chi''(B_z)$) for a system of randomly oriented defects in a crystal powder. The values B_i are defined as $\hbar\omega/\beta g_i$, where g_i are the principal axes of the tensor ($g_1 \neq g_2 \neq g_3$). The dotted line represents the distribution of the resonance fields in the powdered sample due to the random orientations of the spins. The continuous line represents the ESR absorption curve, calculated by convoluting the dotted line with a (much narrower) Lorentzian lineshape. The ESR lineshape that would be observed in this case by a measurement is reported in the inset and corresponds to the derivative of the absorption curve. The case represented here is the most general; in several cases of interest the actual signal appears simpler thanks to the axial symmetry ($g_2 = g_3$) possessed by many defects of interest (such as the E' center).

must be taken into account: also within a set of centers all sharing the same orientation with respect to the magnetic field, an intrinsic site-to-site variation of the principal values of \underline{g} is expected as a consequence of the disordered nature of the amorphous solid. In this sense, the g_i are to be regarded as statistically distributed, this leading to a further broadening of the resonance line.¹

When a nucleus with nonzero spin I is positioned near the electronic spin, the *hyperfine interaction* between the two magnetic moments gives rise to another energy term that must be included to the spin hamiltonian. In general, the hyperfine interaction is accounted for by a *hyperfine tensor* \underline{A} , which contains an anisotropic portion due to the dipolar spin-spin interaction, and an isotropic portion due to the so-called *Fermi contact term*.^{1,217,218} Often, the contact term prevails, so that in first approximation the interaction is completely described by a scalar $A_0 \propto g_e g_N \beta \beta_N |\psi(0)|^2$, where g_N and β_N are the nuclear gyromagnetic ratio and the nuclear Bohr magneton respectively, and $|\psi(0)|^2$ is the probability of finding the electron at the position of the nucleus. The spin hamiltonian assumes the following form:

$$\mathcal{H}_0 = g\beta S_z B_z + A_0 \vec{I} \cdot \vec{S} \quad (3.21)$$

where for simplicity it was neglected the anisotropy of \underline{g} , as well as the (usually minor) nuclear Zeeman term, which describes the interaction between \vec{I} and \vec{B} . Although the treatment proposed here is actually too simplified to thoroughly describe several practical cases of interest, it permits to evidence the main consequence of an hyperfine interaction on the observed ESR spectrum: a splitting of the resonance line in a multiplet of $2I+1$ lines, corresponding to the possible values of the quantum number M_I of the z component of I . At the first order in A_0 , the positions of the resonances are:

$$B_z = \frac{\hbar\omega_0}{g\beta} + \frac{A_0}{g\beta} M_I \quad \text{with} \quad M_I = -I, -I+1, \dots, I-1, I \quad (3.22)$$

When an ESR signal comprises an observable hyperfine interaction, this results to be a very powerful instrument to elucidate the structure of the defect. Indeed, for different isotopes of the same atom, the number of lines in the multiplet depends on the nuclear spin I , and their separation parameter A_0 is proportional to the nuclear magnetic moment: in this way, the nucleus responsible for the hyperfine interaction can be unambiguously identified by experimentally observing how the splitting (3.22) varies in an isotopically-enriched sample.¹ For instance, by substitution of hydrogen ($I=1/2$) with deuterium ($I=1$), it was possible to clarify that the characteristic hyperfine splitting of the ESR signals of the H(I) ($=\text{Si}^\bullet - \text{H}$) and H(II) ($=\text{Ge}^\bullet - \text{H}$) centers in $a\text{-SiO}_2$ is a consequence of the interaction of the unpaired electron with a hydrogen nucleus, thereby demonstrating in a straightforward way the presence of this impurity in the chemical structure of the defect.⁹⁶⁻⁹⁹ Moreover, it can be demonstrated that in the case of *non-isotropic* hyperfine interaction, the parameters of the \underline{A} tensor convey detailed information on the wave function of the electron and its symmetry properties, which can be extracted on the basis of simple models. For instance, by this method it was demonstrated that the unpaired electron of the E' center resides in a sp^3 orbital of a 3-fold coordinated Si atom, thus giving valuable information on the structure of the defect.¹

It is worth noting that also taking into account anisotropy, site-to-site inhomogeneity, and hyperfine interactions, it remains valid the property that the above defined parameter Γ' (doubly-integrated intensity of the ESR spectrum far from saturation, divided by B_x and A_m) is *proportional*

to the number N of paramagnetic centers. In this sense, if a reference sample is available, ESR may be used to provide a measurement of the absolute concentration $\rho = N/V$ of every paramagnetic defect, where V is the volume of the sample.

Part II

Experiments and Results

Chapter 4

Materials and experimental setups

This chapter is concerned with the description of the materials, instruments, and setups, used to perform the experiments discussed in the rest of the work.

4.1 Silica samples

As discussed in Part I of this Thesis, the effects induced by irradiation on α -SiO₂ are often found to be strongly dependent on the manufacturing procedure of the material. In fact, the history of the sample determines the nature and the concentration of pre-existing defects, which may get involved in the processes triggered by radiation. For this reason, in this section we provide information on the samples used in this work.

The specimens involved in our experiments were all of commercial origin, produced by *Heraeus QuarzGlas* and *Quartz & Silice*. An important advantage of commercial samples is that their properties are highly reproducible, since they are manufactured by standardized industrial techniques. Even though commercial silica specimens have been investigated for a long time, in the following chapters we are going to see that significant new information can still be extracted by them by careful experimental work. Commercial samples are usually classified in four categories following the scheme described below.^{215,216}

Natural dry (Type I): Samples produced from natural quartz powder, which is melted by an electric arc in an inert atmosphere and then cooled down to get the amorphous material. These materials feature relatively low (or the order of ~ 10 Parts Per Million [ppm] in weight) concentrations of Si–OH impurities, which is the reason for the name "dry". Usually they contain also significant concentrations (>1 ppm) of extrinsic impurities, mainly metallic, already present in the starting material (quartz). Ge, Al, and alkali are the most common.

Natural wet (Type II): Similar to natural dry, but the melting is performed by a H₂/O₂ flame. Due to the composition of the flame, a higher concentration of Si–OH groups (~ 100 ppm) is incorporated in these materials than in dry silicas. Also here extrinsic impurities are usually present in significant

concentrations.

Synthetic wet (Type III): Produced by oxidation of suitable compounds of Si (typically SiCl_4) in a H_2/O_2 flame. So-produced silica contains a high concentration of Si–OH due to the hydrogen present in the flame. Synthetic $\alpha\text{-SiO}_2$ contains lower concentrations of extrinsic elements with respect to natural samples due to the higher purity of the starting compounds.

Synthetic dry (Type IV): Produced by oxidation of SiCl_4 in a water-free-plasma so as to obtain a low concentration of Si–OH. For what concerns extrinsic elements, these materials usually retain relatively high concentrations of chlorine ($[\text{Cl}]\sim 100$ ppm).

In our experiments we used representatives of each of the four types of $\alpha\text{-SiO}_2$. In Table 4.1 are reported the commercial nicknames of the used samples and the content of some impurities.^{236–238}

Name	Nickname	Type	TMI[ppm]	[Si–OH][cm^{-3}]	[Ge][cm^{-3}]
Infrasil 301	I301	I	~ 20	6.2×10^{17}	$< 0.8 \times 10^{16}$
Silica EQ 906	Q906	I	~ 25	1.6×10^{18}	$(1.4 \pm 0.3) \times 10^{16}$
Herasil 1	HER1	II	~ 20	1.2×10^{19}	$(1.6 \pm 0.3) \times 10^{16}$
Suprasil 1	S1	III	< 1	7.8×10^{19}	$< 10^{15}$
Suprasil 300	S300	IV	< 1	$< 8 \times 10^{16}$	$< 10^{15}$

Table 4.1: Materials used in our experiments, representative of the four categories (defined above) of commercial $\alpha\text{-SiO}_2$. Ppm stands for Parts Per Million (in weight) while TMI stands for Total Metallic Impurities. Silica Q906 is produced by *Quartz and Silice*, while the other 4 materials are produced by *Heraeus*

The reported total concentrations of both metallic impurities and Si–OH are nominal values provided by the manufacturer,^{237, 238} but the latter were subsequently verified by IR spectroscopy.²³⁶ The concentrations of Ge were estimated in previous works²³⁶ by using the *neutron activation* technique: the samples are bombarded with fast neutrons in a nuclear reactor, and Ge impurities become unstable isotopes by trapping neutrons^a; then, the presence and the concentration of Ge is inferred by observing the emission of γ radiation at a characteristic energy that is peculiar of the nuclear decay of a Ge isotope.

The samples were received in slabs of sizes $5 \times 50 \times 1 \text{ mm}^3$ (or $5 \times 50 \times 2 \text{ mm}^3$), optically polished only on the largest surfaces, of sizes $5 \times 50 \text{ mm}^2$, apart from HER1 samples, which were optically polished on all surfaces. Prior to any experiment, they were cut in pieces of size $5 \times 5 \times 1 \text{ mm}^3$ or $5 \times 5 \times 2 \text{ mm}^3$. All the specimens presented no ESR signals before irradiation, as checked by preliminary measurements. Actually, for reasons that will be clear in the following, most of the results presented in this Thesis were obtained from experiments on *natural* silica samples. These materials will be also equivalently indicated with the common expression *fused silica*.

^aIn particular, ^{75}Ge and ^{77}Ge are formed by neutron trapping on the naturally occurring isotopes ^{74}Ge and ^{76}Ge , respectively.²³⁶

4.2 Irradiations and *in situ* optical measurements

To investigate the effects of laser irradiations on α -SiO₂, contextually to this work it was set up an *ad hoc* experimental system suitable to perform *in situ* optical absorption (OA) measurements during laser irradiations. A scheme of the experimental station is reported in Figure 4.1. The main components are a Nd:YAG laser system, an optical fiber spectrophotometer and a cryostat, plus a variety of accessory elements, all mounted on a standard optical table.

4.2.1 The Nd:YAG laser system

The Q-switched Nd:YAG laser (Quanta System SYL-201) emits pulses of 5 ns duration and wavelength $\lambda_0=1064$ nm with a 1-20 Hz repetition rate. The active medium is a Nd:YAG rod 10 mm long and 7 mm in radius, pumped by a pulsed Xe discharge lamp. To achieve Q-switching, the laser cavity is engineered in such a way that the quality factor Q remains very low for most of the time, and is increased only when a strong electric pulse is applied to an electro-optic crystal (Pockel cell, PC) within the cavity, which acts like a switch. When the PC is not polarized, Q is low and a population inversion is obtained by pumping, without any laser oscillations. Then, when the PC is activated, the sudden increase of the Q factor causes the onset of laser action with a strong initial inversion, resulting in the build up of an intense pulse that in a few ns dissipates all the energy stored in the active medium. More details on the principle of Q-switching used to obtain short laser pulses can be found in many bibliographic references.^{239–241}

A nonlinear KD*P (KH₂PO₄) birefringent crystal (NLC₁ in Figure 4.1) is used to perform frequency up-conversion, generating a second harmonic signal at $\lambda_0/2=532$ nm. A further BBO (β -BaB₂O₄) crystal (NLC₂) is used to generate the fourth harmonic at $\lambda_0/4=266$ nm, corresponding to a photon energy of 4.7 eV. The nonlinear conversion process critically depends on the relative orientation of the polarization axis of the incident beam and the NLC₁ and NLC₂ axes. The maximum efficiency is obtained when a condition known as *phase matching* is verified, which assures that the phase velocities of the frequency-doubled and the fundamental waves are the same within the crystal.¹²⁵ For this reason, the laser includes a system that allows to finely rotate (*tune*) separately each of the nonlinear crystals in order to maximize the intensity either of the II or of the IV harmonic beams. The maximum laser energies per pulse are 600 mJ, 280 mJ and 65 mJ, for the I, II, IV harmonic beams respectively. The pulse energy can be controlled by varying the voltage applied on the pumping lamp.

In all the experiments reported in this work, only the IV harmonic UV laser beam was used to irradiate the silica samples. Indeed, preliminary data had shown that the IR I-harmonic and the visible II harmonic have negligible effects on the as-grown samples. Since the output of the laser comprises the I, II and the IV harmonic, a pair of dichroic mirrors (DM₁ and DM₂) is used to reflect selectively the IV harmonic (LB[IV]) towards the sample position. The diameter d_b of LB[IV] can be regulated by an iris (I) from (1.0 ± 0.1) mm up to (6.0 ± 1.0) mm, and an electronic shutter (S) is present on the beam path, permitting to start and end the irradiation session from remote. The

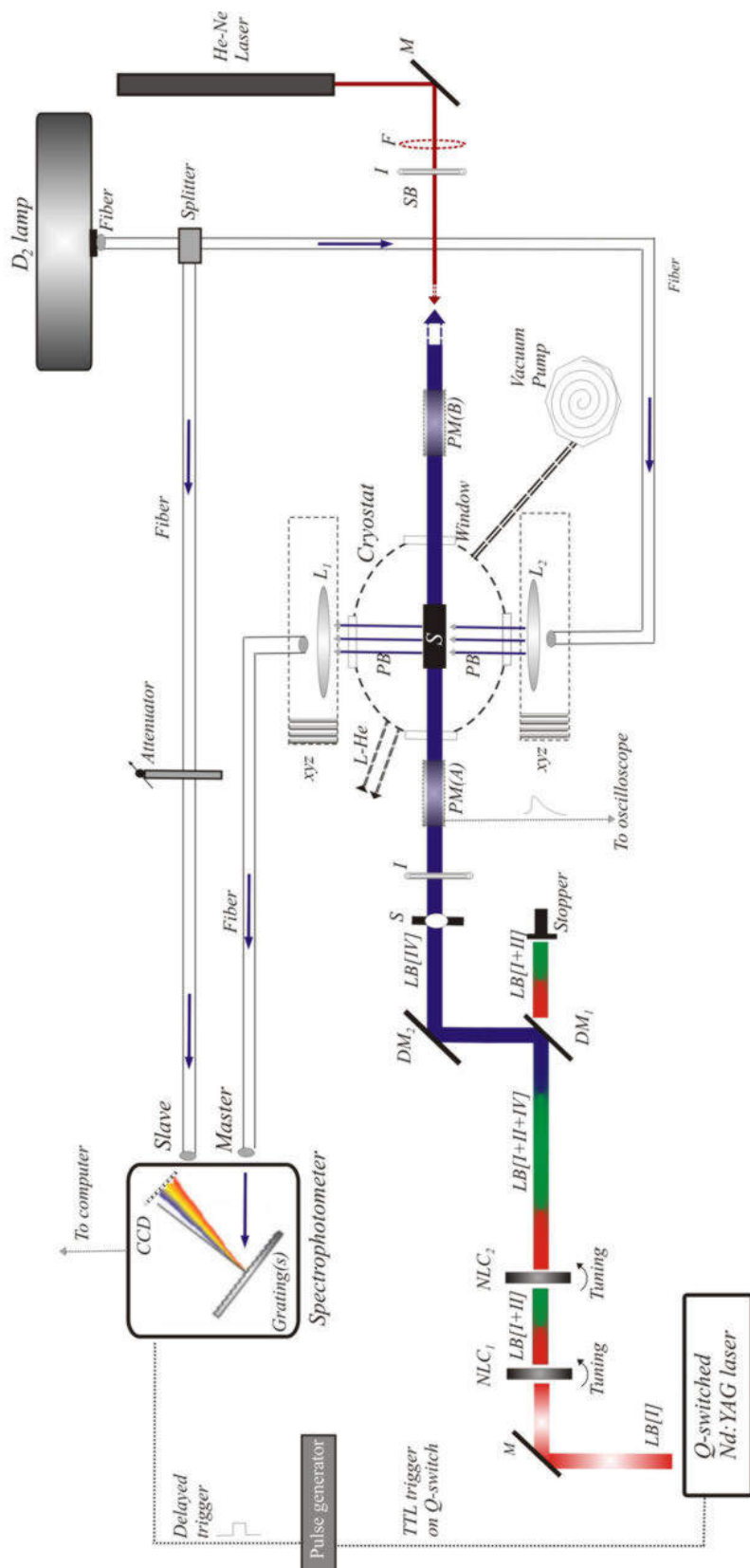


Figure 4.1: Scheme of the experimental station used for Nd:YAG laser irradiations and *in situ* optical absorption measurements. M=Mirror, I=Iris, F=Filter, S=Shutter, NLC = nonlinear crystal, DM = dichroic mirror, LB=laser beam, PM = power meter, S=Sample, PB = probe beam, L= Lens, xyz = micrometric translation stage

beam is unfocused and has an uniform intensity profile, as inferred by verifying that the pulse energy measured after the iris is proportional to d_b^2 .²⁴¹

The irradiation beam enters the cryostat and hits the sample (S) on one of its minor surfaces (5 mm×1 mm). A secondary continuous He:Ne laser is positioned in such a way that it shares a portion of the optical path of the primary beam; its beam (SB) is used to check the alignment of the sample with the 4.7 eV laser beam.

The energy of the laser pulses is measured either with a bolometer or with a pyroelectric detector connected to an oscilloscope, with consistent results. The bolometer measures the mean incident power of the Nd:YAG IV harmonic beam, based on the heating produced upon absorption of the laser light. The pyroelectric detector responds to each laser shot giving in output a short (μ s) electric pulse, whose amplitude is proportional to the energy of the shot; in particular, this detector allows to estimate pulse-to-pulse intensity fluctuations. Each of the two power meters can be positioned either before the sample (PM(A)), to measure the laser intensity before an irradiation begins, or after the sample (PM(B)), to check the stability of laser intensity during long irradiations. The accuracy of pulse energy measurements with the pyroelectric detector is $\sim 5\%$.

4.2.2 The optical fiber spectrophotometer

Optical absorption spectra are performed with an optical fiber AVANTES S2000 spectrophotometer. The optical source is a deuterium lamp that injects light into an optical fiber that splits up in two channels, referred to as *Master* and *Slave*, each 2 m long from source to detector. The optical fibers are multimode pure silica core/F₂-doped silica cladding with diameter of 200 μ m. They are loaded with H₂ to better resist to the prolonged exposure to UV light without being deteriorated.

The light carried by the *master* channel gets out of the fiber and is used as the probe beam (PB). The PB is collimated by a lens (L₁) so as to have a ~ 3 mm diameter; then, it passes through the cryostat windows and arrives on the larger surface of the sample (5×5 mm²). The typical intensity of the PB is $\sim 2 \mu$ W. The transmitted portion of the PB is collected from a second lens (L₂) coupled to another fiber that brings it to the detector. The two lenses are mounted on independent micrometric positioning controls (xyz), which permit both to control the alignment of the PB to the sample and to optimize the collection efficiency after the sample. The *slave* channel passes through a variable attenuator, after which it goes to the detector. Since the slave channel does not traverse the sample, it can be used to correct experimental data for the temporal drift of the lamp when monitoring on the master channel the kinetics of laser-induced OA.

The detector consists in a 1200 lines/mm grating with blaze at 300 nm, dispersing on a 2048 channels Charge Coupled Device (CCD) array. For the two channels are used two different gratings, virtually identical, but a single CCD detector. The latter is coated with a fluorescent compound ("lumogen" coating) to enhance its sensitivity in the UV. The instrument works in the 200 nm–500 nm range with a spectral resolution of 5 nm. It is worth noting that such a relatively low resolution is usually sufficient to study the absorption bands of point defects in *a*-SiO₂, usually very broadened

by both homogeneous and inhomogeneous effects.¹ The detector features a minimum integration time of 3 ms. Including also the time required to transmit to the acquisition system, the instrument takes about 20 ms to perform a complete measurement of the intensity profile $I(\lambda)$ of the light carried by each channel.

We describe now the **experimental procedure** used to perform time dependent absorption measurements *in situ* during and after the end of a laser irradiation. First, the D₂ lamp is disconnected from the fibers and it is acquired a *dark* reference signal on both channels: $D^M(\lambda)$ (master) and $D^S(\lambda)$ (slave). Then, the lamp is connected again; at a time t_0 just before the irradiation begins, a reference signal is acquired for both channels, $I^M(\lambda, t_0)$ (master) and $I^S(\lambda, t_0)$ (slave). Finally, the Nd:YAG laser is turned on (or the shutter S is open) and the irradiation begins. Using an electronic signal provided by the laser concurrently to each Q-switching, a delayed pulse is produced that triggers the spectrophotometer so as to perform measurements only during the time span separating one laser pulse and the successive one (*interpulse*). In this way, it is avoided that scattered laser light may be detected by the CCD altering the measurements. Defining $I^M(\lambda, t)$ (master) and $I^S(\lambda, t)$ the signals acquired at time t by the detector, the *difference absorption induced in the sample by the irradiation* after t is calculated as:

$$\Delta OD(t) = \log_{10} \left(\frac{I^M(\lambda, t_0) - D^M(\lambda)}{I^M(\lambda, t) - D^M(\lambda)} \right) - \log_{10} \left(\frac{I^S(\lambda, t_0) - D^S(\lambda)}{I^S(\lambda, t) - D^S(\lambda)} \right) \quad (4.1)$$

this equation is valid in the approximation in which the dark signal does not depend on time, which results to be a very good one. In eq. (4.1), the first term already represents the difference absorption induced in the sample between t_0 and t . The subtraction of the second term, formally identical apart from being estimated from the slave channel, allows to correct for the temporal drift of the lamp and/or the detector; the correction is necessary since this is a *single beam* system in which the acquisition of the reference is performed only once, at the time t_0 . It is worth noting that the validity of this procedure is necessarily limited by the fact that the drift of the two channels are not, in general, perfectly identical. For this reason, the stability of the *corrected* ΔOD calculated by eq. (4.1) was checked by a test experiment: a not-irradiated sample was monitored for many hours while keeping the laser off; in this way, it was obtained that $\Delta OD(t) < 5 \times 10^{-4} \text{OD/hour}$.

The system can be used also to perform standard *ex situ* absolute absorption measurements, by the following procedure. Two signals are acquired without ($I_0(\lambda)$) and with ($I(\lambda)$) the sample in the probe beam; hence, the absorption profile of the specimen is given by

$$OD = \log_{10} \left(\frac{I_0(\lambda) - D(\lambda)}{I(\lambda) - D(\lambda)} \right) \quad (4.2)$$

Finally, an additional spectrophotometer (JASCO-V560) was used to perform *ex situ* optical absorption measurements on the irradiated samples after removal from the irradiation site. The instrument is a traditional double beam spectrophotometer based upon a D₂ discharge lamp source, a photomultiplier tube detector, and a double monochromator (two gratings with 1200 lines/mm) on the excitation side, which allows to reduce stray light to 0.0003%. Measures with this instruments were performed with a spectral resolution of 2 nm. The optical absorption profiles obtained with the JASCO spectrophotometer are consistent with those detected with the optical fiber instrument.

4.2.3 The cryostat

To perform temperature-controlled experiments, the samples are placed in a continuous liquid Helium flow cryostat (Optistat CF-V) produced by Oxford Instruments working between 4 K and 500 K. The cryostat mounts four synthetic silica windows, reasonably transparent to the UV laser and the probe beams. A two stage rotary/turbomolecular pump (Leybold Vacuum PT 50) is used to achieve high vacuum in the cryostat by overnight pumping (base pressure $\sim 10^{-6}$ mbar). Helium is picked up from a storage dewar by a standard transfer tube and delivered within the cryostat just above the sample holder. Thermal equilibrium within 1 K at the working temperature is achieved by a Oxford-ITC503 instrument, which controls the He flow and the electric current input on a resistor, positioned near the sample holder as well, and acting as a heating element. The experiments started after a delay of ~ 1 hour after reaching each nominal operative temperature, to allow for thermal equilibrium. The cryostat is equipped with an aluminum radiation shield that grants a better thermal isolation of the sample. In addition, in this context the use of the radiation shield is important also to reduce undesired condensation of the residual gases present in the vacuum chamber on the sample surfaces. Indeed, insufficiently clean surfaces may compromise the results of the experiments because laser-induced removal of the condensed film can result in fake negative absorption signals during *in situ* OA measurements under Nd:YAG irradiation.

4.3 Photoluminescence measurements

4.3.1 The instrument

Stationary PL measurements were carried out by a JASCO FP-6500 spectrofluorometer, whose scheme is reported in Figure 4.2. The light emitted by the excitation source (a 150W Xenon discharge lamp) is dispersed by a monochromator (MONO-I), based on a grating with 1800 lines/mm, which permits to select the excitation wavelength λ_0 with variable bandwidth $\Delta\lambda_0$. The monochromatized excitation light is then directed on the sample, which is positioned in a standard 45° backscattering geometrical configuration. The emitted luminescence signal is collected by a second monochromator (MONO-II, 1800 lines/mm) which selects the emission bandwidth λ_e with variable bandwidth $\Delta\lambda_e$. Finally, the emitted photons are detected by a photomultiplier (PMT) giving an output signal $S_R(\lambda_0, \lambda_e)$. The instrument includes a feedback system that corrects the measurements for the temporal fluctuations of the source intensity: to this end, a beam splitter (BM) separates a portion of the excitation light from the main beam and directs it on a secondary PMT (F-PMT), which measures its intensity; hence, the signal detected by the primary PMT is automatically rescaled by the so-obtained reference signal.

Two basic types of measurements are possible: **(i)** the *emission* spectrum, in which $S_R(\lambda_0, \lambda_e)$ is measured as a function of λ_e for fixed λ_0 . This type of acquisition aims to measure the spectral shape and intensity of the band emitted by the center while decaying from the upper electronic state (see Figure 3.1). **(ii)** The *excitation* spectrum, in which $S_R(\lambda_0, \lambda_e)$ is measured as a function of λ_0

for fixed λ_e , representing a measurement of the efficiency of the emission process in dependence of the excitation wavelength.

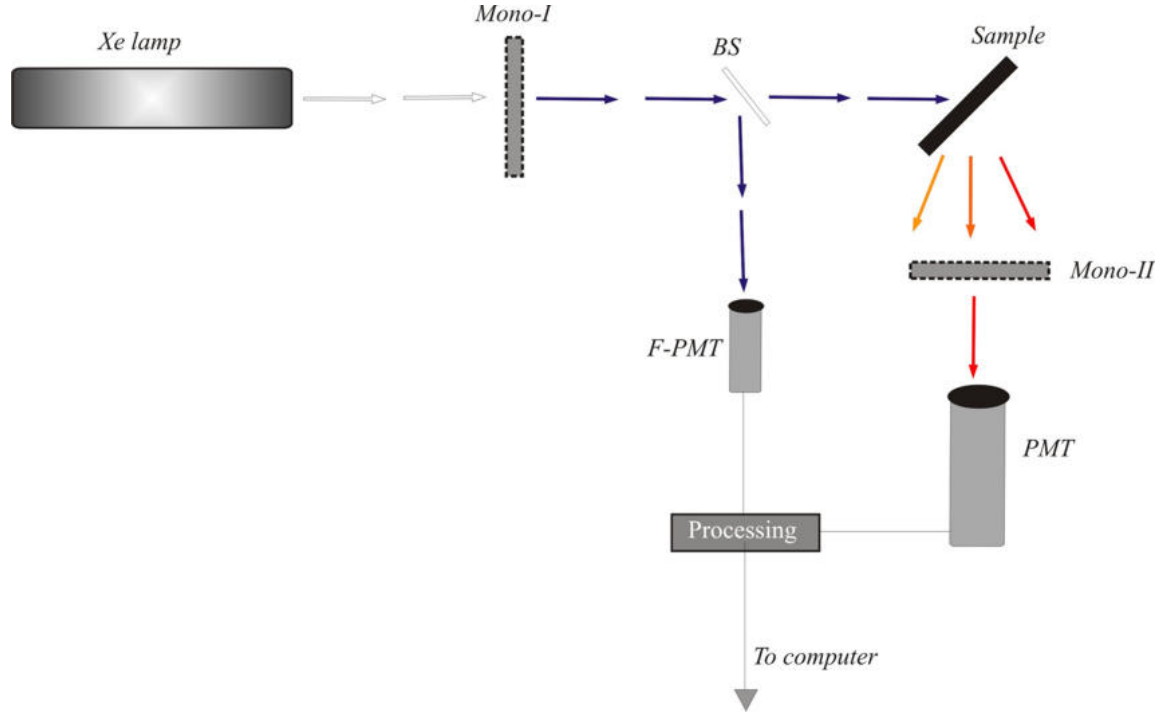


Figure 4.2: Idealized scheme of the spectrofluorometer JASCO-FP 6500

4.3.2 Correction procedures

Luminescence measurements require specific correction procedures before they can be related to physically meaningful quantities. Let us start with considering a thin sample of width dx containing a concentration ρ of identical^b luminescent centers. We express as $\Omega = \Delta\lambda_0 \times [dI_0(\lambda_0)/d\lambda_0]$ the excitation intensity, meaning the number of photons from the source illuminating the sample per unit time. If $\sigma(\lambda_0)$ is the absorption cross section of the defects, the number of absorbed photons per unit time is given by $\rho\Omega\sigma(\lambda_0)dx$. Therefore, recalling the definition of the luminescence quantum yield (section 3.1) η , the number of photons emitted per unit time by the sample with wavelength between λ_e and $\lambda_e + \Delta\lambda_e$ (i.e. the spectral density of the emitted light) is given by:

$$\frac{dI_e}{d\lambda_e}(\lambda_0, \lambda_e)\Delta\lambda_e = \rho\Omega\Delta\lambda_e\eta\sigma(\lambda_0)\Phi(\lambda_e)dx \quad (4.3)$$

where $\Phi(\lambda_e)$ represents the normalized emission lineshape function, which for simplicity we have supposed to be independent of λ_0 .

For a sample of finite thickness d , we substitute Ω in the last equation by $\Omega = \Omega_0 \exp[-\alpha(\lambda_0)x]$, namely the dependence of the excitation intensity on the position x through the sample. Here, $\alpha(\lambda_0)$

^bin the following treatment we are going to suppose a population of identical homogeneous defects, thereby neglecting inhomogeneity effects, common in amorphous silica.^{163–165, 242} However, this approximation does not alter the main conclusions of this subsection.

is the *overall* absorption coefficient, to which in general may contribute also other centers. Then, we integrate on x . In this way we obtain the generalization of eq. (4.3):

$$\frac{dI_e}{d\lambda_e}(\lambda_0, \lambda_e)\Delta\lambda_e = \Omega_0\Delta\lambda_e\eta [1 - \exp(-\alpha(\lambda_0)d)] \frac{\sigma(\lambda_0)\rho}{\alpha(\lambda_0)}\Phi(\lambda_e) \quad (4.4)$$

Now, the measured *raw* signal $S_R(\lambda_0, \lambda_e)$ is proportional to eq. (4.4) multiplied by the spectral response $R_d(\lambda_e)$ of the detecting system (MONO-II + PMT). Furthermore, the action of the feedback system is to substitute Ω_0 (which could be time-dependent due to fluctuations in the lamp) with a term $R_f(\lambda_0)$ expressing the spectral response of the BS plus the F-PMT. Eventually we get:

$$S_R(\lambda_0, \lambda_e) \propto \Delta\lambda_e\eta [1 - \exp(-\alpha(\lambda_0)d)] \frac{\sigma(\lambda_0)\rho}{\alpha(\lambda_0)}\Phi(\lambda_e) \frac{R_d(\lambda_e)}{R_f(\lambda_0)} \quad (4.5)$$

Therefore, to obtain from the raw signal a meaningful physical quantity, it is necessary to divide for $R_d(\lambda_e)$ and multiply for $R_f(\lambda_0)$.^c These two corrections *were performed for all the luminescence data reported in this Thesis*, based upon the measurement of R_d and R_f performed as follows: $R_f(\lambda_0)$ can be estimated (apart from an arbitrary factor) by performing an excitation spectrum on a sample whose luminescent centers feature high absorption ($\sigma(\lambda_0)\rho d \gg 1$) and a quantum yield independent of λ_0 . In fact, in this case the term within squared parentheses in (4.5) may be approximated to unity; moreover, if no other absorbing centers are present in the sample, $\sigma(\lambda_0)\rho/\alpha(\lambda_0) = 1$. In these conditions, eq. (4.5) becomes (retaining only the terms that depend on λ_0):

$$S(\lambda_0) \propto \frac{1}{R_f(\lambda_0)} \quad (4.6)$$

thereby allowing to estimate R_f from an excitation spectrum performed in these conditions. For this purpose it was used a sample of Rhodamine B (in glycerol), which emits at 640 nm and can be excited from 220 nm to 600 nm with a constant (near to 1) quantum yield.²⁴³ To measure $R_d(\lambda_e)$, a mirror was put in the instrument, redirecting the excitation light to the detecting system. Then, an acquisition (*synchronous* spectrum) was performed while keeping $\lambda_0 = \lambda_e$. If we assume that the reflection efficiency of the mirror is independent of λ , it is easy to see that the signal measured in this conditions can be expressed by:

$$S(\lambda) \propto \frac{R_d(\lambda)}{R_f(\lambda)} \quad (4.7)$$

from which it can be derived $R_d(\lambda)$ if $R_f(\lambda)$ has already been measured.

Using these two procedures to eliminate R_d and R_f from eq. (4.5), the corrected signal $S_C(\lambda_0, \lambda_e)$ is finally given by:

$$S_C(\lambda_0, \lambda_e) = y\Delta\lambda_e\eta [1 - \exp(-\alpha(\lambda_0)d)] \frac{\sigma(\lambda_0)\rho}{\alpha(\lambda_0)}\Phi(\lambda_e) \quad (4.8)$$

where the proportionality constant y accounts for geometrical factors that result in a partial collection of the light emitted by the sample.

^cIf one is interested only in the *lineshape*, it is sufficient to divide for $R_d(\lambda_e)$ the raw emission spectra and to multiply for $R_f(\lambda_0)$ the raw excitation spectra

When the absorbance of the sample at the excitation wavelength is low ($\alpha(\lambda_0)d \ll 1$), the last equation can be approximated as follows:

$$S_C(\lambda_0, \lambda_e) = y\Delta\lambda_e\eta\sigma(\lambda_0)\rho d\Phi(\lambda_e) \quad (4.9)$$

As apparent from eq. (4.9), in conditions of low absorbance the intensity of the corrected signal *is proportional to the concentration* ρ of the luminescent centers. It is worth noting that this is untrue in the general case (4.8) because ρ indirectly contributes also to $\alpha(\lambda_0)$ appearing in the exponential term.

Finally, let us focus now on an emission measurement, where λ_0 is kept fixed and λ_e is scanned. As the only term in eq. (4.9) depending from λ_e is $\Phi(\lambda_e)$, we see that after the correction procedure, the *shape* of the corrected emission spectrum resembles the spectral density of the emitted light. Furthermore, comparing with eq. (4.8) we observe that this property in itself does not depend on the low absorbance hypothesis.^d The precision of the measurement of S_C is $\sim 10\%$, being mainly limited by the repeatability of the mounting conditions. From the physical point of view, it is usually preferable to report the spectral density of the emission bands as a function of photon energy $E_e = hc/\lambda_e$, instead of using the wavelength λ_e . To this purpose, the following transformation must be applied:

$$\frac{dI_e}{dE_e} = \frac{dI_e}{d\lambda_e} \left| \frac{d\lambda_e}{dE_e} \right| \propto \lambda_e^2 \frac{dI_e}{d\lambda_e} \quad (4.10)$$

Due to (4.10), all the emission spectra reported in this Thesis (after scaling for $R_d(\lambda_e)$) were further corrected by multiplication for λ_e^2 , before changing the independent variable to E_e . In literature this is usually called correction for the *dispersion* of the detecting system.

4.3.3 Time-resolved photoluminescence measurements

The luminescence decay measurements reported in this work were performed at the I-beamline of SUPERLUMI station at DESY, Hamburg, under excitation by 130 ps synchrotron radiation pulses. The excitation pulses were monochromatized with a bandwidth of 0.3 nm. The emitted light was acquired by a photomultiplier (Hamamatsu R2059) with a time resolution of 0.02 ns and an emission bandwidth of 5 nm. Temperature was varied from 8 K to 300 K by a Helium-based continuous flow cryostat.

4.4 Electron spin resonance measurements

4.4.1 The instrument

The ESR measurements reported in this Thesis were performed by a Bruker EMX spectrometer working at $\omega_0=9.8$ GHz. In Figure 4.3 it is reported a simplified scheme of the instrument. The sample

^dAlso, the corrected excitation spectrum reproduces the shape of the absorption spectrum; this property, however, is true *only* in the case of low absorbance.

is positioned in a resonant cavity, fed by a waveguide transporting microwaves produced by a Gunn Diode source. A variable attenuator permits to regulate the actual power P_i incident to the cavity from a maximum value 200 mW down to 200 nW; In this way, P_i is usually chosen so as to avoid the saturation of the observed magnetic resonance transition.^e The microwaves arriving on the entrance of the cavity are partially reflected and partially transmitted. The reflected power P_R is measured by a detector that gives a current signal I proportional to the square root of P_R . Indicating with B_R the magnetic field amplitude of the reflected microwaves, we have: $P_R \propto B_R^2$, so that $I \propto B_R$. The cavity is positioned within the polar expansions of an electromagnet, which permits to generate a static magnetic field B_z up to 10^4 G. The magnetic field B_i of the incident microwave field is perpendicular to B_z .

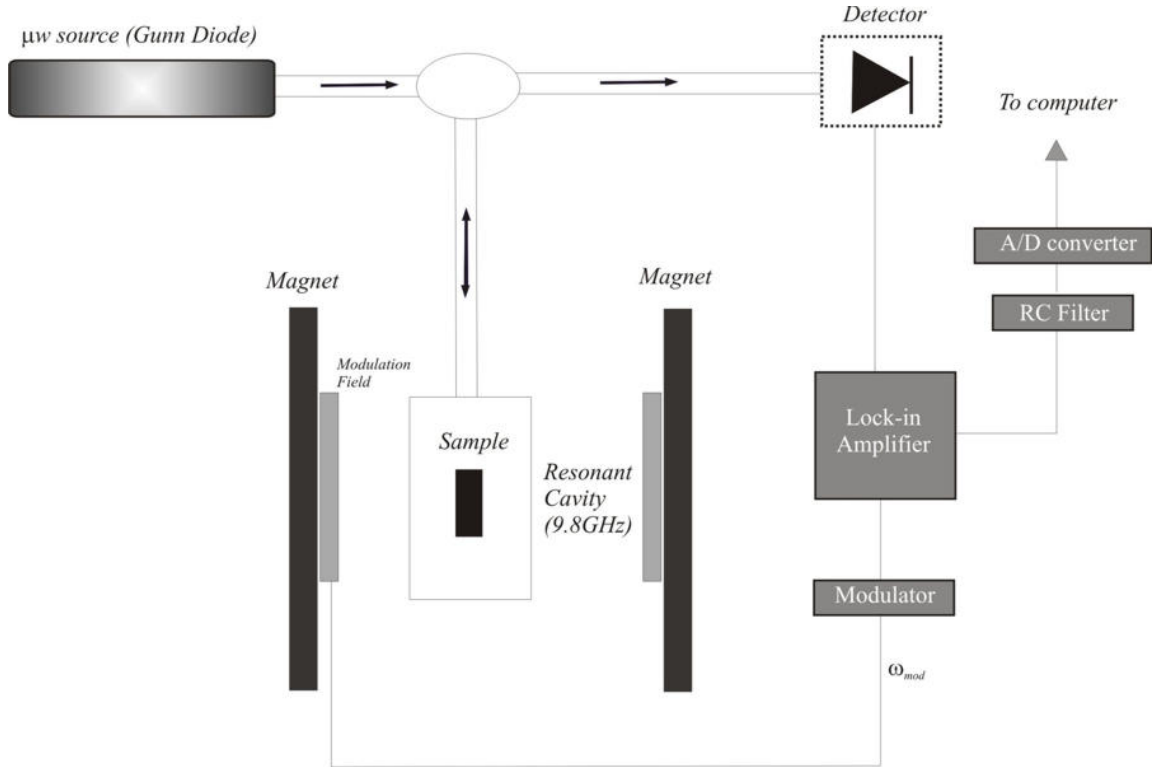


Figure 4.3: Idealized scheme of the Bruker EMX electron spin resonance spectrometer including only the most important elements.

In the typical measurement scheme, a static magnetic field interval of width $\Delta B_z^{sw} = B_z^{max} - B_z^{min}$ is swept in a time T_{sw} . At some value of the magnetic field the onset of the magnetic resonance condition causes the absorption of microwaves by the sample. It can be demonstrated that this leads to a variation $\Delta P_R \propto \Delta B_R^2$ of the reflected power, with $\Delta B_R \propto B_i \chi''$. Hence, we have $\Delta I \propto \Delta B_R \propto B_i \chi''$, so that the variation of the output detector current allows to measure the quantity $\chi'' B_i$. We take into account now the effects of modulation: to the static magnetic field is superimposed a modulation field with frequency ω_m and amplitude A_m . As a consequence of the

^eIn the following, we are going to report the ESR spectra of E' and H(II) centers (see chapter 1). Previous studies have demonstrated that the maximum not-saturating powers for these two defects are 3 mW and 8×10^{-4} mW respectively.²³⁶

modulation of B_z , $\chi''(B_z)$ is modulated as well. A necessary condition to avoid distortion in the measured signal is that A_m is chosen to be significantly smaller than the resonance linewidth. In these conditions, the following relation holds:

$$\begin{aligned}\Delta I \propto B_i \chi''(B_z) &= B_i \chi''[B_z^0 + A_m \sin(\omega_m t)] \\ &\sim B_i \chi''(B_z^0) + B_i \frac{d\chi''}{dB_z}(B_z^0) A_m \sin(\omega_m t)\end{aligned}\quad (4.11)$$

Therefore, the detector signal I has a component oscillating with frequency ω_m that is selectively detected by the *lock-in* acquisition system (see chapter 3), thus allowing for an increasing sensitivity if compared with detection of the non-modulated portion. Therefore, selecting in (4.11) only the component at ω_m , we conclude that the revealed signal is proportional to

$$\frac{d\chi''}{dB_z} B_i A_m \quad (4.12)$$

which is equivalent to eq. (3.17) because the oscillating field in the cavity, B_x , is proportional to the incident amplitude B_i . Finally, to reduce the signal to noise ratio, the last stage of the instrument comprises a RC filter, whose integration time τ_{RC} can be regulated by the user, and must verify the following relation

$$\tau_{RC} \ll T_{sw} \frac{\Delta B_{pp}}{\Delta B_z^{sw}} \quad (4.13)$$

where ΔB_{pp} is the width of the resonance line. This condition prevents from filtering out part of the signal together with the noise, thereby avoiding distortion of the measured lineshape.

4.4.2 Absolute concentration measurements

The precision of the *relative* concentration measurement Γ' (defined in section 3.2) in our experimental system, and in the typical acquisition conditions used throughout this work, is $\sim 10\%$, including both the effects of noise and of repeatability of the mounting conditions^f. Then, as anticipated in chapter 3, to convert this result to an *absolute* concentration measurement it is needed a reference sample. To this purpose, in this work it was used a specimen where the absolute number of E' centers (purposely generated by γ irradiation) was known by spin-echo measurements.^{236,244}

The expression *spin-echo* indicates the characteristic response of the transverse (perpendicular to \vec{B}) magnetization (\vec{M}_\perp) of a spin system submerged in a static magnetic field \vec{B} , to a sequence of two appropriately engineered microwave *pulses* separated by an interpulse time Δt . The phenomenon consists in a partial recovery after the second pulse of the coherence between the spins, which had been lost due to the inhomogeneous spreading of their resonance frequencies causing the decay of \vec{M}_\perp ; as a consequence of the recovery, after a time Δt from the second pulse it is observed a temporary increase (echo) of \vec{M}_\perp .^{218,236,244} By an appropriate experimental setup suitable to perform *transient* ESR spectroscopy,^{236,244} it is possible to measure the intensity of the echo signal as a function of Δt ,

^fThe 10% estimate refers to an ESR signal acquired with a reasonable signal/noise ratio, as it is the case for all the spectra analyzed in this work. When the signal is very noisy due to a very low concentration of defects, the precision can significantly drop below this value.

so as to study in particular its typical decay dynamics at low temperatures. A contribution to the decay arises from the spin-spin magnetic dipole interaction, whose strength is proportional to d^{-3} , where d is the mean spin-spin distance. Hence, the measurement of the decay time of the spin-echo signal permits to find d and the mean concentration $\langle \rho \rangle = d^{-3}$.^{236,244}

The accuracy of the absolute concentration measurements obtained by ESR, based on comparison with the spin-echo reference sample, is estimated as 20%. However, we stress that this error never explicitly appears when reporting in the following the uncertainties on the concentration measurements; indeed, the stated errors represent only the $\sim 10\%$ relative precision of the estimates. The reason for this choice is that the 20% uncertainty coming from spin-echo plays the role of a *systematic* error that affects in the same way all the concentration measurements reported throughout the Thesis.

4.5 Raman measurements

The Raman effect is the anelastic scattering of light (by a molecule or a point defect) due to emission or absorption of a vibrational quantum.^{126,245} If E_i is the energy of the incident photons, scattering at $E_s < E_i$ implies the excitation of a vibrational mode of energy $\hbar\omega = E_i - E_s$. A Raman spectrum consists of a plot of the scattered intensity as a function of ω . This spectroscopy allows to probe the vibrational modes of a molecule or a point defect, sometimes bearing some advantages with respect to common IR spectroscopy. For example, it can happen that a vibrational mode is Raman-active but non IR-active, or *vice versa*.^{126,245} In this Thesis we are going to report Raman measurements aimed to detect the Si-H vibration mode at 2250 cm^{-1} , which is difficult to see in IR due to the overlap with an intrinsic vibration of the α -SiO₂ matrix, but is more easily detectable by Raman spectroscopy.^{40,41} Measurements were performed by the group led by Prof. Y. Ouerdane at the TSI laboratory - Université Jean Monnet - Saint-Etienne (France), using an Argon laser source ($\lambda=488 \text{ nm}$) with P=1–2 W intensity and a photomultiplier detector.

Chapter 5

Effects induced on silica by 4.7eV laser radiation

This is the first of the five chapters in which the report and the discussion of our experimental results is organized. Here we describe and discuss qualitatively the basic defect-related phenomenology induced by 4.7 eV pulsed laser irradiation on amorphous silica, as observed by the combined use of several spectroscopic techniques.

5.1 Introduction

As discussed in detail in the introductory chapters, laser irradiation of amorphous silica triggers a complex landscape of processes manifesting themselves in alterations of the macroscopic properties of the material, and often related to laser-induced generation and transformation processes of point defects. In particular, many studies have investigated the generation of the dangling silicon bond (E') and of the dangling oxygen bond (NBOHC), namely two of the basic intrinsic point defects in α -SiO₂, while other works have focused on the effects of laser radiation on the defects related to Germanium impurities. A last class of processes of relevant scientific and technological interest is that of point defect conversions driven by diffusion of mobile chemical species; in fact, these effects may strongly condition the response of the material to irradiation, and some of their features are a fingerprint of the disordered structure of the amorphous solid. Despite the great amount of work devoted to understand this wide class of processes, the current understanding of many important aspects is mainly qualitative, and several relevant questions remain unanswered.

Starting from this chapter, we present the results of a series of experiments investigating the effects of pulsed UV laser irradiation on amorphous silica. In particular, we are going to show that in a subclass of silica materials, fused silica, 4.7 eV laser photons triggers an articulated landscape of point defect conversion processes, which involve both intrinsic and extrinsic point defects, and whose features permit to use this material as a model system to investigate some important aspects of laser-induced and diffusion-driven effects in α -SiO₂. In this chapter,^{246–250} we basically present

the phenomenology observed in our experiments, which is then discussed on a qualitative basis in order to introduce the main problems that we are going to thoroughly investigate in the rest of the work.

5.2 Optical properties of the as-grown samples

The experiments described throughout this Thesis were carried out on 4 types of silica samples (Table 4.1). The purpose of this section is to introduce the optical properties of the as-grown materials.

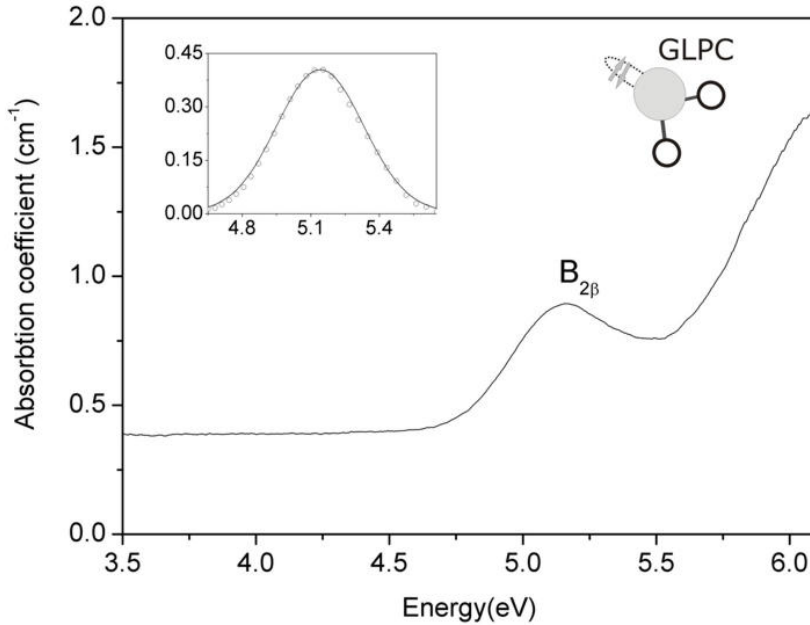


Figure 5.1: Absorption spectrum of an as-grown natural dry I301 silica sample. The main detected signal is the $B_{2\beta}$ band associated to the twofold coordinated Ge center, $=\text{Ge}^{\bullet\bullet}$ (GLPC), represented in the upper right corner. After proper baseline subtraction (the background is representable as the tail of a band peaked at $E > 6$ eV), the $B_{2\beta}$ band is well reproduced by a Gaussian shape (inset)

A typical absorption spectrum of a *natural dry* α - SiO_2 sample in the UV range prior to any treatment, is reported in Figure 5.1. The main detected signal is a band ($B_{2\beta}$ band¹³⁵) peaked at (5.13 ± 0.02) eV with (0.45 ± 0.03) eV Full Width at Half Maximum (FWHM). The area of the band is (0.19 ± 0.02) cm^{-1}eV both for the I301 and Q906 natural dry samples. An analogous absorption profile is detected in as grown *natural wet* HER1 samples, where the intensity of the $B_{2\beta}$ band is (0.13 ± 0.02) cm^{-1}eV .

By exciting the $B_{2\beta}$ absorption, we detect a photoluminescence (PL) emission signal consisting in a band peaked at (3.14 ± 0.02) eV with $\text{FWHM} = (0.42 \pm 0.02)$ eV and a band peaked at (4.28 ± 0.02) eV

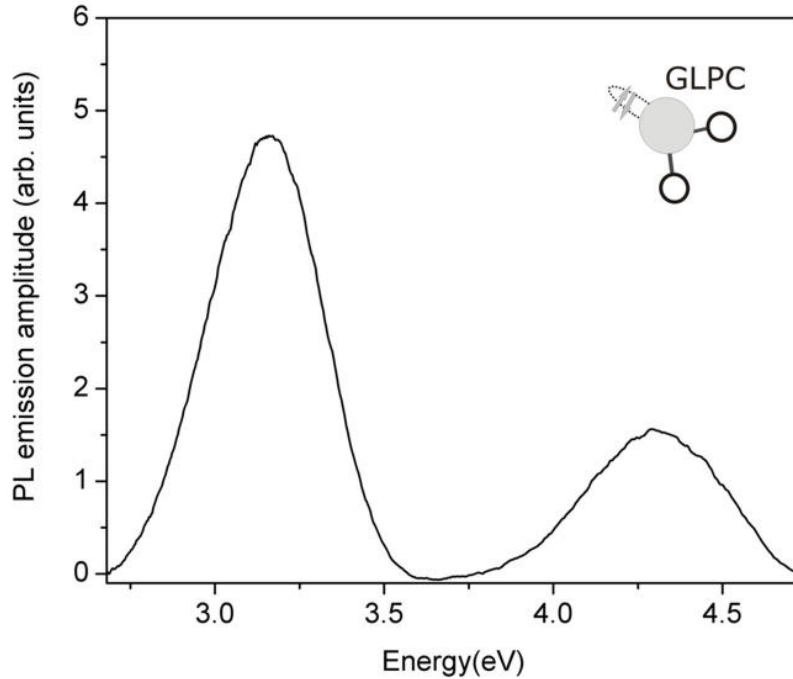


Figure 5.2: PL emission spectrum detected in an as-grown natural silica sample under excitation at 5.0 eV with 3 nm excitation and 3 nm emission bandwidths. The signal is due to the GLPC center represented in the upper right corner

with $\text{FWHM}=(0.46\pm 0.02)$ eV (Figure 5.2). In addition, the excitation spectrum (not reported) of both PL signals closely resembles the 5.1 eV absorption band in Figure 5.1.^{3,163,164,236}

In previous studies it was found a linear correlation between the intensities of the three bands (absorption and the two emissions), valid in a large number of commercial natural silica materials.¹⁶⁵ This evidence strongly suggests the overall optical activity to be due to a single defect. Then, from comparison of the spectroscopic features of the bands with literature, this optical activity can be ascribed to the Germanium Lone Pair Center (GLPC), consisting in a two-fold coordinated Ge impurity ($=\text{Ge}^{\bullet\bullet}$).^{3,93,163,164,166} The presence of this defect in the as-grown material is consistent with the independent observation of Ge impurities in natural silica by neutron activation measurements (see section 4.1 and references therein).^a

As already discussed in the introduction (see Figure 1.13), the 4.3 eV and 3.1 eV PL emissions are associated to the decay from the excited singlet (S_1) and triplet (T_1) electronic states to the

^aTo avoid confusion, it is worth clarifying a subtle difference in the notation we are using here with respect to that of subsection 1.2.3, where Ge-related defects were introduced. Indeed, we had originally used the symbol " $B_{2\beta}$ " to indicate generically the ~ 5.1 eV OA commonly detected in as-grown Ge-doped silica materials; in general, other defects besides GLPC (e.g. the Ge-related neutral oxygen vacancy, NOV) may contribute to this absorption. Now, since the as-grown optical activity of natural silica materials can be completely ascribed to GLPC, here and in the following we are going to use the symbol $B_{2\beta}$ to indicate more specifically only the absorption band at 5.13 eV of the GLPC center.

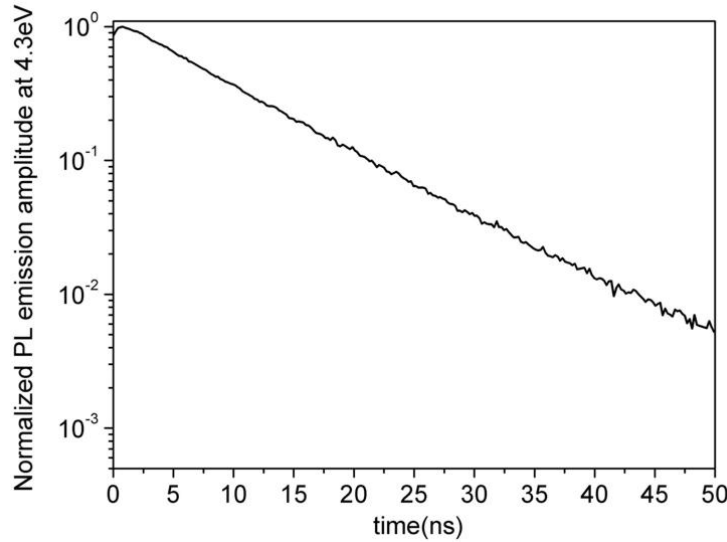


Figure 5.3: Decay curve of PL emission at 4.3 eV (maximum of the emission band) measured at 10 K after excitation with a synchrotron radiation pulse monochromatized at 5.00 eV (near the maximum of the excitation band).

ground singlet (S_0) state respectively. The luminescence activity of GLPC is further characterized by its radiative emission lifetime $\tau=7.8$ ns from S_1 ; τ is estimated by measuring at $T=10$ K the emission decay curve (Figure 5.3) after excitation with pulsed synchrotron radiation at 5.00 eV. It is worth noting that performing this measurement at low temperature is mandatory so as to quench the non-radiative decay channel from S_1 , which at higher temperatures alters the observed lifetime.²⁴²

Differently from natural silica, the native absorption profile of synthetic dry and wet α - SiO_2 samples in the same spectral region does not show any measurable absorption band. This is not surprising, given the lower concentration of impurities typical of synthetic α - SiO_2 with respect to natural silica (chapter 4).

5.3 *In situ* observation of the generation and decay of E' center

One of the main techniques employed in this work to investigate the effects of laser irradiation on α - SiO_2 is *in situ* optical absorption spectroscopy, carried out by the experimental apparatus described in detail in chapter 4. In a representative experiment, an as-grown sample is irradiated at room temperature by 4.7 eV pulsed (5 ns pulsewidth) radiation from a frequency-quadrupled Nd:YAG laser, using a 1 Hz repetition rate and a 40 mJcm^{-2} energy density per pulse. The total duration of the irradiation session is 2520 s. During and for a few $\sim 10^3$ s after irradiation, the absorption profile induced in the UV spectral range is monitored by the optical fiber spectrophotometer. In particular, during the irradiation session 10-20 spectra are collected and averaged during each interpulse time interval. The spectra are corrected for the temporal drift of the lamp using the second reference channel. Hence, we calculate the difference spectra with respect to the native absorption profile

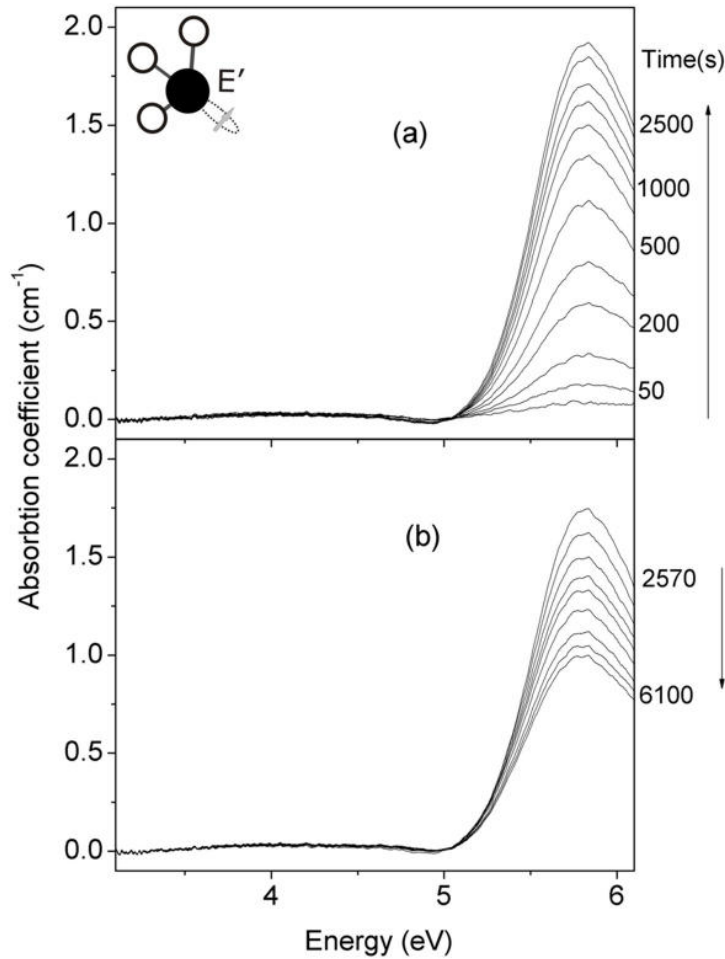


Figure 5.4: Induced OA measured *in situ* at different times during (a) and after (b) an irradiation session with 2520 laser pulses (4.7 eV photon energy, 5 ns pulsewidth, 1 Hz repetition rate, 40 mJcm⁻² energy density per pulse) of a natural dry I301 silica sample. The observed 5.8 eV absorption band is due to the E' center (represented in the upper left corner of panel (a)) induced in the sample by irradiation.

of Figure 5.1, at different times during and after the end of the exposure session: the results are reported in Figure 5.4.

The main detected signal is the band centered at 5.81 ± 0.02 eV with 0.71 ± 0.03 eV FWHM which, as widely known, is associated to one of the fundamental defects in α -SiO₂: the silicon dangling bond, known as E' center^{1-3,8} ($\equiv \text{Si}^\bullet$, see chapter 1). The peak amplitude of the induced band grows up to $(1.90 \pm 0.02) \text{cm}^{-1}$ during the irradiation session (panel (a)); then, as soon as the laser is switched off, we observe that the signal begins spontaneously to decrease with time (panel (b)), its reduction being $\sim 40\%$ in the first 3600 s. Many works in literature have discussed the generation of E' under laser irradiation, suggesting a variety of possible mechanisms, discussed in detail in subsection 1.2.2. Elucidating the specific process that is active in our case is one of the main topics of the next

chapter. For the moment, we proceed to discuss the main features of the process, as apparent from experimental observations.

Within experimental error, both the growth and the decay of the signal take place without changes in shape. Hence, from the peak amplitude $\alpha(5.8\text{eV})$ of the band and the known peak absorption cross section $\sigma(5.8\text{eV})=6.4\times 10^{-17}\text{cm}^2$,^{3,224} we can estimate the concentration of the defects: $[E']=\alpha\sigma^{-1}$, which is plotted in Figure 5.5 as a function of time. In this particular case, during irradiation $[E']$ grows up to $2.9\times 10^{16}\text{cm}^{-3}$. As soon as the laser is switched off ($t=2520\text{s}$), we observe a dramatic change of slope characterizing the beginning of E' decay, as evidenced in the inset. While the growth stage of the curve can be obviously measured *in situ* once for all for a given type of $a\text{-SiO}_2$ and laser intensity, the post-irradiation decay stage of the kinetics depends on the number of pulses after which the irradiation session is interrupted. This is shown in Figure 5.6, where we compare three kinetics of $[E']$ induced by irradiation with different total numbers of pulses. From the same Figure, the degree of overlap of the growth stages of the three curves evidences the high repeatability of the *in situ* OA measurement.

The presence of E' in the irradiated sample is also independently confirmed by *ex situ* ESR measurements carried out starting from $\sim 5\times 10^2\text{s}$ after the end of exposure, which show the typical signal of the paramagnetic center. An example of the characteristic ESR lineshape of E' acquired in optimal conditions in a (natural dry) laser-irradiated specimen is reported in Figure 5.7. Also, by measurements at different delays from the end of exposure, the intensity of the ESR signal is found to decay with time (Figure 5.8), consistently with the results coming from optical measurements.

From Figure 5.5 it is apparent that the decay of E' is still in progress after 1 hour from the end of irradiation. While *in situ* measurement are the only way to investigate the *growth* stage of the kinetics as well as the first $\sim 10^3\text{s}$ of the decay, they are not suitable to follow the post-irradiation kinetics for more than $\sim 10^4\text{s}$, because they are performed with a single-beam system (see chapter 4). For this reason, the most reliable estimate of the asymptotic stationary value $[E']_\infty$ of $[E']$ at the end of the decay process, comes from *ex situ* ESR or OA measurements performed for a few days after irradiation. The two techniques yield consistent results, but ESR allows for a higher precision. In this way, from the intensity of the ESR signal of Figure 5.7, it was determined that $[E']_\infty=(1.0\pm 0.1)\times 10^{16}\text{cm}^{-3}$ for the kinetics in Figure 5.5. This asymptotic value is reached within a few $\sim 10^5\text{s}$ from irradiation, after which the concentration of E' was observed to remain stationary within experimental error on a timescale of (at least) several months.^{b,c}

Similar growth and decay kinetics of the E' absorption band are observed in all the irradiated natural $a\text{-SiO}_2$ materials. In Figure 5.9 we compare the time dependencies of the induced absorp-

^bFor the meaning of the uncertainty affecting $[E']_\infty$, and any other concentration estimate obtained by ESR, please refer to subsection 4.4.2.

^cThe absorption cross section of E' , σ , was estimated from the slope of the linear correlation between $\alpha(5.8\text{eV})$ and the concentration measured by ESR.^{3,224} Since the latter depends on the value of $[E']$ in the spin-echo reference sample (see subsection 4.4.2), σ is affected by the same 20% error featured by any concentration measurement derived by ESR throughout this work. On the other hand, due to the systematic nature of this uncertainty, it does not affect the agreement between the concentrations calculated from ESR and OA data, which are consistent within the repeatability of the respective measurements.

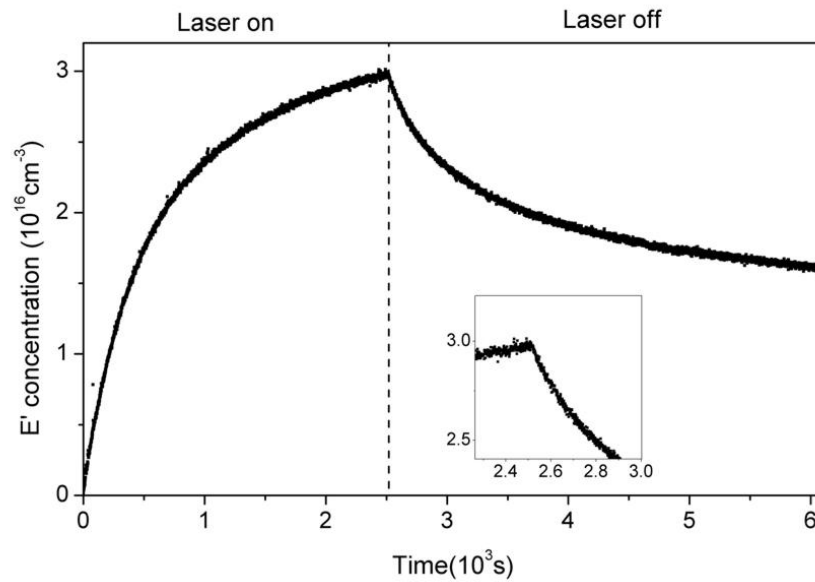


Figure 5.5: Typical kinetics of $[E']$ in a laser-irradiated I301 natural dry α -SiO₂ sample, as calculated from the induced absorption profile measured *in situ* (Figure 5.4). Inset: zoom at the end of the irradiation session.

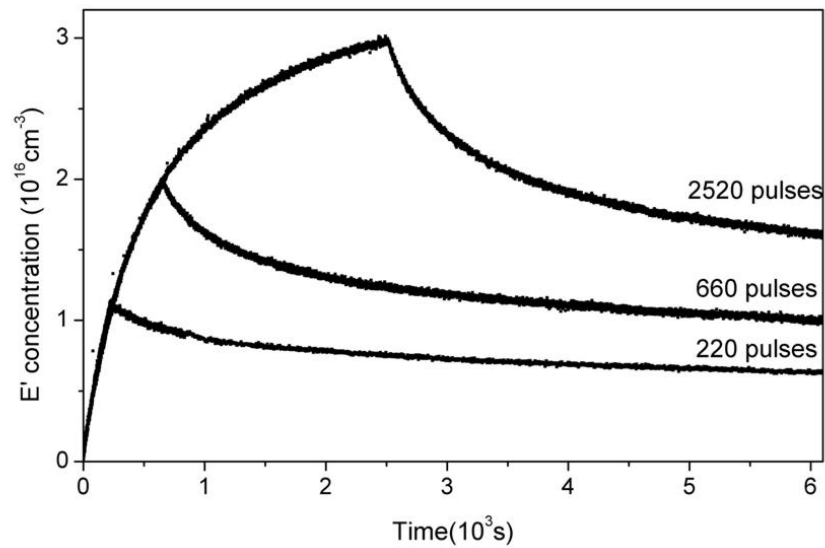


Figure 5.6: Three kinetics of $[E']$ measured during and after irradiation of I301 natural dry silica with different numbers of laser pulses.

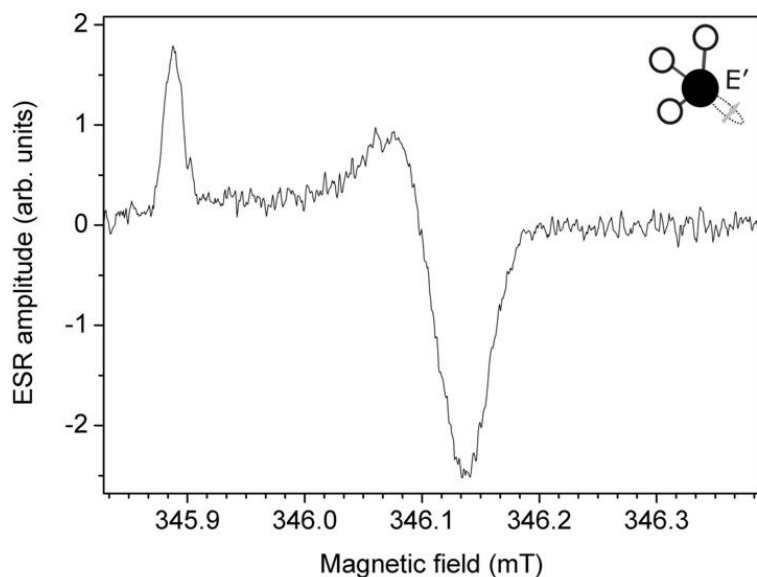


Figure 5.7: ESR signal of E' center (represented in the upper right corner), as detected on the sample of Figure 5.5 a few days after the end of exposure. The signal was detected with a 0.01mT modulation amplitude and with a not-saturating 8×10^{-4} mW microwave power.

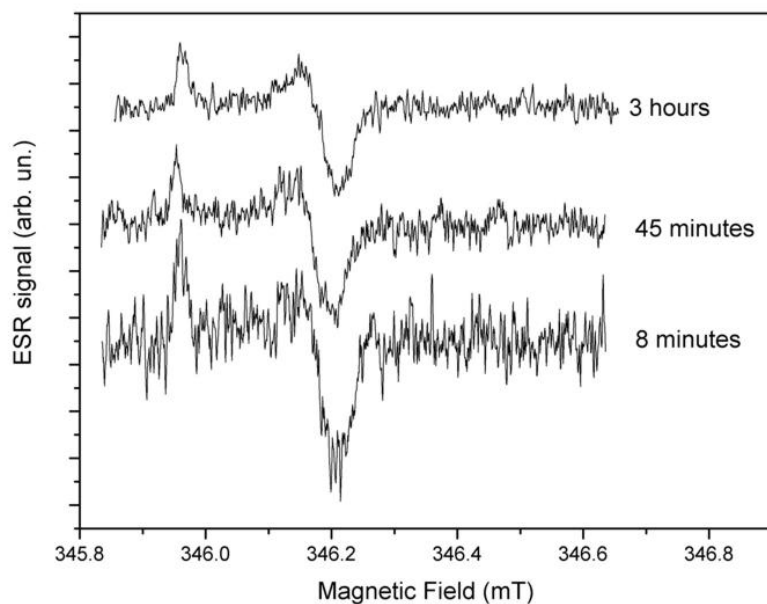


Figure 5.8: ESR signal of E' center detected in a Q906 sample at different delays after the end of laser irradiation. The three spectra have been normalized with respect to the acquisition parameters so that their intensities are proportional to the concentrations of E' ; after normalization, the curves have been vertically shifted to avoid overlap. The signal is much noisier than Figure 5.7 because of the lower (but progressively increasing) integration time used in these measurements, as mandatory to follow the time dependence of the signal.

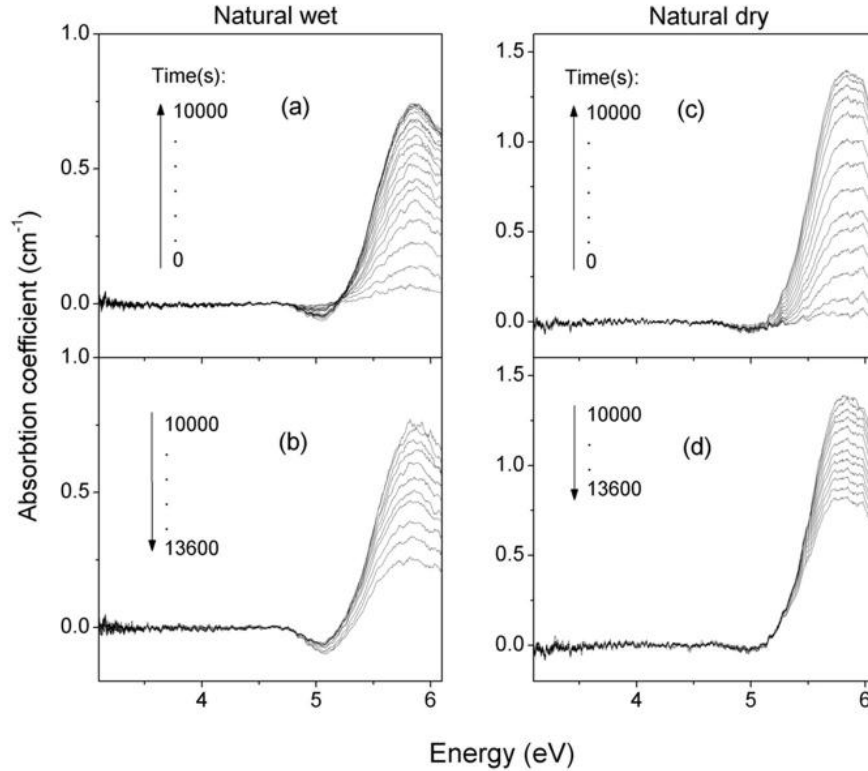


Figure 5.9: Induced OA measured *in situ* during and after a 10000 pulses irradiation with 40 mJcm^{-2} energy density per pulse and 1 Hz repetition rate in wet (HER1) and dry (Q906) natural silica

tion profile, as observed during irradiation and for the first hour of the post-irradiation stage in a wet (panels (a) and (b)) and dry (panels (c) and (d)) natural silica sample irradiated with 10000 laser pulses with 40 mJcm^{-2} energy density per pulse and 1 Hz repetition rate. The kinetics of $[E']$ calculated from these data are reported in Figure 5.10 (kinetics I, dry and II, wet), and compared with the result of the same experiment performed in synthetic dry (III) and wet (IV) silica samples.

These data permit to discuss the different response of the four $\alpha\text{-SiO}_2$ varieties to 4.7 eV laser photons. First, generation of E' is observed only in natural silica, whereas laser irradiation results to be *ineffective on synthetic materials*, (within $\sim 5 \times 10^{14} \text{ cm}^{-3}$), at least at the explored laser intensities, which are unable to induce any detectable absorption band in these specimens. Second, both in wet and dry natural silica the E' centers grow during irradiation until they reach a saturation value after a certain number of pulses, and decay after the laser is switched off, but the kinetics differ in two important aspects: **(i)** more defects are induced in the dry materials for a given irradiation dose (values of curve I are higher than those of II). **(ii)** The decay is more effective in wet silica, where the reduction of $[E']$ in the first hour is already 70%, to be compared with a 40% reduction in the dry material. Further info on this latter point comes from Figure 5.11, where two representative post-irradiation kinetics, as observed in dry or wet silica, are reported in a logarithmic scale, and compared with the asymptotic stationary concentration values obtained by ESR measurements a few days after the end of exposure. In the plot, the origin of the time scale has been redefined to

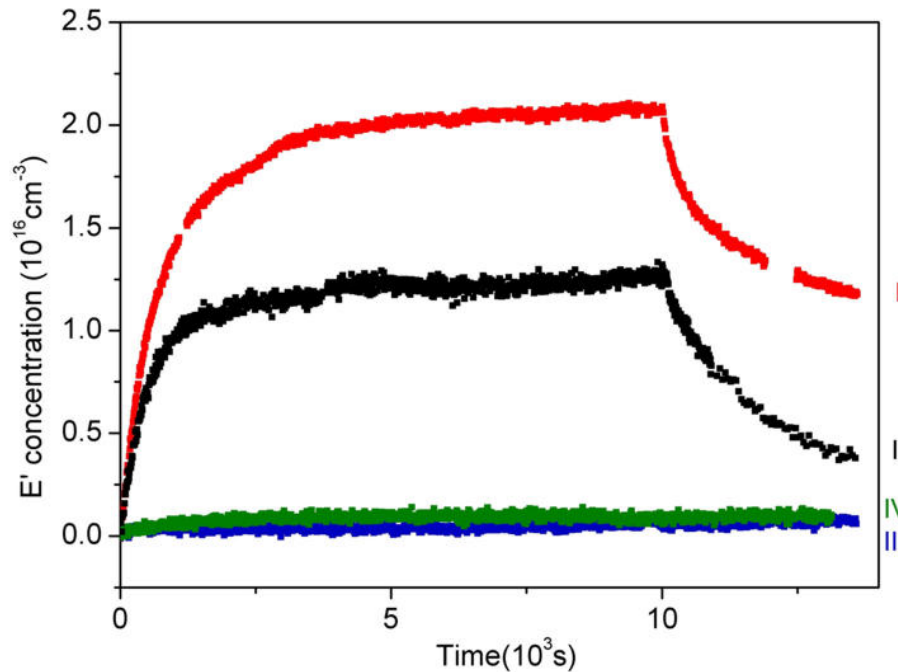


Figure 5.10: Kinetics of E' concentration measured *in situ* during and for 1 hour after the end of a 10000 pulses laser irradiation with 40 mJcm^{-2} energy density per pulse and 1 Hz repetition rate in the four varieties of $\alpha\text{-SiO}_2$: natural dry (I, red), natural wet (II, black), synthetic wet (III, blue) and synthetic dry (IV, green).

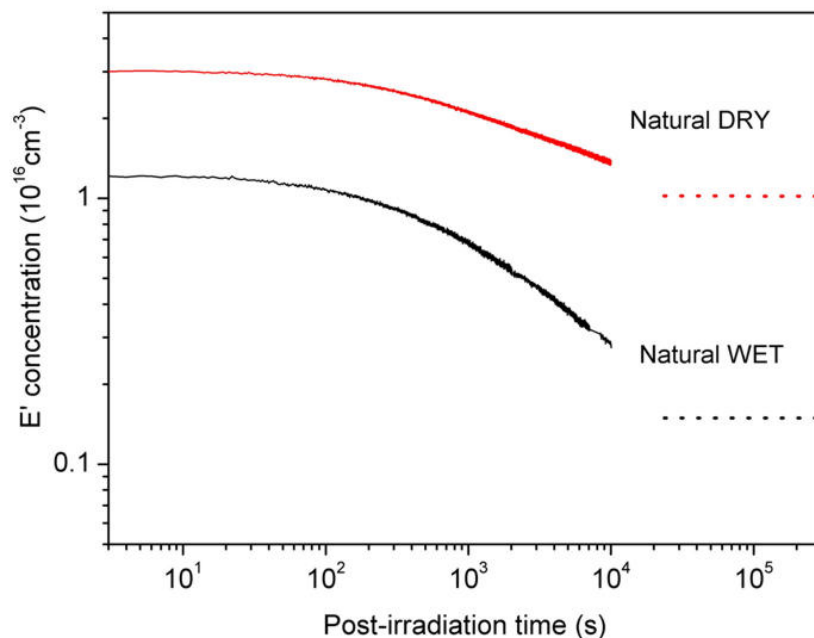


Figure 5.11: Post-irradiation kinetics of $[E']$ measured *in situ* after the end of laser irradiation on dry and wet natural silica samples. Dotted lines: asymptotic stationary values of $[E']$ measured a few days after the end of the irradiation session by ESR. The origin of the time scale corresponds here to the end of exposure.

correspond to the *end* of the irradiation session.

We see that in the wet sample the post-irradiation decay anneals about 90% of the E' centers that had initially been induced by laser exposure, resulting in a stationary concentration of $\sim 1.5 \times 10^{15} \text{ cm}^{-3}$. In contrast, in dry natural silica the portion of annealed centers is lower (67%) and the concentration of stationary centers $\sim 10^{16} \text{ cm}^{-3}$ one order of magnitude higher. These are general features of all the laser-induced kinetics we have observed. Wet natural silica appears to be a remarkable material for what concerns post-irradiation effects, since the E' induced by laser exposure are *almost completely transient*. In contrast, the dry material differs in that a significant concentration of residual E' are still present after the decay is completed. Finally, we can characterize the decay of E' by a typical time scale, defined as the time necessary to achieve half of the total decrease. From data, it can be estimated that this time is close to 10^3 s for both kinetics, although in both cases appreciable concentration variations can be experimentally observed for a few days after irradiation.

5.4 Response of Ge-related defects to irradiation

By a closer look to the induced absorption spectra measured *in situ* (Figures 5.4 and 5.9) we observe that, in addition to the 5.8 eV band, it is detected a weak negative component near $\sim 5 \text{ eV}$.

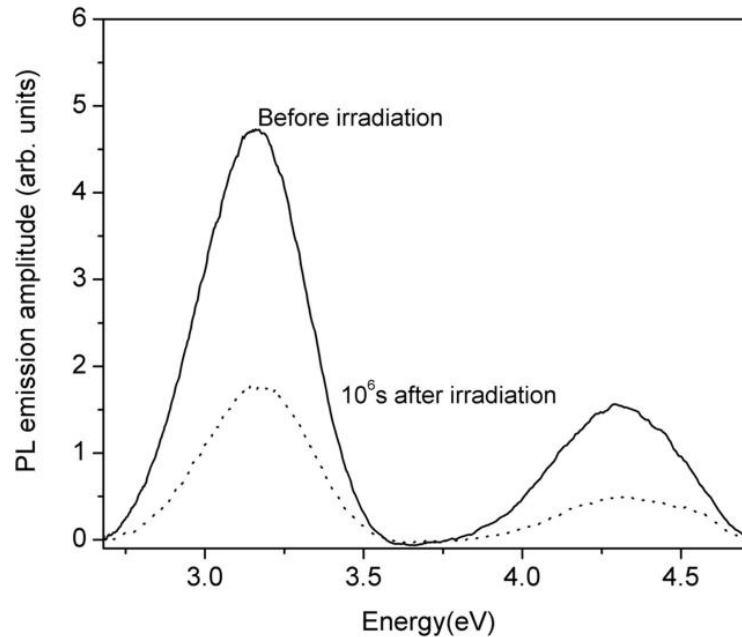


Figure 5.12: Typical PL emission spectrum of GLPC center excited at 5.0 eV in an as-grown natural silica material (continuous line, already reported in Figure 5.2) and in the same sample a few days after being exposed to 2000 laser pulses with 40 mJcm^{-2} energy density per pulse and 1 Hz repetition rate (dashed line).

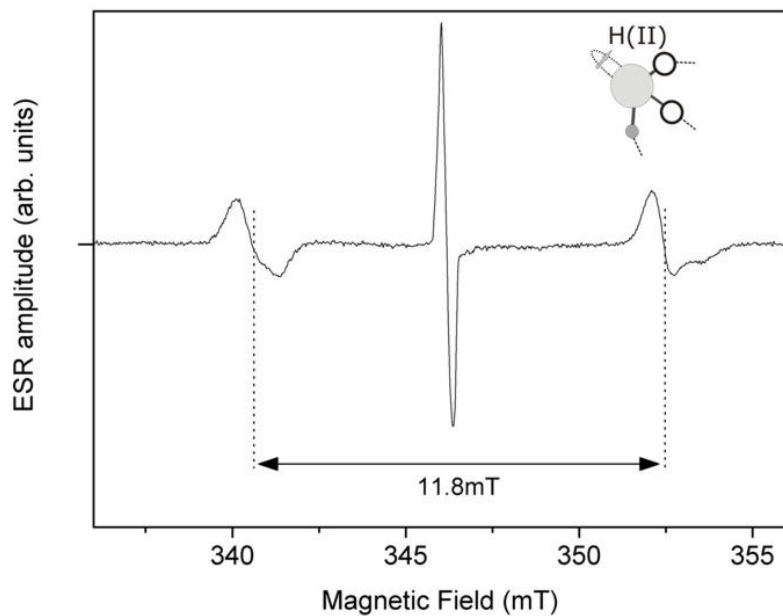


Figure 5.13: Typical ESR spectrum of a laser-irradiated natural dry silica sample, measured in the post-irradiation stage. The signal was acquired with a 3 mW microwave power and a 4 G modulation amplitude. The 11.8 mT doublet is due to the Ge-related H(II) center ($=\text{Ge}^{\bullet}-\text{H}$), represented in the upper right corner.

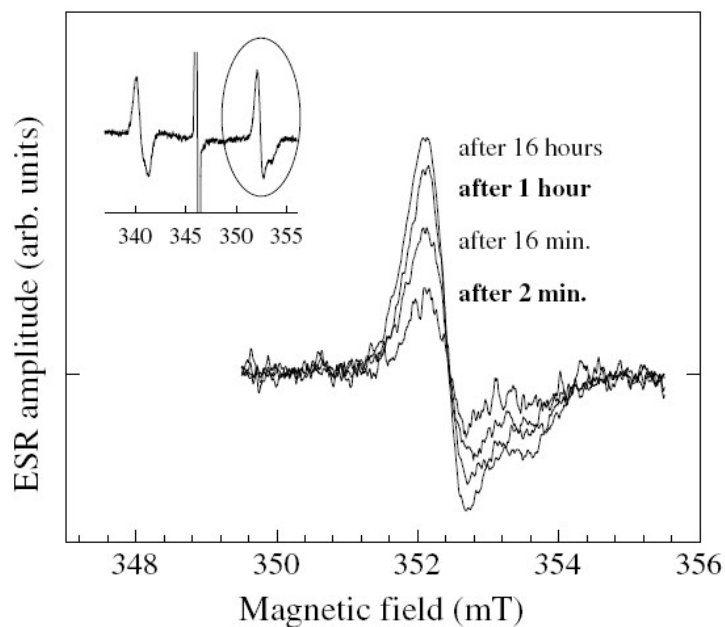


Figure 5.14: High field component of the 11.8 mT ESR doublet of the H(II) center (as evidenced in the inset) as detected at different delays after the end of laser exposure. The signal was acquired using a 3 mW non-saturating²³⁶ microwave power and a 4 G modulation field. Figure taken from Cannas *et al.*²⁴⁶

Due to the presence in the as-grown absorption profile (Figure 5.1) of the $B_{2\beta}$ band, peaked at 5.1 eV, the negative contribution in the difference spectra may be explained as an intensity reduction of this signal. In turn, this finding evidences a partial conversion of the pre-existing Ge-related GLPC centers responsible for the band. Since this signal is partially concealed by the much more intense 5.8 eV component, the conversion of GLPC is more conveniently investigated by luminescence measurements. In fact, in Figure 5.12 we show the PL signal of GLPC in an as-grown sample and in an irradiated specimen, as detected a few days after exposure. It is apparent that laser irradiation induces a reduction (*bleaching*) of the native PL activity, which confirms the occurrence of laser-induced conversion processes transforming the GLPC in other defects. However, we stress that at this stage no information is available on the *kinetics* of the bleaching process.

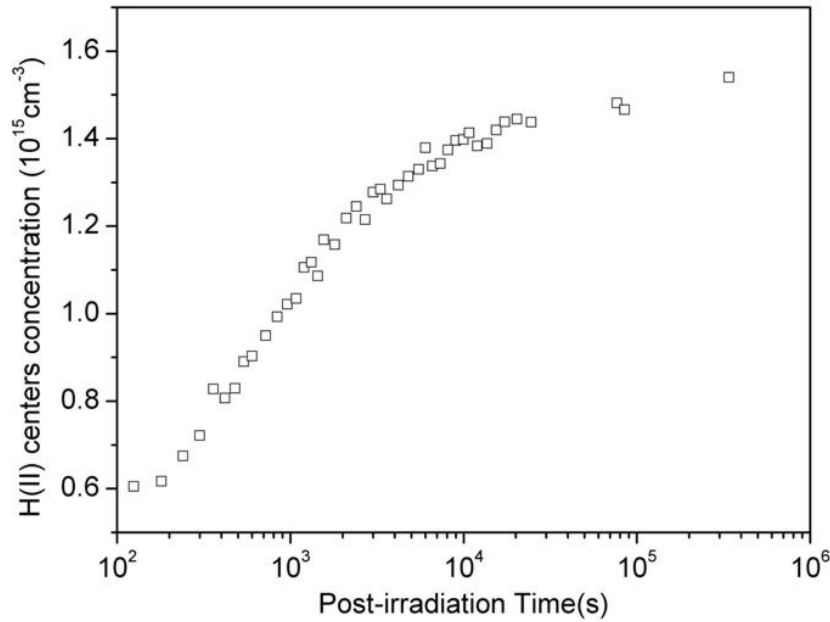


Figure 5.15: Post-irradiation kinetics of H(II) centers in an irradiated Q906 sample, after irradiation with 10000 laser pulses with 40 mJcm^{-2} energy density per pulse and 1 Hz repetition rate, as calculated from the time dependence of their 11.8 mT doublet. $t=0$ represents the end of the irradiation session.

Another process related to Germanium impurities is evidenced by ESR. In detail, if an as-grown natural silica sample is laser-irradiated, and we perform in the post-irradiation stage an *ex situ* ESR measurement on a wide magnetic field region, we detect a typical signal that is reported in Figure 5.13. The strong component near 346 mT is the E' signal in Figure 5.7, which here appears very distorted due to the high modulation field and microwave power being used in the acquisition^d. In addition, the spectrum evidences a doublet split by 11.8 mT, which by comparison with literature can be attributed to the Ge-related H(II) center.^{96,98,155}

^dIn this acquisition, the instrumental parameters were optimized to detect the 11.8 mT doublet, which features a saturation power²³⁶ and a linewidth much larger than E' .

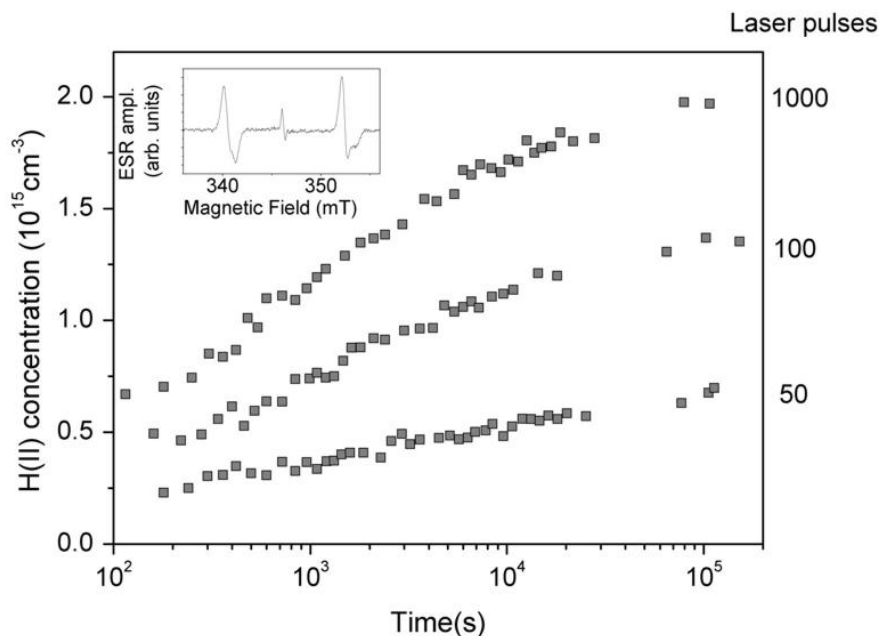


Figure 5.16: Post-irradiation kinetics of H(II) centers observed in HER1 wet natural α -SiO₂ after exposure of several as-grown samples to different numbers of laser pulses with 40 mJcm⁻² energy density per pulse and 1 Hz repetition rate. Inset: typical ESR spectrum showing the 11.8 mT doublet of H(II) centers.

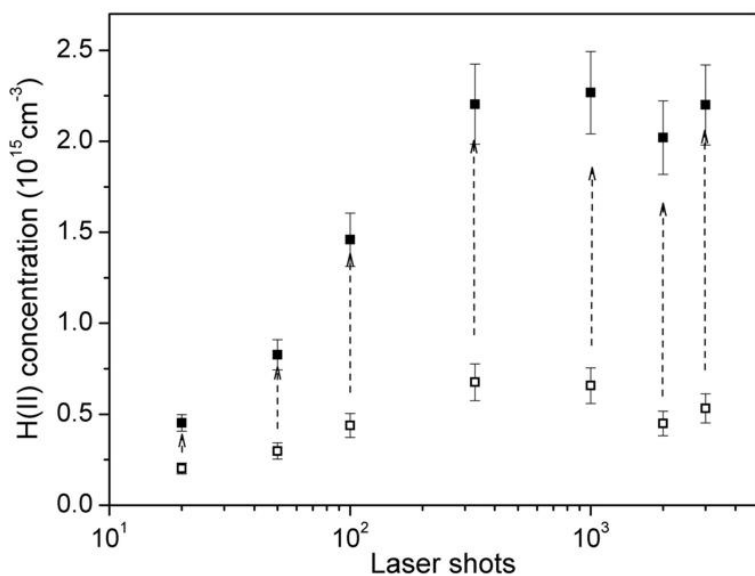


Figure 5.17: Dose-dependence of the concentrations measured a few minutes after the end of irradiation (empty symbols) and at the end of the post-irradiation kinetics (full symbols) for HER1 natural wet α -SiO₂ irradiated with 40 mJcm⁻² energy density per pulse and 1 Hz repetition rate.

The H(II) center consists in a Ge bonded to two oxygen atoms and one hydrogen, and hosting an unpaired electron ($=\text{Ge}^\bullet-\text{H}$); the doublet structure of its ESR signal arises from the hyperfine interaction between the electron and the proton spins. If the ESR measurements are repeated at different delays from the end of exposure, two effects are observed: **(i)** the progressive decrease of the E' signal, above mentioned, consistent with the post-irradiation decay of the 5.8 eV band observed by *in situ* OA, and **(ii)** a progressive *increase* of the intensity of the 11.8 mT doublet, as shown in Figure 5.14 for one of the two components of the signal.

This observation demonstrates a growth of the concentration of H(II) centers taking place in the post-irradiation stage, *simultaneously to the decay of E'* . From the intensity of the doublet, measured^e at different delays from the end of exposure, we calculate the concentration of the defects, which is plotted in Figure 5.15 as a function of time for a natural dry sample irradiated with 10000 laser pulses. The concentration a few minutes after the end of exposure (*initial* concentration) is $\sim 6 \times 10^{14} \text{ cm}^{-3}$, from which it grows up to $\sim 1.5 \times 10^{15} \text{ cm}^{-3}$ (*stationary* concentration) measured after a few days. A similar kinetics is observed in all the irradiated dry and wet natural silica specimens. In all samples, the stationary concentration of H(II) is always $[\text{H(II)}] < 2 \times 10^{15} \text{ cm}^{-3}$. Similarly to E' , also the growth of H(II) can be characterized by a typical time scale, defined as the time necessary to achieve half of the total *growth*. From inspection of Figure 5.15 one can easily estimate that this time is $\sim 10^3$ s, comparable to the time scale of E' decay.

To show the dose-dependence of the H(II) generation process, we report in Figure 5.16 their growth kinetics measured after exposure to different numbers of pulses in natural wet $\alpha\text{-SiO}_2$ samples. From each kinetics we extract the initial and stationary concentrations, which are reported in Figure 5.17 as a function of irradiation dose (number of pulses). We see that the stationary concentration increases with dose, and after ~ 300 pulses it becomes invariant with increasing number of pulses at $(2.1 \pm 0.2) \times 10^{15} \text{ cm}^{-3}$. The initial concentrations show a similar dose-dependence but are always 3-4 times smaller than stationary concentrations, independently of dose. The results of Figure 5.17 are representative of all natural silica samples investigated.

Finally, no ESR signals are detected in irradiated synthetic $\alpha\text{-SiO}_2$ specimens, consistently with the absence of any induced absorption signal in *in situ* measurements. In particular, in regard to the H(II) doublet, it is worth noting that its absence is a necessary consequence of the lack of Ge impurities in synthetic $\alpha\text{-SiO}_2$, differently from the case of natural specimens.

5.5 Discussion

We have shown that one of the main features of natural $\alpha\text{-SiO}_2$ exposed to pulsed 4.7 eV laser irradiation is that the induced E' centers are unstable and decay in the post-irradiation stage. As reviewed in chapter 2, in literature post-irradiation effects have often been attributed to the diffusion

^eWe stress that the signal of H(II) is monitored as a function of post-irradiation time without removing the sample from the ESR spectrometer. This allows to measure the kinetics of $[\text{H(II)}]$ with a higher precision, it being not limited by the repeatability of the mounting conditions.

in $a\text{-SiO}_2$ of mobile species able to react with point defects causing their conversion in other centers. Among the many species whose diffusion in $a\text{-SiO}_2$ was evidenced experimentally, only hydrogen (aside from chemically inert noble gases, see Table 2.1) is able to readily diffuse at room temperature, where the experiments presented up to this point were carried out. Moreover, at room temperature hydrogen in $a\text{-SiO}_2$ is found only in *molecular* H_2 form, because H diffuses so fast and is so reactive that it exists only as a transient species, which rapidly recombines with reactive defects or dimerizes forming H_2 . On this basis, it is natural to hypothesize that the post-irradiation decay of E' ($\equiv \text{Si}^\bullet$) is due to reaction with H_2 :



H produced at the right side of the reaction rapidly dimerizes again in H_2 or passivates another E' :



In literature, the reaction of E' with H_2 has been experimentally observed in several works both for E' in bulk $a\text{-SiO}_2$ and on silica surfaces (see subsection 2.4.3). The overall kinetics of (5.1) and (5.2) is basically driven by the former reaction, because diffusion of H is so fast that the latter follows adiabatically the slow concentration variations of E' driven by H_2 diffusion (see chapter 2). The analysis of the temperature dependence is useful to verify if the post-irradiation decay of E'

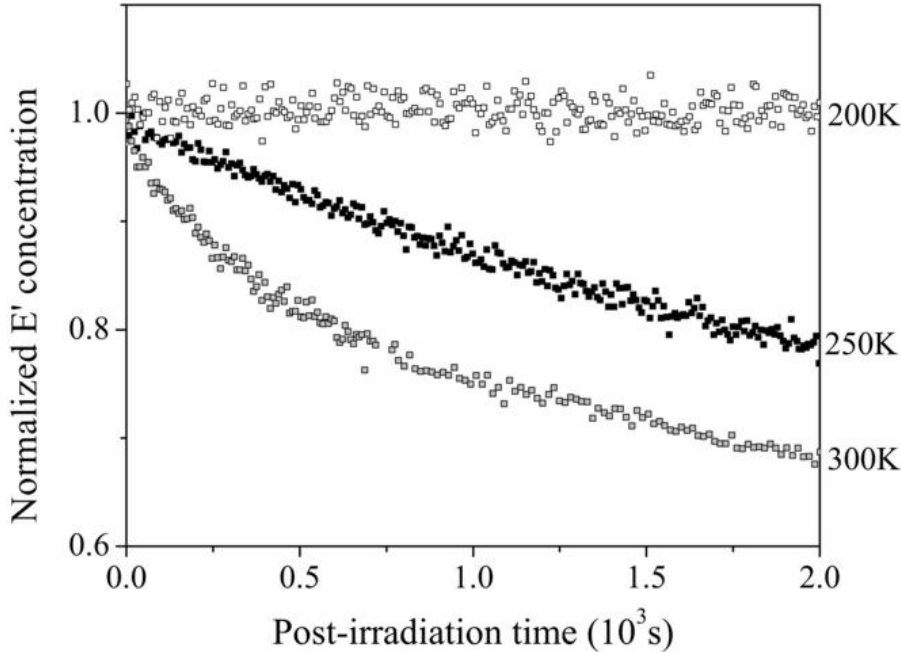


Figure 5.18: Post-irradiation kinetics of E' after irradiation of a natural dry silica sample with 2000 laser pulses with 40 mJcm^{-2} energy density per pulse and 1 Hz repetition rate, performed at three different temperatures. The curves are normalized to the concentration measured at the end of exposure.

is consistent with this interpretation scheme. To this purpose we measured *in situ* the kinetics

of E' during and after irradiation with 2000 laser pulses performed at several temperatures in the $200\text{ K} < T < 300\text{ K}$ interval. Each irradiation experiment consisted in the exposure of the sample to laser radiation at a given temperature and in the observation of the post-irradiation kinetics of E' at the same temperature. Here we focus only on the post-irradiation (decay) stage of the kinetics, some of which are reported in Figure 5.18 after normalization to the concentrations of E' at the end of the exposure session. The decrease becomes progressively slower on decreasing T , and it is absent within experimental uncertainty at $T=200\text{ K}$. These data demonstrate the post-irradiation decay to be a thermally activated process, frozen at $T_0 \sim 200\text{ K}$. This finding is consistent with literature studies^{38,42,185} where diffusion of H_2 in silica has been characterized by the same threshold temperature, thus supporting our interpretation (5.1).

It is interesting to briefly discuss this process on the basis of the Waite theory of diffusion-limited reactions (section 2.3), which allows to estimate from literature parameters of H_2 the *expected* time scale of E' anneal at room temperature: applying eq. (2.29) to the kinetics of E' in dry silica of Figure 5.11, we obtain:

$$\tau \sim 10^{17} \text{ cm}^{-3} \text{ s} \cdot [E']_{\infty}^{-1} \sim 10 \text{ s} \quad (5.3)$$

which is roughly two orders of magnitude lower than the 10^3 s characterizing the experimental decay. On the one hand, this means that our kinetics are actually *compatible* with the idea of a process driven by H_2 diffusion, as the experimental reaction rate does not *overcome* the maximum possible value consistent with the mobility of H_2 in silica at $T=300\text{ K}$. It is easy to see that a similar check excludes that the process may be driven by O_2 or H_2O diffusion, much slower than H_2 (Table 2.1). On the other hand, the difference between the observed and the predicted decay time scales indicates that a physical reason, unaccounted for by purely diffusion-limited reactions theory, slows down the overall reaction rate. This is consistent with the unrealistically small capture radius found in previous works when trying to fit the post-irradiation kinetics measured *ex situ* on the basis of the theoretical predictions obtained by the Waite theory.^{89,224} The reason of this discrepancy will be clarified in chapter 8. Finally, it is worth noting that at this stage we have not yet addressed the problem of the *origin* of mobile H_2 : it may be already present in the as-grown samples due to the manufacturing procedure, or be induced radiolytically by laser-induced rupture of pre-existing precursors, such as Si-OH or Si-H bonds.

Aside from the above considerations, there is another totally independent line of reasoning that strongly suggests hydrogen to be at the basis of the post-irradiation effects. In fact, ESR measurements evidence the growth of H(II) centers occurring concurrently to the decay of E' (Figure 5.15). The features of the paramagnetic signal of H(II) (see Figure 5.13) are an unambiguous *fingerprint of the presence of a hydrogen atom* in its structure, as was proved by studies on isotopically enriched^f samples, which allowed to determine the microscopic structure ($=\text{Ge}^{\bullet}-\text{H}$) of the defect.⁹⁶ Consequently, the post-irradiation growth of the H(II) center is most likely attributable to *trapping of a*

^fIn detail, by substitution of hydrogen with deuterium, the 11.8 mT doublet was shown to become a *triplet*, and its separation to scale (as expected) as the ratio of deuteron and proton magnetic moments.⁹⁶

hydrogen atom on a suitable pre-existing Ge precursor. Now, given the structure of the H(II), the precursor is clearly expected to be ($=\text{Ge}^{\bullet\bullet}$), namely the GLPC center, as also put forward in previous works on γ -irradiated silica or on surface defects:^{12,98,167,236}



the attribution of the post-irradiation kinetics of H(II) to process (5.4) is also consistent with the observed reduction of the GLPC typical optical activity (Figure 5.12), even if it would be necessary to prove that the *kinetics* of GLPC bleaching is correlated with H(II) growth.

Reaction (5.4) necessarily requires *atomic* hydrogen because, as widely known, H_2 does not react spontaneously with *diamagnetic* defects, being a very stable molecule with a high bond energy ($\sim 4.5\text{eV}$). On the contrary, the reaction with (some) *paramagnetic* centers is possible because the presence of an unpaired electron confers to these defects a much higher reactivity.^{38,214} Hence, since the stable form of hydrogen in $\alpha\text{-SiO}_2$ at room temperature is H_2 , for reaction (5.4) to be possible, it is needed a paramagnetic defect that reacts with H_2 thus acting as a *cracking center*, which makes available H to be trapped at the GLPC site. Given the post-irradiation decay of E' , it is clear now that E' is the main candidate for the role of the cracking center.⁸

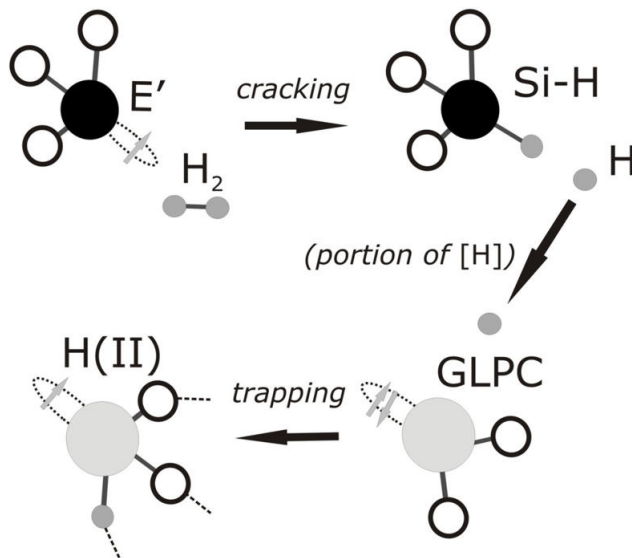


Figure 5.19: Pictorial representation of post-irradiation processes in natural silica. Diffusing H_2 reacts with E' center: this leads to passivation of the defect and produces free atomic hydrogen H. A portion of the population of H migrates until encountering a GLPC center, where it is trapped producing the H(II) center. The remaining portion of H (not represented) passivates another E' or dimerizes in H_2 .

So, in this scheme, displayed in Figure 5.19, diffusing H_2 reacts with E' by (5.1) causing the post-irradiation decay of this paramagnetic center. A *portion* of the population of H produced at the right side of (5.1) is then captured by GLPC (Reaction 5.4) thereby causing the simultaneous

⁸A further indication of the role of E' is the absence here of the other basic defect in silica able to serve as a H_2 cracking center, namely the NBOHC.^{38,42,185} Indeed, the typical 4.8eV absorption band of NBOHC is not observed by *in situ* OA. This point is further discussed in the next chapter.

growth of the H(II) center. This interpretation is also corroborated by the comparable time scales ($\sim 10^3$ s) of the E' decay and the H(II) growth kinetics. Comparing the typical H(II) concentration (Figure 5.15) $\sim 2 \times 10^{15} \text{ cm}^{-3}$ with the entity of the total post-irradiation decrease of E' (Figure 5.11) $\sim 10^{16} \text{ cm}^{-3}$, it appears that hydrogen trapping by GLPC (5.4) can be regarded as a *secondary* reaction, which consumes no more than 10-20% of the available hydrogen atoms, most of which react with E' by (5.1) and (5.2). On the other hand, it is clear that the importance of H(II) in the present context goes much further. In fact, the observation by ESR of this hydrogen-related center whose concentration increases in time, naturally leads to attribute the post-irradiation decay of E' to H_2 , ruling out *a priori* other possibilities, like electron/hole detrapping or diffusion of other mobile species. Then, H(II) may be considered *a probe of the presence of mobile hydrogen*, allowing in some sense to overcome the difficulty of a direct observation of H_2 .

Although the present qualitative considerations offer quite convincing reasons to attribute the post-irradiation effects to the presence of mobile H_2 , the problem of verifying in more detail the quantitative consistency of this model with the observed kinetics will be discussed again in greater detail in chapters 7 and 8.

5.6 Conclusions

Exposure of natural silica to 4.7 eV pulsed laser radiation induces the generation of E' centers. The defects are unstable and decay in the post-irradiation stage in a typical time scale of the order of 10^3 s. The E' is not induced in synthetic silica materials. ESR measurements show that a Ge-related paramagnetic center, the H(II), grows in the post-irradiation stage concurrently to the decay of E' . Since the structure of the H(II) can be unambiguously identified by ESR, this center may be considered as a probe of the presence of mobile hydrogen, so as to attribute both the decay of E' and the growth of H(II) to diffusion of H_2 in the glass after the end of exposure. In this scheme, E' decays by reaction with H_2 , and a portion of the H made available by this process is then captured on pre-existing GLPC centers so as to form H(II). Our interpretation is also confirmed qualitatively by the temperature dependence of the E' decay and by the observed reduction of the PL optical activity of GLPC upon irradiation.

Chapter 6

Generation of E' center

In this chapter we discuss in more detail the *in situ* kinetics of the E' center, with the purpose to understand the generation mechanism of the defect, as well as the origin of the hydrogen responsible for its post-irradiation decay.

6.1 Introduction

The experimental results presented in the previous chapter demonstrate the ability of 4.7 eV laser light to induce at room temperature the generation of E' in natural α -SiO₂ materials. Besides, the induced defects are unstable and decay in the post-irradiation stage, supposedly due to reaction with diffusing H₂. The decay is particularly effective in wet natural silica, where it anneals almost completely the E' induced by irradiation. However, many questions remained open such as the generation mechanism of the E' center and the origin of hydrogen responsible for the post-irradiation decay.

The passivation of E' by H₂ is one of the most important processes among the several defect conversions in silica induced by hydrogen, quite common even well below room temperature due to the high mobility and reactivity of H and H₂. A careful study of the reaction dynamics of defects with diffusing species requires spectroscopic techniques suitable to probe *in situ* their concentration changes. So far, *in situ* photoluminescence measurements have been used to clarify the generation and the decay of another defect of fundamental interest, the non bridging oxygen hole center (NBOHC) induced by photolysis of Si–OH bond.^{42,116,185} In contrast, the current understanding of the generation of E' centers by UV laser (reviewed in subsection 1.2.2) is mainly founded on *ex situ* ESR and OA measurements. Hence, even though the passivation of E' by H₂ (reviewed in subsection 2.4.3) has been repeatedly observed in literature, the interplay between the photo-induced creation of E' and its decay due to reaction with mobile hydrogen is not well understood. Our *in situ* technique is based upon the observation of the complete time-dependent absorption profile in the UV,^{249–253} differently from previous works, which reported only the absorption at a fixed wavelength.^{110,113,114} In addition to the possibility of monitoring the kinetics of induced absorption, another advantage

of our approach is the possibility of clearly determine which transient absorbing centers are induced (and which are not), provided that their absorption line shapes can be unambiguously identified. In this chapter^{249–252} the *in situ* OA technique is applied to perform a comprehensive investigation of the processes controlling the generation and decay dynamics of E' centers. Our discussion starts from wet fused quartz, which is a remarkable material to study transient transmittance losses; in fact, as already shown, in these glasses UV absorption due to E' centers is effective mainly during laser exposure, while *transparency is almost completely recovered in the post-irradiation stage*. In the last part of the chapter we are going to extend our considerations to the other varieties of a -SiO₂.

6.2 E' center in natural wet a -SiO₂

6.2.1 Experiment

The experiments reported in this section were performed on HER1 *natural wet* a -SiO₂ samples (see Table 4.1), of sizes $5 \times 5 \times 1$ mm³ and optically polished on all surfaces. The specimens were irradiated at room temperature ($T_0=300$ K) with 4.7 eV pulsed laser radiation perpendicularly to one of the minor surfaces. We verified that during laser irradiation the temperature of the samples did not vary significantly from T_0 . It was used a repetition rate of the laser pulses of 1 Hz, corresponding to an interpulse time of $\Delta t=1$ s. The diameter $2r$ of the laser beam was (6.0 ± 0.1) mm. Since the intensity profile of the laser beam is uniform (see chapter 4), the ratio of pulse energy to the beam section (πr^2) and duration ($\tau=5$ ns) gives the (*mean*) laser peak intensity Λ . We performed several irradiation sessions on different *virgin* samples at different laser pulse energies, from 3.7 mJ to 27 mJ. These values correspond to peak intensities Λ from $(2.6 \pm 0.2) \times 10^6$ Wcm⁻² to $(19 \pm 1) \times 10^6$ Wcm⁻², respectively.

During each irradiation session (consisting in a few thousand pulses), we measured *in situ* the absorption profile induced in the sample. As described in the previous chapter, these measurements yield the kinetics of the OA on a time scale longer than Δt . For some of the irradiations, the measurements were carried on at the same rate (1 OA spectrum per second) also for a few hours in the post-irradiation stage, so as to follow the decay of the induced absorption profile. Our investigation was completed by ESR spectra performed for a few days after the end of irradiation.

6.2.2 Results

As already discussed, the main signal observed in the induced OA spectrum measured *in situ* during and after laser irradiation of wet natural silica is the 5.8 eV band due to the E' centers; from the knowledge of the peak absorption cross section of the defects, we estimated their concentration [E'] as a function of time. In Figure 6.1 are reported three representative kinetics observed upon exposure of the specimens to radiation with the peak laser intensities $\Lambda_1=2.6 \times 10^6$ Wcm⁻², $\Lambda_2=4.8 \times 10^6$ Wcm⁻², and $\Lambda_3=12 \times 10^6$ Wcm⁻². For practical reasons, the *irradiation stage* of the kinetics is plotted as a function of laser fluence $\Phi = \Lambda \tau \Delta t^{-1}$, while data for the first 10³ s of the *post-irradiation stage* are

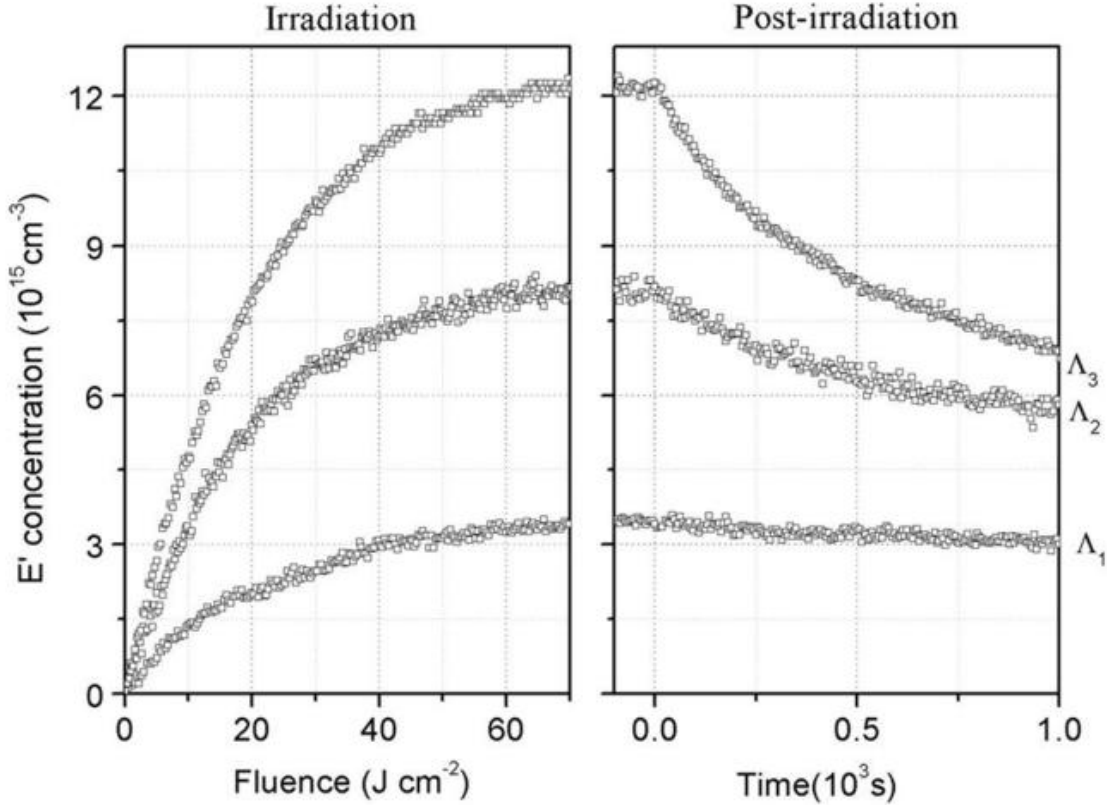


Figure 6.1: Three representative kinetics of induced absorption measured *in situ* during and after pulsed UV laser irradiation of wet natural silica at different laser intensity levels. The origin of the time scale corresponds to the end of the irradiation session. The parameters Λ_i are defined in the text. For graphical reasons, not all datapoints are plotted.

plotted versus time, $t = 0$ corresponding to the end of the irradiation session.

During irradiation, $[E']$ saturates after $\sim 70 \text{ J cm}^{-2}$ to a constant value $[E']_S$ that depends on intensity. For instance, $[E']_S = 1.2 \times 10^{16} \text{ cm}^{-3}$ during irradiation with $\Lambda_3 = 12 \times 10^6 \text{ W cm}^{-2}$. As soon as the laser is switched off, the defects begin to decay. The decay appears to be progressively faster with increasing Λ ; indeed, the concentration of the E' generated with intensity Λ_3 is reduced of $\sim 40\%$ after 10^3 s , whereas for $\Lambda = \Lambda_1$ the decrease is $\sim 15\%$ in the same time interval. However, ESR measurements performed for a few days after irradiation confirm the result of the previous chapter, namely that the E' centers are *almost completely transient* since $[E']$ tends to an asymptotic value lower than 20% of the maximum concentration.

We discuss now in more detail the typical OA profile induced in wet natural silica, as reported in Figure 6.2. Apart from the Gaussian-shaped band centered at $(5.84 \pm 0.03) \text{ eV}$ with $\text{FWHM} = (0.70 \pm 0.04) \text{ eV}$ associated with the E' centers, we observe the small negative component at 5.1 eV, already attributed to conversion of GLPC centers pre-existing in natural a - SiO_2 . Furthermore, no other measurable absorption bands are present in the spectrum: in particular, we stress

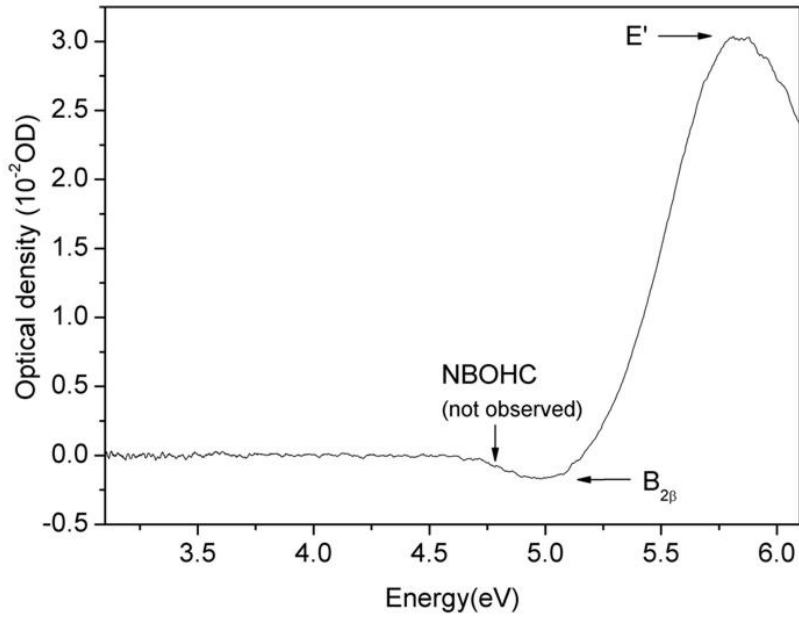


Figure 6.2: Typical UV profile of the transient OA induced by 4.7 eV pulsed laser irradiation in wet natural α -SiO₂.

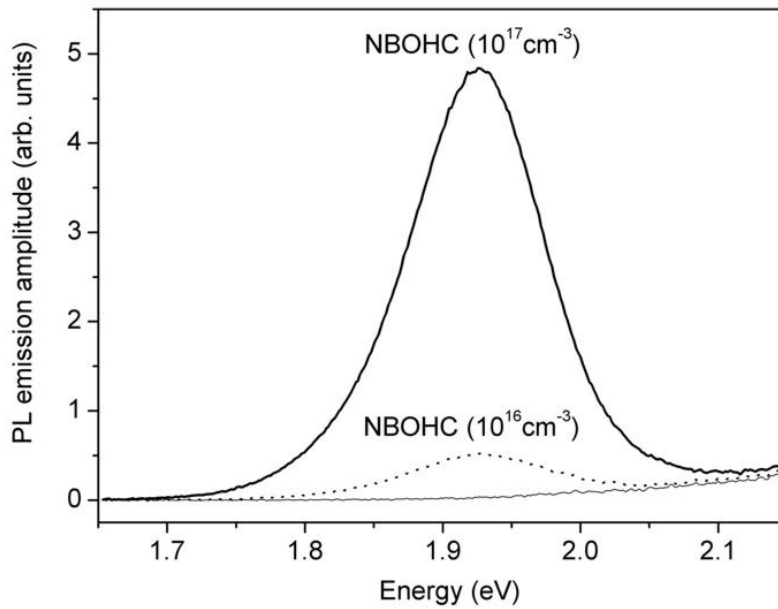


Figure 6.3: Photoluminescence emission spectra excited at 4.8 eV and measured with an emission bandwidth of 10 nm in a γ -irradiated synthetic silica sample that contains 10^{17} cm^{-3} NBOHC centers (spectrum G, thick continuous line), and in a laser-irradiated wet natural silica sample (L, continuous line). The dotted line is a simulation of the signal that would be expected for 10^{16} cm^{-3} NBOHC; it was obtained by adding G/10 to L.

that there is no evidence of the typical 4.8 eV band associated with NBOHC centers ($\equiv \text{Si}-\text{O}^\bullet$, see chapter 1) within our sensitivity, which is $\sim 0.02 \text{ cm}^{-1}$ in optimal conditions (Figure 6.2). The oscillator strength of the NBOHC centers was estimated to be in the interval 0.03–0.05 on the basis of the decay time of their luminescence band at 1.9 eV.^{8,20,254} Hence, the sensitivity limit can be converted by eq. (3.8) to a *concentration* upper limit for NBOHC of $3-5 \times 10^{15} \text{ cm}^{-3}$.

In this way, the *in situ* technique allows to exclude that NBOHC centers are generated in concentrations comparable to E' by IV harmonic Nd:YAG radiation, at least at the investigated intensity levels. To further corroborate this conclusion, we performed photo-luminescence measurements in laser-irradiated wet and dry natural silica samples a few days after the end of irradiation. In fact, it is known that the NBOHC feature a PL emission bands centered at 1.9 eV under excitation at 4.8 eV, which was not observed in the measured emission spectra (Figure 6.3). For comparison, it is shown the 1.9 eV emission band as measured in a γ -irradiated synthetic a -SiO₂ sample, which corresponds to a concentration of NBOHC of $\sim 10^{17} \text{ cm}^{-3}$ as deduced from the intensity of the OA band at 4.8 eV. Since the intensity of the PL emission signal is proportional to the concentration (in conditions of low absorbance, see chapter 4), these data confirm that the concentration of NBOHC in laser-irradiated samples is lower than $\sim 2 \times 10^{15} \text{ cm}^{-3}$. However, it is worth noting that the *in situ* technique yields a stronger information than PL measurements, since it excludes also possible *transient* NBOHC centers. We stress that the absence of NBOHC is going to be a very important point in what follows.

6.2.3 Discussion I: Precursor of E' center

We are going to show now that the analysis of *in situ* OA measurements permits to infer important information about the generation mechanism of the E' center under Nd:YAG laser irradiation. In particular, we begin our discussion with the analysis of the *decay* stage of the process.

A thorough study of the decay of E' due to reaction with mobile hydrogen, must be performed on the basis of a set of chemical rate equations, comprehending also the secondary trapping of atomic hydrogen on preexisting twofold coordinated Ge (Reaction 5.4). This problem will be dealt with in a following chapter, while here we propose an analysis founded on the properties of the *first stage* of the decay. Besides, we neglect here for simplicity the secondary reaction, which involves only a minor portion of hydrogen, and we assume in the following that H₂ is involved only the reaction with E' center, also because it is absent the NBOHC center that would react with a portion of the available hydrogen.^{38,185}

To characterize the first stage of the decay, we can determine by a linear fit in the first ~ 50 s of the post-irradiation stage the *initial decay slope* $d[E']/dt(t=0)$, as shown in Figure 6.4 for the kinetics at $\Lambda = 12 \times 10^6 \text{ W cm}^{-2}$. Then, the slope is normalized dividing by the concentration $[E']_S$, measured at the beginning of the decay as well, so as to give the following parameter Γ :

$$\Gamma = -\frac{1}{[E']_S} \frac{d[E']}{dt}(t=0) \quad (6.1)$$

which represents the probability per unit time that an E' center disappears, estimated immediately

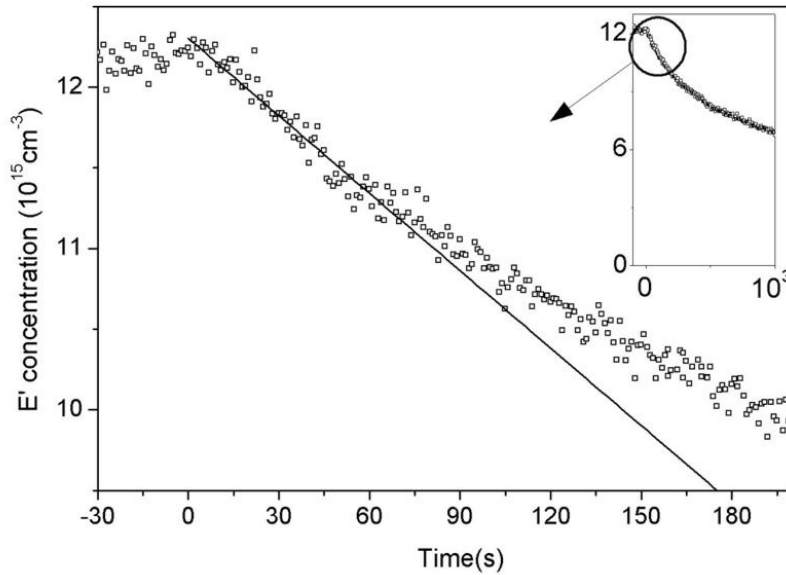


Figure 6.4: Zoom of the first portion of the decay curve Λ_3 of the right panel of Figure 6.1, and reported again in the inset. The continuous line is obtained by a linear least-square fit of the data in the first 50 s.

after the end of irradiation. The importance of the parameter Γ derives from the following considerations. We know that the post-irradiation annealing of E' ($\equiv \text{Si}^\bullet$) in the present experimental conditions is due to the reaction with mobile H_2 , which we rewrite again here:



where H produced at the right side may passivate another E' or dimerize in H_2 . As described in section 2.3, the concentration variations due to reaction (6.2) are accounted for by the following rate equation, valid in the stationary-state approximation:^{39,194}

$$\frac{d[E']}{dt} = 2 \frac{d[\text{H}_2]}{dt} = -2k_0[E'][\text{H}_2] \quad (6.3)$$

where k_0 is the reaction constant between E' and molecular hydrogen, and the factor 2 derives from the fact that one H_2 passivates *two* E' . Hence, evaluating eq. (6.3) at the end of irradiation and dividing both members by $[E']$, we get:

$$\Gamma = -\frac{1}{[E']} \frac{d[E']}{dt}(t=0) = 2k_0[\text{H}_2](t=0) \quad (6.4)$$

which means that the above defined parameter Γ is proportional to the concentration $[\text{H}_2]_S = [\text{H}_2](t=0)$ of molecular hydrogen present in the sample at the end of irradiation. In other words, Γ can be considered as an *indirect measure* of $[\text{H}_2]_S$.

Therefore, in Figure 6.5 we analyze how Γ is related to the concentration of E' at $t=0$, $[E']_S$. To this purpose, Γ is plotted as a function of $[E']_S$ for 5 points obtained at different power levels Λ . We stress that at this stage Λ serves only as a parameter useful to span the concentration of E' . We see

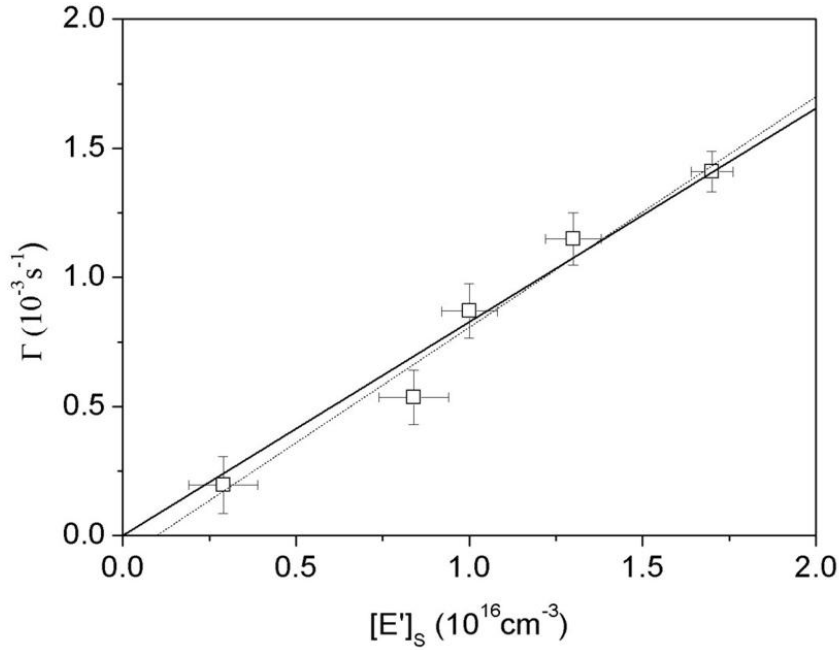


Figure 6.5: Parameter Γ , proportional to the concentration of molecular hydrogen at $t=0$, as a function of the concentration of E' measured at the same time instant. The continuous line is a least-square fit of the data with the function $y=\alpha x$, from which we find: $\alpha=(8.3\pm 0.8)\times 10^{-20}\text{ cm}^3\text{s}^{-1}$. Alternatively, the dotted line is a least-square fit with the function $y=\alpha x+\beta$; in this case, the β coefficient obtained from the fit is consistent with zero within the error of the fitting procedure.

that the plot evidences a linear dependence $y=\alpha x$ with a slope $\alpha=8.3\times 10^{-20}\text{ cm}^3\text{s}^{-1}$. This implies that $[E']_S$ is *proportional* to $[\text{H}_2]_S$.

This observation has very important implications for two of the questions we posed at the beginning of this chapter, i.e. the origin of E' and of mobile H_2 . Let us start with discussing H_2 . In general, molecular hydrogen in a α -SiO₂ sample can be either already present in the material prior to any treatment, or be generated radiolytically by the irradiation itself; in both cases it can then get involved in post-irradiation processes. However, data in Figure 6.5 allow to exclude that H_2 available for reaction with E' is already present in the samples before exposure, since in that case $[\text{H}_2]_S$ would be independent of irradiation, resulting in a constant value of Γ regardless of $[E']_S$. Then hydrogen has a *radiolytic origin*.

To make a step forward, we first observe that the rate equation (6.3) conserves the difference $[E']-2[\text{H}_2]$.^a As a consequence, the total variation of the concentration of E' in the post-irradiation stage is at most the double of the amount of available hydrogen $[\text{H}_2]_S$:

$$\Delta[E'] = 2\Delta[\text{H}_2] < 2[\text{H}_2]_S. \quad (6.5)$$

Now, we observe that radiolytic hydrogen must be generated by breaking of a suitable precursor

^aIn fact, from (6.3): $d/dt([E']-2[\text{H}_2])=0$

in which H is stored in bonded form in the as-grown material. In particular, we have seen in chapter 2 that the two main forms of bonded hydrogen in α -SiO₂ are Si–OH and Si–H,^{8,40,41} whose UV-induced breaking can release atomic H, which dimerizes to form H₂. However, photo-induced breaking of Si–OH generates NBOHC (\equiv Si–O•) as a co-product of H, according to the following reaction:^{1,8,38,42,85}



The absence of the 4.8 eV band in the *in situ* absorption profile, which we have seen to lead to the the absence of NBOHC within a few 10^{15}cm^{-3} , indicates that the photolysis of Si–OH *cannot account* for the available $[\text{H}_2]_S$, expected by eq. (6.5) to be at least one-half of $[E']_S$ since E' centers decay almost completely in the post-irradiation stage. Therefore, we can exclude process (6.6) as a possible source of radiolytic hydrogen.^b

Additionally, the linear correlation between $[\text{H}_2]_S$ and $[E']_S$ of Figure 6.5 strongly suggests that the generation processes of the two species are not independent. Based on this observations, the simplest model is that *hydrogen and E' are formed from a common precursor*, i.e. the Si–H group, whose dissociation produces E' centers and H in the same amount:



where the produced H is supposed to rapidly diffuse (at T=300 K) and dimerize forming H₂. Indeed, as a consequence of this process, $[\text{H}_2]_S=[E']_S/2$, leading to

$$\Gamma = 2k_0[\text{H}_2]_S = k_0[E']_S \quad (6.8)$$

in agreement with the results in Figure 6.5. In this model, the slope $\alpha=8.3\times 10^{-20}\text{cm}^3\text{s}^{-1}$ of Figure 6.5 equals the reaction constant k_0 between E' and H₂; this is corroborated by its close agreement with the value $k=(8.4\pm 0.5)\times 10^{-20}\text{cm}^3\text{s}^{-1}$, which was estimated by fitting the post-irradiation kinetics of E' by a second-order kinetic curve (eq. (2.28) with $k = 4\pi r_0 D_{H_2}$) derived from the Waite theory.^{210,224} Aside from the linear correlation of Figure 6.5, some more considerations further support the attribution to Si–H of the role of precursor of E' centers in wet natural silica:

A. This model explains why in the wet natural silica samples the E' are almost *completely* transient, independently of laser intensity at least in the investigated range. In fact, process (6.7) produces E' and hydrogen *exactly in the same amount*, which recombine in the post-irradiation stage so as to completely anneal the effects of exposure. In this sense, the transient nature of E' may be considered an *intrinsic* property of its very generation process. The fact that ESR measurements a few days after irradiation show a residual small concentration (~ 10 – 20% of $[E']_S$) of E' can be interpreted as a consequence of the minor reaction (5.4), which causes a small portion of the total hydrogen population to escape from recombination with the E' .

^bOur results suggest that 4.7 eV laser is unable to break efficiently Si–OH bonds, differently from 7.9 eV radiation which has been demonstrated to generate NBOHC from Si–OH with high efficiency.⁴² Our finding is consistent with data by Nishikawa *et al.*, according to which Si–H breaking is much more efficient than Si–OH breaking under 6.4 eV laser irradiation.^{72,90} It is possible, however, that the lack of observation of NBOHC under 4.7 eV laser derives from a much higher reactivity of NBOHC (compared to E') with H₂, which prevents the defect from significantly growing during the irradiation session, due to fast recombination with hydrogen during each interpulse time span. The different reaction properties with H₂ of NBOHC and E' are further discussed in chapter 8.

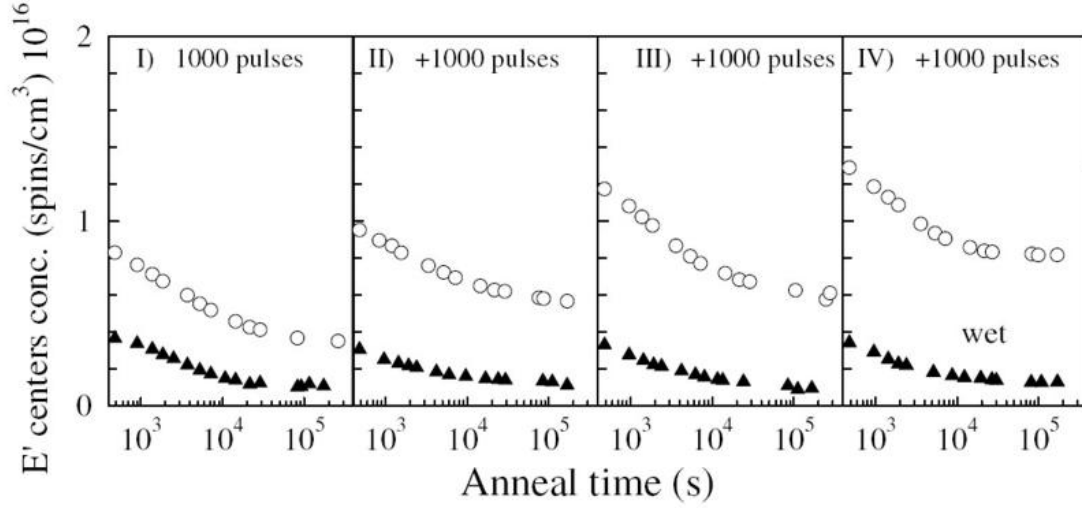


Figure 6.6: Post-irradiation kinetics of E' measured upon a sequence of identical irradiation sessions consisting in 1000 laser pulses with 1 Hz repetition rate, separated by a $\sim 10^6$ s post-irradiation stage. Full and empty symbols represent wet and dry natural silica, respectively. In wet natural silica, the decay curves repeat themselves identically after each exposure. Figure adapted from Cannas *et al.*²²⁴

B. A consequence of the precursor Si-H hypothesis is that the irradiated sample virtually returns to the same condition as the virgin material after the recombination of E' and H_2 in the post-irradiation stage is completed. Hence, the material is expected to show an "elastic" response to irradiation, meaning that if the sample is irradiated once more, the growth and annealing of E' should repeat themselves with the same kinetics as observed after the first exposure. This prediction was confirmed, at least in regard to the post-irradiation stage, by a multiple-irradiation experiment recently performed on wet fused quartz (Figure 6.6),²²⁴ thereby supporting the model proposed here.

C. Finally, further support to the Si-H precursor model comes from the critical analysis of the other possible generation models, as proposed in literature and reviewed in detail in subsection 1.2.2. In general, generation of E' centers under sub-bandgap radiation has been hypothesized to occur either by conversion of pre-existing precursors, such as oxygen deficient centers (ODC(I) and ODC(II)), strained Si-O-Si bonds and impurity bonds (Si-H, Si-Cl), or by intrinsic non-radiative decay of self trapped excitons (STEs), which has been observed only under femtosecond laser radiation or highly focused excimer laser radiation. In the present experiment, where the radiation source was a non-focused ns laser, we expect non-radiative decay of STEs to be inefficient, and the defects to be generated from precursors. The optical properties of the as-grown samples permit to go further. In fact, the typical 7.6 eV band of the ODC(I) (corresponding to an oxygen vacancy $\equiv \text{Si}-\text{Si} \equiv^{12}$) is not observed by spectrophotometric measurements in the vacuum UV (VUV) range on the as-grown natural wet samples.²⁵⁵ On the basis of the known oscillator strength,⁸ this fixes a concentration limit of $\sim 10^{16} \text{ cm}^{-3}$ for this defect. For what concerns the ODC(II) (whose models are a twofold coordinated silicon, $=\text{Si}^{\bullet\bullet}$, or an *unrelaxed* oxygen vacancy¹²), its typical optical activity, consisting in an absorption band peaked at 5.0 eV exciting two emission bands at 2.7 eV and 4.4 eV,^{8,12,93} was not observed in the as-grown materials. From the lack of these signals we infer that ODC(II) is absent

Summary I. Section 6.2 is concerned with the generation of E' centers under 4.7 eV laser irradiation in wet natural silica. To study this process we have measured the growth and decay kinetics of E' induced by irradiation at different laser intensities (Figure 6.1). Our initial aim was to answer to two apparently unrelated questions, namely the origin of E' and of hydrogen responsible for the post-irradiation decay of the defect. Eventually, our experimental observations have led to the unexpected conclusion that the two questions have in natural wet silica a common answer, namely the two species both derive from a common generation mechanism, the breaking of pre-existing Si–H precursors, eq. (6.7). In particular, this model is suggested by the linear correlation between the concentrations of E' and H_2 at the end of irradiation (Figure 6.5), where the latter is indirectly estimated from the decay rate of E' .

within $\sim 10^{15} \text{ cm}^{-3}$. So, the concentration of both varieties of ODCs is too small to account for the observed values of $[E']_S$ (Figure 6.5) and also this precursor can be excluded. Finally, the *strained* $\equiv\text{Si}-\text{O}-\text{Si}\equiv$ bonds are excluded as well, since their photolysis has been proposed in literature to generate E' -NBOHC pairs,^{83–85} but NBOHC is not observed here. In conclusion, by comparison with literature, we deduce by exclusion that the most plausible precursors *a priori* are extrinsic impurity bonds like Si–H, Si–Cl and Si–F. It is clear that among the three only the Si–H is consistent with data in Figure 6.5 and with the post-irradiation decay of E' , as it allows to explain the origin of hydrogen as a byproduct of E' generation. A further comparison with literature is proposed at the end of this section.

Before going on with the discussion, it might be worth clarifying why our treatment was based upon an indirect approach, i.e. the use of the kinetic parameter Γ proportional to $[H_2]$ at the end of the irradiation session: indeed, the *direct* measurement of $[H_2]$ would require a system able to perform *in situ*, and on a time scale of ~ 1 s, a Raman measurement sufficiently sensitive to appreciate a concentration of $\sim 10^{16} \text{ cm}^{-3}$ of the mobile species. Raman techniques, also when performed *ex situ*, are quite insensitive to such a low concentration of H_2 so that an indirect approach results to be much more feasible.

6.2.4 Discussion II: Generation mechanism

Up to now, we have provided experimental evidence that the dominant generation mechanism of E' in wet fused quartz under Nd:YAG laser radiation is the breaking of preexisting Si–H precursors. Moreover, in the irradiated samples no other OA signal significantly overlaps with the 5.8 eV band (Figure 6.2). In this sense, this appears to be a material of choice to isolate and study selectively the generation process (6.7), in order to obtain further information on the underlying mechanism and on its dynamics. This is the purpose of this and the next subsection, which are mainly concerned with the growth stage of the kinetics in Figure 6.1. One of the basic features of the kinetics in Figure 6.1, is the presence of a saturation tendency after a sufficiently high number of pulses. In addition, the saturated concentration $[E']_S$ varies with incident power. This simple observation has an important consequence: the saturation during UV irradiation is not ascribable to exhaustion of the Si–H pre-

cursors, whose initial concentration in the as-grown material would determine $[E']_S$ regardless of the irradiation conditions. Then, the saturation must arise from the reaching of an equilibrium between two competitive process, the photo-induced generation and a concurrent depletion mechanism of the induced E' population. Now, we know that after the laser is switched off, reaction (6.2) causes the decay of almost all the defects initially produced; besides, the typical time scales of growth and decay ($\sim 10^3$ s) are comparable. Due to the behavior of E' in the post-irradiation stage, we argue that reaction (6.2) is also effective in the interpulse time span, and is a possible candidate for the depletion mechanism. So, even the growth kinetics of the defects is conditioned by the interplay between pulse-induced generation (6.7) and interpulse annealing (6.2).

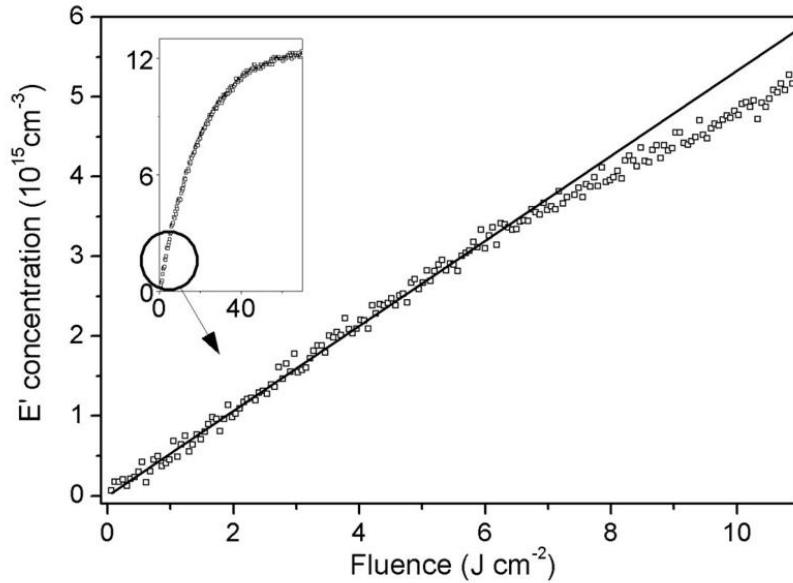


Figure 6.7: Zoom of the first portion of the growth curve Λ_3 of the left panel of Figure 6.1, and reported again in the inset. The continuous line is obtained by a linear least-square fit of the data in the first $\sim 3 \text{ J cm}^{-2}$.

Pulse-induced generation can be isolated by looking at the first stages of the growth of E' , when the growth curve is still approximately linear because the annealing process is still too slow to compete with the generation rate. So, in Figure 6.7, we report a zoom of one the kinetics in Figure 6.1 comprising the first $\sim 11 \text{ J cm}^{-2}$. By a linear fit, we can determine the initial growing slope $d[E']/d\Phi(\Phi=0)$. Then, we convert the so-obtained values to generation rates *per pulse* R :

$$R = \frac{d[E']}{dN}(N=0) = \Lambda\tau \frac{d[E']}{d\Phi}(\Phi=0) \quad (6.9)$$

where the laser pulse duration τ is 5 ns. The quantity R is finally plotted in Figure 6.8 as a function of the peak laser intensity Λ . By a least-square fit of these data with the function $R = a\Lambda^b$ we obtain $b=2.2\pm 0.2$; this means that the behavior of R is consistent with a quadratic dependence from Λ . The data in Figure 6.8 allow to address an important feature of the laser-induced breaking process of Si-H (6.7). Indeed, the quadratic dependence of R on peak laser intensity demonstrates that *two-photon processes* are involved in E' generation.

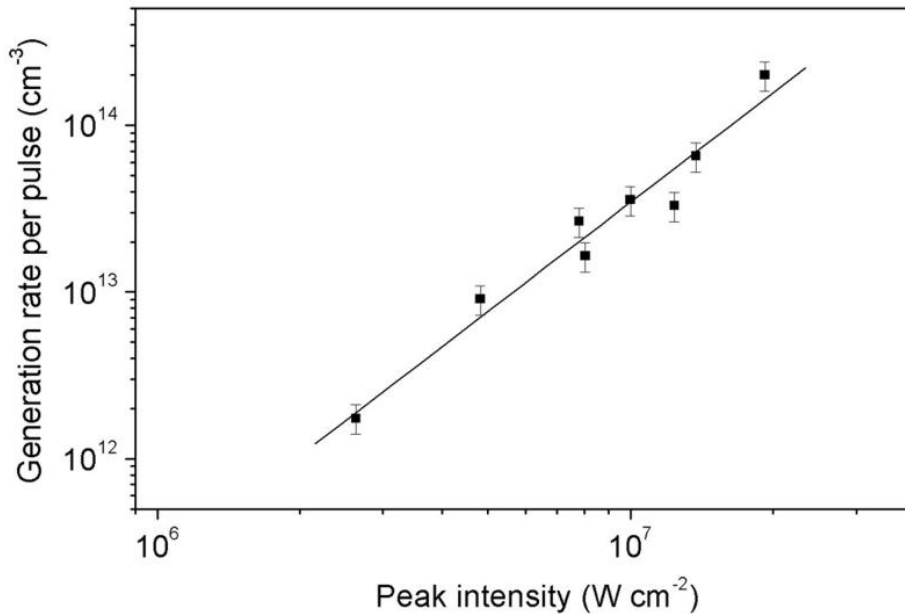


Figure 6.8: Generation rate per pulse R as a function of laser peak intensity Λ . The continuous line in the plot is a least-square fit with the function $R = a\Lambda^b$. In addition to the five irradiations in Figure 6.5, three more exposures were performed to check the repeatability of the results and to extend the explored range of Λ .

The UV absorption properties of Si–H are basically unknown at the moment;⁸ however, we can say that a two-photon mechanism is qualitatively consistent with current, though incomplete, knowledge on Si–H group: indeed, this center does not show any measurable OA at energies below the silica bandgap, and its lowest transition was predicted by theoretical calculations to be at ~ 9 eV, leading to an anti-bonding state.¹⁰⁶ Hence, the simplest E' generation mechanism consistent with present results is two photon absorption by Si–H leading to the excited state with consequent breaking of the bond. Yet, other nonlinear processes are conceivable, such as production of excitons by two photon absorption followed by non-radiative decay on Si–H. In this sense, our work provides valuable experimental support to *ab initio* theoretical calculations on the absorption properties of the hydrogen-related precursor.

As reviewed in detail in subsection 1.2.2, several works in literature have discussed the generation mechanisms of E' in α -SiO₂ under laser radiation, distinguishing between single- and multi-photon processes. Nevertheless, an important distinction must be made at this point: indeed, most of these investigations dealt with *permanent* defects, while only a few have directly observed the transient E' centers originating from the Si–H precursor.^{110,114,115} The reason for this fact is clear: due to the transient nature of the generated E' , the comprehensive study of process (6.7) requires *in situ* measurements, which have only been widely available for a few years and are the most appropriate

way to find out whether UV-induced Si-H breaking is a single- or two-photon process.

Comparing now the present results with previous *in situ* studies, we see that only in two papers^{110,115} was the dependence on laser energy density of the initial generation rate of transient E' centers studied in synthetic a -SiO₂ exposed to KrF (5.0 eV) or ArF (6.4 eV) laser radiation; it was reported to be linear¹¹⁰ and sublinear.¹¹⁵ These results are in disagreement with the quadratic dependence found here, and also difficult to reconcile with the theoretical predictions on UV absorption properties of Si-H.¹⁰⁶ At the moment the reason for this discrepancy is unclear, but it may be related to differences in the materials employed, leading to the activation of different mechanisms leading to Si-H breaking, or to the coexistence of (transient) E' centers not arising from Si-H, whereas the present samples permit a selective observation of process (6.7).

Finally, we point out that the information derived here may also be relevant for the understanding of other systems, such as Si/SiO₂ interfaces, where Si-H breakage is a very common process resulting in the formation of P_b-type interface centers (whose structure is Si₃≡Si• at the (111)Si/SiO₂ interface), this being an important mechanism of degradation of microelectronics devices.^{256,257} In particular, under laser radiation, breakage of Si-H at Si/SiO₂ interfaces has been observed to occur either by a photothermal mechanism or by direct photolysis.²⁵⁸ In these systems, theoretical work has fixed the bonding-nonbonding electronic transition of Si-H to be at 8.5 eV,²⁵⁹ not far from the value of 9 eV found in a -SiO₂;¹⁰⁶ consistently, Si-H photolysis was observed to occur by single-photon absorption of F₂ laser (7.9 eV) radiation.²⁵⁸ Taking into account the lower laser energy used in the present work, it appears that the photochemical Si-H breaking process may be quite similar in the two systems. On the other hand, breaking of Si-H under less energetic photons occurs efficiently by a *photothermal* mechanism peculiar to the Si/SiO₂ system, in which the Si-H bond is broken by providing the ~2.6 eV dissociation energy via heating due to strong absorption of the laser light by the silicon substrate.^{258,260,261}

6.2.5 Discussion III: Generation kinetics

We now proceed to address the issue of quantitatively modeling the growth kinetics of the defects. As above discussed, the growth of E' concentration is conditioned by the interplay between two-photon laser-induced generation, and concurrent annealing due to reaction (6.2). In this scheme, the kinetics of $[E']$ on the scale of many laser pulses should be described by the following rate equation, provided that N is approximately treated as a continuous variable:

$$\frac{d[E']}{dN} \sim \frac{\Delta[E']}{\Delta N} \sim R - 2k_0\Delta t[E'][\text{H}_2] \quad (6.10)$$

where R is the generation rate plotted in Figure 6.8, which equals the initial growth slope of the kinetics, while the negative term accounts for the decrease of $[E']$ during the $\Delta t = 1$ s interpulse due to annealing with H₂. Moreover, the reaction constant k_0 can be fixed to the value obtained by the fit in Figure 6.5. Then, (i) due to the correlated generation of E' and hydrogen of eq. (6.7), (ii) supposing fast dimerization of H after creation, and (iii) based also on the absence of dissolved H

prior to laser exposure, we have $[H_2]=[E']/2$. Substituting in eq. (6.10) we obtain:

$$\frac{d[E']}{dN} \sim R - k_0\Delta t[E']^2 \quad (6.11)$$

We found that this rate equation is in disagreement with the experimental kinetics, being in particular incapable of predicting the observed saturation values of $[E']$. In fact, the saturation concentration of $[E']$, found from eq. (6.11) when $d[E']/dN=0$, is given by $[E']_S = (R/k_0\Delta t)^{1/2}$; for instance we obtain $[E']_S = 2.0 \times 10^{16} \text{ cm}^{-3}$ for the kinetics at $\Lambda=12 \times 10^6 \text{ Wcm}^{-2}$, which is higher than the actual $[E']_S = 1.2 \times 10^{16} \text{ cm}^{-3}$ in Figure 6.1. A similar situation is found for all the kinetics. More to the point, we verified that the agreement with experimental data is not improved by taking into account the statistical distribution of the diffusion parameters of H_2 , which has been proposed in literature to take into account the amorphous structure of the silica matrix.^{38,42,185,206} This implies that annealing driven by H_2 -diffusion (reaction 6.2) significantly slows down the growth of the defects, but alone is insufficient to explain the observed saturation concentrations, which are still lower than predicted; for this reason, an additional negative term has to be added to the rate equation.

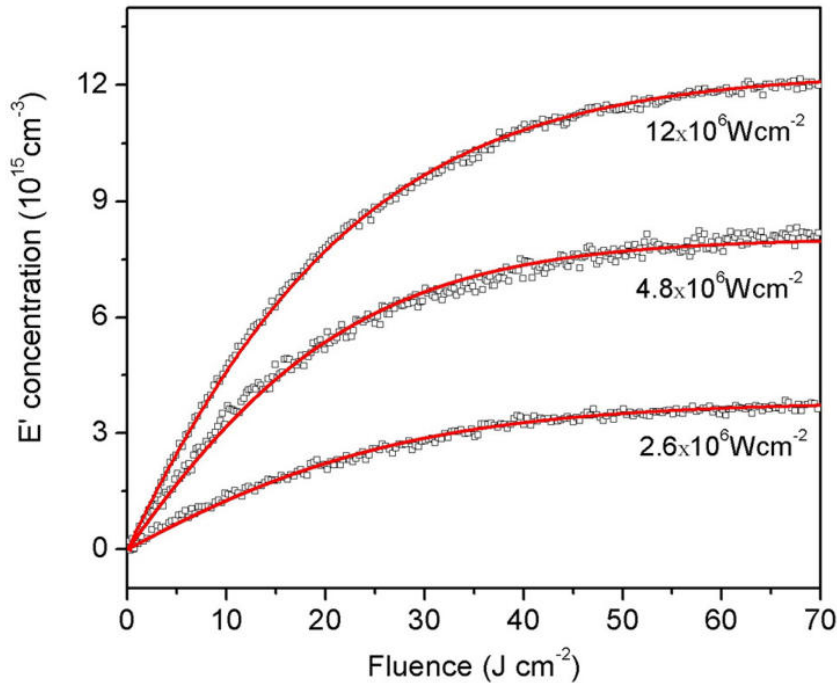


Figure 6.9: Growth kinetics of E' from Figure 6.1 fitted by eq. (6.13) with respect to the free parameter α .

On this basis, we found empirically that all the kinetics can be satisfactorily fitted by adding a linear term to eq. (6.11) as follows:

$$\frac{d[E']}{dN} = R(1 - \alpha[E']) - k_0\Delta t[E']^2 \quad (6.12)$$

this being equivalent to supposing a (linear) concentration dependence of the generation rate. The analytical solution of eq. (6.12) with the initial condition $[E'](N=0)=0$, and changing variable back to fluence ($\Phi=\Lambda\tau N$) is the following:

$$[E'(\Phi)] = \frac{\gamma}{k_0\Delta t} \left[\tanh\left(\frac{\gamma}{\Lambda\tau}\Phi + \beta\right) - \tanh\beta \right] \quad (6.13)$$

where

$$\gamma = \frac{\alpha R}{2} \sqrt{1 + 4\frac{k_0\Delta t}{\alpha^2 R}} \quad \text{and} \quad \tanh\beta = \frac{\alpha R}{2\gamma}$$

Hence, the growth stage of the three representative kinetic curves from Figure 6.1 was fitted with the function (6.13), depending on the free parameter α . The results are reported in Figure 6.9: it is seen that the predicted curves are consistent with experimental data. Similar results are obtained in all Nd:YAG irradiation experiments on wet natural silica. The values of α from the fits all fall in the interval $(5.7\pm 1.4)\times 10^{-17} \text{ cm}^3$.

We discuss now the possible interpretations of the linear term $-R\alpha[E']$. The rate equation (6.10) has been written in the approximation of an infinite population of Si-H. Actually, even if the saturation of $[E']$ is due to the equilibrium between generation and annealing (as above discussed), it is anyway possible that the progressive reduction of the precursors has to be accounted for in the generation term. In this respect, we note that eq. (6.12) can be rewritten as follows

$$\frac{d[E']}{dN} = R'(\alpha^{-1} - [E']) - k_0\Delta t[E']^2 \quad (6.14)$$

where $R' = R\alpha$; this equation can be seen as the generalization of (6.10) in the case of a finite concentration α^{-1} of pre-existing Si-H. This interpretation also seems to be corroborated by the fact that $\alpha^{-1} \sim 1.8\times 10^{16} \text{ cm}^{-3}$ is found by the fits to be reasonably independent of Λ . Hence, to better understand this point, we compared this predicted value of the Si-H concentration in the as-grown specimens with the results of Raman measurements.

A typical Raman spectrum of a HER1 sample is shown in Figure 6.10. The spectrum shows a weak and broad signal between $2000 - 2500 \text{ cm}^{-1}$, in the same spectral region in which it is known to peak the typical 2250 cm^{-1} signal of Si-H groups in $a\text{-SiO}_2$.^{40,41} However, the width of the signal in Figure 6.10 appears to be significantly larger than that reported in literature for Si-H ($<100 \text{ cm}^{-1}$). Hence, it is likely that other components aside from Si-H contribute to the measured signal, a possibility being the intrinsic vibrational peak of the silica matrix whose frequency is reported in literature to fall near the Si-H signal.^{40,41} Hence, our present data permit only to fix a superior limit for [Si-H]. To this purpose, if one tentatively ascribes all the amplitude of the signal in Figure 6.10 to Si-H, the corresponding concentration of the defect can be calculated by comparison with literature data and exploiting the signal (out of scale in Figure 6.10) near 800 cm^{-1} as a benchmark to take into account different instrumental sensitivity.⁴¹ In this way we obtain $[\text{Si-H}] \sim 5\times 10^{17} \text{ cm}^{-3}$. This value is more than one order of magnitude higher than α^{-1} . If taken literally, this estimate suggests that the linear term cannot arise from the finite number of precursors, which is much higher than the maximum concentration of attainable $[E']$. We cannot exclude, however, a much smaller Si-H signal concealed under the broad component observed in Figure 6.10. While the present data do not allow

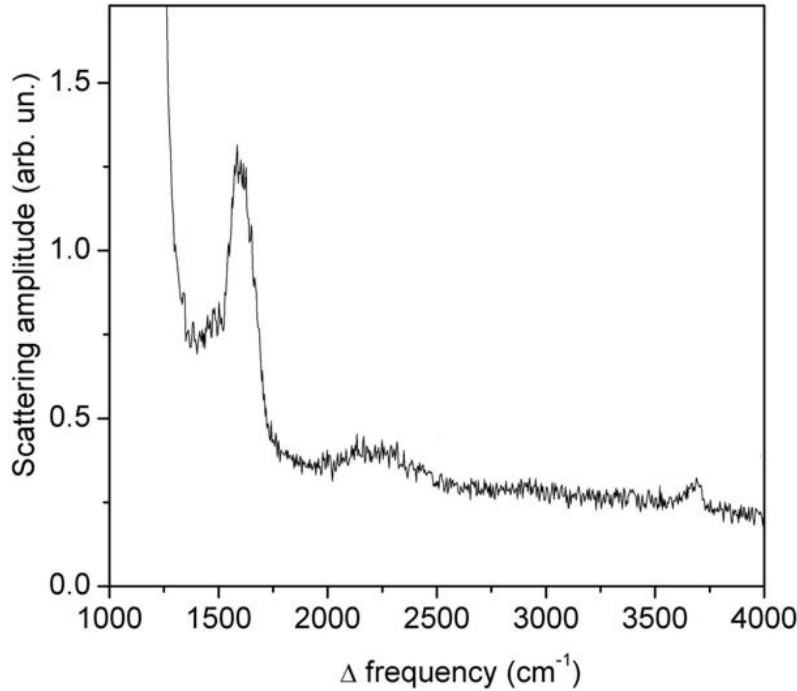


Figure 6.10: Raman spectrum of an as-grown wet natural silica sample. The signal between 2000 cm^{-1} and 2500 cm^{-1} supposedly comprises a contribution (expected at 2250 cm^{-1}) due to the Si-H centers, while the signal near 3700 cm^{-1} is due to Si-OH impurities.

to provide a definite answer to this point, we discuss in the following other two possible explanations of the linear term.

One of them may be the reaction of $[E']$ with molecular hydrogen already dissolved in the sample before laser exposure, in concentration $[\text{H}_2]_0$. In fact, in this case the relation $[\text{H}_2]=[\text{H}_2]_0+[E']/2$ deriving from (6.7) becomes $[\text{H}_2]=[\text{H}_2]_0+[E']/2$, so that eq. (6.11) is generalized as follows:

$$\frac{d[E']}{dN} = R - 2k_0\Delta t[\text{H}_2]_0[E'] - k_0\Delta t[E']^2 \quad (6.15)$$

giving rise to a linear term (whose coefficient should be independent of laser intensity).

Now, as already observed, the linear correlation between E' and H_2 at the end of exposure (Figure 6.5) excludes the presence of H_2 in significant concentrations prior to irradiation. To make quantitative this argument, we note that in presence of $[\text{H}_2]_0$, eq. (6.8) would be modified as follows:

$$\Gamma = 2k_0[\text{H}_2]_0 + k_0[E']_S \quad (6.16)$$

introducing a nonzero intercept in Figure 6.5. On this basis, from the data one can fix a limit for $[\text{H}_2]_0$: $[\text{H}_2]_0 < 10^{15}\text{ cm}^{-3}$, which in turn gives the following estimate of the linear coefficient, $2k_0\Delta t[\text{H}_2]_0 \sim 10^{-4}$. However, this is between one and two orders of magnitude smaller than the values of $R\alpha$ coming

Summary II. *In wet natural silica, the dependence of the generation rate of E' centers from laser intensity is found to be quadratic (Figure 6.8). This suggests that two-photon processes are involved in the photochemical generation mechanism of E' , eq. (6.7). Moreover, a peculiar feature of the generation process of E' from Si–H is to produce mobile hydrogen together with E' centers. As a consequence, the growth of E' during irradiation is limited by the simultaneous occurrence of reaction (6.2). This leads to a characteristic growth curve (Figure 6.9) which can be satisfactorily modeled by a suitable rate equation, eq. (6.12). The ability of eq. (6.12) to fit the growth stage of the kinetics of E' centers is a further, albeit indirect, confirmation of the validity of our interpretation eq. (6.7) of the generation process of the defect.*

from the fits (except at the two lowest laser intensities used). So, this mechanism at the basis of the linear term can be excluded.

Finally, another qualitative interpretation can be tentatively proposed, based on a more accurate discussion of the generation process (6.7): in general, a H produced by (6.7) diffuses in the matrix and may experience two different fates: it can either meet another H and dimerize in H₂ or it can come across an E' and passivate it; for this reason, aside from the slow annealing due to reaction (6.2), the E' centers undergo a much faster decay (FD) due to recombination with a portion of the H population made available by each pulse. In addition, the portion of H involved in the FD is expected to increase with E' concentration, which enhances the probability of encountering an E' before meeting another H. A FD stage with similar features was directly observed *in situ* for NBOHC produced by F₂ laser irradiation at T₀=300 K, and occurs on a typical timescale which is shorter than the 1 s interpulse.¹¹⁶ Besides, the FD is not accounted for in the stationary-state approximation for H, which considers only the H produced at the right side of eq. (6.2): in other words, during the irradiation the stationary-state approximation is expected to fail just after each pulse due to the excess H produced by (6.2) which is still to dimerize. From the experimental standpoint, since the FD cannot be directly observed with the time resolution available here, it is incorporated *de facto* in the generation term, which must actually be interpreted as the net concentration of [E'] generated by (6.7) and surviving fast recombination with H. Now, given that the portion of H quickly recombining with [E'] must increase with E' concentration as the irradiation session progresses, we expect a consequent reduction of the generation rate from its initial value R , which to a first approximation can be represented by a linear term in [E'], as in (6.12).

We acknowledge that understanding the origin of the linear term is not an easy problem, and that more measurements are surely needed to conclusively solve it. However, it is worth pointing out the main merits of the simple model proposed here: it allows to describe the kinetics and the saturation of E' as a consequence of hydrogen-related reactions, and it is able to reproduce independent datasets coming from several irradiation sessions with only one free parameter.

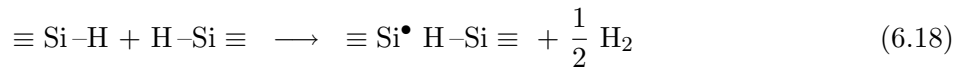
6.2.6 Previous literature on the Si–H generation model

In a sense, the Si–H model provides a particularly straightforward interpretation of the effects of pulsed Nd:YAG laser irradiation in natural wet a -SiO₂: E' and H are generated together by laser light and recombine in the post-irradiation stage, so that the matrix virtually returns to the native state after the decay is completed. Also, this process appears the analogue on Si–H to the generation of NBOHC from Si–OH groups (Reaction 6.6), quite clearly demonstrated in several works.^{38,42,85}

Generation of E' from Si–H under laser irradiation has been repeatedly proposed in literature (see subsection 1.2.2), most of the time on the basis of qualitative considerations. A convincing evidence of this process has been provided by Imai *et al.*, who irradiated an oxygen-deficient sample preliminary treated at high temperature in H₂ atmosphere, so as to strongly increase the concentration of Si–H by the reaction:



As a consequence of reaction (6.17), Si–H becomes one of the dominant impurities in the material. Then, Imai *et al.* reported that after treatment in H₂, the generation efficiency of E' is strongly increased, supposedly because Si–H serves as a precursor for the paramagnetic center. One of the possible generation mechanism of E' proposed by Imai *et al.* to apply in this case is:



where the first term at the right side is to be considered an E' as it contains the ($\equiv\text{Si}^\bullet$) structure. To further confirm the role of Si–H as a precursor, Imai *et al.* also observed that a portion of the paramagnetic centers decay in the post-irradiation stage, supposedly due to reaction with H₂. The circumstance that the decay was not complete indicates either that other precursors still contributed to the generation of E' or that a portion of H₂ was involved in a reaction with another paramagnetic defect.

Some interesting observations arise from comparison of our results with those by Imai *et al.*, obtained on samples in which the Si–H precursor should be present mainly in the form predicted by eq. (6.17), i.e. a *hydrogen-decorated vacancy*. Indeed, in general it is conceivable for Si–H to exist also as an isolated defect, depending on the reactions that control the incorporation of such impurity during the manufacturing procedure of the material.^c For the moment, our results do not allow to understand the prevalent form in which Si–H is incorporated in our samples; more in general, these considerations suggest the need of further studies to understand if different varieties of Si–H actually exist in a -SiO₂ and whether their UV-induced breaking process are different. However, it is worth noting the following: if the H-decorated vacancy happened to be the most common form of Si–H in a -SiO₂ also in the case of *non*-H₂-loaded samples (such as our materials), then it is possible to argue that the generation process eq. (6.7) proposed in this chapter should be re-interpreted as eq. (6.18). This would not invalidate the essence of our conclusions, but it would give further information on

^cA further possibility is that Si–H defects are coupled to nearby Si–OH, if both are formed by reaction of H₂ with the silica matrix within the atmosphere in which the material is produced.^{40,108}

the structure of the E' center produced in our experiments. In fact, while the E' produced from an isolated Si–H is simply an (isolated) silicon dangling bond ($\equiv\text{Si}^\bullet$), the defect at the right side of eq. (6.18) comprises a nearby Si–H group, thereby coinciding with what in literature has been generally called E'_β .^{d,1,38} The E'_β is distinguishable in principle from the other varieties of E' by ESR, as it features a slightly different g tensor.¹ Unfortunately, present ESR data are not accurate enough to operate such a distinction. We note, however, that this is an interesting hypothesis that deserves further investigation, because it implies that the E'_β absorbs at 5.8 eV, contrary to the fact that a 5.4 eV band has been provisionally ascribed to the defect.^{e,12}

After Imai *et al.*, only a few researchers improved the experimental approach by using *in situ* optical absorption to investigate laser-induced generation of E' . In particular, Smith *et al.*¹¹⁴ proposed that laser-induced E' are unstable only in samples containing free dissolved H_2 prior to irradiation. Their conclusion is apparently at variance with the Si–H model, in which H_2 should be always available at the end of irradiation because it is produced radiolytically. In contrast, in the pioneering work by Leclerc *et al.*,¹¹⁰ it was already proposed that generation of transient E' occurs by breakage of Si–H, but the detailed description of the generation process involved a two-step mechanism, in which E' are first produced by unknown precursors, then converted to an unknown \overline{E}' (later identified with Si–H), which successively serves as an efficient precursor for E' for successive generation upon repeated irradiations of the same sample. Finally, as already discussed, disagreeing results were reported in literature when trying to apply *in situ* measurements to find out if transient E' generation occurs by a single- or by a two- photon process.

Present results were obtained in a non- H_2 -loaded silica sample and improve the understanding of this problems in many aspects. Despite previous works had proposed Si–H breaking to be one of the possible channels contributing to E' generation in H_2 -loaded materials, where Si–H is one of the prevalent impurities, our evidences suggest this to be a mechanism that can be dominant in standard non-treated samples. Also, the post-irradiation instability that leads to the almost complete disappearance of the induced defects, is now proposed as an *intrinsic* feature of the E' centers inherent to their very generation process, not being related to hydrogen dissolved prior to laser exposure. Furthermore, we have provided rigorous proofs basically leaving generation of Si–H as the only possible generation mechanism of E' in our experimental conditions. In contrast with previous results, we have obtained a direct proof of a two photon generation mechanism for Si–H breaking, consistently with theoretical and experimental expectations on the UV absorption properties of the Si–H groups. Finally, for the first time we have addressed the issue of quantitatively modeling the growth kinetics of the defects with a suitable rate equations model.

In this sense, *in situ* OA spectroscopy demonstrates its usefulness, as it has permitted to study quantitatively the first stage of the decay, thus yielding the correlation of Figure 6.5, and the first

^dThe E'_β was originally introduced as the reaction product between an oxygen vacancy and a hydrogen atom, giving the same result as reaction (6.18).^{1,38} Actually its microscopic model presupposes a structural relaxation (not represented in (6.18)) at the end of which the unpaired electron points away from the former vacancy.

^eHowever, we stress that the identification of our E' with the E'_β is not a necessary consequence of the decorated vacancy hypothesis; indeed, Imai *et al.* proposed an alternative photochemical reaction, eq. (1.7), which generates the usual E'_γ .

stage of the growth, demonstrating a two-photon mechanism for Si–H breaking. Moreover, only the observation of the complete absorption profile has allowed to exclude the generation of (transient) NBOHC, and in turn to exclude laser-induced breaking of Si–OH.

From a wider point of view, it is expected that the generation processes induced by laser exposure can be triggered as well by ionizing radiation. Consistently, the formation of E' from Si–H precursors has been proposed in literature also as a mechanism activated by γ or β irradiation.^{1,2,28,75} In particular, a recent investigation has supported this generation model on the basis of an accurate study of the ESR lineshape of γ -induced E' centers, carried out in several commercial α -SiO₂ samples including those used in the present work.²⁶² In this context, we remark that also in the case of γ irradiation, the study of the *in situ* kinetics and of the post-irradiation stability of E' may allow to infer additional information complementary to what is known from the *ex situ* investigations.

As a final remark we add that the present results, together with all the others in literature promoting the Si–H generation model, suggest an important hint on the still open problem of understanding the nature of the 5.8 eV transition leading to the E' absorption band. In fact, as anticipated in the introduction, some theoretical calculations^{33,34} have suggested the band to be due to a *charge transfer* transition from the silicon dangling bond ($\equiv\text{Si}\cdot$) to the charged Si⁺, which is expected in front of it when the E' is generated by ionization of a vacancy:



the E' at the right side of eq. (6.19) is what we have defined *vacancy- E'* . On the other hand, this interpretation of the OA band has been questioned by other authors,³⁵ and calculations have also predicted another weaker absorption, falling in the same energy region but due to a transition entirely comprised within the basic $\equiv\text{Si}\cdot$ moiety of the defect.^{12,33} In this context, our results strongly suggest that an E' absorbing in the "standard" 5.8 eV band may come from Si–H breakage. So-produced E' is expected to be structurally different from *vacancy- E'* , not containing the Si⁺ portion and being more similar to an isolated dangling bond. Hence, the lack of the Si⁺ fragment excludes the charge transfer model, and we conclude that our results point towards the *intra-dangling-bond* interpretation of the the 5.8 eV electronic transition.

6.3 E' center in other types of α -SiO₂

6.3.1 Dry natural silica

We have seen in the previous chapter that the generation of E' centers under 4.7 eV pulsed laser irradiation occurs as well in *dry* natural silica materials, and its efficiency is comparable with *wet* natural silica. Moreover, also in the dry materials the E' centers are unstable in the post-irradiation stage due to reaction with mobile H₂. Nonetheless, there is an important difference between the two cases. In fact, while the E' generated in the wet samples are almost completely annealed after the end of exposure by reaction (6.2), in the dry samples the passivation is incomplete, meaning that only a fraction of the E' are annealed and a residual concentration remains in the sample after that

the reaction is completed. This in turn implies that the concentration $[\text{H}_2]_S$ of hydrogen available at the end of irradiation must be insufficient to completely cancel the defects, i.e. $[\text{H}_2]_S < [E']_S/2$, differently from the wet samples where, as a consequence of the generation process (6.7), we have $[\text{H}_2]=[E']/2$.

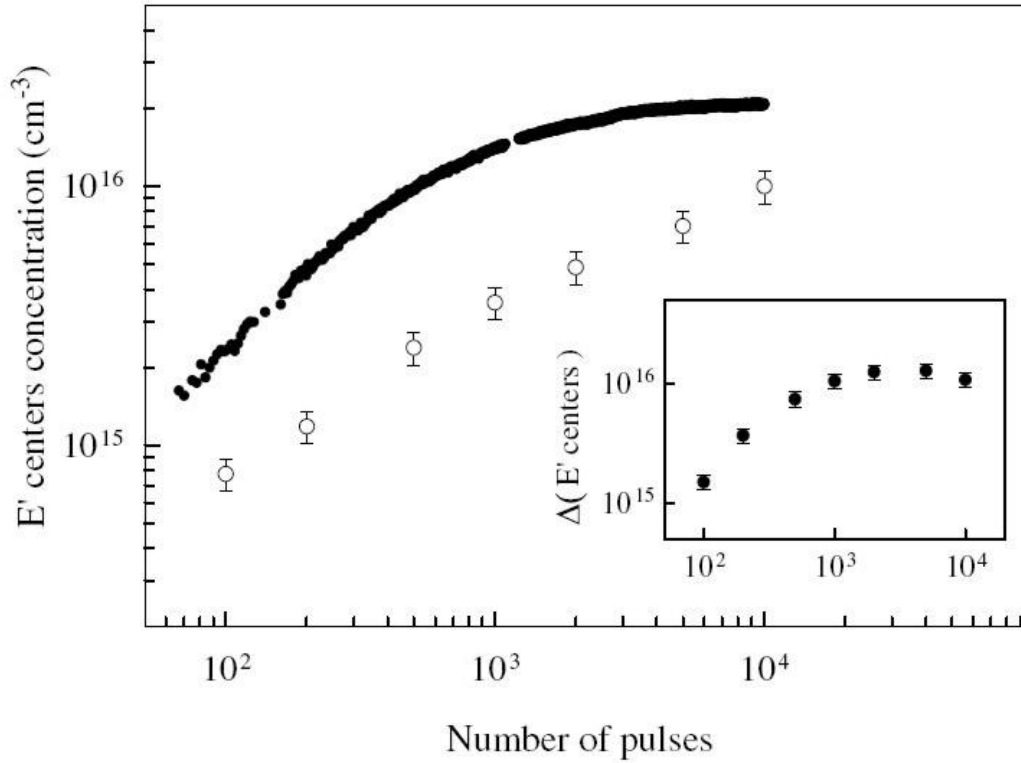


Figure 6.11: Concentration of E' measured *in situ* during laser irradiation (full symbols), and stationary concentrations measured with ESR at the end of the post-irradiation annealing process after exposure to different laser of pulses (empty symbols). Inset: difference between the two curves, representing the post-irradiation reduction of the E' . Figure taken from Messina *et al.*²⁴⁹

To better understand this issue, we performed the following experiment on natural dry Q906 samples. A set of virgin samples were irradiated with different numbers of pulses ranging from 100 to 10000, using a pulse repetition rate of 1 Hz and an energy density of 40 mJcm^{-2} per pulse. For each sample, we waited a few days after the end of the irradiation session, so as to be sure that the post-irradiation kinetics was completed; then, the stationary concentration $[E']_\infty$ was estimated by ESR. On another virgin sample it was measured *in situ* the growth curve of E' during irradiation in the same conditions. In Figure 6.11 the results of the two measurements are compared. These data show that the stationary concentration $[E']_\infty$ follows a sub-linear dependence on the number of received pulses, very different from the behavior of the *transient* concentration measured *in situ*, and different also from wet natural silica, where there is no accumulation of E' with dose, as they are almost completely annealed after the end of irradiation independently of the received number of pulses. In addition, the difference $\Delta[E']$ between transient and stationary concentration, reported in the inset, depends on the irradiation dose as well. Analogous results are obtained on I301 dry fused

silica samples.

Now, the post-irradiation decrease $\Delta[E']$, equals two times $[H_2]_S$, so as to represent another indirect measurement of the amount of available hydrogen at the end of exposure. In this sense, the results in Figure 6.11 demonstrate that *also* in natural dry silica hydrogen has a *radiolytic origin*, since its concentration grows with dose. Furthermore, the same considerations that demonstrate that NBOHC are not generated in significant (comparable to E') concentrations in wet samples apply also here, where the typical induced OA profiles (Figures 5.4 and 5.10) do not contain any appreciable 4.8 eV band and PL measurements do not detect the characteristic 1.9 eV emission.

Based upon these considerations and on comparison with wet samples, the simplest interpretation is the following. Also in dry samples, process (6.7) is the most likely source of the hydrogen responsible for the decay of E' , and generates a *portion* of the total E' population. However, in dry glass a second formation channel of E' apart from (6.7) is active: as a consequence, concentration of generated E' is higher than $[H_2]_S/2$, so that available molecular hydrogen is insufficient to completely cancel the induced defects.^f In this respect it is worth stressing that the entity of the post-irradiation decay of E' is comparable in the two materials (confront Figure 6.11 with the typical concentrations of E' in wet, as in Figure 6.1, or see Figure 5.10). This suggests that dry and wet silica, although differing of more than one order of magnitude for what concerns the concentration of Si–OH impurities (Table 4.1), seem to be unexpectedly similar in the content of Si–H groups.

Within the proposed scheme, the population of E' centers consists in two portions: the defects E'_H coming from Si–H, plus a contribution E'_X arising from the second formation process. Since the concentration of hydrogen made available by each laser pulse is one-to-one correlated to the E'_H component, the stationary concentration $[E']_\infty$ in Figure 6.7 is related only to the presence of E'_X : more precisely, $[E']_\infty$ equals the total concentration of defects generated from the precursor X during the irradiation session^g. Dry and wet materials also differ in the behavior under repeated irradiations: in fact, while wet samples appear to be "elastic" upon re-irradiation, in the dry glass (Figure 6.6) the presence of the additional E'_X component leads to the progressive accumulation of the defects with increasing number of exposures. At the moment it is not possible to identify the generation process of E'_X , although the presence of oxygen deficient centers (Si–Si vacancies) in dry fused glass²⁵⁵ suggests this defect to be a possible precursor. More studies may help to clarify this point.

A last subtle question must be addressed to have a comprehensive scheme of the E' generation-

^fWe have performed Raman measurements also on dry fused silica samples: they show a signal similar to that in Figure 6.10, which supposedly comprises the contribution at 2250 cm^{-1} due to the Si–H groups. In this case, however, the presence of Si–H in the I301 glass, in concentrations exceeding 10^{18} cm^{-3} , was reported also by the manufacturer of the material.²⁶³ This supports the role of Si–H as a precursor of E' also in dry silica, and suggests that the Si–H signal significantly contributes to the broad component between $2000\text{--}2500\text{ cm}^{-1}$ observed in our Raman spectra.

^gThis does not imply, however, that $[E']_\infty$ equals the concentration of E'_X at the end of exposure. In fact, since both E'_X and E'_H react with H_2 (see later), $[E'_X]$ at the end of exposure is already depleted of the portion of defects which have been passivated by H_2 during the irradiation session. What is true is only that $[E']_\infty$ (times the volume of the sample) equals the number of generation *events* from the precursor X which have occurred during all the irradiation session.

annealing dynamics in these materials. Indeed, in the case of dry natural silica, it is not obvious *a priori* if reaction with H_2 involves *all* E' centers generated by irradiation or only the portion coming from the Si-H precursor. To clarify this issue, we performed the following repeated irradiation experiment. An I301 natural dry sample was preliminarily irradiated with $N_1=2500$ laser pulses of 70 mJcm^{-2} energy density. After the post-irradiation kinetics is completed, we measured with ESR that $[E']_\infty(N_1)=(1.0\pm 0.1)\times 10^{16}\text{ cm}^{-3}$. Then, the sample was irradiated a second time with 50 laser pulses. The concentration kinetics of E' during and after this second exposure is reported in panel (a) of Figure 6.12. For comparison, we report in panel (b) the result of the same 50 pulses irradiation on an as-grown sample. The two kinetics are different; indeed, on the as-grown sample, 50 pulses induce

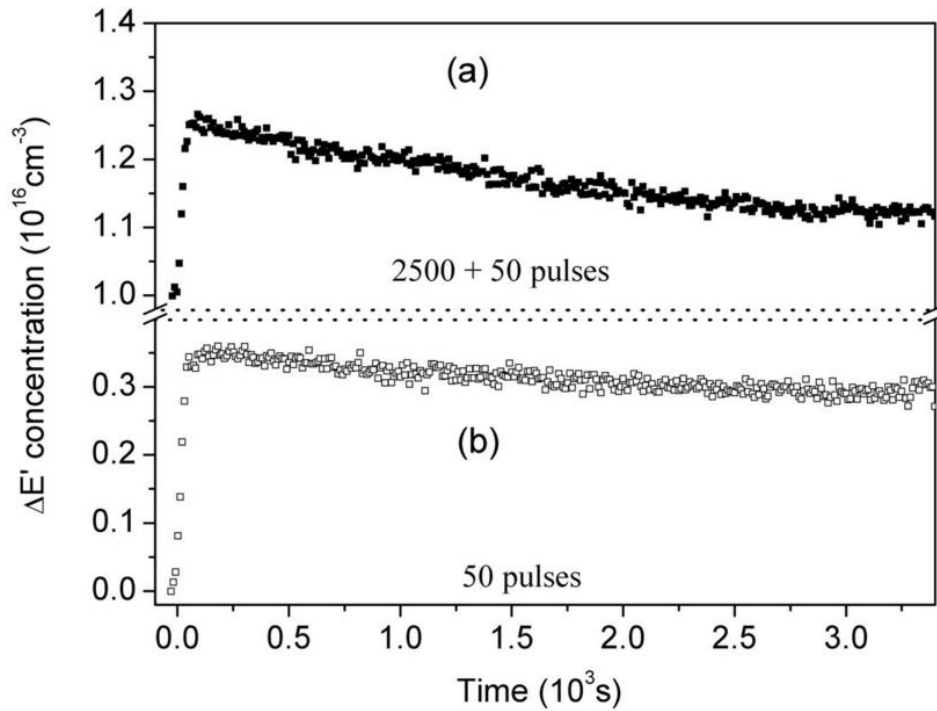


Figure 6.12: Panel (b): Kinetics of $[E']$ induced on an as-grown I301 sample by irradiation with 50 pulses. Panel (a): the same experiment, but performed on a sample which already contained $[E']\sim 10^{16}\text{ cm}^{-3}$ due to a previous irradiation.

the generation of $[E']_S(50)=(0.36\pm 0.04)\times 10^{16}\text{ cm}^{-3}$ defects, $\sim 17\%$ of which decay after 1 hour of the post-irradiation stage; in contrast, the re-irradiation of the sample which had already received 2500 pulses induces a smaller variation of $[E']$ from $[E']_\infty(N_1)$: $(0.25\pm 0.02)\times 10^{16}\text{ cm}^{-3}$; most important, the decay of the induced defects is faster ($\sim 55\%$ after 1 hour).

To discuss this experimental result, let us consider again the expression for the reaction rate (6.3). If only the E'_H centers were reactive with H_2 , $[E']$ on the right side of (6.3) should be identified with $[E'_H]$ and the decay kinetics would be independent of the previous history of the sample, not influenced by other contributions to the *total* E' concentration. Results in Figure 6.12 are at variance

Summary III. *After discussing the generation of E' in wet natural silica, the last part of this chapter discusses the experimental results found on other varieties of amorphous a - SiO_2 . The kinetics of E' centers in dry natural silica are found to be different from wet natural silica, in that the post-irradiation decay of the defects induced in the dry specimens is only partial (Figure 6.11). This can be explained by supposing a second generation channel of E' active in dry silica concurrently to Si-H breaking, so that the concentration of hydrogen available for reaction (6.2) is always smaller than that of E' centers. Finally, 4.7 eV laser irradiation appears to be basically unable to generate E' centers in synthetic silica; several interpretations of this finding are conceivable and discussed in the text.*

with this picture, as the decay of the defects induced by 50 pulses is accelerated when the sample, prior to irradiation, already hosts a concentration $[E']_\infty(N_1)$ due to a previous exposure. This is a consequence of the increase of the right side of (6.3) due to the addition of $[E']_\infty(N_1)$ to the total population of reacting centers. Then we conclude that *all* E' centers participate in the reaction of H_2 independently of their origin.

6.3.2 Synthetic silica

As described in the previous chapter, no E' centers generation is observed in synthetic silica upon laser irradiation, at least within the same intensity range used in the experiments on natural silica. Within the interpretation proposed so far, the simplest explanation of this result would be the absence of Si-H precursors in synthetic a - SiO_2 . Nonetheless, this seems somewhat unlikely, since we have seen that both dry and wet natural a - SiO_2 contain appreciable concentrations of Si-H , which must be incorporated during the manufacturing process, and is not expected to depend on properties of the starting material (quartz *vs* SiCl_4). Raman measurements aimed to investigate the presence of Si-H in synthetic S1 and S300 samples (see Table 4.1) were not able to observe any signal in the 2000–2500 cm^{-1} region, because of the presence of an unknown luminescence signal which made impossible the observation of the Raman scattering in this spectral range. Finally, differently from the case of Si-OH no comprehensive literature data are available to clarify how the concentration of Si-H depends on the type of silica.

Another possible explanation is that E' are not efficiently generated due to the presence of pre-existing H_2 already dissolved in the as-grown samples in high concentration. In fact, in this case the generated E' would be immediately annealed by reaction with H_2 so as to prevent their growth. This could be the case for synthetic *wet* materials, which several authors have claimed to be impregnated with high (up to $\sim 10^{18} \text{ cm}^{-3}$) concentrations of hydrogen molecules even when as-grown.^{42, 221} This hypothesis need to be verified by applying to the samples a degassing procedure prior to irradiation, or by studying the effects of irradiation at low ($< 200 \text{ K}$) temperatures, so as to block molecular hydrogen mobility.

Finally, we should consider the possibility of extrinsic impurities in the material playing some

indirect role in E' generation. Even if the (main) precursor of the paramagnetic center is Si–H, impurities may for example serve as intermediate states in *two step absorption* assisting the generation of hole-electron pairs, which then could form excitons whose non-radiative decay on the Si–H precursor would give the E' . In conclusion, the lack of observation of E' by 4.7 eV pulsed laser radiation in synthetic silica remains here as an open issue that requires further investigation.

6.4 Conclusions

We studied the generation and annealing dynamics of E' centers induced by 4.7 eV pulsed laser irradiation in α -SiO₂, mainly on the basis of *in situ* optical absorption spectroscopy. We first discussed the process as observed in wet natural silica. The experimental results indicate that hydrogen responsible for the decay of E' in the post-irradiation stage has a radiolytic origin. Furthermore, the generation processes of E' and hydrogen are correlated, consistently with a model in which the two species are formed by photo-induced breaking of a common precursor Si–H. The dependence of the initial generation rate on laser intensity is quadratic, demonstrating a two-photon mechanism for E' generation. The kinetics and the saturation of the process are the result of competition between the action of radiation and the annealing of E' due to reaction with H₂. On this basis, a rate equation model was proposed and tested against experimental data. In dry natural silica, also a second generation process contributes to the total concentration of the defects; both types of E' centers participate in the reaction with H₂. The possible reasons of the lack of E' in irradiated synthetic silicas are discussed from a qualitative point of view. These results prove the usefulness of *in situ* time-resolved detection of absorption spectra to perform comprehensive studies on transient point defect conversion processes and their effect on the transparency of optical materials during UV exposure.

Chapter 7

Post-irradiation conversion processes at room temperature

This chapter focuses on the kinetics of point defects in natural α -SiO₂ after the end of laser irradiation at room temperature. The results, obtained exclusively by *ex situ* experimental techniques, provide a deeper understanding of the processes involving Ge-related impurities and of the kinetics driven by diffusion and reaction of H₂.

7.1 Introduction

In the previous chapter we have carried out a detailed analysis of the *in situ* kinetics of E' , permitting in particular to clarify several aspects of its generation mechanism and growth kinetics. We make now a step backwards, returning to the interpretation of post-irradiation processes that in chapter 5 was proposed mostly on the basis on qualitative considerations. Indeed, in our initial discussion, one of the most convincing reasons to interpret the decay of E' as a consequence of reaction with mobile H₂ has been the observation of the simultaneous growth of the Ge-related H(II) centers (=Ge[•]-H), attributed to H trapping on pre-existing GLPC (=Ge^{••}) impurities:



where atomic hydrogen at the left side of reaction (7.1) was supposed to be made available by cracking of H₂ on E' centers. Hence, the conversion of GLPC in H(II) played the central role of *probing* the presence of diffusing hydrogen, strongly suggesting its involvement also in the decay of E' .

Nevertheless, several questions were left open by our discussion in chapter 5: **(i)** to convincingly prove our interpretation of the post-irradiation processes we still have to demonstrate that the time dependencies of GLPC, H(II) and E' can be quantitatively accounted for by a chemical kinetics model describing the diffusion and reactions of mobile H₂ and H. **(ii)** Although process (7.1) very reasonably explains the growth of H(II), to prove it we still need to evidence an anticorrelation

between the reduction of GLPC^a and the growth of H(II). **(iii)** The reason why the concentration of H(II) remains very low *during* irradiation is still to be elucidated. **(iv)** Finally, it is interesting to find out if GLPC subjected to laser irradiation undergoes other conversion processes parallel to (7.1). For these reasons, in this chapter^{247,264,265} we extend the discussion of chapter 5 on the post-irradiation processes observed in natural silica, with the aim to clarify these unsolved problems.

Aside from the present relation with the kinetics of E' center, there is also another reason motivating us to further investigate the conversion process of GLPC into H(II). In fact, we recall from subsection 1.2.3 that the laser-induced conversion processes of Ge-related defects in α -SiO₂ currently attract a strong research interest because of a variety of properties featured by Ge-doped silica under laser exposure, e.g. photosensitivity and second harmonic generation, quite relevant for applications and partly ascribable to Ge-related defects. The existing experimental investigations on these topics have been invariably carried out on samples of Ge-doped silica (with typical Ge concentrations of a few %), material of choice in the fabrication of optical fibers. As-grown Ge-doped α -SiO₂ usually features an OA band at ~ 5.1 eV: the defects contributing to this signal are widely believed to behave as efficient precursors readily convertible in paramagnetic centers by laser radiation. Nonetheless, while this absorption band seems to play a central role in laser-induced processes in Ge-doped silica, the current understanding of the microscopic conversion mechanisms is still incomplete. Also, the presence of H₂ has been demonstrated to enhance Ge-related conversion processes and photosensitivity, but the underlying microscopic interactions between Ge defects and H₂ are unclear to a large extent. Finally, scanty literature data exist on the kinetics of these phenomena, since most of the studies have been carried out by investigating only the stationary defect concentrations before and after laser irradiation.

In this context, natural α -SiO₂ is a potentially interesting material since it contains Ge in concentrations (a few ppm, see Table 4.1) much lower than Ge-doped silica. In this sense, Ge atoms are incorporated as *dispersed* impurities, as opposed to the high concentrations deliberately obtained by doping procedures. Hence, one can wonder whether laser-induced conversion processes of Ge-related defects in these conditions are different from those observed in Ge-doped silica, and it is possible that such a simple model system may allow to isolate some specific Ge-related process within the complex landscape emerging from literature. Another important difference exists between Ge impurities in natural silica and Ge-doped α -SiO₂. Indeed, it was demonstrated that in as-grown natural α -SiO₂ the majority (50%–100%) of Ge impurities are incorporated in twofold coordinated form,^{93,164–166,172} i.e. as GLPC centers (=Ge^{••}). This situation is quite different from Ge-doped α -SiO₂, where the portion of Ge atoms in the two-coordinated configuration is much lower (10^{-4} – 10^{-2}), while significant portions of Ge are present in the three- and four-fold coordinated arrangements or as Ge clusters.^{136,172} The reasons why Ge impurities in α -SiO₂ prevalently choose the GLPC arrangement only when their total concentration is low are not completely clear at the moment. Even so, this circumstance can be exploited for our purposes: indeed, natural silica can be regarded as a material of choice to investigate *selectively* the conversion processes of the GLPC center elicited by UV radiation. The experiments presented in this chapter aim also to investigate this point.

^awhich can be monitored by the reduction (*bleaching*) of the typical optical activity of GLPC centers, consisting in the B_{2β} absorption band at 5.1 eV exciting the two emissions at 3.1 eV and 4.3 eV.⁹³ See Figure 5.12.

7.2 Conversion processes of GLPC center

7.2.1 Results

ESR measurements

As-grown dry Q906 and wet HER1 samples were irradiated at room temperature with 2000 pulses of 4.7 eV laser radiation with 40 mJcm^{-2} energy density per pulse and 1 Hz repetition rate.

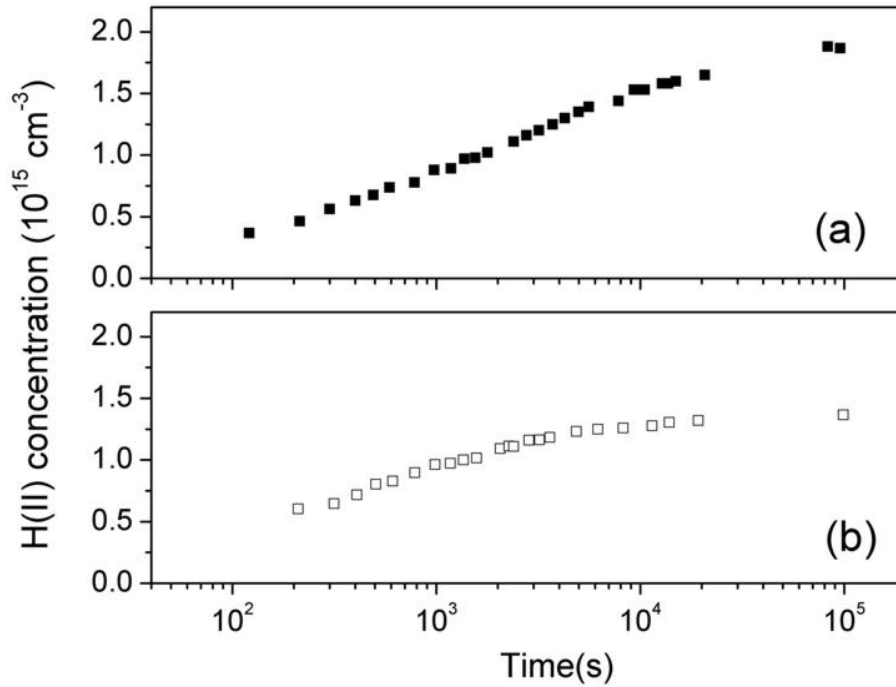


Figure 7.1: Post-irradiation kinetics of H(II) centers induced in wet (a) and dry (b) natural α -SiO₂ by 2000 4.7 eV laser pulses with 40 mJcm^{-2} energy density per pulse and 1 Hz repetition rate at room temperature. The origin of the time scale corresponds to the end of irradiation.

As already described, by ESR measurements performed in the post-irradiation stage we are able to detect the 11.8 mT doublet typical of the H(II) center. From the time dependence of the intensity of the doublet, we calculated the two kinetics $[\text{H(II)}](t)$, which are reported in Figure 7.1. In both materials we observed the usual post-irradiation growth of $[\text{H(II)}]$, which increases from the initial values of $(3.7 \pm 0.4) \times 10^{14} \text{ cm}^{-3}$ (wet) and $(6.0 \pm 0.6) \times 10^{14} \text{ cm}^{-3}$ (dry), measured at $t \sim 10^2$ s from the end of irradiation, to the stationary values of $(1.9 \pm 0.2) \times 10^{15} \text{ cm}^{-3}$ (wet) and $(1.4 \pm 0.1) \times 10^{15} \text{ cm}^{-3}$ (dry), measured at $t \sim 10^5$ s.

We have seen in chapter 5 that the two main signals detected by ESR in irradiated natural silica are H(II) and E' . Aside from these two, a further very weak component (Figure 7.2) is detected, which is known in literature as Ge(2) center. In particular, the characteristic negative peak of the Ge(2) ESR signal is found in our spectra in the expected spectral position, being a clear fingerprint

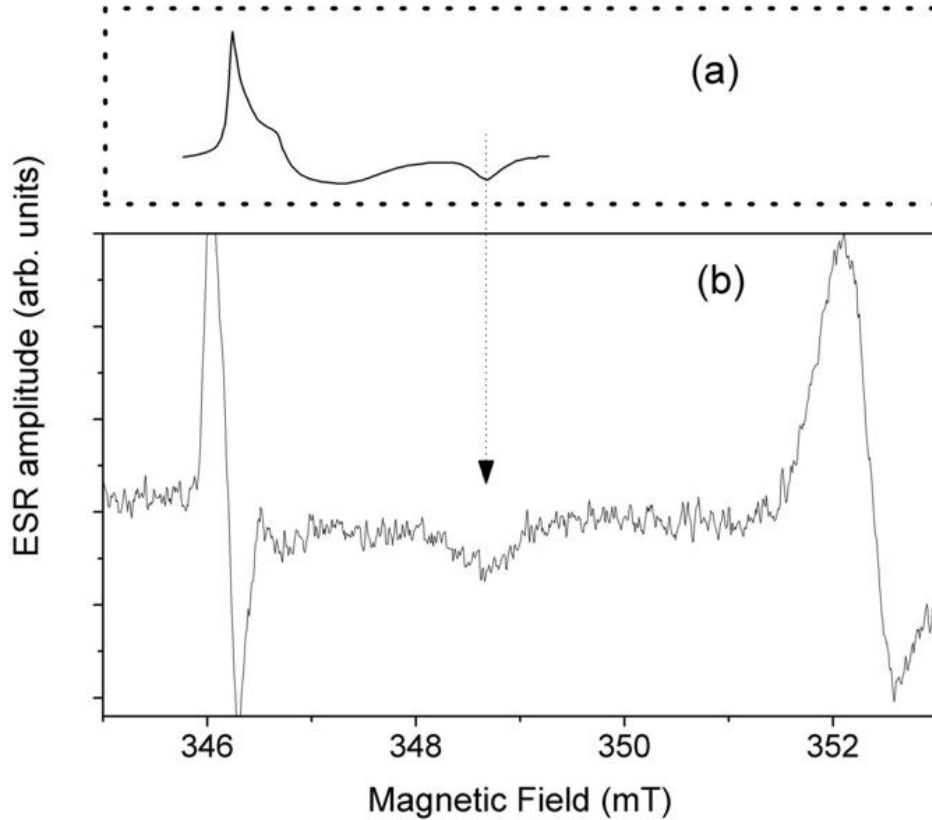


Figure 7.2: ESR spectrum (b) of a natural dry a -SiO₂ a few days after exposure to 500 laser pulses with 40 mJcm^{-2} energy density per pulse and 1 Hz repetition rate. The signal was acquired with a 2G modulation amplitude and a $P=6 \text{ mW}$ microwave power. Panel (a): simulated Ge(2) lineshape taken from Friebele *et al.*¹⁴³ with purpose of comparison.

of the presence of this defect.¹⁴³ Ge(2) is a paramagnetic Ge-related center, whose microscopic structure is currently debated to be either a ionized twofold coordinated Ge ($=\text{Ge}^\bullet$),^{134, 139, 147, 158} or an electron trapped at a GeO_4 site (GeO_4^\bullet)⁻.^{138, 152-154, 157} Even if the signal is very weak and partially superimposed to the much stronger E' resonance, it is possible to approximately assess the concentration of Ge(2) by comparing the negative peak with a reference lineshape available in literature;¹⁴³ by this procedure we obtain: $[\text{Ge}(2)] \sim 2 \times 10^{14} \text{ cm}^{-3}$. The concentration of Ge(2) never exceeds this order of magnitude in all the investigated samples. H(II) and Ge(2) are the only Ge-related defects observed by ESR in irradiated natural a -SiO₂. In particular, we do not detect either the $\text{Ge}-E'$ ($\equiv \text{Ge}^\bullet$),¹⁴²⁻¹⁴⁶ or the Ge(1) ($(\text{GeO}_4^\bullet)^-$) centers,^{134, 145, 152-154} both commonly found in Ge-doped silica exposed to laser radiation.

PL measurements

We already reported in chapter 5 that laser irradiation induces the bleaching of the native optical activity of the GLPC, although no information was provided on the *kinetics* of this bleaching process. However, if H(II) are generated by (7.1), it is expected that the reduction of the GLPC occurs in the

post-irradiation stage, i.e. simultaneously to the observed growth of H(II). To investigate this issue, we carried out other two irradiation experiments on as-grown wet and dry natural α -SiO₂ specimens in the same conditions as those of Figure 7.1. PL measurements under lamp excitation at 5.0 eV were performed on both samples, before and at different delays (10^2 - 10^5) s from the end of irradiation. In particular, to monitor the intensity variations of the PL signal of GLPC in the post-irradiation stage, Δ PL, the irradiated specimens were positioned into the sample chamber of the spectrofluorometer about 10^2 s after exposure, after which they were kept in place and measured for 10^4 - 10^5 s; with this choice, the precision of Δ PL is not limited by repeatability of the mounting conditions and increases to $\sim 1\%$ of PL intensity.

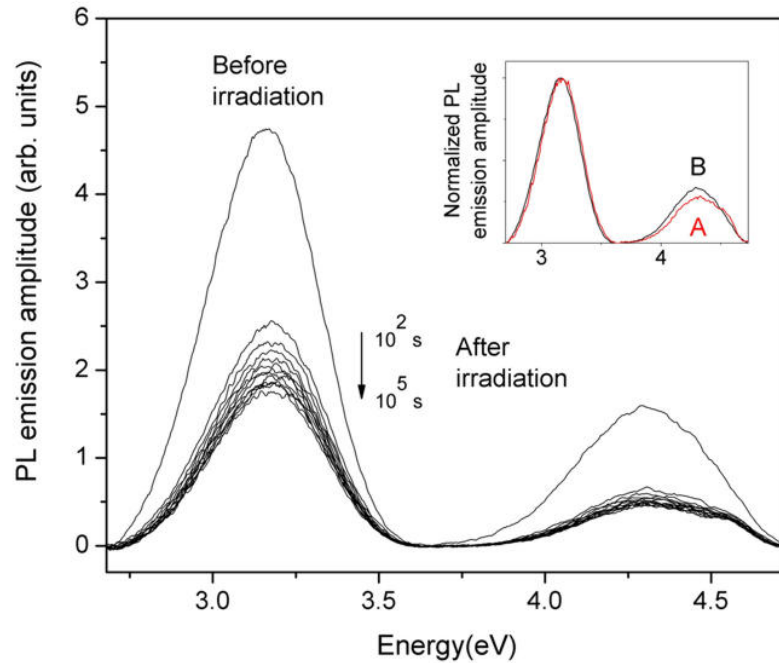


Figure 7.3: PL signal of GLPC before irradiation and at several times from 10^2 s up to 10^5 s after irradiation, all detected in a HER1 natural wet sample irradiated with 2000 laser pulses with 40 mJcm^{-2} energy density per pulse and 1 Hz repetition rate. Inset: normalized spectra before (B) and after (A) irradiation.

The detected emission spectra consist in the 3.1 eV and 4.3 eV bands. We found that the signal intensity reduction induced by irradiation occurs in two clearly distinguishable stages (see Figure 7.3): (i) during illumination, an intensity reduction of 50% in wet and 15% in dry silica takes place, as we observe by comparing the as-grown PL spectrum with the first detected after exposure at $t \sim 10^2$ s (ii) after the end of irradiation, the PL intensity further decreases in time, as apparent from the spectra measured in the wet specimen at different delays from the end of exposure. An analogous result was obtained on the dry material. In both cases, measures were continued until a constant PL intensity was reached within experimental error. Finally, we observed that the bleaching is accompanied by a small alteration of the ratio between the 3.1 eV and 4.3 eV PL bands of GLPC, as shown in the inset of Figure 7.3.

The post-irradiation kinetics of the GLPC is summarized in Figure 7.4, where the integrated intensity PL(GLPC) of the signal is plotted for the two materials against time. Luminescence inten-

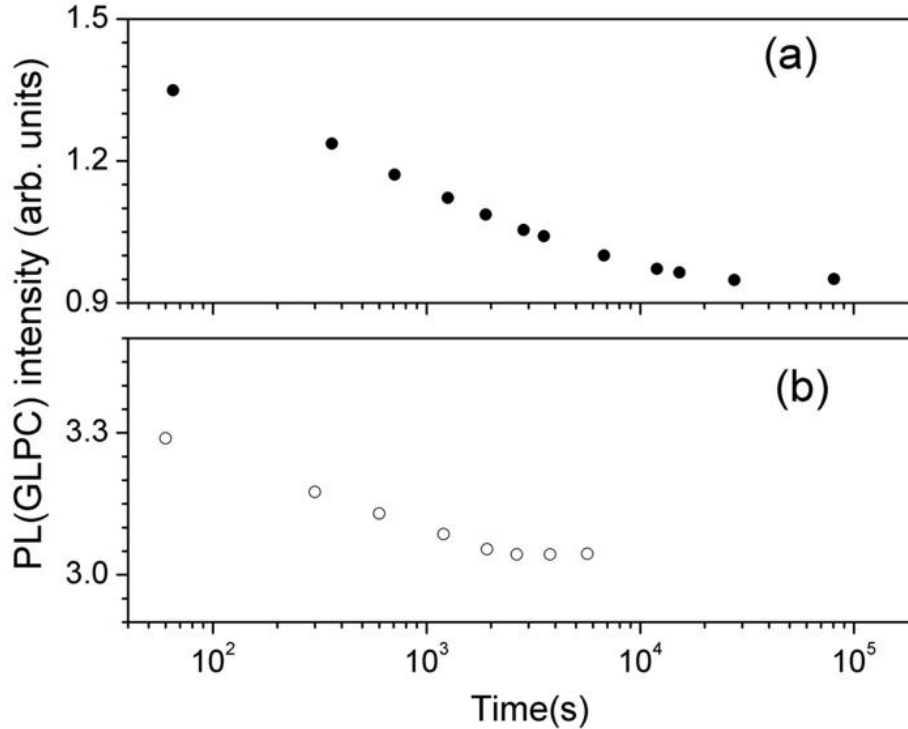


Figure 7.4: Post-irradiation kinetics of the intensity of the PL signal of GLPC after exposure of a wet (a) or a dry (b) natural α -SiO₂ sample to 2000 laser pulses with 40 mJcm⁻² energy density per pulse and 1 Hz repetition rate at room temperature.

sity decreases of 0.40 ± 0.01 arb.units from 65 s to 8×10^4 s in the wet sample. In the dry specimen, the decrease is 0.24 ± 0.03 arb.units from 60 s to 6×10^3 s.

Repeated irradiations

To deeper analyze the relationship between H(II) and GLPC, we investigated the concentration variations of both defects under repeated irradiations. In general, this approach is useful in that it allows to observe the interaction of already formed defects with laser light; besides, the application of multiple exposures separated by dark intervals reproduces a situation often encountered in optical applications of amorphous silica. In this case, an experiment was performed in which a natural wet specimen was irradiated 3 times with 2000 laser pulses; after each exposure, the post-irradiation kinetics of PL(GLPC) was measured until completion. Results are shown in Figure 7.5-(a). On a second sample subjected to the same irradiation sequence, the post-irradiation kinetics of H(II) centers was measured after each exposure (Figure 7.5-(b)). As apparent from experimental data, each exposure destroys most of H(II) that had formed upon the previous illumination, their concentration decreasing approximately to the same value as immediately after the previous irradiation; simultaneously, we observe a rebuild of luminescence intensity to approximately the same value found at the same time after the previous exposure. After every re-irradiation, the sample *loses memory* of its previous history, meaning that both PL(GLPC) and [H(II)] repeat again the same decrease/growth

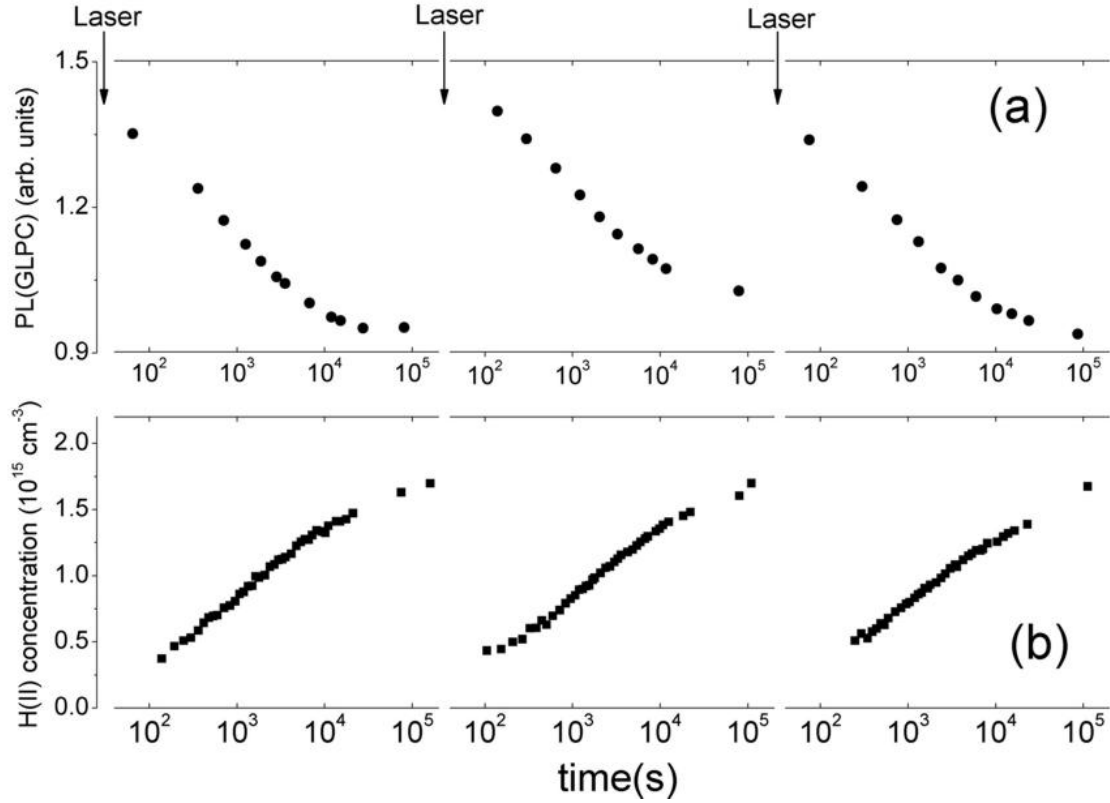


Figure 7.5: PL signal of GLPC (a) and concentration of H(II) (b) induced in a wet natural α -SiO₂ sample by a cycle of 3 irradiations of 2000 laser pulses with 40 mJcm^{-2} energy density per pulse and 1 Hz repetition rate. Each arrow represents an irradiation session. The irradiation sessions are separated by a waiting time of $\sim 10^6$ s to allow the post-irradiation kinetics to be completed.

kinetics.

We stress that the repeatable decay and recovery cycles of GLPC observed upon multiple irradiations involve only the portion bleached in the post-irradiation stage, whereas the reduction observed *during* exposure occurs irreversibly only during the earliest irradiation. However, we clarify that the term "irreversibly" is used here only in relation to the effects of further irradiations. Indeed, data obtained by a thermal treatment experiment show that the "irreversible" portion of the bleaching can actually be reversed by heating the irradiated material at 300C° for 3 hours. This aspect is of no concern here and will be not further discussed.

7.2.2 Discussion I: Correlation between GLPC and H(II) centers

Being the optical density of our samples at 5.0 eV smaller than 0.02 (see for example Figure 5.1), PL(GLPC) is proportional to the concentration of the twofold coordinated center (chapter 4). Hence, the bleaching induced by irradiation is a manifestation of conversion processes triggered by UV exposure, which transform the diamagnetic center in other defects. Results in Figures 7.3 and 7.4, allow to isolate two different stages of GLPC conversion: the "irreversible" stage, occurring only once

during the earliest irradiation, and that taking place after each irradiation. In particular, the second stage was expected from our preliminary discussion, since it occurs simultaneously to the growth of H(II) consistently with reaction (7.1). Now, we have to find out if a quantitative anti-correlation between the two effects exists *and* if the amount of the absolute concentration growth of H(II) is compatible with the absolute concentration decrease of GLPC.

To this aim, we begin with converting the PL intensity PL(GLPC) to an absolute concentration measurement $[GLPC]=\xi PL(GLPC)$. The coefficient ξ can be estimated from the radiative emission lifetime $\tau=7.8$ ns of the defect from the excited singlet state (see Figure 5.3) in two steps. First, by using the Förster equation (3.12), we can calculate from τ the oscillator strength^b of GLPC, or equivalently the proportionality coefficient ξ' between $[GLPC]$ and the area $A(B_{2\beta})$ of the *absorption* band at 5.1 eV of the defect, $[GLPC]=\xi' A(B_{2\beta})$. Hence, we find ξ by multiplying ξ' for the known constant ratio between the intensities $A(B_{2\beta})$ and PL(GLPC) of absorption and emission signals.¹⁶⁵ In this way we estimate^c: $\xi=(4.4\pm 0.7)\times 10^{15} \text{cm}^{-3}$.

Being now able to transform PL intensities in absolute concentrations, we first discuss the irreversible conversion of GLPC occurring during irradiation. Using ξ , we estimate the concentrations of the centers converted in this stage, $\Delta_0=(6.0\pm 0.9)\times 10^{15} \text{cm}^{-3}$ (wet) and $\Delta_0=(2.7\pm 0.4)\times 10^{15} \text{cm}^{-3}$ (dry). Present data do not allow to clarify in what is transformed this portion of GLPC, thereby leaving open this specific issue. Nonetheless, we can rule out H(II) and Ge(2), whose concentration (at $t=0$) are both too small to account for Δ_0 , and Ge- E' and Ge(1), which are absent in the exposed specimen within the EPR sensitivity of $\sim 2\times 10^{14} \text{cm}^{-3}$. Then, we infer that during irradiation a portion of GLPC is most likely converted to some unknown *diamagnetic* center that happens to be virtually invisible at this concentration.

Hence, we proceed to examine the relation between the post-irradiation decay of GLPC and the simultaneous growth of H(II). To this aim, we plot in Figure 7.6 the increase $\Delta[H(II)]$ of H(II) concentration as a function of the decrease of $[GLPC]$, $-\Delta[GLPC]=-\xi\Delta PL(GLPC)$. For each of the two materials, $\Delta[H(II)]$ and $\Delta[GLPC]$ were calculated from the same time instant t_0 ; ESR data used to calculate $\Delta[H(II)]$ were obtained by extrapolation at the same time instants at which luminescence spectra had been acquired. For practical reasons, t_0 was chosen to be the time at which the first ESR spectrum was acquired, i.e. the x-coordinate of the first point in Figure 7.1 ($t_0\sim 10^2$ for the wet sample and $t_0\sim 2\times 10^2$ for the dry sample).

We see that data from both materials fall on a single line for short times, whereas for long times they tend to depart from the line towards the upper semiplane. In the short time region, H(II) and GLPC are indeed anti-correlated, with a correlation coefficient independent of the material and represented by the slope of the line, $S\sim 0.7$, as estimated by a best fit procedure on the first points (corresponding to $t<2\times 10^3$ s). This value of S , which is founded on two completely independent

^bAs a result of this calculation, using the Lorentz-Lorenz effective field correction we get an oscillator strength of: $f\sim 0.07$. We stress, however, that the value of ξ' does *not* depend on the expression chosen for the effective field correction.

^cIt is worth noting that the value of ξ (as well as PL(GLPC), but differently from ξ') does not possess an absolute meaning. In fact, ξ is a function of the instrumental parameters used to acquire the luminescence spectrum. The present calculation refers to the acquisition conditions used for all the PL data reported in this chapter.

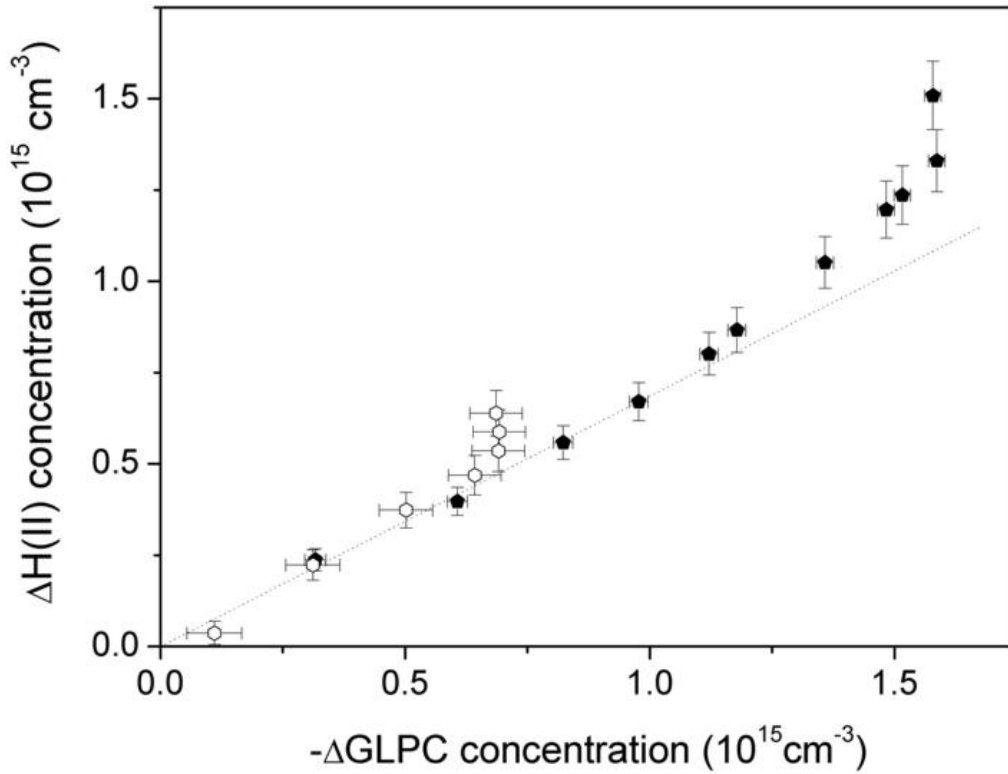


Figure 7.6: Correlation plot between the increase of [H(II)] and the decrease of [GLPC], measured from $t \sim 10^2$ from the end of irradiation. Full (empty) symbols correspond to wet (dry) natural α -SiO₂.

concentration measurements^d, can be considered to be in a reasonable agreement with unity for our present purposes. Also, the circumstance that data obtained on two different materials fall on a single line strengthens the result.

Therefore, the following interpretation of Figure 7.6 is proposed: the linear relationship approximately valid at short times represents a one-to-one conversion between GLPC and H(II) centers by process (7.1), whereas the deviations from linear correlation indicate that H(II) centers are generated also by a second channel prevailing over the main reaction (7.1) at long times. In both samples, this second generation channel accounts for $\sim 30\%$ of the total $\Delta[\text{H(II)}]$. Since we detect a low concentration of Ge(2) centers after irradiation (Figure 7.2), if we assume the model of Ge(2) as a ionized twofold coordinated Ge impurity ($=\text{Ge}^\bullet$), a possible mechanism producing the portion of H(II) not anti-correlated to GLPC may be the successive H and electron trapping on Ge(2), as proposed by Fujimaki *et al.*¹⁷⁵



^dIn contrast to the case discussed in footnote c of Chapter 5, the errors on the concentration measurements derived from PL and ESR are completely independent. Then, the accuracy (rather than the repeatability only) of these two concentration estimates becomes important when assessing the closeness of the parameter S to unity. In this sense, we recall that the uncertainty on [H(II)] measured by ESR is $\sim 20\%$. As for the concentration of GLPC derived from PL data, it is more difficult to obtain a precise estimate of the experimental error due to the relative complexity of the procedure; however, it can be argued that also in this case the uncertainty is at least (another) 20–30%

However, it may be possible that the deviations from a straight line of Figure 7.6 arise from a not-perfect proportionality between PL(GLPC) and [GLPC], due to inhomogeneities in the optical properties of the GLPC defect embedded in the disordered solid.^{163–165, 242, 266} Indeed, it is conceivable that both the oscillator strength and the reactivity of GLPC with H fluctuate within the population of defects due to site-to-site inhomogeneity. Suppose now that the two statistical distributions are inter-correlated^e: in this scheme, the progress of reaction (7.1) is expected to lead to a variation of the *mean* value of ξ , above supposed for simplicity to be unique, which could explain the deviations from a perfect linear correlation. The possible influence of such effects in the present context is also suggested by the laser-induced variation of the ratio between the 3.1 eV and the 4.3 eV PL bands in the PL signal (inset of Figure 7.3). This evidence indicates a variation of the (mean) value of the intersystem crossing (ISC) rate (see the level scheme of GLPC in Figure 1.13); this parameter in GLPC has been clearly proved to be affected by inhomogeneity effects.¹⁶⁵ Hence, similarly to ISC, it is likely that inhomogeneity may affect also other parameters controlling the luminescence intensity, such as the PL quantum yield or the oscillator strength (see chapter 3).

Even though a definite interpretation cannot be proposed for the deviations of Figure 7.6, the correlation at short times, found for both materials and with a common slope S near unity, is sufficient to conclude that our results are in a good agreement with the hypothesized model that ascribes the formation of H(II) to process (7.1). It is worth noting that our present approach significantly differs from the customary way in which this kind of problems are addressed in literature. In fact, a correlation between *relative* concentration measurements (i.e. the intensities of spectroscopic signals) is often considered sufficient to confirm a supposed conversion mechanism between a diamagnetic precursor and a paramagnetic center. Then, since it is usually easier to obtain an *absolute* concentration estimate by ESR measurements than by optical data, the slope of the correlation is exploited to "calibrate" the signal of the diamagnetic center to its absolute concentration. In contrast, we have proceeded here in a more rigorous way. Starting from two independent concentration measurements, each potentially affected by several sources of experimental uncertainty (see footnote d), we have verified not only the existence of a linear correlation, but also that the linear coefficient, when expressed as an absolute dimensionless quantity, is sufficiently close to one for the conversion process (7.1) to be reliable.

Comparison with literature on conversion processes of Ge-related defects

As reviewed in subsection 1.2.3, literature studies on conversion process of Ge-related centers are usually carried out on Ge-doped silica, with a typical Ge impurity concentration of the order of a few %. Most of these works report a reduction of the pre-existing ~ 5.1 eV band accompanied by the generation of Ge(1), Ge(2) and Ge- E' centers.^{134, 136–141} Several models have been proposed to explain the formation of these paramagnetic centers, often on the basis of observed correlations

^ethis may occur for example if the two distributions actually reflect the randomization of a single "structural" parameter (bond length, angle, etc..) that varies from site to site, and on which both quantities depend. It is relatively common in α -SiO₂ to find situations in which such cross-correlations effects alter the perfect proportionality between two parameters associated to the same defect, and expected to be proportional in absence of inhomogeneity effects.¹²

Summary I. *Aside from the generation of E' centers discussed in the previous chapter, 4.7 eV laser irradiation induces in natural silica conversion processes of defects related to the Ge impurities present in low concentration in this material. In particular, in the post-irradiation stage GLPC defects (monitored by PL spectroscopy, Figure 7.4) are converted in H(II) centers (monitored by ESR, Figure 7.1) by hydrogen trapping, eq. (7.1), as proved by the anti-correlated concentration variations of the two defects (Figure 7.6). The conversion of GLPC into H(II) can be temporarily reversed by re-irradiating the material (Figure 7.5). Indeed, re-irradiation causes the photo-induced destruction of the H(II) centers, (Figure 7.7) and eq. (7.3), which are back-converted to GLPC. Natural silica permits a selective study of the interplay between GLPC and H(II) centers triggered by UV radiation, differently from Ge-doped materials where several conversion processes of Ge-related defects have been reported to be active at the same time.*

between the stationary concentrations of the induced defects or between the reduction of the native OA and the concentration of the induced defects (see subsection 1.2.3-B). Present results show that Ge-related processes induced by laser irradiation in natural silica, where the concentration of Ge is only a few ppm, are remarkably different. In fact, we did not observe either Ge(1) or Ge- E' centers. Ge(1) has been proposed to arise from trapping of an electron on 4-fold coordinated Ge precursors,^{138,139,157,173–175} while Ge- E' is supposed to be induced by ionization of pre-existing Neutral Oxygen Vacancies (NOV) on Ge, in which the Ge atom is 3-fold coordinated.¹³⁶ While the NOV is believed to contribute to the ~ 5.1 eV absorption without emitting luminescence,¹³⁶ no measurable optical activity below bandgap has been ascribed to the 4-fold coordinated Ge precursor of Ge(1).

On this basis, the lack of Ge(1) and Ge- E' in irradiated natural silica is likely due to the lower concentration of 4-fold and 3-fold coordinated Ge precursors with respect to Ge-doped glass, as already anticipated in the introduction of this chapter. Two considerations support this idea: **(i)** The close resemblance in natural silica between the PLE spectrum of the 3.1 eV and 4.3 eV bands and the 5.1 eV absorption profile, as well as the strong linear correlation between the three bands, exclude the presence of the NOV in this material in concentration comparable to GLPC. **(ii)** The concentration of native two-fold coordinated GLPC centers, calculated using the conversion ratio ξ between PL intensity and GLPC concentration estimated above, is 1.2×10^{16} in wet specimens. This corresponds to about 75% of the total Ge content estimated from neutron activation measurements (see section 4.1 and references therein). The ratio $[\text{GLPC}]/[\text{Ge}] \sim 0.75$, is to be compared with Ge-doped samples where it was measured to be $[\text{GLPC}]/[\text{Ge}] \sim 10^{-4} - 10^{-2}$.^{136,172} Such a difference confirms the much lower concentration of 3- and 4-fold Ge precursors in natural α -SiO₂, where Germanium is almost completely arranged as GLPC. The reasons of the difference between the prevalent arrangements of the Ge impurities in the two materials are not completely understood at the moment.

In this sense, our results can be regarded as a selective investigation of the laser-induced conversion processes of the GLPC centers, very difficult to isolate in Ge-doped silica due to the presence

of NOVs and other configurations of Ge. Our results strongly suggest that a significant portion of GLPC can be converted to a diamagnetic center, at variance with the common practice in literature to ascribe the conversion of GLPC to the formation of paramagnetic signals only, mainly the Ge(2).^{139,174,175} Consistently with our view, in recent times the conversion of GLPC in another diamagnetic defect has been proposed by a few other experimental and computational works.^{160–162} In our system, the prevalent paramagnetic Ge-related center induced by irradiation is H(II), formed by process (7.1). The role of H(II) as one of the main products of GLPC conversion was evidenced in γ -irradiated natural silica,^{167,236} even if no evidence was found of other parallel conversion processes of GLPC. In contrast, in laser-irradiated Ge-doped silica the generation of H(II) has been reported only as a minor process occurring in H₂-loaded samples, and being accompanied by the disappearance of Ge(2).¹⁷⁵ This further difference with our result could be due to the absence of available mobile H₂ in common irradiated Ge-doped *a*-SiO₂ samples, whereas natural silica contains an intrinsic source of radiolytic hydrogen (supposedly Si–H) so as to allow for the growth of H(II) (and possibly cause the passivation of Ge(2)).

As a final remark, we stress that the present results are founded on the choice of studying the *time-dependence* of the Ge-related defects. *A posteriori*, we can say this choice to be mandatory in order to isolate process (7.1) from the conversion channels active during exposure and possibly at long times. Our approach is innovative in that it differs from the common practice in literature of studying (and trying to correlate) only the *stationary* concentrations of the defects. In this sense, we propose that also in Ge-doped materials or in other systems, kinetic investigations may help to clarify the picture of laser-induced conversion processes.

7.2.3 Discussion II: Correlation under repeated irradiations and photo-induced decay of H(II) center

The data in Figure 7.5 show evidence that the two defects have an anticorrelated behavior also under repeated irradiations. In fact, each exposure causes a photo-induced decay of the H(II) grown during the last post-irradiation kinetics, and simultaneously restores the GLPC. This finding indicates that H(II) centers, generated by reaction (7.1) activated by irradiation, are also *reduced* by laser exposure. This observation allows us to understand the feature of the growth kinetics of H(II) center, that are formed mostly in the post-irradiation stage rather than during it, so that the final concentrations are always 3-4 times higher than initial concentrations (chapter 5). In fact, this property can be now explained as follows: the growth of H(II) *during* irradiation by reaction (7.1) is inhibited because of the competition with the photo-induced decay of the centers. Also, it is interesting to note the similarity between the present finding and the photo-induced decay of H(I) (=Si[•]–H) center observed by Radtsig et al;²¹⁴ H(I) and H(II) both belong to an isoelectronic series of defects, localized on a Si, Ge, Sn atom, which are known to have similar formation and spectroscopic properties.^{93,155} From this point of view, we suggest that the isoelectronic defects share also similar photo-induced decay properties.

The re-growth of GLPC concurrent to the disappearance of H(II), combined with the structural

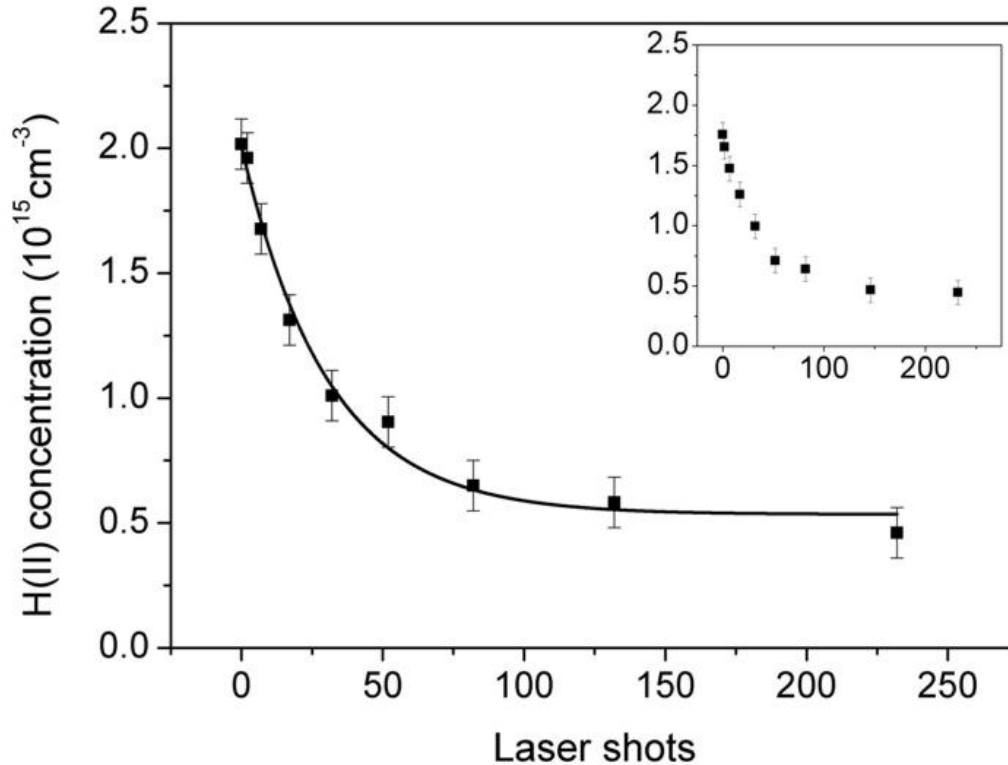


Figure 7.7: Variations of [H(II)] induced in a natural wet sample by reirradiation after preliminary exposure to 2000 laser shots. Continuous line: least-square fit by an exponential function. Inset: result of the same experiment on a dry natural sample.

relationship existing between H(II) ($=\text{Ge}^\bullet - \text{H}$) and GLPC ($=\text{Ge}^{\bullet\bullet}$), suggest the following microscopic mechanism responsible for the photo-induced decay of H(II):



namely, exposure of H(II) to 4.7 eV photons causes detaching of the hydrogen atom from the Ge–H bond reconstructing the precursor GLPC. We found that H(II) can be destroyed also by exposure of the sample to light from a Xe lamp. Due to the much lower peak intensity with respect to laser, this observation suggests process (7.3) to occur by single-photon absorption at the defect site.^f A further experiment was carried out to measure the cross section of process (7.3): we started with a natural wet sample exposed to an irradiation dose large enough (2000 pulses, see Figure 5.17) to produce the maximum H(II) concentration. Such a dose is referred to as a *high-dose*. After waiting the H(II) post-irradiation kinetics to be completed, we measured $[\text{H(II)}] = (2.0 \pm 0.2) \times 10^{15} \text{ cm}^{-3}$. Then, we irradiated again the specimen with an increasing number of pulses of $W = 40 \text{ mJ cm}^{-2}$ energy density per pulse. We found that after each exposure, the defect concentration remains almost invariant (within 10%)

^fOn the other hand, this leads to the necessity of some precautions when measuring the post-irradiation kinetics of the GLPC (subsection 7.2.1); indeed, to prevent H(II) from being destroyed during PL measurements due to the excitation light, in all PL measurements reported above we used a high scan speed (500 nm min^{-1}) to reduce as much as possible the exposure time of the sample to the Xe lamp. We verified that this choice avoids the photo-decay of H(II) as well as any appreciable distortion of the experimentally observed PL kinetics.

during the time interval required for the ESR measurement (~ 500 s). Hence, between successive exposures we measured the defect concentration, obtaining the results in Figure 7.7. Consistently with Figure 7.5, we observed that the new irradiation results in the destruction of H(II) generated by the first dose, their concentration decreasing to $\sim 25\%$ of the initial value after ~ 250 laser pulses. An identical effect was observed also on natural dry samples (inset). The same response of H(II) embedded in the two materials agrees with our interpretation in which the decay is due to the direct absorption of UV light at the defect site (process 7.3). After the whole 250 pulses sequence, [H(II)] increases again but does not recover its initial magnitude within the investigated time scale: their concentration increases to $(1.4 \pm 0.1) \times 10^{15} \text{ cm}^{-3}$ in 2×10^6 s. This behavior is different from the observed repeatability of the kinetics after 2000 pulses (Figure 7.5); in other words, only a high-dose irradiation is able to cause a memory loss by the sample. Finally we note that the concentration of $\sim 5 \times 10^{14} \text{ cm}^{-3}$ to which [H(II)] tends at the end of the 250 pulses sequence, is in good agreement with the value observed in Figure 7.5 just after each re-irradiation. It is reasonable to assume that this concentration represents an equilibrium between the photo-induced decay of H(II) and the growth of the defect due to reaction (7.1) taking place during each interpulse time span.

The H(II) reduction with the number of pulses N is fitted by an exponential function:

$$[\text{H(II)}] = A_1 \exp\left(-\frac{N}{N_0}\right) + A_2 \quad (7.4)$$

where $N_0 = 30 \pm 3$, $A_1 = (1.5 \pm 0.1) \times 10^{15} \text{ cm}^{-3}$, $A_2 = (0.5 \pm 0.1) \times 10^{15} \text{ cm}^{-3}$. From these data, we calculate the cross section of process (7.3), $\sigma_D = N_0^{-1}(h\nu/W) = (6.2 \pm 0.6) \times 10^{-19} \text{ cm}^2$.

Given that the H(II) is able to absorb 4.7 eV light (though destructively), at this point one could wonder why this does not correspond to a OA signal near 4.7 eV, present in the observed absorption profiles due to the presence of the defect. In this sense, we note that the H(II) concentration, $\text{H(II)} = 2.1 \times 10^{15} \text{ cm}^{-3}$, leads to the following estimate of the 4.7 eV absorption coefficient of the defects, $\alpha = \sigma_D [\text{H(II)}] = 1.3 \times 10^{-3} \text{ cm}^{-1}$, if we suppose that each absorbed photon results in the destruction of a center. Therefore, the presence of the much stronger $B_{2\beta}$ band overlapping in same spectral region prevents us from detecting the anticipated signal that could be ascribed to H(II). On the other hand, as carried out in a recent experiment,²⁶⁷ a tunable UV radiation source can be used to measure σ_D as a function of wavelength; this method allows to reconstruct indirectly the absorption profile of the H(II) center, thus overcoming the difficulty of directly observing the weak OA signal of the defect by a standard spectrophotometric approach.

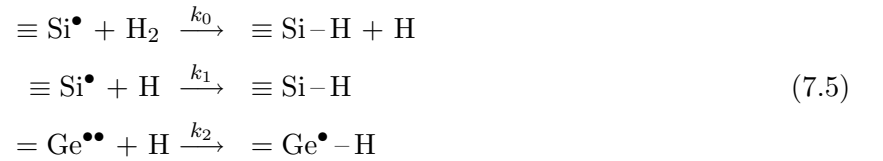
Finally, we briefly comment the observed repeatability of the post-irradiation kinetics. The kinetics of H(II) and GLPC centers repeat themselves after each *high-dose* exposure cycle (Figure 7.5). In principle, the post-irradiation kinetics is determined by the concentrations at $t=0$ of all the centers involved in the reactions that induce the growth of H(II). In the model we have proposed starting from section 5.5, these defects are GLPC, hydrogen and E' , the latter playing the role of a cracking center for H_2 . So, the memory loss implies that each 2000 pulses re-irradiation is able to reset the concentrations of H(II), GLPC, E' and hydrogen to fixed concentration values independent of the previous history of the sample. The first step to achieve this effect is process (7.3), which destroys the H(II) and rebuilds their precursors GLPC, this being completed just after the first 250

shots (Figure 7.7). As for the E' centers, in wet natural silica their concentration is almost null at the beginning of each exposure, as the post-irradiation annealing leads to the almost complete disappearance of the defect; moreover, also E' is consistently found to repeat "elastically" the same decay kinetics after each high dose re-irradiation (see Figure 6.6). The combination of these findings suggest the following picture for wet natural silica: in a 2000 pulses exposure E' , H(II), GLPC and hydrogen reach some equilibrium concentrations regardless of the previous history of the sample, thereby leading to repeatability of the post-irradiation kinetics. This scheme is also consistent with the observed *in situ* kinetics of E' in natural wet silica (Figure 5.10), where 2000 pulses (with the same laser intensity 40 mJcm^{-2} and repetition rate 1 Hz used here) were found to (almost) saturate $[E']$.

Apparently, this scheme does not apply to the dry material, where it was observed a progressive accumulation of E' upon successive irradiations (Figure 6.6) and 2000 pulses are not enough to saturate $[E']$ (Figure 5.10). In principle, this could alter the post-irradiation kinetics leading to a not perfect repeatability. Likely, the influence of the slowly increasing concentration of E' from an irradiation to the successive one is negligible within the experimental conditions explored so far.

7.3 Modeling the reaction kinetics

According to our results, the post-irradiation processes in natural $\alpha\text{-SiO}_2$ after 4.7 eV irradiation are the result of the following system of reactions, involving E' ($\equiv \text{Si}^\bullet$), GLPC ($=\text{Ge}^{\bullet\bullet}$), and giving Si-H and H(II) ($=\text{Ge}^\bullet\text{-H}$) as the final results:



However, it is still necessary to find out if the model inherent in (7.5) is able to account for the measured time dependence of the concentrations of all the involved species. To this aim, we start with writing down the chemical rate equations governing the kinetics of (7.5):

$$\left\{ \begin{array}{l} \frac{d[E']}{dt} = -k_0[E'][\text{H}_2] - k_1[E'][\text{H}] \\ \frac{d[\text{H}_2]}{dt} = -k_0[E'][\text{H}_2] \\ \frac{d[\text{GLPC}]}{dt} = -k_2[\text{GLPC}][\text{H}] \\ \frac{d[\text{H}]}{dt} = k_0[E'][\text{H}_2] - k_1[E'][\text{H}] - k_2[\text{GLPC}][\text{H}] \end{array} \right. \tag{7.6}$$

Based on the fact that H is an intermediate reaction product, and the reaction constants driven by the fast diffusion of H are much larger than that depending on H_2 diffusion ($k_1, k_2 \gg k_0$), we can apply to this system the *stationary state approximation*.^{39,194} As described in detail in chapter 2,

this consists in assuming that both the concentration of H and its time derivative remain negligible during the progress of the kinetics, so as to set:

$$\frac{d[\text{H}]}{dt} = k_0[E'][\text{H}_2] - k_1[E'][\text{H}] - k_2[\text{GLPC}][\text{H}] \sim 0 \quad (7.7)$$

this equation can be used to express [H] as a function of the other concentrations, and eliminate it from system (7.5). In this way, we obtain:

$$\begin{cases} \frac{d[E']}{dt} = -k_0[E'][\text{H}_2] \left(1 + \frac{1}{1 + \zeta \frac{[\text{GLPC}]}{[E']}} \right) \\ \frac{d[\text{GLPC}]}{dt} = -\frac{d[\text{H}(\text{II})]}{dt} = -k_0[E'][\text{H}_2] \left(1 - \frac{1}{1 + \zeta \frac{[\text{GLPC}]}{[E']}} \right) \\ \frac{d[\text{H}_2]}{dt} = -k_0[E'][\text{H}_2] \end{cases} \quad (7.8)$$

where $\zeta = k_2/k_1$ is a parameter that controls the ratio between the amount of H captured by GLPC and that captured by E' . This ratio is usually referred to as the *branching ratio* of the last two reactions in (7.5). System (7.8) explicitly shows that the main parameter controlling the overall reaction rate is k_0 , namely the reaction constant between H_2 and E' : the whole post-irradiation stage of the processes is driven by H_2 diffusion.

Before discussing the fit of experimental data with the rate equations (7.8), we recall that chemical reaction constants such as k_0 typically depend on temperature according to the Arrhenius equation:^{108,194}

$$k_0(\epsilon) = A \exp\left(-\frac{\epsilon}{k_B T}\right) \quad (7.9)$$

where A and ϵ are referred to as pre-exponential factor and activation energy for the reaction of E' with H_2 , respectively. In the particular case of a *diffusion-limited reaction*⁸, the theoretical model by Waite (chapter 2) can be applied. In this case the value of the reaction constant k_0 is predicted to be (from eq. 2.12):

$$k_0 = 4\pi r_0 D_{0L} \exp(-E(\text{H}_2)/k_B T) \quad (7.10)$$

In (7.10), $D = D_{0L} \exp(-E(\text{H}_2)/k_B T)$ is the diffusion constant of H_2 in silica glass, where $D_{0L} = 5.65 \times 10^{-4} \text{ cm}^2 \text{ s}^{-1}$ and $E(\text{H}_2) = 0.45 \text{ eV}$, as reported in literature from macroscopic diffusion experiments of H_2 in $\alpha\text{-SiO}_2$.^{38,108,197} The parameter r_0 is the capture radius of the defect, i.e. a distance of the order of a few 10^{-8} cm under which E' is supposed to react instantaneously with H_2 . Comparing (7.9) with (7.10), we see that within the Waite model for diffusion-limited reactions, the activation energy ϵ coincides with that for H_2 diffusion in $\alpha\text{-SiO}_2$, i.e. $E(\text{H}_2)$, while the value for the pre-exponential factor A is:

$$A_W = 4\pi r_0 D_{0L} \quad (7.11)$$

⁸In a diffusion-limited reaction (see chapter 2), the diffusion of the mobile species (rather than the local interaction with the other reagent) is the bottleneck in determining the overall kinetics of the process. This is regarded as the most common situation for reactions in solids, where diffusion is quite a slow process.^{38,42,108,185,194}

Summary II. *In the last part of this chapter we deal with the problem of fitting with a suitable rate equation model the kinetics of E' , GLPC and H(II) centers, observed after the end of laser irradiation and due to the reactions eqs. (7.5) driven by diffusion of H_2 . Consistently with previous findings on other point defects embedded in the disordered silica matrix, we show that our task can be accomplished only by incorporating in the mathematical treatment (eqs. (7.8)) a statistical distribution of the activation energy ϵ which controls the reaction constant of E' with H_2 . By a fit procedure (Figure 7.8) we are able to estimate the width of this (gaussian) distribution to be $FWHM=(0.12\pm 0.02)$ eV.*

We measured the post-irradiation decay kinetics of E' in a natural wet a -SiO₂ HER1 sample subjected to 2000 laser pulses, from the amplitude of the 5.8 eV OA band and using the known value of the peak absorption cross section of the paramagnetic center. In this context it becomes important to follow the kinetics until completion (for a few days); hence, we monitored E' by *ex situ* OA measurements performed with the JASCO spectrophotometer. In fact, as already mentioned, the *in situ* approach is useful to follow the first $\sim 10^4$ s of the decay, but not suitable to perform measurements on a very extensive time range. An obvious drawback of the present choice is the loss of information on the first $\sim 10^2$ s of the kinetics, which is a necessary compromise for the present purposes. The results are reported in Figure 7.8 as full square points. In the same graph are reported again the kinetics of [H(II)] from Figure 7.1, and of [GLPC], calculated from the data in Figure 7.4 using the conversion coefficient ξ . Then, the solutions of system (7.8), calculated numerically, were fitted to the experimental datasets. In the fitting procedure, the initial concentrations of E' , GLPC and H(II) were constrained to the values obtained by extrapolating the experimental curves at $t=0$, $[E'](t=0)=(8.6\pm 0.5)\times 10^{15}$ cm⁻³, $[GLPC](t=0)=(4.7\pm 0.2)\times 10^{15}$ cm⁻³ and $[H(II)](t=0)=(2.0\pm 0.2)\times 10^{14}$ cm⁻³. Hence, the fitting parameters that remain to be determined are $[H_2](t=0)$, ζ and k_0 ; the best fit values of the first two were found to be $[H_2](t=0)=(4.1\pm 0.3)\times 10^{15}$ cm⁻³ and $\zeta=(1.1\pm 0.2)$.

For what concerns k_0 , a more complex picture emerges. In fact, as already known from literature,^{38,42,185} we found that a good fit to the data on all the 10^2 - 10^6 s time scale can be achieved only by introducing a *statistical distribution* of the activation energy ϵ . This is done by fitting experimental data with a *linear combination of solutions* of (7.8): individual solutions are first calculated for different values of ϵ , resulting in correspondent values of k_0 from (7.9); then, the weight of each solution in the linear combination equals the weight of the associated value of ϵ within the distribution curve of the activation energy. Such a situation is referred to by saying that the kinetics of point defects in glasses are "anomalous". This result is commonly interpreted as a consequence of the amorphous nature of silica, which manifests itself in a statistical distribution of activation energies, this being a fingerprint of site-to-site inhomogeneity of the a -SiO₂ matrix. A comment is mandatory before applying this procedure to the current case. In fact, present data at the single temperature $T=300$ K do not allow to estimate *separately* ϵ and A , since only k_0 appears in the rate equations. This limitation will be overcome in the next chapter on the basis of the study of the temperature dependence of k_0 . In the present context, before using the statistical distribution of ϵ

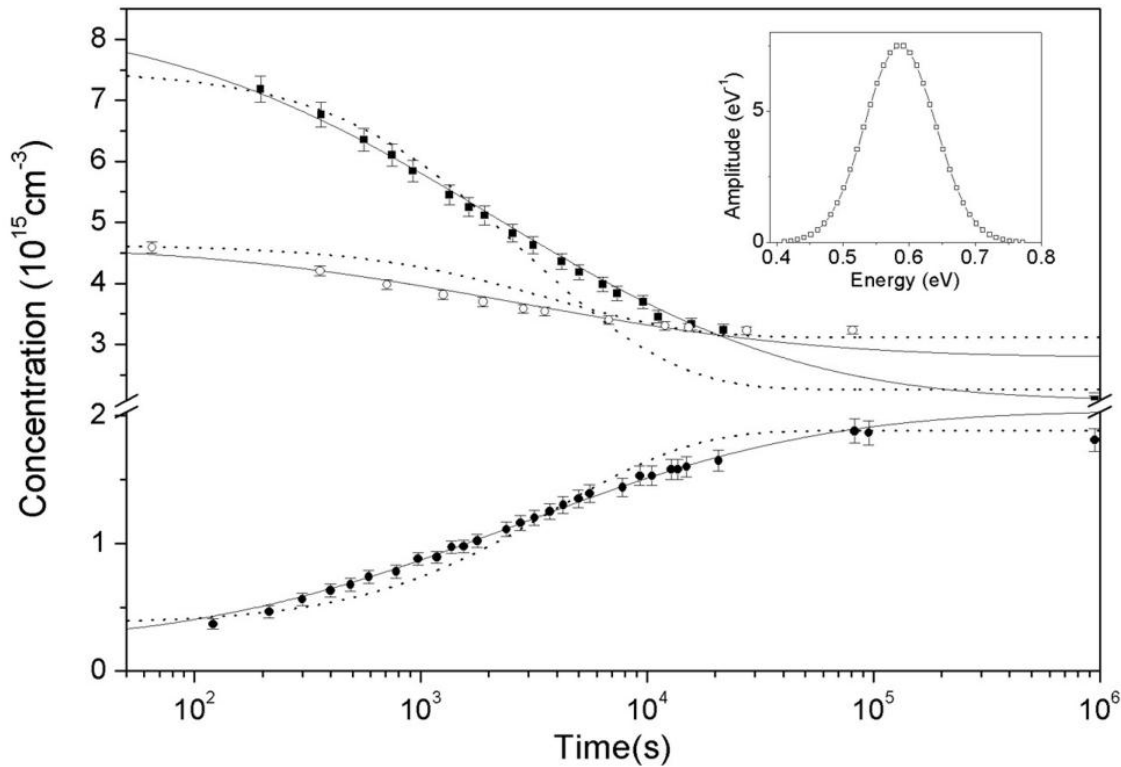


Figure 7.8: Concentrations of E' (squares), GLPC (empty circles) and H(II) (circles) in a natural wet sample after exposure to 2000 laser shots with 40 mJcm^{-2} energy density per pulse and 1 Hz repetition rate. Dotted lines are numerical solutions of system 7.8. Solid lines take also into account the statistical distribution of the activation energy ϵ (represented in the inset) which controls by (7.9) the reaction constant between E' and H_2 .

to calculate the correspondent values of k_0 from (7.9), it is first necessary to *choose* a value of the pre-exponential factor A . As the simplest hypothesis, to this purpose we used the expression (7.11) valid within the Waite theory of diffusion-limited reactions, with a capture radius arbitrarily chosen to be $r_0 = 5 \times 10^{-8} \text{ cm}$. Of course, it must be kept in mind that the distribution of ϵ could be *shifted*, giving in particular a different mean value, by a different choice of A leading to the same distribution of k_0 .

Based on these premises, we show as dotted lines in Figure 7.8 the typical solutions of eqs. (7.8) obtained with a single value of ϵ , which manifestly fail to reproduce the shape of the experimental kinetics. In contrast, we found that an excellent agreement (solid curves) is attained introducing a Gaussian distribution of ϵ with mean $\langle \epsilon \rangle = (0.59 \pm 0.01) \text{ eV}$ and FWHM $\Delta \epsilon = (0.12 \pm 0.02) \text{ eV}$. The finding that all three independent experimental datasets can be fitted at once for a suitable choice of parameters, is a clear proof of the validity of the chemical model (7.5) hypothesized to explain the post-irradiation processes, thus accomplishing one of the goals that we wished to fulfill at the beginning of this chapter. This is particularly true if we consider the approximations implicit in eqs. (7.8), such as neglecting every other generation channel of H(II) and the stationary state approximation. We propose in the following some comments on the values of the fitting parameters.

I. As explained above, present data do not allow to separate the contributions of A and ϵ to the reaction constant k_0 , and in particular the distribution of ϵ could be *shifted*, giving a different $\langle\epsilon\rangle$, by a different choice of A leading to the same distribution of k_0 . Hence, apart from k_0 only the parameter $\Delta\epsilon=(0.12\pm 0.02)$ eV has an *absolute* meaning, and it can be said to represent a measure of the effect of inhomogeneity on the reaction properties of E' with H_2 .

II. Nevertheless, the circumstance that $\langle\epsilon\rangle=0.59$ eV is higher than the $E(H_2)=0.45$ eV value reported for H_2 diffusion in α - SiO_2 , contrary to what should be expected from (7.10), is not to be underestimated. In fact, although $\langle\epsilon\rangle$ does not possess an absolute meaning, this disagreement can be restated saying that the value of the reaction constant $k_0(\langle\epsilon\rangle)$, given by (7.9) with the value (7.11) for the pre-exponential factor A , is *lower* than expected (eq. (7.10)) from the Waite model for a diffusion-limited reaction. Hence, it *unambiguously* indicates the inadequacy of the Waite theory to describe the reaction between E' and H_2 , in the sense that the present reaction is much *slower* than expected for a purely diffusion-limited process.^h Such a result is analogous to the comparison proposed in chapter 5, in which the typical decay time of E' was found to be *longer* than expected for a purely diffusion-limited reaction with H_2 . These findings (as well as a few other similar results in literature^{89,224}) suggest the idea that the passivation of E' by H_2 is also *reaction-limited*, so as to yield an effective value of ϵ *lower* than $E(H_2)$ because k_0 incorporates somehow also the activation energy *for reaction*.

III. In regard to the statistical distribution of the activation energy, the situation we have found for E' is subtly different from previous works, in which a similar "anomalous" decay kinetics was evidenced for the decay of NBOHC centers. In fact, differently from the present case, the mean value of ϵ for NBOHC was found close to $E(H_2)$.^{42,185} This permitted to conclude that the reaction of NBOHC with H_2 is diffusion-limited and, most important, to identify $\langle\epsilon\rangle$ coming from the fit with the activation energy for H_2 diffusion, so as to interpret the very existence of a randomization of $\langle\epsilon\rangle$ as a property *inherent to diffusion* in silica. Consistently with this view, macroscopic diffusion experiments directly showed an anomalous temperature-dependence of the diffusion constant of some species in α - SiO_2 , which can be explained on the basis of a distribution of the activation energy for diffusion.²⁰⁶ In comparison, even if the present results extend from NBOHC to E' the observation of the influence of inhomogeneity on the reaction properties with H_2 , at this stage it is not completely clear how to interpret from a physical point of view the distribution of ϵ introduced to treat the kinetics. All these problems will be dealt with in the next chapter.

IV. In some works in literature it was used a *flat* statistical distribution of ϵ to describe anomalous reaction kinetics in glass, the advantage being the possibility of finding an analytical expression for the kinetics in some cases.²²⁷ Anyway, more recent studies on the reaction between NBOHC and H_2 have confirmed to a large extent the applicability of a Gaussian distribution of ϵ to the modeling

^hTo see this point: we could have chosen A so as to *fix* the mean activation energy $\langle\epsilon\rangle$ to $E(H_2)$, but this would have not reconciled the results of the fit with the Waite model; indeed, notwithstanding the agreement of ϵ , in this case the chosen A would have been much lower than given by (7.11).

of both isothermal and isochronous reaction kinetics.¹⁸⁵ We observe here that, due to the heuristic nature of the approach itself of fitting the kinetics with a linear combination of solutions of the rate equation system, it is difficult to predict *a priori* if the correct form of the distribution should be flat or Gaussian. Moreover, this detail is not particularly important to our purposes; in fact, the main results of our line of reasoning (the demonstration that model (7.5) is consistent with experimental data, and the evidence of an anomalous kinetics) are not influenced by this choice, which could only bear consequences on the precise estimate of $\Delta\epsilon$.

V. The concentration of H_2 at $t=0$ found from the fit is approximately one half of E' at the same time instant. This is consistent with the model for the generation of E' proposed in chapter 6 for wet natural silica: E' and H are generated during irradiation from the common precursor Si–H. Also, the present fit procedure quantitatively confirms that the small residual concentration of E' ($\sim 2 \times 10^{15} \text{ cm}^{-3}$) still remaining at the end of the post-irradiation stage in wet samples is due to the portion of hydrogen which escapes recombination with E' and is trapped on GLPC.

VI. Finally, we note that a value of ζ of the order of unity is to be expected if the reactions of E' and GLPC with *atomic* hydrogen are diffusion-limited. In fact, in the framework of the Waite model,²¹⁰ ζ should equal the ratio of the capture radii of GLPC and E' for H, which both should be of the order of an atomic dimension if the model is applicable at all.

7.4 Conclusions

We investigated the post-irradiation kinetics of point defects induced at room temperature in natural $\alpha\text{-SiO}_2$ by 4.7 eV laser irradiation, with particular attention to the conversion processes of Ge-related defects. The analysis of the time dependence of the PL signal of the GLPC center permits to isolate the post-irradiation stage of its conversion process, which is ascribed to trapping of H at the defect site leading to the generation of H(II) center, on the basis of the anti-correlated concentration variations of the two species. This process can be reversed by a second laser exposure, which destroys H(II) and restores the precursor GLPC. We provide a measure of the cross section of photo-induced rupture of H(II): $\sigma_D = 6.2 \times 10^{-19} \text{ cm}^2$. Multiple high-dose irradiations result in the repetition of the same post-irradiation kinetics of H(II) centers after each exposure. This effect is achieved by the photo-decomposition of previously formed defects and by the ability of each high dose exposure to reset to fixed values the concentrations of the centers involved in the post-irradiation phenomena. Atomic hydrogen to be trapped at the GLPC site is produced by breaking of diffusing H_2 on E' centers. Consistently, the time dependence of E' , H(II), and GLPC concentrations can be fitted by a suitable set of coupled rate equations describing the chemical reactions occurring in the post-irradiation stage. The kinetics of the three species are mainly controlled by the reaction between E' and H_2 and their features suggest a statistical distribution of the activation energy controlling the reaction constant. The results of the fit suggest that the reaction kinetics of E' with H_2 is not purely diffusion-limited.

Chapter 8

Temperature dependence of the generation and decay of E' center

This chapter completes our experimental investigation by the study of the temperature dependence of the generation and decay of E' center in natural silica by 4.7 eV laser radiation.

8.1 Introduction

The experimental results have shown that natural α -SiO₂ is an interesting system in that it allows to investigate the generation of E' by 4.7 eV pulsed laser radiation, the decay of E' due to reaction with H₂, and some conversion processes of Ge-related defects. Although the experiments presented up to now have provided many important information on these phenomena, a thorough investigation must necessarily include also the temperature dependence of these processes.

For what concerns E' (\equiv Si \bullet), temperature may be expected *a priori* to influence both its generation and its stability through several effects. In particular, the investigation of the temperature dependence of the post-irradiation decay of the defect due to reaction with H₂:



is motivated by a variety of reasons. Indeed, process (8.1) basically represents the passivation of a silicon dangling bond (E') in the "archetypal" α -SiO₂ amorphous solid by the ubiquitous diffusing species H₂; from this point of view, it is to be regarded as one of the basic interaction processes between point defects and mobile species in amorphous solids. Besides, from the technological point of view, this process takes an important place in the general topic of passivation of many defects detrimental for applications, such as the NBOHC, the other fundamental paramagnetic defect in silica glass,^{38,42,185} and the P_b center, (Si₃ \equiv Si \bullet), common at the Si/SiO₂ interface in metal-oxide-semiconductor (MOS) devices.^{256,268,269} The reaction of E' with H₂ has been discussed in literature by several experimental and theoretical works, aiming to estimate the kinetic parameters of the process (subsection 2.4.3). One of the most debated issues has been whether the reaction kinetics is

diffusion- or reaction-limited: in fact, contrary to the common assumption that the reaction kinetics of defects with migrating species in solids are diffusion-limited (due to the slowness of the diffusion process in solids), some results in literature and in the previous chapters have indicated the reaction of E' with H_2 to proceed more slowly than expected for a purely diffusion-limited process; consistently, computational investigations proposed the interaction between E' and H_2 to be characterized by an activation barrier.^{1,229,230,232} The possibility that the diffusion-limited model may be unapplicable to such a "basic" reaction deserves to be thoroughly investigated. In this sense, besides the specific interest in elucidating the properties of a very common point defect in α - SiO_2 , the interest of this problem extends well beyond the "silica community".

Nevertheless, until now detailed kinetic studies of reaction (8.1) have been carried out only for surface E' centers^{a,214} or for E' centers in thin silica films.²²⁶ The advantage of these systems is that the reaction can be directly investigated by exposure of the surfaces to gaseous H_2 . These two works report disagreeing results: the measured rates of the reaction at $T=300$ K differ by two orders of magnitude, while the activation energies are 0.4 eV and 0.3 eV respectively.^{214,226} The process has been also discussed by computational studies, where it was shown to require an activation energy of a few tenth of eV.^{1,229,230,232,234} In contrast, for E' centers in bulk silica, the task of studying experimentally the reaction becomes more difficult, since here the concentration of available H_2 is not an external controllable parameter, and diffusion of H_2 in the bulk α - SiO_2 matrix becomes a necessary step to bring the reagents in contact. Furthermore, it is needed to measure *in situ* the kinetics of the transient defects in temperature-controlled experiments. For these reasons, even if process (8.1) has been repeatedly observed to spontaneously passivate radiation-induced E' centers *in bulk*,^{89,114,223,224} its thermal activation properties have still to be thoroughly investigated. Studying these problems by *in situ* OA spectroscopy is the purpose of this chapter.

8.2 Experiments and Results

The experiments were performed on I301 natural dry specimens, placed in the He flow cryostat and irradiated with 4.7 eV laser radiation of 40 mJcm^{-2} energy density per pulse and 1 Hz repetition rate. We performed isothermal irradiations at temperatures $10 \text{ K} < T < 475 \text{ K}$ on different as-grown samples. Each sample was exposed to laser radiation for a time $\tau=2 \times 10^3$ s at a given temperature, and its OA spectrum was monitored *in situ* during exposure. Then, the measurements continued for a few 10^3 s after the end of exposure while keeping the specimen at the same temperature at which it had been irradiated.

In Figure 8.1 the typical absorption profile is reported as observed at different times during (a) and after the end (b) of the irradiation session at 250 K. Similarly to what we observe at room temperature (see chapter 5) on the same materials, the main detected signal is the 5.8 eV band of the E' centers, accompanied by the negative component near 5.1 eV due to bleaching of the $B_{2\beta}$

^aThe *surface* E' is a $\equiv Si^\bullet$ isolated dangling bond existing on the surface of α - SiO_2 . It features slightly different spectroscopic properties with respect to bulk E' .^{8,12}

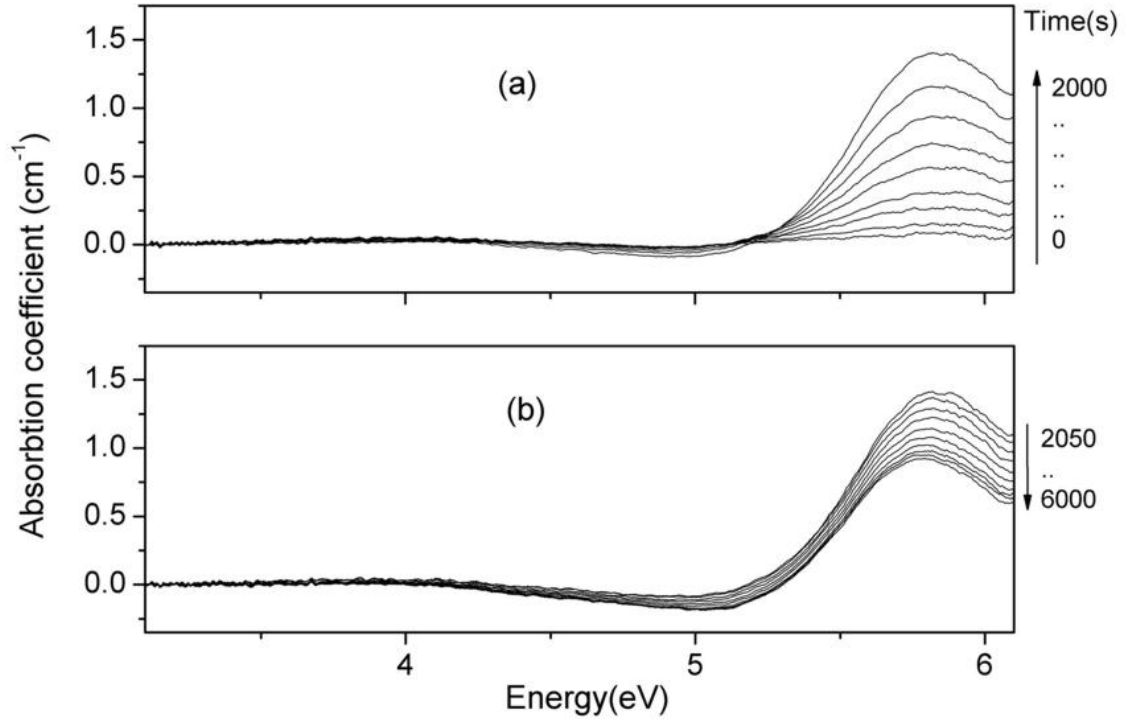


Figure 8.1: Difference absorption induced on natural dry silica by laser irradiation with 2000 pulses of 40 mJcm^{-2} energy density per pulse and 1 Hz repetition rate at 250 K, as detected *in situ* at several time instants during (a) and after the end (b) of the irradiation session.

band and by a very weak and broad component^b peaked at $\sim 4 \text{ eV}$. The profiles in Figure 8.1 are representative of all the investigated temperatures. The shape of the laser-induced 5.8 eV band weakly depends on temperature^c. For example, as shown in Figure 8.2, in the experiment at 225 K the band is peaked at $(5.85 \pm 0.02) \text{ eV}$ with a $(0.68 \pm 0.02) \text{ eV}$ FWHM, while at 450 K the peak is at $(5.78 \pm 0.02) \text{ eV}$ with $(0.71 \text{ eV} \pm 0.02) \text{ eV}$ FWHM. Nevertheless, such variations are sufficiently small to be neglected for what concerns the procedure used to estimate the E' concentration. Hence, also here $[E']$ can be calculated in a good approximation by multiplying the peak amplitude of the band by the known cross section, similarly to what we have seen in chapter 5. These calculated kinetics $[E'](t, T)$ at different representative temperatures are reported in Figure 8.3. The concentration of E' grows during the irradiation session of duration τ to a final value $[E'](\tau, T)$. Inspection of the curves shows that $[E'](\tau, T)$ has a maximum at $T=250 \text{ K}$. As for the post-irradiation stage, only for the experiments at $T > 200 \text{ K}$ we observe a measurable decay of E' , supposedly due to reaction (8.1). Both the entity of the decay and its typical time scale are influenced by temperature, in a way that is going to be analyzed in the following.

Let us focus now our attention on the 200 K–475 K temperature range, i.e. we temporarily exclude from our considerations the kinetics at temperatures so low that the diffusion and reaction of

^bThis signal, detected only in the natural dry I301 samples, has been ascribed to Ge-related impurities.³ However, it is of no concern for our present purposes.

^cIn contrast, the oscillator strength of the 5.8 eV band (controlling the ratio between $[E']$ and OA intensity), does not depend on temperature.²⁷¹

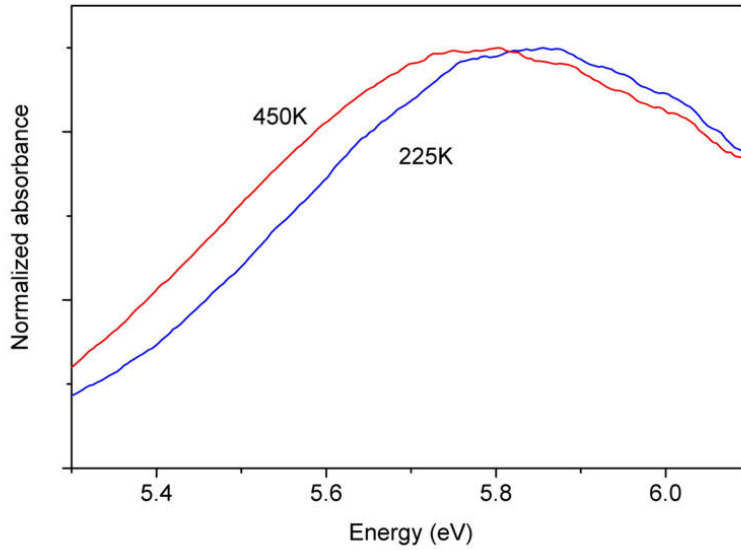


Figure 8.2: Shape of the 5.8 eV band induced by laser irradiation in natural dry silica at two representative temperatures.

H_2 with E' are quenched. Consistently with our results at room temperature, we are going to assume in the following that reaction (8.1) is the only cause of E' decay in all this temperature range^d. In addition we assume that hydrogen is consumed only by E' : indeed, the reaction (5.4) with GLPC of H produced at the right side of reaction (8.1) involves only a minor portion of the total hydrogen population, and NBOHC centers, which are known to react with H_2 ,^{38,42,185} are virtually absent, as inferred from the lack of their 4.8 eV OA and 1.9 eV PL optical activities. Hence, we write again the rate equation accounting for the time variations of $[E']$ in the post-irradiation stage due to reaction (8.1):

$$\frac{d[E']}{dt} = 2 \frac{d[H_2]}{dt} = -2k_0(T)[E'][H_2] \quad (8.2)$$

A consequence of this equation is that the total decay $\Delta[E'](T)$ equals twice the amount of radiolytic hydrogen $[H_2](\tau, T)$ available at the end of irradiation:

$$\Delta[E'](T) = [E'](\tau, T) - [E']_{\infty}(T) = 2[H_2](\tau, T) \quad (8.3)$$

where $[E']_{\infty}(T)$ is the stationary asymptotic concentration of E' at the end of the decay. On the one hand, this equation permits to indirectly estimate the concentration of available hydrogen if both the maximum and the stationary concentrations of E' are known. On the other hand, eq. (8.3) uniquely determines $[E']_{\infty}(T)$ at each temperature given $[E'](\tau, T)$ and $[H_2](\tau, T)$; in fact, the decrease of E' only depends on the amount of hydrogen made available by irradiation, since the decay of the defect ends as soon as H_2 is completely exhausted. This simple observation has an important consequence: if a sample is irradiated at a given T and then heated up (cooled down) to room temperature some time

^dAs usual, the parallel reaction of E' with atomic hydrogen is automatically accounted for when treating reaction (8.1) within the stationary state approximation.

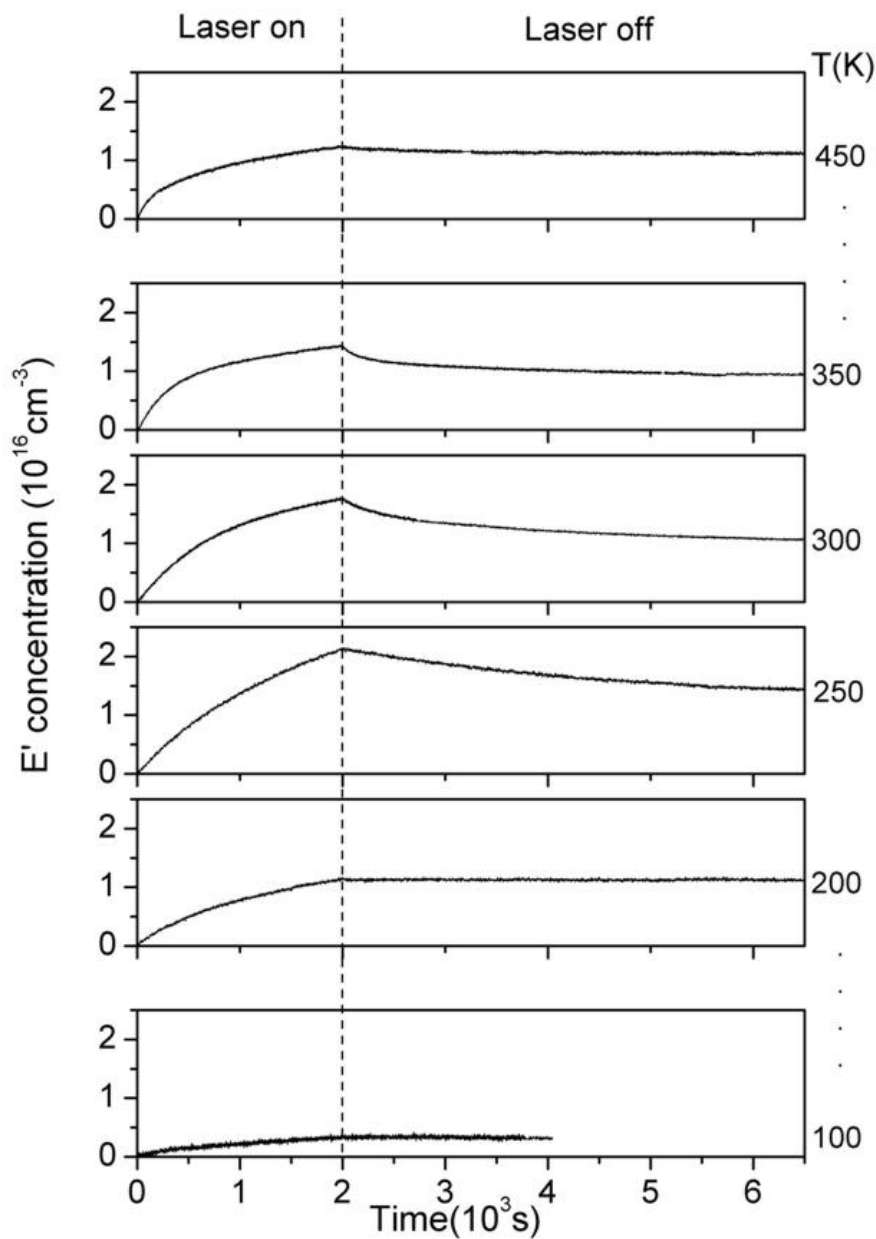


Figure 8.3: Kinetics of E' concentration induced by laser irradiation at several representative temperatures.

after the end of irradiation, this does not alter $[E']_{\infty}(T)$, which depends only on the concentrations of E' and hydrogen created by irradiation, $[E'](\tau, T)$ and $[H_2](\tau, T)$ respectively. The only effect of returning to room temperature is an acceleration (slowing down) of the decay. On this basis, for each irradiation, after observing *in situ* for a few 10^3 s the kinetics of E' , we brought back the sample at room temperature, where we continued to monitor the decay of $[E']$ for a few days after irradiation, so as to determine $[E']_{\infty}(T)$ by *ex situ* ESR measurements.

Measuring the stationary concentration *after* that the sample has returned to room temperature is particularly convenient for low temperature experiments, where an *in situ* measurement of $[E']_{\infty}(T)$

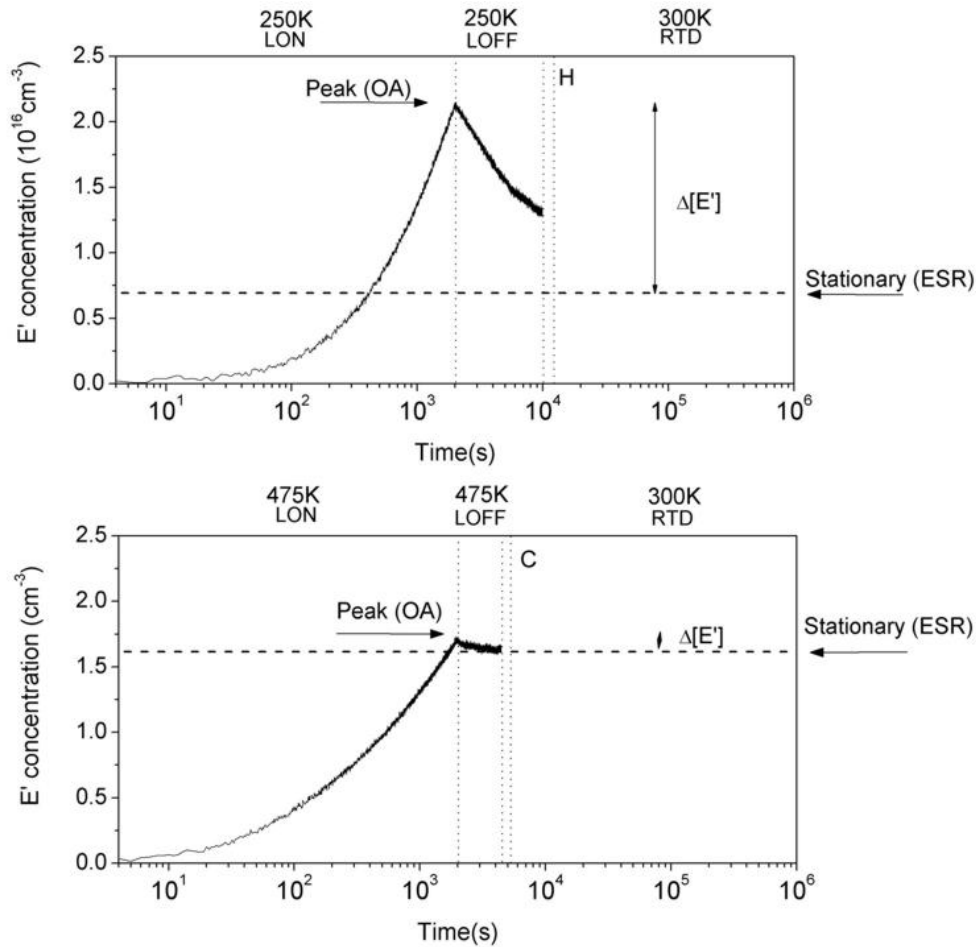


Figure 8.4: Representation of the experimental procedure used to extract some relevant parameters from the kinetics $[E'](t)$ induced by laser irradiation at two representative temperatures, 250 K (upper panel) and 475 K (lower panel). After remaining a few 10^3 s at the irradiation temperature, the specimen returns to room temperature, where the decay of E' continues till the stationary concentration is measured by ESR. Consistent results are obtained by measuring the stationary concentration by *ex situ* OA, but ESR allows for a higher precision when the concentration is a few 10^{15} cm^{-3} . LON stands for "laser on", LOFF stands for "laser off", H stands for "heating up at 300 K", C for "cooling at 300 K", RTD stands for Room Temperature Decay.

would require to follow the slow decay kinetics for a very long time. Two examples of this approach are displayed in Figure 8.4. The upper panel shows the *in situ* kinetics at 250 K. After a few hours from the end of exposure, when the decay is still in progress, the specimen was heated at room temperature. Then, a few days after the experiment we measured by ESR the stationary concentration represented in the Figure. The same approach was used at all temperatures, even if for T significantly higher than >300 K (e.g. lower panel), the permanence of the sample at T for a few 10^3 s is enough to complete the kinetics, so that the last *in situ* measurement agrees with the stationary ESR measurement performed after cooling back at room temperature.

Finally, at the beginning of this discussion we had momentarily left aside the low temperature ($T < 200$ K) kinetics, i.e. the regime in which H_2 diffusion and reaction are quenched. In this case, the stationary concentration $[E']_{\infty}(T)$ (measured after returning to room temperature) assumes a slightly

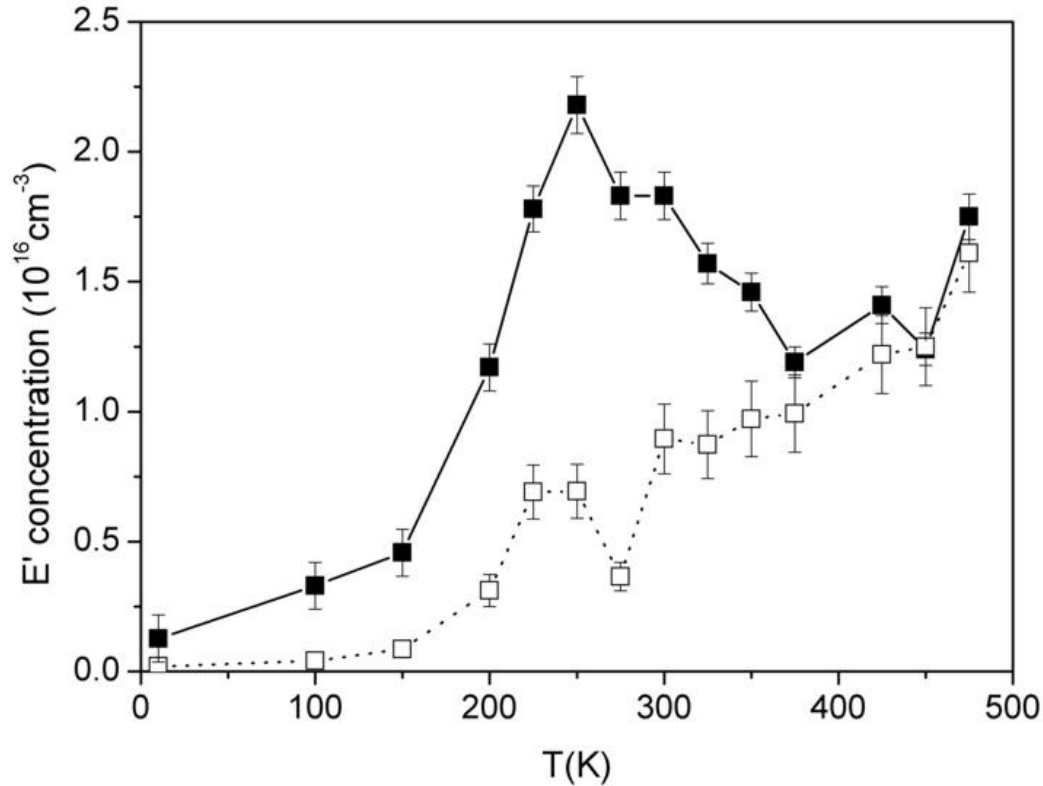


Figure 8.5: Concentration of E' measured *in situ* at the end of laser irradiation (full symbols) and stationary concentrations measured by ESR after the end of the decay process (empty symbols), as a function of the irradiation temperature.

different meaning. Indeed, even if we are not going to discuss in detail the post-irradiation stability of E' at low temperatures, we expect that when process (8.1) is quenched, $[E']_{\infty}(T)$ measured at room temperature does not coincide with the asymptotic concentration theoretically reached at the end of the isothermal decay. In fact, in this case the post-irradiation stage is controlled by *atomic* hydrogen diffusion only, as H_2 is immobile; hence, after conclusion of the post-irradiation stage, the E' centers can still coexist with a concentration of stationary (immobile) H_2 , after that H has been exhausted by dimerization and reaction with E' . In particular, in the extreme case of the 10 K kinetics also H is immobile, so that *all* E' are expected to be stationary before heating. For comparison, we stress that there is no stationary H_2 when process (8.1) is active (above 200 K). However, notwithstanding the fact that the values $[E']_{\infty}(T)$ at the three lowest investigated temperatures (150 K, 100 K and 10 K) cannot be literally interpreted as asymptotic isothermal concentrations, the differences $\Delta[E'](T)$ continue to represent the amount of hydrogen made available by irradiation^e. In fact, this property depends only on the circumstances that reaction(s) with H and H_2 are the only cause of E' decay, and each hydrogen atom (or half a hydrogen molecule) passivates a single E' .

With these considerations in mind, the values of $[E'](\tau, T)$ and $[E']_{\infty}(T)$ measured with the above procedures are plotted in Figure 8.5. Apart from a certain scattering of the data, mainly due

^ewhich at the irradiation temperature is expected to be stored partly in atomic and partly in molecular form.

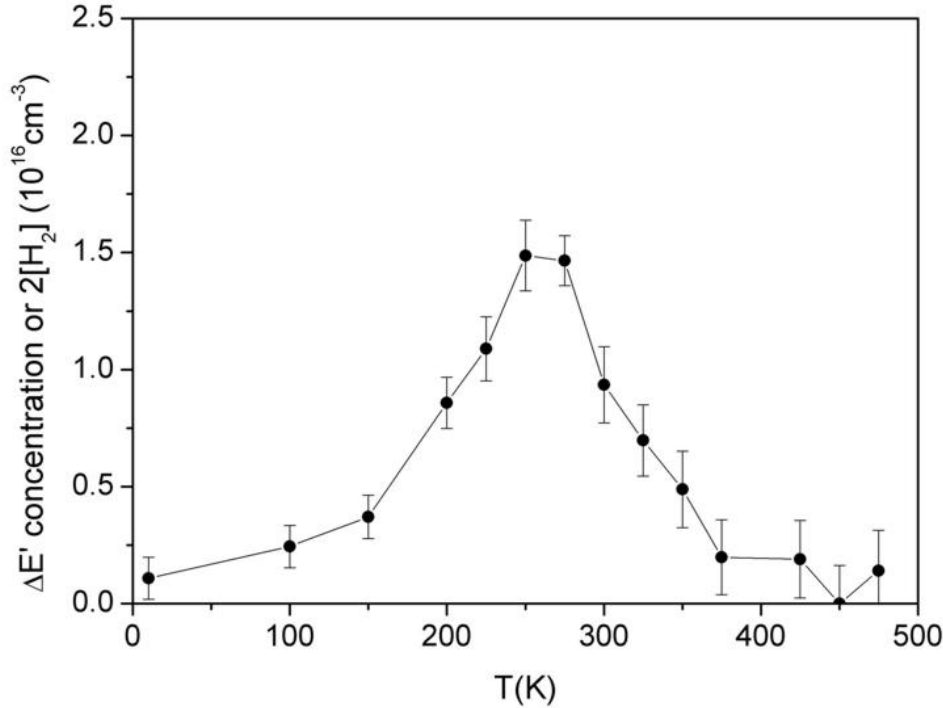


Figure 8.6: Concentration decrease of E' in the post-irradiation stage (which equals two times the concentration of radiolytic hydrogen $2[H_2]$) after irradiation with 2000 laser pulses, as a function of the irradiation temperature.

to limited repeatability of the irradiation conditions, the basic qualitative features of the process are (i): the stationary concentration is very low below ~ 150 K, and above this threshold it monotonically increases with temperature; (ii): also the maximum *in situ* concentration increases starting from ~ 150 K; above this temperature, it grows to a maximum at ~ 250 K, and then it decreases and joins the stationary concentration curve above ~ 400 K. The variation $\Delta[E'](T)$ in the post-irradiation stage, calculated as the difference between the two curves in Figure 8.5, is reported in Figure 8.6; its temperature dependence is roughly bell-shaped and features a maximum near 250 K.

From a phenomenological point of view, we can summarize the results as follows. First, the generation of E' is a thermally activated process, quite inefficient below ~ 150 K. Above this threshold, a general feature of the generated E' is their post-irradiation instability, which leads to a difference $\Delta[E'](T)$ between the maximum *in situ* concentrations and the stationary concentrations. As a consequence, we stress that up to ~ 400 K, a thorough study of laser-induced E' cannot rely only on measurements of the stationary concentration; on the contrary, the *in situ* approach is mandatory to have a full picture of the laser-induced process based on the observation of the kinetics of the defects. Above ~ 400 K, $\Delta[E'](T)$ tends to zero, meaning that the generated E' are basically stable in the post-irradiation stage, and the stationary concentration almost coincides with the maximum *in situ* concentrations. The conceptual distinction between the two measurements is lost and in these conditions the *in situ* and *ex situ* techniques yield the same information.

Before going on to discuss the results, we also note that the behaviors in Figure 8.5 and Figure 8.6

have been observed for a given number (2000) of laser shots; hence, although the qualitative features of the process are expected to be basically independent of irradiation dose, detailed features such as the position of the peak in Figure 8.6 may vary with the number of pulses. However, this consideration does not apply to the value of the reaction constant between E' and H_2 ,^f which is calculated and analyzed as a function of temperature in the following section.

8.3 Discussion I: Character of the reaction between E' center and H_2

8.3.1 Rate constant of the reaction

We are going now to focus on the post-irradiation stage of the laser-induced processes, and estimate from experimental data the reaction constant between E' and H_2 . By inverting eq. (8.2) calculated at the end of irradiation ($t=\tau$), and using (8.3), the rate constant $k_0(T)$ of the reaction can be expressed as follows:

$$\begin{aligned} k_0(T) &= -\frac{d[E']}{dt}(\tau, T) \frac{1}{2[E'](\tau, T)[H_2](\tau, T)} \\ &= -\frac{d[E']}{dt}(\tau, T) \frac{1}{[E'](\tau, T)([E'](\tau, T) - [E']_{\infty}(T))} \end{aligned} \quad (8.4)$$

This equation generalizes to dry natural silica, and at all temperatures, the line of reasoning that permitted in chapter 6 to estimate the reaction constant at room temperature $k_0(T=300\text{ K})= 8.3 \times 10^{-20} \text{ cm}^3 \text{ s}^{-1}$. Also in this case, the initial decay slopes $d[E']/dt(\tau, T)$ appearing in (8.4) can be estimated by a linear fit in the first ~ 50 s of the post-irradiation stage of the kinetics of Figure 8.3. Hence, inserting in (8.4) these decay slopes and the values in Figure 8.5, we calculate $k_0(T)$, which is plotted against temperature in Figure 8.7 as empty symbols. The uncertainties were estimated by repeating many times the experiment at $T=300\text{ K}$. The useful temperature range where it was possible to estimate k_0 extends from 225 K to 375 K, outside which interval the initial decay slope is respectively too slow or too fast to be accurately measured. Data are consistent with an Arrhenius dependence:

$$k_0 = A_i \exp\left(-\frac{E_i}{k_B T}\right); \quad (8.5)$$

where the index "i" in E_i and A_i reminds us that k_0 was determined from the initial decay slope. From a linear fit, we obtain the following values for the activation energy and for the pre-exponential factor: $E_i=(0.28 \pm 0.01)\text{ eV}$ and $A_i=3 \times 10^{-15} \text{ cm}^3 \text{ s}^{-1}$.

We must now take into account the effects of the disorder in the glass matrix, causing an inhomogeneous distribution of the activation energy, and consequently also of the reaction constant

^fEven if the maximum or asymptotic concentration of E' (as well as the concentration of radiolytic hydrogen) depend on the number of laser shots received by the specimen, the reaction constant clearly does not, being an intrinsic property of the reaction process determined only by temperature.

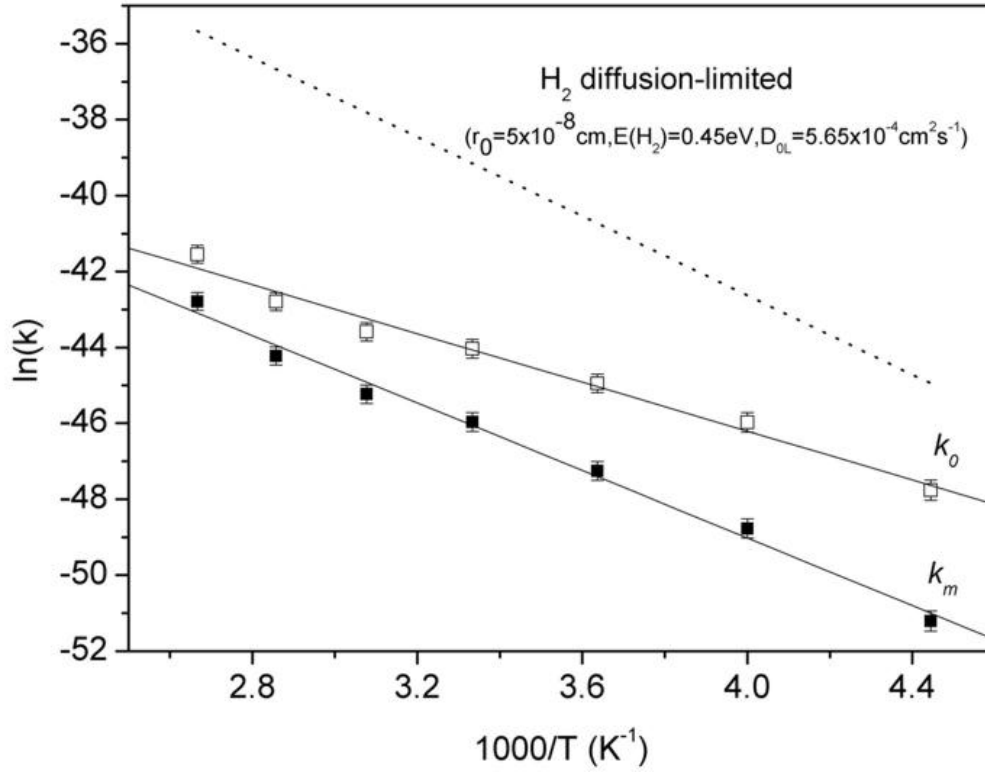


Figure 8.7: Reaction constant between E' and H_2 , taking (k_m , full symbols) or not taking (k_0 , empty symbols) into account the distribution of activation energy. Dotted line: prediction based upon a purely diffusion-limited reaction model. Full lines: fits with Arrhenius equations.

k . Indeed, according to what is known from literature,^{38,42,185} we have demonstrated in the previous chapter that the post-irradiation kinetics of E' in natural silica at room temperature can be fitted only by linear combinations of solutions of the chemical rate equations obtained with different reaction constants $k = A \exp(-\epsilon/k_B T)$ weighted by a Gaussian distribution of ϵ centered at a mean value E_m . The pre-exponential factor, as usual in literature, was taken as undistributed. In particular, we estimated the FWHM of the distribution to be (0.12 ± 0.02) eV, corresponding to a standard deviation of $\sigma_0 = (0.05 \pm 0.01)$ eV.

This bears important consequences on the interpretation of the constant k_0 evaluated from the initial decay slope. In fact, due to such inhomogeneity effects, k_0 actually corresponds to the *mean* $\langle k \rangle$ calculated on the distribution of ϵ :

$$\begin{aligned}
 k_0 = \langle k \rangle &= \int A \exp\left(-\frac{\epsilon}{k_B T}\right) \times \frac{1}{\sigma\sqrt{2\pi}} \exp\left[-\frac{(E_m - \epsilon)^2}{2\sigma^2}\right] d\epsilon \\
 &= A \exp\left[\frac{\sigma^2}{2k_B^2 T^2}\right] \exp\left(-\frac{E_m}{k_B T}\right) \\
 &= k_m \exp\left[\frac{\sigma^2}{2k_B^2 T^2}\right]
 \end{aligned} \tag{8.6}$$

where

$$k_m = A \exp\left(-\frac{E_m}{k_B T}\right) < k_0 \quad (8.7)$$

Hence, k_0 is *larger* than the value k_m corresponding to the mean activation energy E_m : for this reason, the above derived value $E_i=0.28$ eV must be interpreted as a phenomenological *effective* energy, describing the fastest stage of the decay. The analysis based on the initial decay slope actually samples only the most reactive subset within the whole population of species participating in the reaction. Strictly speaking, only k_m is expected to exhibit an Arrhenius behavior, whereas k_0 should deviate from it due to the term in $1/T^2$ introduced by eq. (8.6). Likely, the investigated temperature range is not wide enough to directly observe these deviations. We also observe that our estimate in chapter 6 of the reaction constant at room temperature on wet natural silica, $k_0(T=300\text{ K})=8.3\times 10^{-20}\text{ cm}^3\text{ s}^{-1}$ is to be interpreted as well as a *mean* value on the distribution, and is in a good agreement with the value at $k_0(300\text{ K})$ of Figure 8.7 estimated here on dry natural silica^{g,h}.

From the physical point of view, the parameter k_m appears most suitable to be compared with theoretical predictions. For this reason, we calculate k_m from k_0 by inverting eq. (8.6). In the simplest assumption, in this calculation we fix $\sigma=\sigma_0$ at all temperatures. k_m is reported as full symbols in Figure 8.7, and is consistent with an Arrhenius dependence from T , the best fit values for activation energy and pre-exponential factor being $E_m=(0.38\pm 0.04)$ eV and $A=3\times 10^{-14}\text{ cm}^3\text{ s}^{-1}$. The uncertainty in E_m mainly derives from the error on σ_0 .

Before going on with the discussion it is worth comparing the mean activation energy E_m with the value $\langle\epsilon\rangle=0.59$ eV found in the previous chapter from room temperature data. As already discussed, measurements at a single temperature do not allow to distinguish the contribution to k_0 of the pre-exponential factor from that of the activation energy; hence, the 0.59 eV value does not have an absolute meaning, because it is based upon a specific choice A_W of the pre-exponential factor coming from the Waite theory of diffusion-limited reactions. Recalling eq. (7.11) we see that:

$$A_W = 4\pi r_0 D_{0L} \sim 3.55 \times 10^{-10} \text{ cm}^3 \text{ s}^{-1} \quad (8.8)$$

using $r_0=5\times 10^{-8}$ cm. Now, data presented here show that the *real* value $A=3\times 10^{-14}\text{ cm}^3\text{ s}^{-1}$, estimated from the temperature-dependence of k_0 , is 4 orders of magnitude lower than A_W . Therefore, one can redefine *a posteriori* the pre-exponential factor used in the previous chapter, this leading to a *shift* of the statistical distribution of the activation energy that makes $\langle\epsilon\rangle$ coincide with E_m , as verified by the following equation

$$A_W \exp\left(\frac{-0.59\text{ eV}}{k_B \times 300\text{ K}}\right) \sim A \exp\left(\frac{-0.38\text{ eV}}{k_B \times 300\text{ K}}\right) \quad (8.9)$$

^gIn dry silica E' center are supposedly generated by two different channels, only one of which is active in wet α -SiO₂ (see chapter 6). The good agreement between k_0 in dry and wet silica is consistent with a simple picture in which the reaction properties of E' centers with H_2 are the same regardless the origin of the defect, despite the fact that different generation mechanisms may result in structural variations. This idea is strongly confirmed by the comparison (see below) with *surface* E' .

^hWe apologize for a slight difference in the notation used here with respect to the previous chapter. Here, k_0 represents (as in chapter 6) the mean value of the distributed reaction constant k . In contrast, in section 7.3 we implicitly used k_0 to indicate what here is referred to as k .

valid within the experimental errors of the two activation energies. In conclusion, present results are actually consistent with the treatment proposed in the previous chapter, although the observation of the temperature dependence of the decay permits now to attribute to E_m , A (and to A_i , E_i) an *absolute* meaning.

8.3.2 Comparison with theoretical models and previous literature

Reactions of bulk defects in solids with mobile species are generally assumed to be diffusion-limited, meaning that their rate is determined by the mobility of the diffuser, whose migration is usually the bottleneck of the process. In the Waite treatment of diffusion-limited reactions, the rate constant of eq. (8.1) is predicted to be (from eq. 2.12):

$$k_{WD} = 4\pi r_0 D_{0L} \exp\left(\frac{-E(\text{H}_2)}{k_B T}\right) \quad (8.10)$$

k_{WD} , calculated with a value $r_0 = 5 \times 10^{-8}$ for the capture radius of E' and $E(\text{H}_2)$, D_{0L} set to the literature parameters for H_2 diffusion in $\alpha\text{-SiO}_2$,^{38,197} is reported (dashed line) in Figure 8.7 for comparison with present results. We observe that k_{WD} is everywhere much larger than the experimental data.ⁱ This result is consistent with our repeated observations that the reaction proceeds more slowly than expected for a purely diffusion-limited reaction, and with the unrealistically small values of the capture radius r_0 , which were found in previous works trying to reproduce the kinetics of reaction (8.1) at $T=300$ K within the Waite theory.^{89,224}

For the measured macroscopic reaction rate to be so small, it must be limited also by the rate of the reaction itself, i.e. the interaction between H_2 and E' below the pair separation r_0 , rather than by the diffusion of H_2 only. These effects can be included in the expression for the rate constant as discussed in chapter 2:^{210,212,213} it is assumed that below r_0 the reaction is no longer diffusion-controlled, but proceeds by first order chemical kinetics, characterized by a rate constant w [s^{-1}]. Hence, the generalized expression for the overall rate constant is found to be eq. (2.15), which we rewrite here in a slightly simplified form:

$$k_{WR} = 4\pi r_0 D \frac{w}{w + Dr_0^{-2}} \quad (8.11)$$

where $D = D_{0L} \exp\left(\frac{-E(\text{H}_2)}{k_B T}\right)$. When $w \gg Dr_0^{-2}$, $k_{WR} \sim k_{WD}$ and the reaction is diffusion-limited, but if $w \ll Dr_0^{-2}$, $k_{WR} \sim 4\pi r_0^3 w$; in this case, the overall rate k_{WR} is much smaller than k_{WD} and, most important, it is not related to the diffusion constant D . From Figure 8.7 it is now clear that reaction (8.1) falls in the latter case: the theory of diffusion-limited reactions is inapplicable to the reaction between E' and H_2 , whose rate is mainly determined by the reaction process in itself rather than by the migration of H_2 . We stress that this conclusion is independent of the simplifications used to treat the effects of the statistical distribution of the activation energy (such as having supposed a σ independent of T), because it is founded only on the result: $k_m < k_0 \ll k_{WD}$. For the same reason, it would be valid also assuming a non-Gaussian distribution of ϵ .

ⁱThis remains true with any reasonable choice of r_0 , or using any of the slightly different values of $E(\text{H}_2)$ (0.38 eV–0.45 eV) which have been reported in literature.^{37,197,198,207}

Summary I. *The reaction constant k_0 between E' and H_2 can be extracted by eq. (8.4) from the post-irradiation kinetics of E' measured at several temperatures (Figure 8.3). In this procedure, one must take into account the fact that the reaction constant is statistical distributed, as shown in the previous chapter. As a consequence, the mean value k_0 directly extracted from data must be conveniently manipulated by eq. (8.6), in order to obtain a parameter k_m suitable to evaluate the mean activation energy of the reaction. A detailed study of the temperature dependence of the reaction constant (Figure 8.7) and the comparison with theoretical models reveal an important result: the kinetics of the passivation of E' by H_2 is reaction-limited rather than diffusion-limited. Aside from clarifying the reaction properties of the E' center, this finding is important in that it is remarkably different from the properties of other defects in $a\text{-SiO}_2$ reported by previous works.*

Our result on E' strikingly differs from what was found on the other basic defect in silica, the NBOHC, whose reaction with H_2 is diffusion-limited.^{38,42,185} This remarkable difference indicates that, differently from NBOHC, the recombination of E' with H_2 is not spontaneous, but requires overcoming an energy barrier, to such an extent that the character of the reaction is overwhelmingly determined by the local features of the defect rather than by the matrix in which it is embedded. The different reactivities of NBOHC and E' with H_2 had been anticipated by some computational works.^{1,230}

Since the reaction rate is unrelated to D , our best estimates for the mean activation energy $E_m=(0.38\pm 0.04)$ eV and for the pre-exponential factor $A=3\times 10^{-14}\text{cm}^3\text{s}^{-1}$, must be interpreted as features of the local reaction, not related to the diffusion of H_2 . In this sense, it is worth noting that the similarity between E_m and the activation energy 0.45 eV for hydrogen diffusion in $a\text{-SiO}_2$ is purely accidental.^{108,197} What's more, as anticipated in the previous chapter, also the existence *per se* of a distribution in the activation energy, and its width σ_0 , are not interpretable here as features of H_2 diffusion in the amorphous solid. In this sense, one must distinguish between two physically different effects of disorder: inhomogeneity affecting the *diffusion process* in $a\text{-SiO}_2$, and inhomogeneity affecting the *reaction properties* of a specific point defect. The former shows up in the randomization of the diffusion constant D , and in turn of any diffusion-limited reaction constant. In contrast, the latter effect is probed by a defect whose distributed reaction constant is *not* diffusion-limited. The physics of $a\text{-SiO}_2$ provides good examples of these two conceptually different phenomena in the two basic defects, the NBOHC and the E' respectively.

Present experimental results may be used as a benchmark to be compared with computational works, in which several estimates of the activation energy for process (8.1) ranging from 0.2 eV to 0.7 eV were proposed, depending on the calculation method.^{1,229,230,232,234} In this sense, the closest agreement is found with the ~ 0.5 eV value reported by Vitiello *et al.*²³⁰

For what concerns the reaction of surface E' with H_2 , where diffusion is clearly not a rate limiting factor, the mean activation energy was reported to be (0.43 ± 0.04) eV, consistent with our value E_m .²¹⁴ Also the mean rate constant k at room temperature $k(T=300\text{K})=8.2\times 10^{-20}\text{cm}^3\text{s}^{-1}$,

closely agrees with our estimate $k_0(T=300\text{ K})=8.3\times 10^{-20}\text{ cm}^3\text{ s}^{-1}$. The two observations lead also to consistent pre-exponential factors. Since the reaction properties of surface and bulk E' with H_2 are found to be very similar, we conclude that the surroundings of the defect do not influence its interaction with the H_2 molecule, and only the $\text{O}_3\equiv\text{Si}^\bullet$ moiety determines the reaction dynamics^j. Such a simple conclusion is far from being obvious *a priori*, since surface and bulk varieties of E' are known to differ in basic spectroscopic features, such as the OA peak (which falls at energies higher than 6 eV for surface centers) and ESR signal.¹ For comparison, we also observe that the P_b centers ($\text{Si}_3\equiv\text{Si}^\bullet$) on Si/SiO₂ interfaces have been found to react with H_2 with a much higher (~ 1.7 eV) activation energy,^{268–270} this meaning that the nature of the three silicon bonds is a factor that strongly influences the activation energy.

The reaction kinetics of E' with H_2 was also investigated in a pioneering work by Li *et al.* dealing with E' embedded in thermal SiO₂ films exposed to H_2 in a vessel,²²⁶ (see Figure 2.9), where it was estimated an activation energy of 0.3 eV and a rate constant at room temperature of $\sim 5\times 10^{-22}\text{ cm}^3\text{ s}^{-1}$, which is two orders of magnitude lower than our $k_0(300\text{ K})$. Consequently, the authors had qualitatively drawn the same conclusion that is rigorously confirmed here, i.e. reaction (8.1) is not diffusion-limited. Although the comparison with our findings could lead to conclude that reaction parameters of E' in thin films are significantly different from bulk E' , these results cannot be directly compared to ours. In fact, within the experimental approach by Li *et al.*, one must take into account also the entry and permeation processes of H_2 in SiO₂ as additional steps in the process which may condition the measure of the reaction parameters, as clearly discussed by the same authors.

8.4 Discussion II: Temperature dependence of the generation process

Apart from reaction (8.1), also the *generation* of E' appears to be (see Figure 8.5) a thermally activated process, quenched below $\sim 150\text{ K}$. The activation and the progressive increase of the generation efficiency with temperature is even more apparent in Figure 8.8, where we report a zoom of the first 150 s of the kinetics in Figure 8.3 at some representative temperatures. Further information comes from the analysis of the initial generation rate per pulse R [cm^{-3}] at the beginning of irradiation, defined in chapter 6, which can be estimated by a linear fit in the first ~ 100 s of the exposure session^k. R is plotted against temperature in the 150 K–475 K range in Figure 8.9-(a). The values below 150 K were too small to be accurately estimated. We see that R is consistent with an Arrhenius dependence from T , with activation energy of 44 meV as estimated from a least-square linear fit.

^jPut in other words, with respect to the reaction with H_2 the E' centers (at least the type(s) of E' found in our laser-irradiated samples) basically behave as isolated dangling bonds

^kWe recall that R is given by $R=d[E']/dN(N=0)=\nu_r^{-1}d[E']/dt(t=0)$, where ν_r is the repetition rate of laser pulses. As R is derived from the initial linear range of the *in situ* growth curve of E' , it represents the "pure" generation efficiency, not yet affected by the competition with any concurrent annealing processes of the defect.

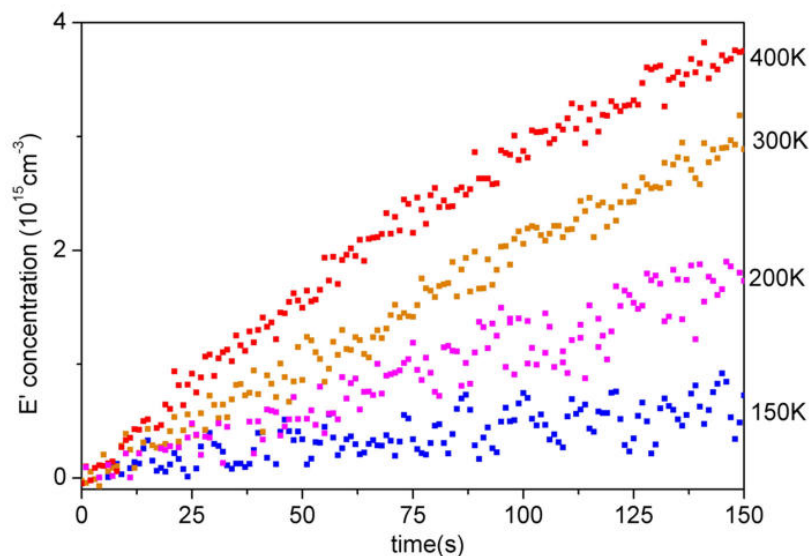


Figure 8.8: Zoom of the first stage of the growth kinetics of Figure 8.3 at 4 representative temperatures. It is apparent the progressive increase of the generation efficiency with temperature.

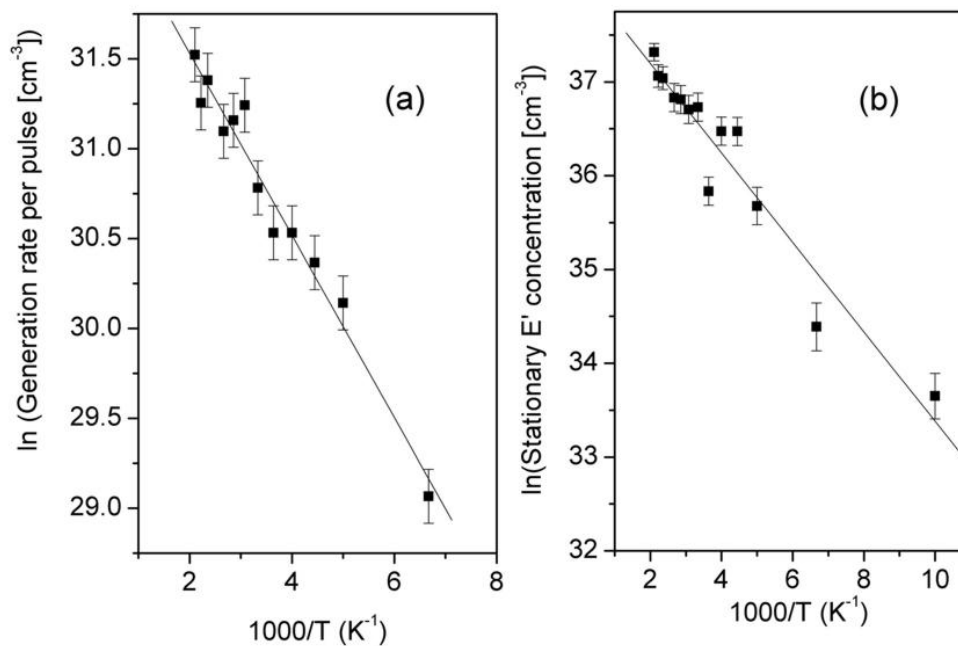


Figure 8.9: Panel (a): Arrhenius plot of the initial generation rate per pulse of E' in the 150 K–475 K interval, extracted from the kinetics in Figure 8.3. Panel (b): Arrhenius plot of the stationary E' concentration (empty symbols in Figure 8.5) in the 100 K–475 K interval.

In literature, the temperature-dependence of *stationary* laser-generated E' was investigated in a few works,^{77–79} which reported a result not dissimilar to the present one, namely the formation of E' is quenched below ~ 150 K, above which its efficiency monotonically increases with T (see for example

Figure 1.6). This finding was explained as the consequence of E' being generated by non-radiative decay of self-trapped excitons (STE), based on the anti-correlated temperature dependence of the luminescence decay time of STE. However, to understand if also in the present case STE are involved in E' generation, more experiments are necessary in order to directly observe STE by detecting *in situ* their luminescence signal (reported^{2,58} between 2.0 eV–2.3 eV) during low temperature irradiations, and to verify if also here their luminescence lifetime is anti-correlated to the E' generation efficiency.

As proposed in chapter 6, in dry natural silica under laser irradiation the E' centers arise partly from Si–H precursors, whose laser-induced breaking generates the defect together with H:



and partly from a second unknown precursor X . After irradiation, the E' centers partially decay, all of them participating in the reaction with H_2 independently of their origin. Within this scheme, the parameter R in Figure 8.9-(a) accounts for both generation channels. In contrast, the contribution to the E' population arising from the precursor X can be isolated as it equals the stationary concentration $[E']_\infty$ of Figure 8.5 (on this point see subsection 6.3.1). As shown in Figure 8.9-(b), also $[E']_\infty$ approximately follows an Arrhenius temperature-dependence from 100 K to 475 K with 41 meV activation energy, although the agreement with the Arrhenius curve is less satisfactory than for the parameter R .¹ Within our interpretation scheme, on the whole, the data in Figure 8.9 suggest that both generation mechanisms of E' are thermally activated and feature comparable activation energies. Although this behavior is very clear from a purely phenomenological point of view, it is difficult at the moment to provide a satisfactory interpretation without further experiments^m. We just remark that the similarity of the two activation energies seems to suggest a correlation between the two generation mechanisms. The simplest explanation of this finding would be that the two processes are both controlled by non-radiative decay of STE. Nevertheless, other interpretations are possible, and more experiments are needed to clarify this point.

As a last point, we discuss qualitatively the data in Figure 8.6. The variation $\Delta[E'](T)$ in the post-irradiation stage, is an indirect measurement of the amount of radiolytic hydrogen $[\text{H}_2](\tau, T)$ made available by irradiationⁿ. Its temperature-dependence is roughly bell-shaped with a maximum near 250 K. This finding may be understood as follows. In chapter 6 it was proposed a rate equation able to model the growth of E' by process (8.12) during irradiation of wet natural silica. The basic idea was the competition between laser-induced rupture of the precursor, and the concurrent annealing of E' by H_2 due to reaction (8.1). This mathematical model cannot be directly applied here because of

¹The value at 10 K (not included in the plot) is not consistent with the Arrhenius dependence; however, the availability of a single data point below 100 K does not permit for the moment to discuss possible deviations from the Arrhenius behavior in the low temperature range.

^mClearly, the circumstance that in the present experimental conditions two distinct processes supposedly contribute to the formation of E' complicates the interpretation. This difficulty could be overcome by performing a similar investigation on *wet* natural silica, where E' was proposed to arise only from Si–H breaking. Actually, the experiments presented in this chapter were carried out on dry specimens because they feature a higher E' generation efficiency, thereby allowing for more accurate measurements of the reaction constant k_0 , this being the primary aim of this investigation.

ⁿAlthough at the lowest temperatures hydrogen is likely to be stored in atomic form before heating causes its dimerization.

the second channel contributing in dry specimens to the generation of E' . Even so, a similar line of reasoning allows to understand the temperature-dependence of $\Delta[E']$. In detail, also here radiolytic hydrogen and a portion of E' are generated by Si–H breaking, which is a thermally activated process (Figure 8.5); hence, $\Delta[E'](T)=2[\text{H}_2](\tau,T)$ remains very low under ~ 150 K. Above this threshold $\Delta[E'](T)$ grows till the onset (~ 200 K) of H_2 diffusion activates the E' – H_2 reaction: when this occurs, the accumulation of H_2 coming from process (8.12) during the 2000 pulses irradiation is limited by the interplay with the concurrent reaction with E' , which at the same time consumes the produced H_2 . The reaction constant k_0 grows with temperature, and an "optimal" condition is reached around 250 K, where generation and annealing of radiolytic H_2 balance at the highest concentration. Then, at even higher temperatures, the reaction becomes so fast that it prevents H_2 to grow during irradiation, because it is too rapidly consumed by the simultaneously growing E' . For this reason, $\Delta[E'](T)$ decreases back to zero. The main difference from the simpler case of wet natural silica, where process (8.12) leads to $[E']=[\text{H}_2]/2$, is that here, due to the presence of a second generation channel for E' , we have $[E'](\tau,T)>[\text{H}_2](\tau,T)/2$, so that the concentration of E' can be nonzero even if H_2 tends to zero. Consistently, at $T>400$ K, the generation of E' is still efficient, even if $\text{H}_2=\Delta[E'](T)/2$ fails to grow during irradiation so that the post-irradiation decay of E' almost disappears. It is expected that in a similar experiment in wet natural silica at $T>400$ K, one should observe *both* $[E'](\tau,T)$ and $[\text{H}_2](\tau,T)$ decreasing to zero. Once understood qualitatively the bell-shaped temperature dependence of $\Delta[E'](T)$ and the Arrhenius behavior of $[E']_\infty(T)$ (Figure 8.9-(b)), the peculiar temperature dependence of the maximum *in situ* concentration $[E'](\tau,T)=[E']_\infty(T)+\Delta[E'](T)$ in Figure 8.5 can be simply regarded as the sum of the two effects, thus completing our qualitative understanding of data in Figure 8.5 and Figure 8.6. Work is in progress to translate these considerations in a system of rate equations fitting experimental data.

8.5 Conclusions

We investigated by *in situ* optical absorption spectroscopy the generation and post-irradiation decay of E' centers induced at several temperatures on dry natural silica by laser-irradiation. We provided a measurement of the temperature dependence of the reaction constant between bulk E' in α - SiO_2 and mobile H_2 . The values of the activation energy and pre-exponential factor of the process lead to the conclusion that the reaction kinetics is not diffusion-limited. This result remarkably differs from what is known for the other basic point defect in α - SiO_2 , the NBOHC, whose reaction with H_2 is purely diffusion-limited. The comparison with properties of surface E' centers investigated in previous works suggests that the reaction properties of E' are independent of its surroundings. Besides the reaction with H_2 , also the generation of E' appears to be thermally activated. The competition between the laser-induced breaking of Si–H that produces radiolytic hydrogen, and the concurrent reaction of H_2 with E' , leads to a characteristic temperature-dependence of the concentration of the defect at the end of irradiation, and to the factual deactivation of the post-irradiation decay process above ~ 400 K.

Chapter 9

Conclusions

In this Thesis we have reported an experimental study of the generation and decay kinetics of point defects induced by 4.7 eV pulsed laser radiation on amorphous silicon dioxide. Our investigation was founded on the combined use of several experimental techniques, mainly *in situ* optical absorption (OA), electron spin resonance (ESR) and photoluminescence (PL). The results show that natural α -SiO₂ samples, produced by fusion of quartz, feature an articulated landscape of processes triggered by exposure to laser light.

One of them is the generation of the silicon dangling bond defect ($\equiv\text{Si}^\bullet$), a paramagnetic center known as E' in the specialized literature, which is one of the most important point defects in silica. A characteristic feature of the laser-induced E' centers, is that after the end of exposure they are unstable and undergo a spontaneous decay with a typical time scale of a few 10^3 s. The growth kinetics of E' during irradiation and the first stages of the post-irradiation decay have been studied by *in situ* optical absorption spectroscopy. Starting from a few minutes from the end of exposure, the decay can also be monitored by ESR, with consistent results. Although laser-induced E' has been investigated by plenty of works in the specialized literature, the current knowledge on its laser- or radiation-induced generation is mainly based on stationary measurements unable to monitor the kinetics of the defects. Only a few works have studied *in situ* the generation and decay of the center; furthermore, most previous *in situ* studies mainly reported single-wavelength measurements, while the observation of the complete absorption profile provides important information that goes beyond the estimate of the concentration of E' .

Simultaneously to the post-irradiation decay of E' , we have observed by ESR the growth of a defect related to the presence of Ge impurities, known as H(II) ($=\text{Ge}^\bullet-\text{H}$). Based on the structure of H(II), which may be regarded as a probe of the presence in the solid of mobile hydrogen, and on the typical time scale and temperature dependence of the post-irradiation processes, we have interpreted both the decay of E' and the formation of H(II) as effects of molecular hydrogen diffusion in the silica matrix. In our interpretation, the decay of E' is due to its reaction with mobile H₂, which converts the paramagnetic defect to a Si-H group and makes available an hydrogen atom H, while the formation of H(II) is a consequence of subsequent trapping of H on already present twofold

coordinated Ge impurities ($=\text{Ge}^{\bullet\bullet}$), known as GLPC. This model has been proved by showing that the post-irradiation kinetics of GLPC and H(II) are anti-correlated, and that the time dependence of the concentrations of E' , GLPC and H(II) after the end of laser exposure can be reproduced by a chemical rate equation model describing the diffusion and reactions of mobile H_2 and H. In addition, we have shown that the features of the kinetics are a fingerprint of the disordered structure of the amorphous solid, which manifests itself in a statistical distribution of the activation energy controlling the reaction constant of E' and H_2 . Till now, this kind of property had been pointed out only for the other "basic" defect in amorphous silica, the oxygen dangling bond, known as Non Bridging Oxygen Hole Center (NBOHC).

The detailed study *in situ* of the kinetics of E' during and after irradiation, has led us to conclude that this defect is generated by laser radiation by breakage of pre-existing Si–H bond. This process is also the origin of the radiolytic hydrogen responsible for the post-irradiation processes; in this sense, the instability of the generated E' centers is, in the present context, an intrinsic property of their very generation process. Although generation of E' from Si–H had already been proposed in literature, we have shown that natural (wet) silica allows to isolate this process from other formation mechanisms of E' . Exploiting this favorable and rather new circumstance, we have been able to carry out a quantitative study of the generation kinetics of E' : the growth of the defect has been found to be conditioned by the interplay between laser-induced generation and concurrent annealing of the induced defects by H_2 . Based upon this idea, we proposed a rate equation model able to describe the kinetics and successfully tested it against experimental data. Moreover, for the first time to our knowledge, we have provided a clear experimental proof that Si–H bond breakage occurs by a two photon absorption process, thus giving support to previous theoretical calculations.

As a further step, we have studied the temperature dependence of the kinetics of E' induced by laser irradiation. For what concerns the post-irradiation reaction of E' with H_2 , previous literature data existed only for surface E' and for E' in thin films, and they were contradictory. In contrast, our study has focused on the E' in bulk silica, and has permitted to clarify the character of the reaction between E' and H_2 , whose kinetics is reaction-limited rather than diffusion-limited. This is a remarkable new result that contrasts with the common assumption that kinetics of reactions in solids driven by diffusion of mobile species are diffusion-limited due to the slowness of the diffusion process. Moreover, our result is remarkably different from what is known for the NBOHC center in silica, whose reaction with H_2 is diffusion-limited. It is worth noting that our results lead to alternative interpretations of the randomization of the activation energy for chemical reactions typical of processes in an amorphous solid.

Another interesting aspect of natural silica is that it allows to study selectively the laser-induced conversion processes of a specific and important Ge-related defect, the GLPC. Our findings strongly suggest that a significant portion of GLPC is converted by radiation to a diamagnetic defect. This is at variance with most literature investigations, carried out on Ge-doped silica samples, in which the GLPC is generally supposed to be converted to paramagnetic defects. Also, our results underline the importance of monitoring the kinetics of Ge-related conversion processes, choice which provides information not available by common studies focusing only on the stationary concentration of defects.

Then, we have studied the effects of repeated irradiations, demonstrating that after each high-dose exposure the samples lose memory of their previous history, namely the post-irradiation kinetics repeat identically after each new irradiation. A necessary step for the achievement of such an effect, is the destruction of already-formed H(II) centers by laser light, which are back-converted to GLPC by breaking of the Ge-H bond. We have measured the cross section for this process and have proposed that it occurs by direct single photon absorption at the defect site.

We argue that these results constitute significant advancements in the understanding of laser-induced processes in silica. From the experimental and technological points of view, they prove the usefulness of *in situ* time-resolved detection of absorption spectra to perform comprehensive studies on transient point defect conversion processes and their effect on the transparency of optical materials during UV exposure.

Several interesting questions remain open and could be investigated by further experiments. To mention some, more details on the generation process of E' could be inferred by studying the dependence of the process from the laser wavelength or by observing the process with pump-and-probe techniques on the femtosecond scale. Also, an increase of the available time resolution, possible with slight modifications of our experimental apparatus, would permit to study the fast (<1 s) stages of the decay of E' supposedly involving atomic hydrogen. Loading with O_2 or H_2O and an extension of the temperature range of the experiments would allow to comprehensively investigate the reaction properties of E' with other mobile species. Finally, our *in situ* approach could be applied also to other systems, such as pure silica under ionizing (γ or β) radiation, or Ge-doped silica under laser exposure.

List of related papers

- M. Cannas, S. Agnello, R. Boscaino, S. Costa, F. M. Gelardi, and F. Messina, *Growth of H(II) centers in natural silica after UV laser exposure*, J. Non-Cryst. Solids **322**, 90 (2003).
- M. Cannas and F. Messina, *Bleaching of optical activity induced by UV laser exposure in natural silica*, J. Non-Cryst. Solids **345**, 433 (2004).
- F. Messina, M. Cannas, and R. Boscaino, *Influence of hydrogen on paramagnetic defects induced by UV laser exposure in natural silica*, Phys. Stat. Sol. (C) **2**, 616 (2005).
- M. Cannas and F. Messina, *Nd:YAG laser induced E' centers probed by in situ absorption measurements*, J. Non-Cryst. Solids **351**, 1780 (2005).
- F. Messina, M. Cannas, and R. Boscaino, *H(II) centers in natural silica under repeated UV laser irradiations*, J. Non-Cryst. Solids **351**, 1770 (2005).
- F. Messina and M. Cannas, *In situ observation of the generation and annealing kinetics of E' centers induced in amorphous SiO₂ by 4.7 eV laser irradiation*, J. Phys.: Condens. Matter **17**, 3837 (2005).
- F. Messina, M. Cannas, K. Médjahdi, A. Boukenter, and Y. Ouerdane, *UV-Photoinduced defects in Ge-doped optical fibers*, Proceedings of 2005 IEEE/LEOS Workshop on Fibres and Optical Passive Components, ISBN 0-7803-8949-2, S. Riva-Sanseverino, M. Artiglia (Eds.), pag. 313 (2005).
- F. Messina and M. Cannas, *Hydrogen-related conversion processes of Ge-related point defects in silica triggered by UV laser irradiation*, Phys. Rev. B **72**, 195212 (2005).
- K. Médjahdi, A. Boukenter, Y. Ouerdane, F. Messina, and M. Cannas, *Ultraviolet-induced paramagnetic centers and absorption changes in singlemode Ge-doped optical fibers*, Optics Express **14**, 5885 (2006).
- F. Messina and M. Cannas, *Photochemical generation of E' centres from Si-H in amorphous SiO₂ under pulsed ultraviolet laser irradiation*, J. Phys.: Condens. Matter **18**, 9967 (2006).
- F. Messina, S. Agnello, R. Boscaino, M. Cannas, S. Grandi, and E. Quartarone, *Optical properties of Ge-oxygen defect center embedded in silica films*, in press on J. Non-Cryst. Solids (2007).
- K. Médjahdi, A. Boukenter, Y. Ouerdane, F. Messina, and M. Cannas, *Role of diffusing molecular hydrogen on relaxation processes in Ge-doped glass*, in press on J. Non-Cryst. Solids (2007).
- F. Messina and M. Cannas, *Stability of E' centers induced by 4.7 eV laser irradiation in SiO₂*, in press on J. Non-Cryst. Solids (2007).
- F. Messina, M. Cannas, R. Boscaino, S. Grandi, and P. Mustarelli, *Optical absorption induced by UV laser radiation in Ge-doped amorphous silica probed by in situ spectroscopy*, in press on Physica Status Solidi (2007).

- S. Agnello, G. Buscarino, M. Cannas, F. Messina, S. Grandi, and A. Magistris, *Structural inhomogeneity of Ge-doped amorphous SiO₂ probed by photoluminescence lifetime measurements under synchrotron radiation*, in press on Physica Status Solidi (2007).

References

1. G. Pacchioni, L. Skuja, and D. L. Griscom (Eds.), *Defects in SiO₂ and Related Dielectrics: Science and Technology*, ISBN 0-7923-6685-9, Kluwer Academic Publishers, USA (2000).
2. R. A. B. Devine, J.-P. Duraud, and E. Dooryhée (Eds.) *Structure and imperfections in amorphous and crystalline silicon dioxide*, ISBN 0-471-97536-2, John Wiley & Sons, UK (2000).
3. H. S. Nalwa (Ed.) *Silicon-based Materials and Devices*, ISBN 0-12-513909-8, Academic Press, USA (2001).
4. W. H. Zachariasen, *J. Am. Chem. Soc.* **54**, 3841 (1932).
5. R. L. Mozzi and B. E. Warren, *J. Appl. Crystallogr.* **2**, 164 (1969).
6. R. J. Bell and P. Dean, *Phyl. Mag.* **25**, 1381 (1972).
7. D. L. Griscom, *Journ. Cer. Soc. Japan.* **99**, 899 (1991).
8. L. Skuja, H. Hosono, and M. Hirano, *Proc. SPIE* **4347**, 155 (2001).
9. P. St. J. Russell, *Science* **299**, 358 (2003).
10. L. Tong, R. R. Gattass, J. B. Ashcom, S. He, J. Lou, M. Shen, I. Z. Maxwell, and E. Mazur, *Nature* **426**, 816 (2003).
11. A. I. Kingon, J.-P. Maria, and S. K. Streiffer, *Nature* **406**, 1032 (2000).
12. L. Skuja, *J. Non-Cryst. Solids* **239**, 16 (1998).
13. A. J. Ikushima, T. Fujiwara, and K. Saito, *J. Appl. Phys.* **88**, 1201 (2000).
14. R. A. Weeks, *J. Appl. Phys.* **27**, 1376 (1956).
15. R. A. Weeks and E. Sonders in *Paramagnetic Resonance*, Vol. 2, W. Low (Ed.), Academic Press, USA (1963).
16. A. R. Silin, L. Skuja, and A. V. Shendrik, *Sov. Phys. Chem. Glass* **4**, 405 (1978).
17. M. Stapelbroek, D. L. Griscom, E. J. Friebele, and G. H. Sigel, *J. Non-Cryst. Solids* **32**, 313 (1979).
18. L. Skuja, *J. Non-Cryst. Solids* **179**, 51 (1994).
19. H. Hosono, K. Kajihara, T. Suzuki, Y. Ikuta, L. Skuja, and M. Hirano, *Solid State Commun.* **122**, 117 (2002).
20. M. Cannas and F. M. Gelardi, *Phys. Rev. B* **69**, 153201 (2004).
21. H. Nishikawa, E. Watanabe, D. Ito, and Y. Ohki, *J. Non-Cryst. Solids* **179**, 179 (1994).
22. R. Boscaino, M. Cannas, F. M. Gelardi, and M. Leone, *Nucl. Instr. and Meth. in Phys. Res. B* **116**, 373 (1996).
23. D. L. Griscom, *Nucl. Instr. and Meth. B* **1**, 481 (1984).
24. F. J. Feigl, W. B. Fowler, and K. L. Yip, *Solid State Commun.* **14**, 225 (1974).
25. D. L. Griscom, E. J. Friebele, and G. H. Sigel, *Solid State Commun.* **15**, 479 (1974).
26. D. L. Griscom, *Phys. Rev. B* **20**, 1823 (1979).
27. A. Stirling and A. Pasquarello, *J. Phys.: Condens. Matter* **17**, S2099 (2005).
28. H. Imai and H. Hirashima, *J. Non-Cryst. Solids* **179**, 202 (1994).
29. G. Buscarino, S. Agnello, and F. M. Gelardi, *Phys. Rev. B* **73**, 045208 (2006).
30. G. Buscarino, S. Agnello, and F. M. Gelardi, *Phys. Rev. Lett.* **94**, 125501 (2005).
31. G. Buscarino, S. Agnello, and F. M. Gelardi, *Mod. Phys. Lett. B* **20**, 451 (2006).
32. G. Buscarino, S. Agnello, and F. M. Gelardi, *Phys. Rev. Lett.* **97**, 135502 (2006).
33. G. Pacchioni and G. Ieranò, *Phys. Rev. B* **57**, 818 (1998).
34. G. Pacchioni, G. Ieranò, and A. M. Márquez, *Phys. Rev. Lett.* **81**, 377 (1998).
35. E. P. O'Reilly and J. Robertson, *Phys. Rev. B* **27**, 3780 (1983).

36. M. Cannas and M. Leone, *J. Non-Cryst. Solids* **280**, 183 (2001).
37. J. E. Shelby, *J. Appl. Phys.* **48**, (1977) 3387.
38. D. L. Griscom, *J. Non-Cryst. Solids* **68**, 301 (1984).
39. D. L. Griscom, *J. Appl. Phys.* **58**, 2524 (1985).
40. J. E. Shelby, *J. Non-Cryst. Solids* **179**, 138 (1994).
41. B. C. Schmidt, F. M. Holtz, and J.-M. Bény, *J. Non-Cryst. Solids* **240**, 91 (1998).
42. K. Kajihara, L. Skuja, M. Hirano, and H. Hosono, *Phys. Rev. Lett.* **89**, 135507 (2002).
43. W. W. Duley, *UV lasers: effects and applications in materials science*, ISBN 0-521-46498-6, Cambridge University Press, UK (1996).
44. J. H. Stathis and M. A. Kastner, *Phys. Rev. B* **29**, 7079 (1984).
45. K. Miura, H. Inouye, J. Qiu, T. Mitsuyu, and K. Hirao, *Nucl. Instr. and Meth. in Phys. Res. B* **141**, 726 (1998).
46. J. Qiu, K. Miura, H. Inouye, J. Nishii, and K. Hirao, *Nucl. Instr. and Meth. In Phys. Res. B* **141**, 6 (1998).
47. K.-I. Kawamura, N. Sarukura, M. Hirano, N. Ito, and H. Hosono, *Appl. Phys. Lett.* **79**, 1228 (2001).
48. K.-I. Kawamura, M. Hirano, T. Kamiya, and H. Hosono, *Appl. Phys. Lett.* **81**, 1137 (2002).
49. N. F. Borrelli, C. M. Smith, J. J. Price, and D. C. Allan, *Appl. Phys. Lett.* **80**, 219 (2002).
50. C. Corbari, J. D. Mills, O. Deparis, B. G. Klappauf, and P. G. Kazansky, *Appl. Phys. Lett.* **81**, 1586 (2002).
51. H. Y. Li, W. Watanabe, K. Itoh, and X. Sun, *Appl. Phys. Lett.* **81**, 1953 (2002).
52. C. Fiori and R. A. B. Devine, *Phys. Rev. B* **33**, 2972 (1986).
53. T. P. Seward III, C. Smith, N. F. Borrelli, and D. C. Allan, *J. Non-Cryst. Solids* **222**, 407 (2000).
54. M. Shimbo, T. Nakajima, N. Tsuji, Z. Zhonga, H. Yamaguch, T. Kahuno, and T. Obara, *J. Appl. Phys.* **88**, 6052 (2000).
55. T. E. Tsai, D. L. Griscom, and E. J. Friebele, *Phys. Rev. Lett.* **61**, 444 (1988).
56. K. Arai, H. Imai, H. Hosono, Y. Abe, and H. Imagawa, *Appl. Phys. Lett.* **53**, 1891 (1988).
57. H. Nishikawa, R. Nakamura, Y. Ohki, and Y. Hama, *Phys. Rev. B* **48**, 15584 (1993).
58. A. N. Trukhin, *J. Non-Cryst. Solids* **149**, 32 (1992).
59. N. W. Ashcroft and N. D. Mermin, *Solid State Physics*, ISBN 0-03-049346-3, Holt-Saunders International Editions, JAPAN (1981).
60. A. J. Dekker, *Solid State Physics*, Prentice-Hall, USA (1957).
61. A. L. Shluger and E. Stefanovich, *Phys. Rev. B* **42**, 9664 (1990).
62. P. N. Saeta and B. I. Greene, *Phys. Rev. Lett.* **70**, 3588 (1993).
63. S. I. Beigi and S. G. Louie, *Phys. Rev. Lett.* **95**, 156401 (2005).
64. K. Tanimura, T. Tanaka, and N. Itoh, *Phys. Rev. Lett.* **51**, 423 (1983).
65. A. L. Shluger, *J. Phys. C: Solid State Phys.* **21**, L431 (1988).
66. K. Tanimura, C. Itoh, and N. Itoh, *J. Phys. C* **21**, 1869 (1988).
67. C. Itoh, T. Suzuki, and N. Itoh, *Phys. Rev. B* **41**, 3794 (1990).
68. A. J. Fisher, W. Hayes, and A. M. Stoneham, *Phys. Rev. Lett.* **64**, 2667 (1990).
69. G. Petite, S. Guizard, W. Joosen, and P. Martin, *Nucl. Instr. and Meth. in Phys. Res. B* **91**, 338 (1994).
70. S. Guizard, P. Martin, G. Petite, P. D'Oliveira, and P. Meynadier, *J. Phys.: Condens. Matter* **8**, 1281 (1996).
71. A. L. Shluger and K. Tanimura, *Phys. Rev. B* **61**, 5392 (2000).
72. H. Nishikawa, R. Nakamura, R. Tohmon, Y. Ohki, Y. Sakurai, K. Nagasawa, and Y. Hama, *Phys. Rev. B* **41**, 7828 (1990).
73. R. A. B. Devine and J. Arndt, *Phys. Rev. B* **42**, 2617 (1990).
74. T. E. Tsai and D. L. Griscom, *Phys. Rev. Lett.* **67**, 2517 (1991).
75. H. Imai, K. Arai, J. Isoya, H. Hosono, Y. Abe, and H. Imagawa, *Phys. Rev. B* **48**, 3116 (1993).
76. N. Fukata, Y. Yamamoto, K. Murakami, M. Hase, and M. Kitajima, *Appl. Phys. Lett.* **83**, 3495 (2003).
77. R. A. B. Devine, C. Fiori, and J. Robertson, *Mater. Res. Soc. Symp. Proc.* **61**, 177 (1986).

78. R. A. B. Devine, Nucl. Instrum. and Meth in Phys. Res. B **91**, 378 (1994).
79. M. Rothschild, D. J. Ehrlich, and D. C. Shaver, Appl. Phys. Lett. **55**, 1276 (1989).
80. R. A. B. Devine, Phys. Rev. Lett. **62**, 340 (1989).
81. R. A. B. Devine and J. Arndt, Phys. Rev. B **39**, 5132 (1989).
82. K. Arai, H. Imai, J. Isoya, H. Hosono, Y. Abe, and H. Imagawa, Phys. Rev. B **45**, 10818 (1992).
83. D. Donadio and M. Bernasconi, Phys. Rev. B **71**, 073307 (2005).
84. H. Hosono, Y. Ikuta, T. Kinoshita, K. Kajihara, and M. Hirano, Phys. Rev. Lett. **87**, 175501 (2001).
85. K. Kajihara, Y. Ikuta, M. Hirano, and H. Hosono, J. Non-Cryst. Solids **322**, 73 (2003).
86. P. Karlitschek, G. Hillrichs, and K.-F. Klein, Opt. Commun. **155**, 376 (1998).
87. P. Karlitschek, G. Hillrichs, and K.-F. Klein, Opt. Commun. **116**, 219 (1995).
88. H. Imai, K. Arai, H. Imagawa, H. Hosono, and Y. Abe, Phys. Rev. B **38**, 12772 (1988).
89. H. Imai, K. Arai, H. Hosono, Y. Abe, T. Arai, and H. Imagawa, Phys. Rev. B **44**, 4812 (1991).
90. H. Nishikawa, R. Nakamura, Y. Ohki, and Y. Hama, Phys. Rev. B **48**, 2968 (1993).
91. A. Zoubir, C. Rivero, R. Grodsky, K. Richardson, M. Richardson, T. Cardinal, and M. Couzi, Phys. Rev. B **73**, 224117 (2006).
92. L. N. Skuja, A. N. Streletsky, and A. B. Pakovich, Solid State Commun. **50**, 1069 (1984).
93. L. Skuja, J. Non-Cryst. Solids **149**, 77 (1992).
94. H. Hosono, Y. Abe, H. Imagawa, H. Imai, and K. Arai, Phys. Rev. B **44**, 12043 (1991).
95. N. Kuzuu and M. Murahara, Phys. Rev. B **52**, 3241 (1995).
96. J. Vitko, J. Appl. Phys. **49**, 5530 (1978).
97. V. A. Radtsig, Kin. Katal. **20**, 456 (1979).
98. V. A. Radtsig and A. A. Bobyshev, Phys. Stat. Sol. B **133**, 621 (1986).
99. T. Tsai and D.L. Griscom, J. Non-Cryst. Solids **91**, 170 (1987).
100. A. H. Edwards, G. Germann, Nucl. Instr. and Meth. in Phys. Res. B **32**, 238 (1988).
101. D. Donadio, M. Bernasconi, and M. Boero, Phys. Rev. Lett. **87**, 195504 (2001).
102. A. N. Trukhin, L. N. Skuja, A. G. Boganov, and V. S. Rudenko, J. Non-Cryst. Solids **149**, 96 (1992).
103. R. Boscaino, M. Cannas, F. M. Gelardi, and M. Leone, Phys. Rev. B **54**, 6194 (1996).
104. T. Uchino, M. Takahashi, and T. Yoko, Phys. Rev. Lett. **86**, 1777 (2001).
105. S. Agnello, R. Boscaino, M. Cannas, F. M. Gelardi, M. Leone, and B. Boizot, Phys. Rev. B **67**, 033202 (2003).
106. J. Robertson in: *The Physics and Technology of Amorphous SiO₂*, R. A. B. Devine (Ed.), ISBN 0306429292, Plenum Press, USA (1988).
107. V. V. Afanas'ev and A. Stesmans, J. Phys.: Condens. Matter **12**, 2285 (2000).
108. R. H. Doremus, *Diffusion of Reactive Molecules in Solids and Melts*, ISBN 0-471-38545-X, John Wiley & Sons, USA (2002).
109. N. Leclerc, C. Pfeiderer, J. Wolfrum, K. Greulich, W. P. Leung, M. Kulkarni, and A. C. Tam, Appl. Phys. Lett. **59**, 3369 (1991).
110. N. Leclerc, C. Pfeiderer, H. Hitzler, J. Wolfrum, K-O Greulich, S. Thomas, and W. Englisch, J. Non-Cryst. Solids **149**, 115 (1992).
111. H. Hitzler, C. Pfeiderer, N. Leclerc, J. Wolfrum, K. O. Greulich, and H. Fabian, J. Non-Cryst. Solids **149**, 107 (1992).
112. M. Shimbo and K. Sato, Jpn. J. Appl. Phys. **34**, 5640 (1995).
113. C. D. Marshall, J. A. Speth, and S. A. Payne, J. Non-Cryst. Solids **212**, 59 (1997).
114. C. M. Smith, N. F. Borrelli, and R. J. Araujo, Appl. Opt. **39**, 5778 (2000).
115. M. Shimbo, T. Nakajima, N. Tsuji, T. Kakuno, and T. Obara, Jpn. J. Appl. Phys. **40**, 5962 (2001).
116. K. Kajihara, L. Skuja, M. Hirano, and H. Hosono, Appl. Phys. Lett. **79**, 1757 (2001).
117. A. Anedda, G. Bongiovanni, M. Cannas, F. Congiu, A. Mura, and M. Martini, J. Appl. Phys. **74**, 6993 (1993).

118. S. Agnello and B. Boizot, *J. Non-Cryst. Solids* **322**, 84 (2003).
119. K. O. Hill, Y. Fujii, D. C. Johnson, and B. S. Kawasaki, *Appl. Phys. Lett.* **32**, 647 (1978).
120. F. Bilodeau, D. C. Johnson, S. Theriault, B. Malo, J. Albert, and K. O. Hill, *IEEE Phot. Techn. Lett.* **7**, 1041 (1995).
121. N. Chiodini, S. Ghidini, and A. Paleari, *Phys. Rev. B* **64**, 073102-1 (2001).
122. M. Watanabe, S. Juodkazis, H.-B. Sun, S. Matsuo, and H. Misawa, *Appl. Phys. Lett.* **77**, 13 (2000).
123. U. Osterberg, and W. Margulis, *Opt. Lett.* **11**, 516 (1986).
124. U. Osterberg, and W. Margulis, *Opt. Lett.* **12**, 57 (1987).
125. P. G. Harper and B. S. Wherret (Eds.), *Nonlinear Optics*, ISBN 0-12-325950-9, Academic Press Inc., UK (1977).
126. A. Thorne, U. Litzén, and S. Johansson, *Spectrophysics: principles and applications*, ISBN 3-540-65117-9, Springer-Verlag, Germany (1999).
127. T. Fujiwara, D. Wong, Y. Zhao, S. Fleming, S. Poole, and M. Sceats, *Electron. Lett.* **31**, 573 (1995).
128. T. Fujiwara, M. Takahashi, and A. J. Ikushima, *Appl. Phys. Lett.* **71**, 1032 (1997).
129. M. Takahashi, T. Fujiwara, T. Kawachi, and A. J. Ikushima, *Appl. Phys. Lett.* **71**, 993 (1997).
130. A. Kameyama, A. Yokotani, and K. Kurosawa, *J. Appl. Phys.* **89**, 4707 (2001).
131. R. Atkins, *Electron. Lett.* **29**, 385 (1993).
132. L. Dong, J. L. Archambault, L. Reekie, P. St. J. Russell, and D. N. Payne, *Appl. Opt.* **34**, 3436 (1995).
133. M. Essid, J. L. Brebner, J. Albert, and K. Awazui, *Nucl. Instr. and Meth. In Phys. Res. B* **141**, 616 (1998).
134. V. B. Neustrev, *J. Phys.: Condens. Matter* **6**, 6901 (1994).
135. R. Tohmon, H. Mizuno, Y. Ohki, K. Sasagane, K. Nagasawa, and Y. Hama, *Phys. Rev. B* **39**, 1337 (1989).
136. H. Hosono, Y. Abe, D. L. Kinser, R. A. Weeks, and K. M. H. Kawazoe, *Phys. Rev. B* **46**, 11445 (1992).
137. J. Nishii, H. Yamanaka, H. Hosono, and H. Kawazoe, *Appl. Phys. Lett.* **64**, 282 (1994).
138. J. Nishii, N. Fukumi, H. Yamanaka, K. Kawamura, H. Hosono, and H. Kawazoe, *Phys. Rev. B* **52**, 1661 (1995).
139. M. Fujimaki, T. Watanabe, T. Katoh, T. Kasahara, N. Miyazaki, Y. Ohki, and H. Nishikawa, *Phys. Rev. B* **57**, 3920 (1998).
140. A. Sakoh, M. Takahashi, T. Yoko, J. Nishii, H. Nishiyama, and I. Miyamoto, *Opt. Express* **11**, 2679 (2003).
141. M. Takahashi, A. Sakoh, K. Ichii, Y. Tokuda, T. Yoko, and J. Nishii, *Appl. Opt.* **42**, 4594 (2003).
142. T. Purcell and R. A. Weeks, *Phys. Chem. Glasses* **10**, 198 (1969).
143. E.-J. Friebele, D. L. Griscom, and G. H. Sigel Jr., *J. Appl. Phys.* **45**, 3424 (1974).
144. T.-E. Tsai, D. L. Griscom, E.-J. Friebele, and J. W. Fleming, *J. Appl. Phys.* **62**, 2264 (1987).
145. G. Pacchioni and C. Mazzeo, *Phys. Rev. B.* **62**, 5452 (2000).
146. T. Tamura, G.-H. Lu, M. Kohyama, and R. Yamamoto, *Phys. Rev B* **70**, 153201 (2004).
147. E. V. Anoikin, A. N. Guryanov, D. D. Gusovsky, V. M. Mashinsky, S. I. Miroshnichenko, V. B. Neustrev, and V. A. Tikhomirov, *Sov. Lightwave Commun.* **1**, 29 (1991).
148. H. Hosono, H. Mizuguchi, H. Kawazoe, and J. Nishii, *Jpn. J. Appl. Phys., Part 2* **35**, L234 (1996).
149. N. Chiodini, F. Meinardi, F. Morazzoni, A. Paleari, and R. Scotti, *Phys. Rev. B* **60**, 2429 (1999).
150. K. Awazu, H. Onuki, and K. Muta, *J. Non-Cryst. Solids* **211**, 158 (1997).
151. T.-E. Tsai, G. M. Williams, and E. J. Friebele, *Opt. Letters* **22**, 224 (1997).
152. H. Kawazoe, *J. Non-Cryst. Solids* **71**, 231 (1985).
153. E. J. Friebele and D. L. Griscom in *Defects in Glasses*, F. L. Galeener, D. L. Griscom, and M. J. Weber (Eds.), ISBN 0-931837-26-X, Material Research Society, USA (1986).
154. T. E. Tsai, D. L. Griscom, and E. J. Friebele, *Diffus. Defect Data, Part B* **5354**, 469 (1987).
155. G. Pacchioni, and R. Ferrario, *Phys. Rev. B* **58**, 6090 (1998).
156. K. Awazu, K.-I. Muta, H. Kawazoe, *J. Appl. Phys.* **74**, 2237 (1993).
157. J. Nishi, K. Kintaka, H. Hosono, H. Kawazoe, M. Kato, and K. Muta, *Phys. Rev. B* **60**, 7166 (1999).
158. M. Yamaguchi, K. Saito, and A. J. Ikushima, *Phys. Rev. B* **66**, 132106 (2002).

159. D. P. Poulios, N. P. Bigelow, and J. P. Spoonhower, *J. Phys.: Condens. Matter* **12**, 8309 (2000).
160. T. Uchino, M. Takahashi, and T. Yoko, *Phys. Rev. Lett.* **84**, 1475 (2000).
161. T. Uchino, M. Takahashi, K. Ichii, and T. Yoko, *Phys. Rev. B.* **65**, 172202 (2002).
162. M. Takahashi, K. Ichii, Y. Tokuda, T. Uchino, T. Yoko, J. Nishii, and T. Fujiwara, *J. Appl. Phys.* **92**, 3442 (2002).
163. A. Cannizzo, *Optical properties of point defects in silica: Role of the local dynamics of the host matrix*, PhD Thesis (2005). Dipartimento di Scienze Fisiche ed Astronomiche, Università di Palermo (Italy).
164. M. Cannas, *Point Defects in Amorphous SiO₂: Optical Activity in the Visible, UV and Vacuum-UV Spectral Regions*, PhD Thesis (1998). Dipartimento di Scienze Fisiche ed Astronomiche, Università di Palermo (Italy).
165. M. Leone, S. Agnello, R. Boscaino, M. Cannas, and F.M. Gelardi, *Phys Rev. B* **60**, 11475 (1999).
166. L. N. Skuja, A. N. Trukhin, and A. E. Plaudis, *Phys. Stat. Sol. A* **84**, 153 (1984).
167. S. Agnello, R. Boscaino, M. Cannas, F. M. Gelardi, and M. Leone, *Phys. Rev. B* **61**, 1946 (2000).
168. B. L. Zhang and K. Raghavachari, *Phys. Rev. B* **55**, R15993 (1997).
169. B. Poumellec, M. Douay, J.C. Krupa, J. Garapon, and P. Niay, *J. Non-Cryst. Solids* **317**, 319 (2003).
170. D. P. Poulios, J. P. Spoonhower, and N. P. Bigelow, *J. Lumin.* **101**, 23 (2003).
171. H. Shigemura, Y. Kawamoto, J. Nishii, and M. Takahashi, *J. Appl. Phys.* **85**, 3413 (1999).
172. S. Grandi, P.C. Mustarelli, S. Agnello, M. Cannas, and A. Cannizzo, *J. Sol-Gel Sci. Technol.* **26**, 915 (2003).
173. H. Hosono, H. Kawazoe, and J. Nishii, *Phys. Rev. B* **53**, R11921 (1996).
174. M. Fujimaki, K. Yagi, Y. Ohki, H. Nishikawa, and K. Awazu, *Phys. Rev. B* **53**, 9859 (1996).
175. M. Fujimaki, T. Kasahara, S. Shimoto, N. Miyazaki, S. Tokuhira, K. S. Seol, and Y. Ohki, *Phys. Rev. B* **60**, 4682 (1999).
176. P. J. Lemaire, R. M. Atkins, V. Mizrahi, and W. A. Reed, *Electron. Lett.* **29**, 1191 (1993).
177. K. Médjahdi, A. Boukenter, Y. Ouerdane, F. Messina, and M. Cannas, *Opt. Express* **14**, 5885 (2006).
178. F. Messina, M. Cannas, K. Médjahdi, A. Boukenter, Y. Ouerdane, *Proceedings of 2005 IEEE/LEOS Workshop on Fibres and Optical Passive Components*, ISBN 0-7803-8949-2, S. Riva-Sanseverino, M. Artiglia (Eds.), pag. 313 (2005).
179. K. Médjahdi, A. Boukenter, Y. Ouerdane, F. Messina, and M. Cannas, in press on *J. Non-Cryst. Solids* (2007).
180. K. Médjahdi, A. Boukenter, and Y. Ouerdane, *J. Chem. Phys.* **123**, 214701 (2005).
181. D. L. Griscom, *J. Non-Cryst. Solids* **73**, 71 (1985).
182. B. D. Evans, *IEEE Trans. on Nucl. Science* **35**, 1215 (1988).
183. D. L. Griscom, M. E. Gingerich, and E. J. Friebele, *Phys. Rev. Lett.* **71**, 1019 (1993).
184. D. L. Griscom, *Phys. Rev. B* **64**, 174201 (2001).
185. K. Kajihara, L. Skuja, M. Hirano, and H. Hosono, *Phys. Rev. B* **74**, 094202 (2006).
186. P. Borgermans and B. Brichard, *IEEE Trans. on Nucl. Science* **49**, 1439 (2002).
187. D. L. Griscom in *Structure and bonding in noncrystalline solids*, G. E. Walrafen and A. G. Revesz (Eds.), ISBN 0306423960, Plenum Press, USA (1986).
188. S. N. Rashkeev, D. M. Fleetwood, R. D. Schrimpf, and S. T. Pantelides, *Phys. Rev. Lett.* **87**, 165506 (2001).
189. A. Bongiorno and A. Pasquarello, *Phys. Rev. Lett.* **88**, 125901 (2002).
190. T. Bakos, S. N. Rashkeev, and S. T. Pantelides, *Phys. Rev. B* **69**, 195206 (2004).
191. K. Kajihara, L. Skuja, M. Hirano, and H. Hosono, *Phys. Rev. Lett.* **92**, 015504 (2004).
192. J. Godet and A. Pasquarello, *Phys. Rev. Lett.* **97**, 155901 (2006).
193. S. Agnello and L. Nuccio, *Phys. Rev. B* **73**, 115203 (2006).
194. P. W. Atkins and J. De Paula, *Atkins Physical Chemistry*, ISBN 0-19-879285-9, Oxford University Press, UK (2004).
195. D. B.-Avraham and S. Havlin, *Diffusion and Reactions in Fractals and Disordered Systems*, ISBN 0-521-62278-6, Cambridge University Press, UK (2000).

196. P. G. Shewmon, *Diffusion in solids*, McGraw-Hill, USA (1963).
197. R. W. Lee, *J. Chem. Phys.* **38**, 448 (1963).
198. R. W. Lee, R. C. Frank, and D. E. Swets, *J. Chem. Phys.* **36**, 1062 (1962).
199. J. E. Shelby, *J. Appl. Phys.* **51**, 2589 (1980).
200. V. Lou, R. Sato, and M. Tomozawa, *J. Non-Cryst. Solids* **315**, 13 (2003).
201. A. J. Moulson and J. P. Roberts, *Trans. Brit. Ceram. Soc.* **59**, 388 (1960).
202. K. L. Brower, P. M. Lenahan, and P. V. Dressendorfer, *Appl. Phys. Lett.* **41**, 251 (1982).
203. I. A. Shkrob and A. D. Trifunac, *Phys. Rev. B* **54**, 15073 (1996).
204. D. E. Swets, R. W. Lee, and R. C. Franck, *J. Chem. Phys.* **34**, 17 (1961).
205. J. E. Shelby, *J. Am. Ceram. Soc.* **55**, 61 (1972).
206. J. E. Shelby and S. C. Keeton, *J. Appl. Phys.* **45**, 1458 (1974).
207. W. G. Perkins and D. R. Begeal, *J. Chem. Phys.* **54**, 1683 (1971).
208. F. J. Norton, *Nature* **191**, 701 (1961).
209. R. H. Doremus, *J. Mater. Res.* **10**, 2379 (1995).
210. T. R. Waite, *Phys. Rev.* **107**, 463 (1957).
211. M. V. Smoluchowski, *Z. Physik. Chem.* **92**, 192 (1917).
212. F. Collins and G. Kimball, *J. Colloid. Sci.* **4**, 425 (1949).
213. S. Kuchinsky, *J. Non-Cryst. Solids* **352**, 3356 (2006).
214. V. A. Radtsig, V. N. Bagratashvili, S. I. Tsykina, P. V. Chernov, and O. Rybaltovskii, *Journ. Phys. Chem.* **99**, 6640 (1995).
215. G. Hetherington, K. H. Jack, and M. W. Ramsay, *Phys. Chem. Glasses* **6**, 6 (1965).
216. R. Brukner, *J. Non-Cryst. Solids* **5**, 123 (1970).
217. A. Abragam and B. Bleaney, *Electronic paramagnetic resonance of transition ions*, ISBN 0198512503, Clarendon Press, UK (1970).
218. C. P. Slichter, *Principles of Magnetic Resonance*, ISBN 962-430-004-6, Springer-Verlag, Hong Kong (1991).
219. G. H. A. M. Van Der Steen and H. Van Der Boom, *J. Non-Cryst. Solids* **23**, 279 (1977).
220. C. M. Hartwig and J. Vitko Jr., *Phys. Rev. B* **18**, 3006 (1978).
221. Y. Morimoto, T. Igarashi, H. Sugahara, and S. Nasu, *J. Non-Cryst. Solids* **139**, 35 (1992).
222. L. Verdi and A. Miotello, *Phys. Rev. B* **47**, 14187 (1993).
223. N. Kuzuu, Y. Komatzu, and M. Murahara, *Phys. Rev. B* **44**, 9265 (1991).
224. M. Cannas, S. Costa, R. Boscaino, and F. M. Gelardi, *J. Non-Cryst. Solids* **337**, 9 (2004).
225. B. I. Vikhrev, N. N. Gerasimenko, and G. B. Lebedev, *Mikroelektronika* **6**, 71 (1977).
226. Z. Li, S. J. Fonash, E. H. Poindexter, M. Harmatz, F. Rong, and W. R. Buchwald, *J. Non-Cryst. Solids* **126**, 173 (1990).
227. A. A. Bobyshev and V. A. Radtsig, *Kinet. Katal.* **31**, 931 (1990).
228. J. F. Conley and P. M. Lenahan, *Appl. Phys. Lett.* **62**, 40 (1992).
229. A. H. Edwards, J. A. Pickard, and R. E. Stahlbush, *J. Non-Cryst. Solids* **179**, 148 (1994).
230. M. Vitiello, N. Lopez, F. Illas, and G. Pacchioni, *J. Phys. Chem. A* **104**, 4674 (2000).
231. G. Lucovsky, H. Yang, Z. Jing, and J. L. Whitten, *Appl. Surf. Sci.* **117/118**, 192 (1997).
232. A. H. Edwards, *J. Non-Cryst. Solids* **187**, 232 (1995).
233. B. J. Mrstik, *J. Electron. Mater.* **20**, 627 (1991).
234. G. Pacchioni and M. Vitiello, *Phys. Rev. B* **58**, 7745 (1998).
235. D. C. Harris and M. D. Bertolucci, *Symmetry and Spectroscopy*, ISBN 0195020014, Oxford University Press, USA (1979).
236. S. Agnello, *Gamma ray induced processes of point defect conversion in silica*, PhD Thesis (2000). Dipartimento di Scienze Fisiche ed Astronomiche, Università di Palermo (Italy).

237. Heraeus Quarzglas, Hanau, Germany, Base materials Catalogue.
238. Quartz & Silice, Nemours, France, Catalogue.
239. H. Haken, *Light. Volume II - Laser light dynamics*, ISBN 0-444-86021-5, North Holland Physics Publishing, USA (1985).
240. B. E. A. Saleh and M. C. Teich in *Fundamentals of Photonics*, ISBN 0-471-83965-5, John Wiley & Sons, USA (1991).
241. S. Costa, Master's degree Thesis, (2002). Dipartimento di Scienze Fisiche ed Astronomiche, Università di Palermo (Italy).
242. S. Agnello, R. Boscaino, M. Cannas, A. Cannizzo, F. M. Gelardi, S. Grandi, and M. Leone, *Phys. Rev. B* **68**, 165201 (2003).
243. J. R. Lakowicz, *Principles of Fluorescence Spectroscopy*, ISBN 0306460939, Plenum Press, USA (1983).
244. S. Agnello, R. Boscaino, M. Cannas, and F. M. Gelardi, *Phys. Rev. B* **64**, 174423 (2001).
245. J. R. Ferraro, K. Namamoto, C. W. Brown, *Introductory Raman Spectroscopy*, ISBN 0-12-254105-7, Academic Press, UK (2003).
246. M. Cannas, S. Agnello, R. Boscaino, S. Costa, F. M. Gelardi, and F. Messina, *J. Non-Cryst. Solids* **322**, 90 (2003).
247. M. Cannas and F. Messina, *J. Non-Cryst. Solids* **345**, 433 (2004).
248. F. Messina, M. Cannas, and R. Boscaino, *Phys. Stat. Sol. (C)* **2**, 616 (2005).
249. M. Cannas and F. Messina, *J. Non-Cryst. Solids* **351**, 1780 (2005).
250. F. Messina and M. Cannas, in press on *J. Non-Cryst. Solids* (2007).
251. F. Messina and M. Cannas, *J. Phys.: Condens. Matter* **17**, 3837 (2005).
252. F. Messina and M. Cannas, *J. Phys.: Condens. Matter* **18**, 9967 (2006) 9967.
253. F. Messina, M. Cannas, R. Boscaino, S. Grandi, and P. Mustarelli, in press on *Physica Status Solidi* (2007).
254. M. Cannas, L. Vaccaro, and B. Boizot, *J. Non-Cryst. Solids* **352**, 20 (2006).
255. M. Cannas, F. M. Gelardi, F. Pullara, M. Barbera, A. Collura, and S. Varisco, *J. Non-Cryst. Solids*, **280**, 188 (2001).
256. E. H. Poindexter, *Semicond. Sci. Technol.* **4**, 961 (1989).
257. K. L. Brower, *Semicond. Sci. Technol.* **4**, 970 (1989).
258. A. Pusel, U. Wetterauer, and P. Hess, *Phys. Rev. Lett.* **81**, 645 (1998).
259. R. S. Becker, G. S. Higashi, Y. J. Chabal, and A. J. Becker, *Phys. Rev. Lett.* **65**, 1917 (1990).
260. K. L. Brower, *Phys. Rev. B* **42**, 3444 (1990).
261. B. Tuttle and C. G. Van de Walle, *Phys. Rev. B* **59**, 12884 (1999).
262. G. Buscarino, *Experimental investigation on the microscopic structure of intrinsic paramagnetic point defects in amorphous silicon dioxide*, PhD Thesis (2007). Dipartimento di Scienze Fisiche ed Astronomiche, Università di Palermo (Italy).
263. Mr. Bodo Kühn (Heraeus Quarzglas GmbH), private communication.
264. F. Messina and M. Cannas, *Phys. Rev. B* **72**, 195212 (2005).
265. F. Messina, M. Cannas, and R. Boscaino, *J. Non-Cryst. Solids* **351**, 1770 (2005).
266. S. Agnello, G. Buscarino, M. Cannas, F. Messina, S. Grandi, and A. Magistris, in press on *Physica Status Solidi* (2007).
267. M. Cannas and G. Origlio, unpublished data.
268. K. L. Brower, *Phys. Rev. B* **38**, 9657 (1988).
269. A. Stesmans, *Appl. Phys. Lett.* **68**, 19 (1996).
270. A. H. Edwards, *Phys. Rev. B* **44**, 1832 (1991).
271. M. Cannas and A. Cannizzo, unpublished data.

